



QUEENSLAND UNIVERSITY OF TECHNOLOGY

**MICRO-CT BASED CHARACTERISATION OF
CHANGES TO THE VASCULAR NETWORK
FOLLOWING CLOSED SOFT TISSUE TRAUMA
AND CRYOTHERAPY**

Zohreh Barani Lonbani

BSc (Obstetrics), M.E. (Medical Eng., Biomechanics), M.E. (Mechanical Eng.)

Submitted to the School of Chemistry, Physics & Mechanical Engineering,
Science and Engineering Faculty, Queensland University of Technology in
fulfilment of the requirements for the degree of Doctor of Philosophy

2015

Keywords

Closed soft tissue trauma

Micro-CT

Characterisation

Vascular morphology

Vascular network

Vascular injury model

Angiogenesis

Blood vessels

Quantification

Imaging

Rat model

Abstract

It is known that the functionality of the vascular network is affected by closed soft tissue trauma (CSTT) resulting from high-energy impact. Furthermore, it has been shown that the revascularisation after muscle injuries is necessary for tissue healing. Currently, the objective and scientific evaluation of the efficacy of clinical therapeutic methods for the treatment of CSTT is hampered by a lack of quantitative diagnostic tools to monitor the revascularisation of the injured tissue. Even the most common treatments such as cryotherapy (icing) are based on anecdotal evidence rather than scientific studies. While revascularisation after muscle injuries is necessary for tissue healing, knowledge regarding the vascular morphology changes following CSTT during the natural healing process and during cryotherapy is missing.

Therefore, this research aimed to investigate the effects of CSTT and cryotherapy on the vascular morphology in 3D in a well-characterised rat model using contrast-enhanced micro-computed tomography (micro-CT) imaging and histological analysis.

In the injury group, an impact device was used to apply a reproducible CSTT to the left thigh of anaesthetised rats. This group was divided into two untreated (sham) and treated groups (icing) where the icing group received cryotherapy on the injured region. The injured animals were also compared with non-injured and non-treated group (control).

To visualise the vasculature, the blood vessels of euthanised rats were perfused with a contrast agent using an infusion pump. The hindlimbs were then imaged using a micro-CT scanner to characterise the 3D vascular morphology using the parameters such as vessel diameter, volume, and density. The results derived from micro-CT imaging were then interpreted and validated by histomorphometry.

Through the CSTT model, it was found that there are measureable changes to the vascular morphology after traumatic injuries and during the natural healing period.

Also, it was confirmed that the recovery of the injured vasculature is affected by therapeutic modalities such as icing. The perfused vessel volume, diameter and number increased from the first day after trauma in non-treated injuries, while the increase of these parameters is reduced in the early time points as a result of icing. Therefore, while cryotherapy reduces the inflammation and pain in the early days following CSTT, the results obtained from this research suggest that this may delay the restoration of the vasculature and consequently the healing of the injured tissue. Although the exact mechanisms responsible for these changes need to be evaluated further, these findings will be useful for the development of future clinical monitoring, diagnosis and treatment of CSTT. In addition, characterisation of the vascular morphology allows for assessment of the severity of CSTT and for monitoring the effect of treatment modalities on healing progression.

Table of Contents

Keywords.....	i
Abstract.....	ii
Table of Contents.....	iv
List of Figures.....	vii
List of Tables.....	x
List of Abbreviations and Acronyms.....	xi
Terminology and applications.....	xii
List of publications.....	xiv
Statement of Original Authorship.....	xvi
Acknowledgements.....	xvii
CHAPTER 1: INTRODUCTION.....	1
1.1 Problem statement and research motivation.....	1
CHAPTER 2: LITERATURE REVIEW.....	5
2.1 Overview.....	5
2.2 CSTT, vasculature damage and healing mechanisms.....	5
2.2.1 Destruction phase.....	6
2.2.2 Repair phase.....	8
2.2.3 Remodelling Phase.....	9
2.2.4 The necessity of vasculature for the healing of the injured muscles.....	10
2.2.5 Vascular regeneration mechanisms.....	11
2.3 Clinical CHARACTERISATION of vascular damage and CSTT.....	13
2.3.1 Definition of CSTT characterisation.....	13
2.3.2 Current clinical CSTT classifications and limitations.....	13
2.4 Experimental models of CSTT and vascular injury.....	16
2.4.1 Rat models.....	16
2.4.2 Impact Models.....	19
2.4.3 Crush models.....	20
2.4.4 Ischemia models.....	20
2.4.5 Characterisation of vascular injury following CSTT.....	21
2.5 Experimental assessment of CSTT and vascular injury.....	23
2.5.1 Advanced imaging methods in vascular injury models.....	23
2.5.2 Histological evaluation.....	27
2.6 Current clinical treatment of CSTT.....	29
2.6.1 Icing (cryotherapy).....	29
2.6.2 Adverse effects of cryotherapy and controversies.....	30
2.6.3 Cryotherapy application following CSTT.....	32
2.7 Statistical approaches for vascular morphometric analysis.....	35
2.8 gaps in knowledge.....	36
2.9 Findings and summary.....	37
2.10 Research Significance.....	39
2.11 Research questions.....	40
2.12 Research hypothesis.....	40

2.13 key goal and Research aims	40
CHAPTER 3: DEVELOPMENT AND CHARACTERISATION OF THE CSTT MODEL.....	41
3.1 Introduction.....	41
3.2 Methodology	41
3.2.1 Structural design and the functionality of the impact device	41
3.2.2 Characterising the impact device	42
3.2.3 Development of a standardised CSTT model using the impact device	48
3.2.4 CSTT and muscle injury characterisation using ImageJ software.....	50
3.2.5 Histology analysis.....	51
3.2.6 General statistics.....	54
3.3 Results	55
3.3.1 Impact velocity characterisation	55
3.3.2 Impact weight characterisation.....	58
3.3.3 CSTT characterisation.....	60
3.4 Discussion	64
3.4.1 The impact device characterisation.....	64
3.4.2 Characterisation of the CSTT model.....	65
CHAPTER 4: DEVELOPMENT OF PERFUSION AND MICRO-CT EVALUATION PROTOCOLS FOR CHARACTERISATION OF THE VASCULAR INJURY FOLLOWING CSTT	68
4.1 Introduction.....	68
4.2 Material and Methods.....	70
4.2.1 Rat hindlimb injury model.....	70
4.2.2 Vascular perfusion protocol.....	70
4.2.3 Vascular visualisation and quantification using micro-CT	73
4.2.4 Validation of the vascular injury model following CSTT	79
4.2.5 Statistical analysis for the reproducibility and validity of the vascular injury model.....	85
4.3 Results	86
4.3.1 Characterisation of the vascular injury model.....	86
4.3.2 Microvascular injury visualisation (biopsies) using micro-CT.....	94
4.3.3 Optimising the quantification by defining a cut-off diameter.....	95
4.3.4 Quantification of microvascular morphometric parameters (biopsy)	105
4.4 Verification and validation.....	111
4.4.1 The reproducibility of the vascular injury model (biopsy)	111
4.4.2 Perfusion of the smallest capillaries.....	112
4.4.3 Validation of the micro-CT analysis using histology (biopsies).....	114
4.4.4 Verification of the PVN and RVP using histomorphometry	117
4.4.5 Evaluation of the microfil shrinkage	119
4.5 Discussion	120
4.5.1 Limitation of the vascular injury model	125
4.5.2 Concluding remarks.....	127
CHAPTER 5: THE EFFECT OF CRYOTHERAPY ON CSTT AND INJURED VASCULATURE	129
5.1 Introduction.....	129
5.2 Methodology and study design	130
5.2.1 Sample size analysis	130
5.2.2 Animal preparation and treatment groups	130
5.2.3 Statistical analysis	132
5.3 Results	133
5.3.1 CSTT qualitative and quantitative assessment.....	133
5.3.2 CSTT and muscle injury verification using histology.....	139
5.3.3 Vascular injury following CSTT and cryotherapy.....	143
5.3.4 The reproducibility of the micro-CT results obtained from the ROI evaluation	146

5.3.5 Microvascular injury visualisation (biopsies) using micro-CT	147
5.3.6 Quantifications of microvascular morphometric parameters (biopsy)	149
5.3.7 The reproducibility of the results obtained from the biopsy evaluation.....	157
5.4 Verifications.....	158
5.4.1 Angiogenesis indication using the PVN over time	159
5.5 Discussion.....	161
5.5.1 The effect of cryotherapy on muscle injury following CSTT	161
5.5.2 The effect of CSTT and cryotherapy on the vascular injury.....	163
5.5.3 Verification of vasodilation	166
5.5.4 Indications of Angiogenesis	167
5.5.5 Alternatives for cryotherapy application.....	169
5.5.6 Limitations of the icing study.....	171
5.5.7 Concluding remarks	172
CHAPTER 6: DISCUSSION AND CONCLUSIONS	174
6.1 GENERAL DISCUSSION	174
6.1.1 What is novel?	177
6.1.2 Limitations and recommendations.....	178
6.2 Research Implications and contributions towards knowledge	182
6.3 Future Directions	183
6.4 CONCLUSION	187
BIBLIOGRAPHY	I
APPENDIX A	XI
APPENDIX B	XVII
APPENDIX C	XIX
APPENDIX D	XXV
APPENDIX E	XXXIII

List of Figures

<i>Figure 2-1: A schematic of the muscle structure.</i>	6
<i>Figure 2-2: The CSTT healing phases and the time points.</i>	10
<i>Figure 2-3: The rat's muscle anatomy.</i>	17
<i>Figure 2-4: The deep muscles of the lateral surface of the rat's hindlimb.</i>	18
<i>Figure 2-5: CT angiograms of rat hindlimb vessels with reference to vessel name.</i>	18
<i>Figure 2-6: The impact device developed by Claes and his group (Claes et al. 2006).</i>	19
<i>Figure 3-1: A schematic of the impact device's structure.</i>	42
<i>Figure 3-2: The structure and functionality of the impact device.</i>	43
<i>Figure 3-3: A schematic of the mechanical functionality of the impact device.</i>	44
<i>Figure 3-4: A set up for characterising the impact speed with a high-speed camera.</i>	46
<i>Figure 3-5: A representation of the captured images by the high-speed camera.</i>	47
<i>Figure 3-6: Defining a region of interest (ROI).</i>	49
<i>Figure 3-7: A configuration of the CSTT showing the inflamed area.</i>	51
<i>Figure 3-8: The geometrical technique for taking corresponding biopsy specimens.</i>	52
<i>Figure 3-9: Calculated velocities of the drop weight versus various distances.</i>	55
<i>Figure 3-10: Measured velocities obtained from a high-speed camera (HSC).</i>	56
<i>Figure 3-11: Comparisons between the calculated and measured velocities.</i>	57
<i>Figure 3-12: Determining the degree of CSTT and muscle injury.</i>	58
<i>Figure 3-13: The evaluation of the skin surface of the rat's hindlimbs.</i>	59
<i>Figure 3-14: Bone fracture inspection following CSTT.</i>	59
<i>Figure 3-15: Skin evaluation after CSTT.</i>	61
<i>Figure 3-16: The CSTT and muscle injury evaluation following an impact.</i>	62
<i>Figure 3-17: The histological analysis following CSTT.</i>	63
<i>Figure 3-18: The quantitative analysis of inflamed areas due to CSTT.</i>	63
<i>Figure 4-1: Two schematic views representing set ups for the perfusion protocol.</i>	72
<i>Figure 4-2: The designed set ups for perfusing the vascular network.</i>	73
<i>Figure 4-3: Micro-CT images of the rat's hindlimb (ROI).</i>	76
<i>Figure 4-4: Selection of a biopsy stack for micro-CT imaging.</i>	78
<i>Figure 4-5: A gridded histology image and a randomly generated section.</i>	79
<i>Figure 4-6: Counting the perfused vessel number using ImageJ.</i>	82
<i>Figure 4-7: Correlating the micro-CT and histological slices.</i>	83
<i>Figure 4-8: The correlated cross sections of a biopsy sample captured from micro-CT and histological analysis (H&E).</i>	84
<i>Figure 4-9: Micro-CT visualisation of the vascular network.</i>	87
<i>Figure 4-10: A 3D micro-CT visualisation of the vascular architecture.</i>	88
<i>Figure 4-11: Bone volume evaluation.</i>	90
<i>Figure 4-12: The quantitative analysis of the TSV.</i>	91

Figure 4-13: The comparisons between the total segmented volume (TSV) and vessel volume (VV).....	93
Figure 4-14: The microvascular visualisation obtained from biopsy samples.	94
Figure 4-15: Identifying the largest blood vessels in the micro-CT images.	95
Figure 4-16: The vessel diameter distribution versus their population.	97
Figure 4-17: Identifying the largest blood vessels in the micro-CT images.	97
Figure 4-18: Determining the cut-off diameter for the vessel diameter (VD).....	100
Figure 4-19: Determining the cut-off diameter for the vessel volume (VV).....	101
Figure 4-20: The frequency distribution of the vessel diameter at day 28.....	103
Figure 4-21: The recalculated vessel diameter (VD) at various cut-off diameters.	104
Figure 4-22: The recalculated vessel volume (VV) at various cut-off diameters.	104
Figure 4-23: Comparisons for the vessel volume (VV) parameter.	106
Figure 4-24: Comparisons for the vessel diameter (VD) parameter.	107
Figure 4-25: Comparisons for the vessel number (VN) parameter.	108
Figure 4-26: Comparisons for the vessel spacing (VSp) parameter.	109
Figure 4-27: Comparisons for the vessel connectivity (VConn) parameter.	110
Figure 4-28: Comparisons for the vascular degree of anisotropy (DA) parameter.	111
Figure 4-29: The smallest capillary filled with microfil contrast agent.....	113
Figure 4-30: Perfused vessels with microfil in a histology image.	114
Figure 4-31: Evaluation of the length (depth) of the biopsy samples.	115
Figure 4-32: Validations between micro-CT and histomorphometry for the PVN.....	115
Figure 4-33: Validations between micro-CT and histomorphometry.	116
Figure 4-34: The perfused vessel number (PVN) from histological analysis.	117
Figure 4-35: The relative vascular perfusion (RVP) parameter per tissue area (mm ²).	118
Figure 4-36: Vasodilation one day after trauma using histomorphometry.	119
Figure 4-37: The microfil shrinkage.	120
Figure 5-1: Skin evaluation.	133
Figure 5-2: Muscle injury evaluation.....	136
Figure 5-3: Quantitative evaluation of the CSTT area.	138
Figure 5-4: Inflammatory cell influx in a histology image (H&E).....	139
Figure 5-5: Histological evaluation of the CSTT at day 1.	140
Figure 5-6: Histological evaluation of the CSTT at day 3.....	141
Figure 5-7: Histological evaluation of the CSTT at day 7.....	142
Figure 5-8: Histological evaluation of the CSTT at day 28.	143
Figure 5-9: 3D visualisation of the vascular network using micro-CT.....	144
Figure 5-10: Total segmented volume (TSV) results obtained from the ROI.	146
Figure 5-11: Micro-CT visualisation of the microvascular morphology.	148
Figure 5-12: The results for the vessel volume (VV) parameter.....	150
Figure 5-13: The results for the vessel diameter (VD) parameter.....	152
Figure 5-14: The results for the vessel number (VN) parameter.	153

Figure 5-15: The results for the vessel spacing (VSp) parameter.	154
Figure 5-16: The results for the vessel connectivity (VConn) parameter.	155
Figure 5-17: The results for the vascular degree of anisotropy (DA) parameter.	156
Figure 5-18: Indications of vasodilation using the VD.	158
Figure 5-19: The perfused vessel number (PVN) per tissue area (mm ²).	159
Figure 5-20: The positively stained blood vasculature with the vWF antibody	160
Figure 6-1: 3D of the vascular network using AMIRA software.	186
Figure C-6-2: The schematic of the impact device's structure.	XXI

List of Tables

Table 2-1: The Tscherne (Tscherne et al. 1984) and AO (Rüedi et al. 2007) CSTT Classification with the injury descriptions.	14
Table 3-1: The initial and final conditions of the drop weight.	45
Table 4-1: The colour coding and symbols used for presenting the results.	86
Table 4-2: The evaluation of the coefficient of variation (CV).	92
Table 4-3: The recalculation methods for the VV and VD parameters.	98
Table 4-4: Reproducibility of the VD and VV at various cut-off diameters.	102
Table 4-5: Comparisons of coefficient of variations at various cut-off diameters.	105
Table 4-6: The CV values for all vascular morphometric parameters.	112
Table 4-7: Validations between micro-CT and histomorphometry for the PVN.	116
Table 5-1: The colour coding and symbols used for presenting the results.	133
Table 5-2: CSTT and muscle injury descriptions.	137
Table 5-3: The CV results for the TSV parameter.	147
Table 5-4: The CV results for the vascular morphometric parameters.	157

List of Abbreviations and Acronyms

CSTT: closed soft tissue trauma

ROI: region of interest

CT: computed tomography

MRI: magnetic resonance imaging

VV: vessel volume

VD: vessel diameter

VSp: vessel spacing

VN: vessel number

VConn: vessel connectivity

DA: degree of anisotropy

v : velocity

PVN: perfused vessel number

TVN: total number of blood vessels

TSV: total segmented volume

TV: total volume of interest

RVP: relative vascular perfusion

Terminology and applications

Reliability: Reliability here refers to the magnitude of the error in observed measurements. Reliability can be described by measuring the variability between repeat measurements which can be quantified by the standard deviation (SD) of the measured values. A high reliability indicates a small measurement error and therefore, any measured differences between two measurements can be genuinely assumed as true values. The reliability may also be described through the intraclass correlation (ICC), which is a measure for the correlation between two independent measurements of the same parameter (Bartlett et al. 2008).

Reproducibility (consistency): Reproducibility of the results means that independent researchers can achieve the same numerical outcomes by repeating the original study using the same techniques on the same data (Boylan *et al.* 2015). Reproducibility is perhaps the most important interpretation of reliability (Krippendorff, 2004, p.215).

Efficiency: The ratio of the useful output to the total input in any system (Badiru 2013). In this research the efficiency of the perfusion protocol was characterised by the “relative vascular perfusion” (RVP) and was defined as a percentage of the number of vessels Perfused with contrast agent over the total number of blood vessels (summation of filled and non-filled vessels).

Sensitivity: Here the sensitivity means the ability of a method or instrument to easily detect/record the slight changes of a variable due to a condition.

Agreement: It quantifies the closeness of two measurements made on the same parameter obtained from two independent modalities where the differences in measurements may be due to biases between the observers or systems (Bartlett et al. 2008). One popular way of quantifying agreement is to estimate the 95% limits of agreement, as proposed by Bland and Altman (Bartlett *et al.* 2008, Bland *et al.* 2010).

Accuracy: The accuracy of a measurement relates on the precision and the trueness of the method and is how close a result comes to the true value (International Organization for Standardization (ISO) 1994, Feinberg 2007).

List of publications

- ✚ Zohreh Barani Lonbani, Daniel Singh, Tony Parker, Michael Schuetz, Mia Woodruff, Jonathan Peake and Roland Steck, “Icing (cryotherapy) delays the vascular healing following closed soft tissue trauma”, The American journal of sports medicine (In preparation).
- ✚ Zohreh Barani Lonbani, Daniel Singh, Tony Parker, Michael Schuetz, Mia Woodruff, Jonathan Peake and Roland Steck, “Morphological changes to blood vessels following closed soft tissue trauma”, Submitted to Journal of Orthopaedic Research.
- ✚ Zohreh Barani Lonbani, Daniel Singh, Tony Parker, Michael Schuetz, Mia Woodruff, Jonathan Peake and Roland Steck, “Development and characterisation of a standardised model of closed soft tissue trauma and vascular injury”, Journal of Orthopaedic Research (In preparation).
- ✚ Zohreh Barani Lonbani, Daniel Singh, Tony Parker, Michael Schuetz, Mia Woodruff, Jonathan Peake and Roland Steck, “The effect of cryotherapy on the vascular regeneration following closed soft tissue trauma”, Oral presentation, Australian and New Zealand orthopaedic research society (ANZORS), Flinders University, Adelaide, Sep 2014 (Nominated for the ANZORS PhD student award).
- ✚ Zohreh Barani Lonbani, Tony Parker, Michael Schuetz and Roland Steck, “The importance of vascular characterisation following closed soft tissue trauma in the orthopaedic field”, Oral presentation, Australian and New Zealand orthopaedic research society (ANZORS), Darlington Centre, Sydney, Sep 2013.

- ✚ Zohreh Barani Lonbani, Tony Parker, Michael A. Schuetz, Roland Steck, “A novel characterisation model for microvasculature changes following closed soft tissue trauma using micro-CT imaging”, Poster presentation, Translational Research Institute (TRI) Inaugural Annual Poster Symposium, Princes Alexandra Hospital, Brisbane, Australia.
- ✚ Zohreh Barani Lonbani, Michael A. Schuetz, Roland Steck, “How Can Closed Soft Tissue Trauma Be Characterised Based on Vasculature Morphological Changes?” Poster presentation, Institute of Health and Biomedical Innovation (IHBI) Inspire Conference, Gold Coast, Australia.
- ✚ Zohreh Barani Lonbani, Michael A. Schuetz, Roland Steck, “Characterization of closed soft tissue trauma with a focus on changes to the microvasculature”, Poster presentation, Australian Society of Medical Research (ASMR) Conference (Postgraduate), University of Queensland, Brisbane, Australia, 2012.

Statement of Original Authorship

The work contained in this thesis has not been previously submitted to meet requirements for an award at this or any other higher education institution. To the best of my knowledge and belief, the thesis contains no material previously published or written by another person except where due reference is made.

Signature: *Zohreh Barani Lonbani*

[QUT Verified Signature](#)

Date: December 2015

Acknowledgements

I would like to count my blessings and thank those who helped me along my PhD pathway and I owe them for their help and support.

I am grateful to God, the unlimited universal energy, for this learning opportunity and for my three advisors, Dr Roland Steck, Dr Tony Parker and Professor Michael Schuetz who were my lanterns and directed me whenever I could not see the path clearly. I am heartily thankful for all I have learned from them and their support.

I would like to extend my thanks to other indirect advisors, Dr Jonathan Peake and A/Prof Mia Woodruff for their useful advice and also the assistance of Daniel Singh and the Trauma Research Group from time to time when it was needed. I also appreciate QUT, IHBI and MERF for providing the facilities and support for this project.

I could not be luckier and happier for having a great family who always supported me with their unconditional love. Thank you God for this gift!

And last but not least, my great gratitude goes to my husband Jeff Wilkie, who has always been beside me with his great support and unlimited love. Thank you for the times I had to stay until late at University and you made dinner and waited for me to come home to have dinner together. I am truly speechless how I can appreciate all that you have done for me so let me dedicate this thesis to you.

Chapter 1: Introduction

1.1 PROBLEM STATEMENT AND RESEARCH MOTIVATION

Closed soft tissue trauma (CSTT) may result from slow crushing or high-energy impact, causing vascular and muscle injuries. These contusion injuries commonly occur during high intensity sports, traffic accidents, or workplace accidents. The damage to the vascular network and tissue leads to bleeding along with a series of inflammatory reactions triggering early acute symptoms. The acute symptoms appear as inflammation, haematoma and swelling, which in severe cases may lead to compartment syndrome, necrosis (tissue loss) and even amputation of the limb (Blaisdell 2002).

While acute CSTT injuries generally heal over time, chronic symptoms such as swelling and pain may take time to heal, which may delay the patient's return to normal life. Despite the problems created by CSTT for individuals, the musculoskeletal complications cause a substantial socio-economic burden due to their cost of treatment (Australian Institute of Health and Welfare 2012). This indicates the importance of musculoskeletal injuries, as well as their diagnosis and monitoring based on a systematic classification. However, an objective classification for closed soft tissue trauma is currently lacking. Available clinical classifications of soft tissue injuries by Tscherne (Tscherne *et al.* 1984, Moore 2011) and also the AO foundation (Arbeitsgemeinschaft für Osteosynthesefragen; Association for the Study of Internal Fixation) (Rüedi *et al.* 2007) categorise only macroscopic symptoms qualitatively which makes the diagnosis and also the monitoring of treatment efficacy subjective and extremely challenging in regard to its accuracy.

From research reported in the literature, where animal models were used to assess CSTT, there has been some evidence indicating that there is a disruption of microvascular circulation following CSTT (Schaser *et al.* 1999) causing hypoxia and necrosis in the injured soft tissue. Also, a reduction in blood flow has been reported one day following CSTT (Claes *et al.* 2006).

Furthermore, the necessity of blood vessel formation for the regeneration of injured muscle tissue has been emphasised in the literature (Bauer *et al.* 2005, Järvinen *et al.* 2005).

In ischemia research models of rat hindlimbs, the vital role of mechanisms such as angiogenesis (sprouting new capillaries from pre-existing vessels) and arteriogenesis (widening the pre-existing arteries) during the healing process has been highlighted by characterising the vascular morphology (Tonnesen *et al.* 2000, Scholz *et al.* 2002, Duvall *et al.* 2004). Collectively, these studies show that during the natural healing process following an ischemic muscle injury, changes to vascular morphology are necessary for adequate perfusion, in order to provide sufficient oxygen and nutrients for successful tissue regeneration.

However, most methods that have been previously used in research studying the effect of CSTT on the vascular network are either evaluated based on two-dimensional (2D) imaging modalities, or focused on the changes to vascular functionality (e.g. blood flow). These do not provide comprehensive information on the detailed morphological changes to the vascular morphology following CSTT in three dimensions (3D) (Schaser *et al.* 1999, Claes *et al.* 2006). Also, while there is more detailed information available regarding vascular morphology, this originates from ischemia research models where the injury is created by arterial ligation (Duvall *et al.* 2004), which is fundamentally different from a CSTT resulting from a high energy impact. To date, detailed knowledge regarding vascular morphology changes following CSTT is lacking.

Current clinical treatments for CSTT include immobilisation, elevation, compression and icing (cryotherapy) for reducing the haematoma, inflammation and swelling (Järvinen *et al.* 2007). It has been emphasised that the application of appropriate treatments to restore the vascular network can potentially accelerate muscle tissue healing (Järvinen *et al.* 2005). In this regard, oxygen therapy has also been suggested as a remedy for reduction of hypoxia post injury (Gottrup 2004).

To date, the research on the application of these methods remains mostly qualitative without sufficient scientific evidence to demonstrate its efficacy.

One traditional non-invasive treatment that has been extensively used in sport and discussed in literature is the immediate application of ice to the injured region to reduce pain (Hubbard *et al.* 2004) and the development of a haematoma (Schaser *et al.* 2007) following trauma. Despite a few studies that have recommended cryotherapy as a possible method for the treatment of closed soft tissue injuries (Schaser *et al.* 2006, Schaser *et al.* 2007), this method still remains controversial with regard to its efficacy for treating the injured muscle *per se* (Collins 2008, Takagi *et al.* 2011, Tseng *et al.* 2013).

Overall, a scientific research model that could be applied for the quantitative and objective study of the changes to the vascular structure following CSTT during the natural healing process and also after icing is not currently available. While methods for the assessment of CSTT healing are mostly qualitative and in 2D, a 3D quantitative characterisation of the vascular injury following CSTT may provide more comprehensive information that can be used for the assessment and monitoring of the muscle injury and its healing. This experimental framework may also facilitate the development of an efficient CSTT treatment by assessing the effect of therapeutic modalities (e.g. icing) on the vascular injuries following CSTT.

Therefore, the goal of this research is to develop and characterise an experimental rat injury model to investigate the effects of CSTT and cryotherapy on the vascular morphology (3D) at various time points.

Chapter 2: Literature Review

2.1 OVERVIEW

This chapter provides an overview of the pathophysiological pathways involved with vascular damage following soft tissue injuries. The discussion is continued by evaluating CSTT and vascular injury from two perspectives; clinical and experimental. This is then followed by an introduction to injury models and advanced imaging techniques available for the assessment of vascular injuries. Current clinical treatments are also outlined and the subsequent discussion is focused on cryotherapy, the method applied in this research. Current gaps found in the literature regarding vascular injury following CSTT are also summarised. In the light of the literature review, the hypothesis, aims and finally the research questions are stated at the end of this chapter.

2.2 CSTT, VASCULATURE DAMAGE AND HEALING MECHANISMS

Prior to explaining the CSTT pathophysiology, it is important to know the structure of the healthy muscle tissue. Muscle fibres as functional units are long cylindrical cells surrounded by a connective tissue called an endomysium. Each muscle fibre includes many nuclei that are peripherally attached to the muscle fibre beneath the covering membrane called a sarcolemma. Parallel muscle fibres are surrounded by another connective tissue layer called the perimysium that together form a fascicle. A group of fascicles are encapsulated by a thick connective tissue layer called an epimysium (Gillies *et al.* 2011)(Figure 2-1).

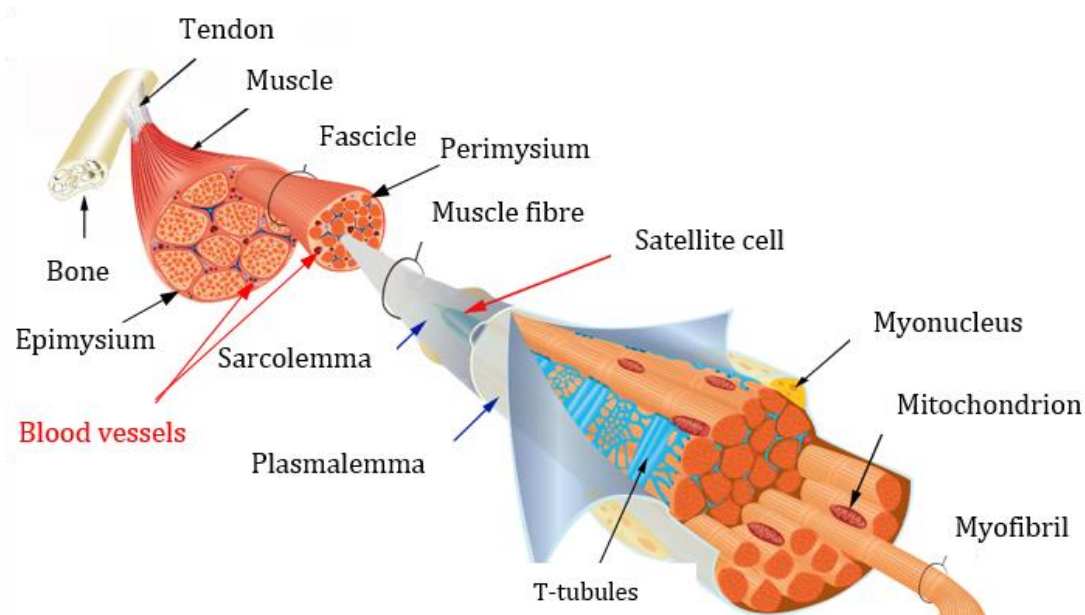


Figure 2-1: A schematic of the muscle structure.

A cross section of the muscle tissue including several fascicles and blood vessels located inside and outside the fascicles. Each fascicle is surrounded by a layer called perimysium and contains several muscle fibres. Each muscle fibre is also covered by a layer of connective tissue called an endomysium and includes many peripherally located nuclei. The original image illustrated here has been kindly provided by Relaix and Zammit (Relaix *et al.* 2012) and modified for this thesis.

Wound healing mechanisms can be classified into three main phases as suggested by Järvinen and colleagues (Järvinen *et al.* 2005). Many of these mechanisms overlap and the classification discussed here is only to provide a simple explanation of these terms.

The wound healing phases are described as the:

- ✚ Destruction phase
- ✚ Repair phase
- ✚ Remodelling phase

2.2.1 Destruction phase

Depending on the severity of the injury, the damage to the soft tissues including muscles and blood vessels leads to the formation of a haematoma as well as a vascular and cellular inflammatory response (Hunt 1988, Nauta *et al.* 2011).

CSTT is often the result of an external compressive force such as a blunt impact (Gierer *et al.* 2010), or a prolonged crush (Akimau *et al.* 2005). Such forces increase the internal mechanical stresses (pressure) in the affected tissue causing deformation (strain) and damage to the skin, muscle and the neurovascular system. In the case of CSTT, even though the skin is not perforated, rupturing of the muscle fibres along with vasculature walls usually leads to internal bleeding and the formation of a haematoma under the skin (Lovering 2008).

Meanwhile, the processes of haemostasis begins to control and reduce the internal bleeding through three mechanisms (Linares 1996). The first mechanism is vasoconstriction which is the contraction of blood vessels to reduce blood flow to the affected region (Casey *et al.* 2012). The second mechanism is the formation of platelet plugs, which is the accumulation and adherence of platelets within the injured vasculature to seal the ruptured regions (Nauta *et al.* 2011). The last mechanism is blood clot development through initiation of the coagulation cascade and production of a fibrin mesh around the platelet plug to seal the ruptured microvasculature preventing further haemorrhage (Norris 2003). Blaisdell (2002) has reported that a secondary effect of the haemostasis is hypoxia that is caused by a reduction of blood flow, and consequently oxygen perfusion to the injured site. He has explained that this is accompanied by a blockage of the microvasculature due to swollen endothelial cells of capillaries, blood clot formation and finally adhesion of other blood cells (leukocytes, lymphocytes and monocytes) in the microvasculature lumen. He has also suggested that this effect may be followed by depletion of adenosine triphosphate (ATP) following ischemia leading to necrosis of muscle cells (Blaisdell 2002). Soon after the haemostasis phase, a series of inflammatory reactions begin to deliver biochemical mediators such as histamine, heparin and prostaglandins from ruptured mast cells located in the injury site (Metcalf *et al.* 1997). Both haemostasis and inflammatory phases are associated with early microcirculation changes after CSTT (Schaser *et al.* 1999, Blaisdell 2002).

The vascular response starts soon after the haemostasis phase through the following processes.

Vasoconstriction refers to the narrowing (contraction) of blood vessels and vasodilation is the enlargement of blood vessels through relaxation of the vascular smooth muscles. While vasoconstriction narrows the surviving blood vessels to reduce the blood flow, the vasodilation mechanism widens the vessels to increase the blood flow following the injury (Dodd *et al.* 1993, Williamson *et al.* 2004, Casey *et al.* 2012). Another mechanism is increasing vaso-permeability which results in an increased plasma passage across blood vessel walls. These early changes in the microvasculature such as vasodilation and increasing vaso-permeability trigger plasma leakage into the surrounding connective tissue and the accumulation of fluid in the extracellular matrix (ECM) which eventually results in swelling of the tissue (Williamson *et al.* 2004).

Usually, symptoms of the inflammatory phase are identified as pain, inflammation, swelling (oedema), redness, and local temperature elevation (Goodman *et al.* 2014). Compartment syndrome is a serious and painful complication that occurs when the intramuscular pressure is increased. Severe injuries may lead to compartment syndrome due to excessive swelling (Gourgiotis *et al.* 2007).

2.2.2 Repair phase

Following the destruction phase, the repair phase begins where the damaged tissue is repaired through two mechanisms; regeneration of the disrupted tissue (muscles and vasculature), and the establishment of the scar (connective tissue) providing the muscle strength to tolerate contractions. These two mechanisms independently commence at the same time and a successful repair depends upon a balance between these two mechanisms (Clark 1996, Baoge *et al.* 2012). Damage to the integrity of the tissue activates a number of growth factors such as the fibroblast growth factor (FGF) and the vascular endothelial growth factor (VEGF) which are already stored in the ECM of myocytes in an inactive form (Hodde *et al.* 2007). Growth factors are natural regulators in the form of proteins that participate in cell proliferation, growth, and differentiation.

For example, FGF is involved in myogenesis by promoting the proliferation and differentiation of myofibres and VEGF stimulates angiogenesis by initiating the formation of new blood vessels and capillaries (Enoch *et al.* 2008).

During the repair phase, proliferation and differentiation of new myoblasts begin from satellite cells which are mono-nucleated myogenic cells located on the surface of the myofibre (Anderson *et al.* 2004, Schmalbruch H. 2006, Relaix *et al.* 2012). After myoblasts are regenerated, several new myoblasts join together to form the multinucleated myotubes. The newly shaped myotubes eventually attach to the pre-existing myofibres to mend the broken muscle fibres (Gilbert 2006, Turner *et al.* 2012).

In parallel with muscle regeneration, the repair of the damaged vasculature begins with regenerating endothelial cells that form a loose granular tissue enriched with capillaries. Gradually the new capillaries begin to grow from pre-existing vessels towards the injured area to provide the necessary nutrition and oxygen for the aerobic metabolism required for the development of myofibres and capillaries. Finding evidence of wound re-vascularisation after trauma is a sign of successful regeneration within the tissue (Enoch *et al.* 2008, Tu *et al.* 2008, Wullschleger 2010).

Besides the regeneration of the muscle fibres and vasculature during the repair phase, the connective tissue and other elements of the ECM are produced to provide an early frame for embedding the myofibres and capillaries (Stroncek *et al.* 2007). In this phase, fibroblasts are responsible for synthesizing the ECM, collagen and connective tissue scar. As the repair procedure progresses, collagen fibres begin to cross-link to form a stronger structure for the tissue scar (Veikkola *et al.* 1999).

2.2.3 Remodelling Phase

The remodelling phase is the final stage of wound healing. The scar formation including cross-linking and orientation of collagen fibres transforms the granulation tissue which has been developed in the regeneration phase within the skin and muscles into a strong fibrous frame (Driessen *et al.* 2003).

The remodelling stage is also identified by the maturation of the newly produced muscle fibres and arteries to restore muscle functionality (Smith *et al.* 2008). It should be pointed out that although the mechanisms involved with the repair and remodelling phases (e.g. muscle and scar formation) are independent processes, they are significantly associated and may overlap (Stroncek *et al.* 2007, Smith *et al.* 2008). Usually, the remodelling phase is a long process and it may take weeks or months for soft tissue to heal and return to its original functional and morphological condition prior to injury (Kannus 2000, Stroncek *et al.* 2007). The CSTT healing phases and the approximate time points are summarised in Figure 2-2 based on the finding from literature (Li *et al.* 2007, Smith *et al.* 2008).

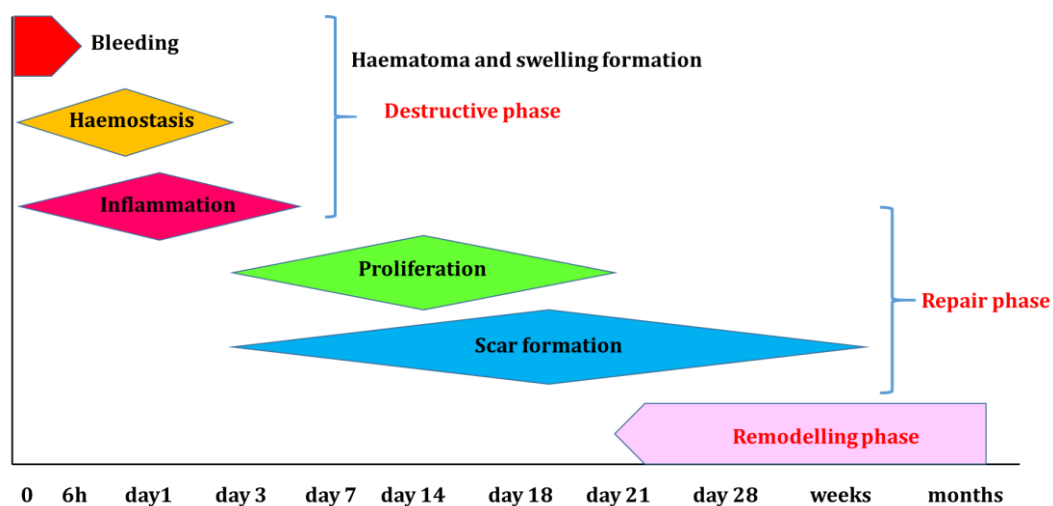


Figure 2-2: The CSTT healing phases and the time points.

2.2.4 The necessity of vasculature for the healing of the injured muscles

The vital role of vascularisation for the healing of damaged tissue and muscle fibre regeneration has been highlighted previously (Bauer *et al.* 2005, Nauta *et al.* 2011, Turner *et al.* 2012). The first sign of regeneration is the restoration of the vascular supply, which is essential for the morphological and functional recovery of the injured muscles (Longo *et al.* 2012).

The growth of new capillaries in the injury site is necessary to restore the blood perfusion and supply sufficient oxygen facilitating aerobic metabolism and consequently the energy required for regeneration of muscle fibres (Järvinen *et al.* 2005, Järvinen *et al.* 2007, van Wessel *et al.* 2010). Research has shown that vascular functionality and morphology changes following injury (Duvall *et al.* 2004, Claes *et al.* 2006). In animal CSTT models, early changes of vascular functionality following CSTT have been demonstrated through disruption of the microvascular circulation causing hypoxia and necrosis in the injured soft tissue (Schaser *et al.* 1999). This is aligned with other findings which have shown a reduction of blood flow following trauma (Claes *et al.* 2006).

Changes to vascular morphology have been reported in animal models of ischemia, where ischemia is established by ligation of the collateral hindlimb artery. There was a demonstrated increase in the number, diameter and volume of blood vessels during the natural wound healing process in the hindlimb of the ligated artery compared to the control hindlimb (Tonnesen *et al.* 2000, Scholz *et al.* 2002, Duvall *et al.* 2004, Lu *et al.* 2010). These results indicate that in the natural healing process, these changes to the vascular morphology are necessary for adequate perfusion providing enough oxygen and nutritional supply for successful tissue regeneration.

2.2.5 Vascular regeneration mechanisms

Following injury, the vasculature within the impaired tissue is regenerated through three mechanisms. The first mechanism is 'angiogenesis' or neovascularisation which is initiated after injury (e.g. ischemic condition). Angiogenesis is the sprouting of new capillaries derived from endothelial cells of pre-existing vessels towards the ECM (within the first 5 days) in response to the reduction of the tissue oxygen level and the presence of angiogenesis stimulators such as VEGF (Greenhalgh 1998, Hershey *et al.* 2001, van Oostrom *et al.* 2008). In animal models, several authors have shown evidence that the application of an angiogenesis inhibitor can suppress revascularization (Couffinhal *et al.* 1998, Murohara *et al.* 1998, Hausman *et al.* 2001).

Therefore, since a direct correlation between vascular growth and tissue repair has been demonstrated, the suppressed angiogenesis and subsequent revascularisation may cause the impairment of muscle regeneration following injury (Zhu *et al.* 2011).

The second mechanism for revascularisation is 'arteriogenesis' which is the growth of new arteries through two mechanisms; arterial branching and the formation of pre-existing collateral arterioles (Zhuang *et al.* 2006). In this process, the pre-existing arterioles which are naturally bridging the larger arteries (bypasses) remodel and grow to form functional arteries (Heil *et al.* 2006). This mechanism involves the enlargement of the lumen diameter, wall thickness and the length of the collateral arterioles through endothelial cell growth and proliferation (Herzog *et al.* 2002, Heil *et al.* 2004). Arteriogenesis is stimulated to recover blood flow at the injury site in response to the changes in shear stresses due to an artery ligation or blockage (Heil *et al.* 2004, van Oostrom *et al.* 2008). It has been shown that after ischemia due to ligation of the femoral artery, the diameter of the collateral artery is increased (Scholz 2002). It should be pointed out that although both angiogenesis and arteriogenesis facilitate restoration of blood flow following injury, these mechanisms act independently (Herzog *et al.* 2002).

The third mechanism is 'vasculogenesis' which is the migration and differentiation of endothelial precursor cells (angioblasts) to the injured area to produce and form new blood vessels (*de novo*) in response to the growth factors including VEGF and FGF (Bauer *et al.* 2005, Schmidt *et al.* 2007). The newly formed blood vessels are initially immature and after lumen formation eventually turn into capillaries and then subsequently into matured arterioles, venules, arteries, and veins (Bauer *et al.* 2005).

2.3 CLINICAL CHARACTERISATION OF VASCULAR DAMAGE AND CSTT

2.3.1 Definition of CSTT characterisation

In this research, the term “CSTT characterisation” is generally used to describe both clinical (*in vivo*) and experimental (*in vivo* and *ex vivo*) approaches for monitoring, assessing and diagnosing CSTT. This represents both the qualitative and quantitative evaluation of CSTT using criteria that together form the characterisation package. These criteria can be identified as morphological (structural), biochemical, functional, physiological or biomechanical in nature.

2.3.2 Current clinical CSTT classifications and limitations

For better clinical management of injuries, several CSTT classifications have been developed. The most commonly used clinical classification systems for CSTT are the Tscherne and AO classifications. The Tscherne classification (Tscherne *et al.* 1984) divides closed fractures accompanied with CSTT into four categories that range from minimal injuries (grade 0) to extensive damage (grade 3). While the Tscherne classification system scores a variety of symptoms within the same category, the AO grading system provides more detailed information regarding the CSTT in combination with closed fractures (Südkamp 2004). This method classifies CSTT into the various anatomical structures including skin, muscles, neurovascular and then based on the severity of the injury assigns them into five categories. The muscle-tendon (MT) injuries range from mild (MT1) to severe (MT5) and neurovascular (NV) injuries range from mild (NV1) to severe (NV5) (Rüedi *et al.* 2007) (Table 2-1). However, these classification systems are based on a qualitative assessment of macroscopic symptoms and palpation, which makes the characterisation subjective. They can be applied for the qualitative characterisation of CSTT whereas quantitative classification will allow for a more accurate initial diagnosis, thereby leading to a better treatment.

Table 2-1: The Tscherne (Tscherne et al. 1984) and AO (Rüedi et al. 2007) CSTT Classification with the injury descriptions.

Tscherne classification			
Grade	Description		
0	Minimal soft tissue damage, simple pattern		
1	Superficial abrasion with local contusion damage to skin or muscle caused by pressure from within, mild to moderate pattern		
2	Deep contaminated abrasion with local contusion damage to skin and muscle, impending compartment syndrome, severe pattern		
3	Extensive contusion or crushing of skin or destruction of muscle, underlying severe muscle, decompensate compartment syndrome, associated with a major vascular injury, severe pattern		
AO classification			
Muscle/tendon injury (MT)		Neurovascular injury (NV)	
Grade	Description	Grade	Description
MT 1	No muscle injury	NV 1	No neurovascular injury
MT 2	Circumscribed muscle injury, one compartment only	NV 2	Isolated nerve injury
MT 3	Considerable muscle injury, two compartments	NV 3	Localized vascular injury
MT 4	Muscle defect, tendon laceration, extensive muscle contusion	NV 4	Extensive segmental vascular injury
MT 5	Compartment syndrome/crush, syndrome with wide injury zone	NV 5	Combined neurovascular injury including partial or total amputation

In general, it was found that the most common clinical classifications for CSTT diagnosis are non-specific, qualitative and subjective, failing to provide enough information regarding the injury status of the microvasculature after the CSTT.

Another clinical avenue to characterise the injured tissue following a CSTT is by monitoring levels of systemic markers such as Creatine Kinase (CK) and Lactate Dehydrogenase (LDH). The elevation of these biochemical markers in the blood serum indirectly indicates damage to skeletal muscle and tissue (Brancaccio et al. 2006, Sudhakar et al. 2012). However, any muscle breakdown releases CK into the blood serum and any general tissue damage elevates the LDH (Wullschleger 2010).

Therefore, these systemic markers are non-specific for the accurate characterisation of soft tissue injury, and these non-specific systemic markers cannot monitor individual injuries in multi-trauma patients.

In general, inaccessibility of the subcutaneous microvasculature restricts the detailed assessment of the microvascular network following trauma during clinical monitoring and treatment administration (Levin *et al.* 1996). Most clinical imaging modalities are hampered by limitations that restrict the comprehensive visualisation of changes to the microvasculature anatomy and detailed microvascular quantification considerably.

While conventional X-ray (radiography) is useful for assessing hard tissues such as bone, it may not be able to visualise soft tissue accurately (Li *et al.* 2004, Zhang *et al.* 2011). Contrast-enhanced angiography for vascular imaging using fluoroscopy is limited by an inadequate number of fixed viewing angles as well as difficulties to differentiate the overlap between pre-existing and regenerated vessels (Zhuang *et al.* 2006).

Ultrasound may be used to measure general blood perfusion within a defined area, but its use is highly dependent on the radiologist's expertise (Canadian Society of Diagnostic Medical Sonography 2008). The visualisation or quantification of individual blood vessels or the vascular morphology using ultrasound is currently not possible in a clinical setting.

Magnetic resonance imaging (MRI) and computed tomography (CT) are currently available as advanced clinical imaging tools for visualisation of changes to the soft tissue. These systems are being used for vascular imaging such as MR-angiography and CT-angiography. The highest resolution range that these systems are able to visualise the vascular network is within a resolution range of 80-100 μm for MR-angiography (Qian *et al.* 2012) and 75-100 μm for CT-angiography (Gakhal *et al.* 2009, Funama *et al.* 2012). This means that the small blood vessels and capillaries less than 75 μm cannot be observed using these systems.

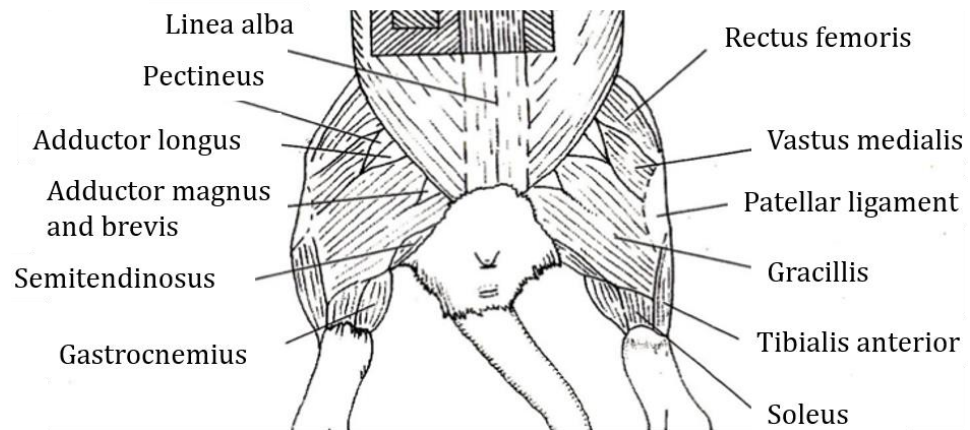
Therefore, these systems may not be suitable for evaluating capillaries which are mainly less than 10 μm (Tata *et al.* 2002) and also the events that occur at the capillary level such as angiogenesis (Hershey *et al.* 2001).

2.4 EXPERIMENTAL MODELS OF CSTT AND VASCULAR INJURY

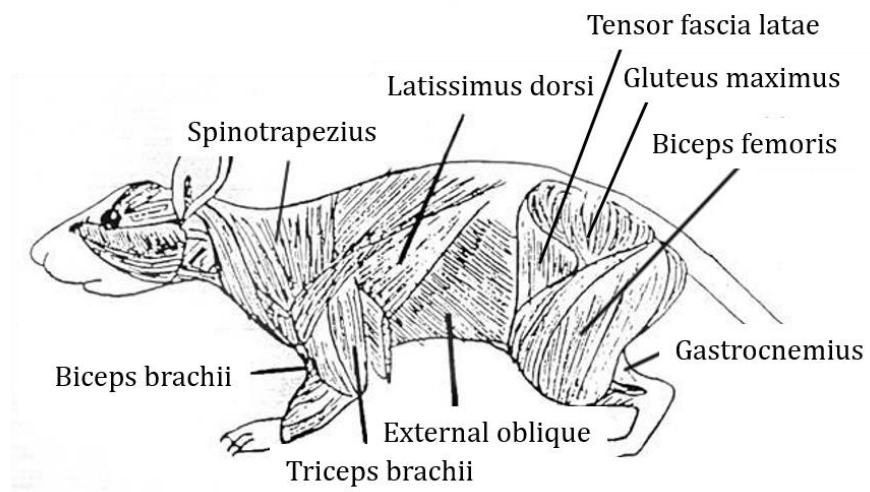
2.4.1 Rat models

Animal models are important for pre-clinical investigation, simulation of traumatic injuries, assessment of healing processes, and testing the efficiency of therapeutic modalities. Rat models have been used for research on CSTT (Kälicke *et al.* 2003) to show vascular perfusion disruption following traumatic injuries (Schaser *et al.* 1999, Claes *et al.* 2006) and for testing the efficacy of treatment modalities such as cryotherapy (Smith *et al.* 1994, Dolan *et al.* 1997). In order to simulate clinical cases of musculoskeletal damage including CSTT and ischemia models, many authors have used rat models for their experiments (Kälicke *et al.* 2003, Lomas-Niera *et al.* 2005, Khattak *et al.* 2010, Frink *et al.* 2011). Furthermore, rat models have been applied for investigation of vascular growth and tissue healing (Ishii *et al.* 2002, Boerckel *et al.* 2011) as well as the effect of cold therapy on swelling following a blunt injury (Dolan *et al.* 1997). Rats are favoured for studies of CSTT because they are quickly acclimatised to their environment as well as being easy to handle, easy to maintain and house due to their small size. Also, their lower cost compared with larger animals is another advantage especially when research requires a large number of animals. Based on these reasons, rats are good candidates to be used for the investigation of the CSTT and therefore, it is essential to be familiar with their basic anatomy including muscles and hindlimb vessels (Figures 2-3, 2-4 and 2-5).

While rat models in musculoskeletal research are well documented, there are only limited studies reported on quantification of the CSTT healing process, particularly with respect to the characterisation of the vascular injury. Experimentally, few models are available in which detailed characterisation *in vivo* and *ex vivo* of the vascular and muscle injuries have been conducted. Some of these models including trauma-induced models (i.e. impact and crush) as well as ischemic models (based on arterial ligation) are explained here.



A



B

Figure 2-3: The rat's muscle anatomy.

The rat's muscle anatomy is shown in particular the medial (A) and lateral (B) views of the hindlimbs. Adapted from (Bismarck Public School 2014) and (Creative Commons 2007, Fastol 2012) respectively.



Figure 2-4: The deep muscles of the lateral surface of the rat's hindlimb.

1. Deep Gluteus superficialis, (reflected), 2. Gluteus medius, 3. Piriformis, 4. Semitendinosus, 5. Biceps femoris (reflected), 6. Semimembranosus, 7. Vastus lateralis, 8. Gastrocnemius. This image has been kindly permitted to use in this thesis by Deborah Sillman, Penn State University, USA (Sillman 2007).

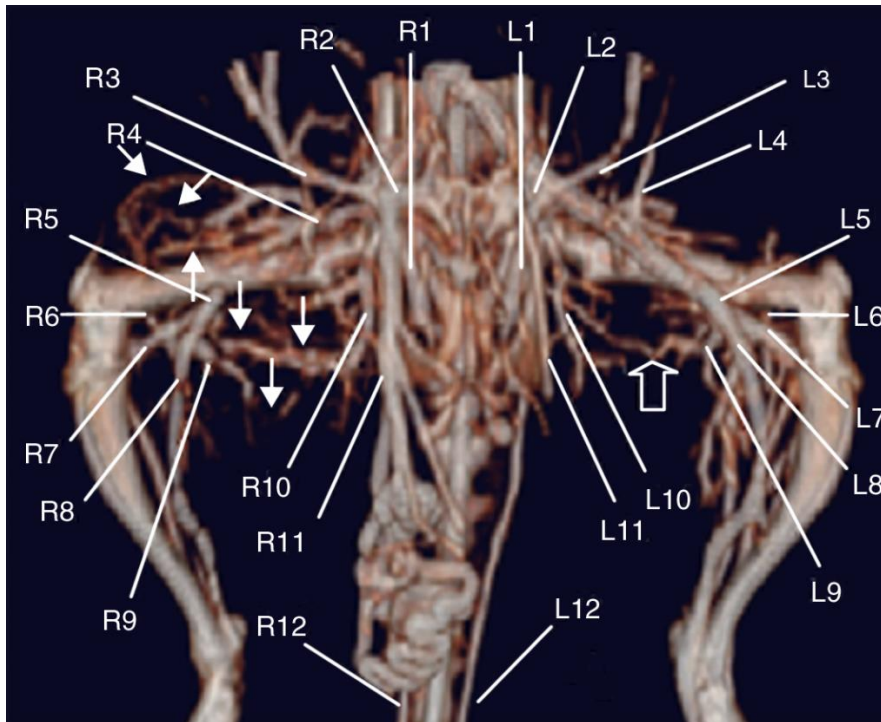


Figure 2-5: CT angiograms of rat hindlimb vessels with reference to vessel name.

L_left leg, R_right leg, 1_arteria circumflexa femoris caudalis, 2_arteria iliaca interna, 3_arteria epigastrica caudalis, 4_circumflexa femoris lateralis, 5_arteria femoralis, 6_arteria genus descendens, 7_arteria saphena, 8_arteria poplitea, 9_arteria caudalis femoris distalis; 10_arteria profunda femoris; 11_arteria ductus deferentis, 12_arteria caudalis dorsolateralis. This image has been kindly provided to use in this thesis by the Radiological Society of North America (RSNA) (Zhuang et al. 2006).

2.4.2 Impact Models

Several animal impact models using an impact device have been developed to study closed soft tissue trauma. One of the first impact trauma devices reported in the literature was developed by Francis (Francis 1985). This impact device was based on a drop weight mechanism and utilised an impactor to produce a uniform CSTT on the lateral thighs of rats. Later, similar impact devices have been developed by other authors, while only a few reported impact characteristics such as impact height, impactor weight and the velocity of the impactor (Claes *et al.* 2006) (Figure 2-6).

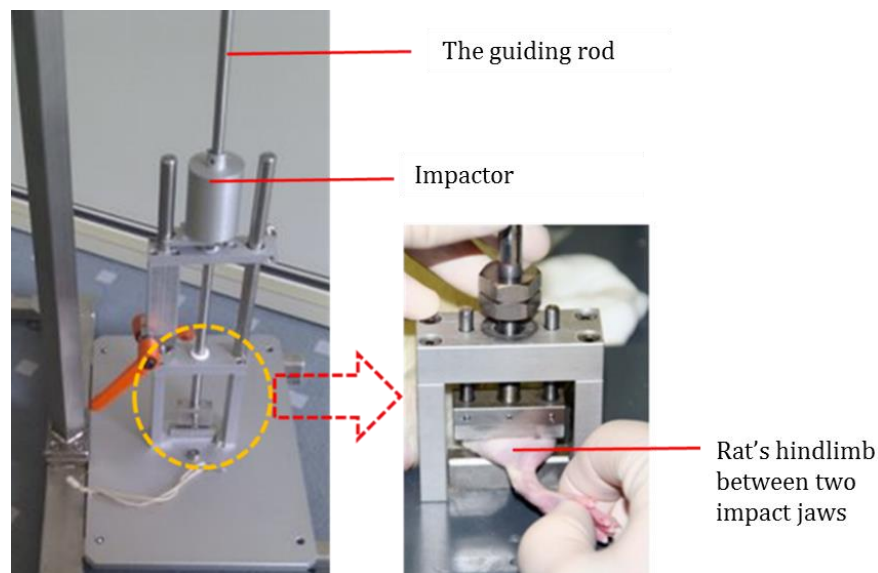


Figure 2-6: The impact device developed by Claes and his group (Claes *et al.* 2006). These images have been kindly provided by Lutz Claes and his group and are reproduced here with his permission.

Schaser and colleagues produced a standardised CSTT using a computer-assisted impact device on rat hindlimbs to simulate the clinical condition of impact to the inferior extremities (Schaser *et al.* 1999, Schaser *et al.* 2003). Their device included a compressed nitrogen gas supply, a plastic container for locating the hindlimb, an adjustable impactor, a displacement transducer, and a computer for time and displacement data examination. Their impact device provided sufficient information regarding the measurement of the depth of the injury due to the impact and other mechanical parameters such as impact speed.

2.4.3 Crush models

A rat crush injury model was developed by Akimau and colleagues to evaluate local and systemic responses (crush syndrome) using systemic markers (CK and LDH) under a mechanical compression load for three hours. They found that there is a correlation between the severity of the crush injury shown by elevated CK and LDH and the volume of the injured muscle (Akimau *et al.* 2005). Through the measurement of the capillary pressure, Korthuis and colleagues have also demonstrated in a canine model that microvasculature permeability is increased in a crush skeletal muscle injury after 4 hours. They have indicated that this may be due to oxygen free radicals and histamine produced by mast cells causing oedema and compartment syndrome (Korthuis *et al.* 1985).

2.4.4 Ischemia models

Many ischemia models have studied the vascular morphology and functionality changes following injury induced by the ligation of arteries in collateral hindlimbs (Couffinhal *et al.* 1998, Scholz *et al.* 2002, Zhuang *et al.* 2006, Oses *et al.* 2009, Lu *et al.* 2010, Orbay *et al.* 2013, Nebuloni *et al.* 2014). Some authors have conducted comprehensive assessments of the changes to the vascular morphology resulting from an ischemia model by quantifying vascular morphometric parameters such as vessel volume and density after ligating the femoral artery in mice using micro-CT and a silicon rubber contrast agent (Microfil: MV-122 Microfil, Flow Tech, Carver, MA) (Duvall *et al.* 2004, Bolland *et al.* 2008). The authors confirmed that high resolution micro-CT scanning along with an appropriate contrast agent provides an accurate visualisation of the 3D microvascular architecture and is capable of sophisticated quantitative evaluation (Duvall *et al.* 2004). This was a significant advancement towards the characterisation of vascular morphology.

2.4.5 Characterisation of vascular injury following CSTT

Currently, there are only a few reported CSTT models and they are mostly focused on changes to the vascular functionality (e.g. blood flow) following trauma (Schaser *et al.* 1999, Claes *et al.* 2006). Claes and colleagues have applied a CSTT (grade 2 according to Tscherne) to the thighs (biceps femoris muscle) of 38 rats. Laser Doppler flowmetry (LDF) was utilised to document blood flow of the injured muscles before and after trauma. The rats were then sacrificed at days 1, 3, 7, 14 (n=3) and on day 28 (n=7). The authors found that moderate CSTT reduced blood flow in the injured muscle for the first 24 hours after trauma (Claes *et al.* 2006). They also demonstrated that the blood flow could recover during healing after 3 days. Despite the fact that LDF can provide information regarding the blood flow changes of the superficial injured tissue, it may not be suitable for deeper tissue injury evaluation as this method cannot detect the blood flow at a depth of more than 2mm.

Regarding the vascular functionality after CSTT, other studies were carried out by Schaser and colleagues (Schaser *et al.* 1999, Schaser *et al.* 2003), who analysed the microcirculation versus capillary size using *in vivo* fluorescence microscopy at various time points (1.5, 24, 72 and 120 hours after injury). They found that perfusion of the skeletal muscle microvasculature was significantly reduced whereas the capillary diameter and microvasculature permeability were increased. This was accompanied by a loss of endothelial integrity, macromolecule leakage through microvasculature causing intramuscular pressure and swelling. They concluded that the initial changes in microvasculature following CSTT ultimately cause tissue death.

Their findings draw attention to the importance of early detection of functionality changes to the vasculature due to trauma (Schaser *et al.* 1999, Schaser *et al.* 2003). Although the changes to individual blood vessels *in vivo* investigated by Schaser and colleagues have delivered important information, they have used fluorescent microscopy, which restricts the study to highly localised and superficial regions.

Through reviewing the literature, the importance of capillaries and skeletal muscle perfusion to supply nutrients and oxygen for cellular metabolism during the wound healing process was found (Landry *et al.* 2000, Wolfard *et al.* 2002, Schaser *et al.* 2003, Zhang *et al.* 2003, Järvinen *et al.* 2005, Claes *et al.* 2006, Duda *et al.* 2008).

On the other hand, using ischemia animal models, vascular morphological changes have been shown to include an increase in the number, diameter and volume of blood vessels during the wound healing process (Oses *et al.* 2009). They have confirmed that during the natural wound healing process, changes to vascular morphology are necessary for adequate perfusion, providing sufficient oxygen and nutritional supply for successful tissue regeneration (Tonnesen *et al.* 2000, Scholz *et al.* 2002, Duvall *et al.* 2004, Lu *et al.* 2010).

While the necessity of revascularisation (Hershey *et al.* 2001) and changes to the vascular morphometric parameters (Duvall *et al.* 2004) is clear for wound healing in ischemia models, an adequate investigation into the morphological changes to the vasculature following CSTT is lacking. Current vascular morphometric information is mostly derived from ischemia models where the injury is invasively created by ligation of the main artery (e.g. arterial femoralis) and disconnecting it completely from the vascular network. These injuries are fundamentally different from a CSTT resulting from a high-energy impact where the skin and the connections between the main arteries and the vascular network remain intact.

An additional drawback is that current CSTT models are limited to localised and superficial assessments, which may not provide comprehensive information regarding the anatomical changes of blood vessels in 3D.

This emphasises the necessity for the development of a 3D vascular assessment model to facilitate a detailed exploration of the morphometric changes following CSTT, during the natural healing process and in response to treatment.

2.5 EXPERIMENTAL ASSESSMENT OF CSTT AND VASCULAR INJURY

2.5.1 Advanced imaging methods in vascular injury models

Contrast-enhanced MR-angiography and CT-angiography have been used for 3D vascular assessment using small animals (Zhuang *et al.* 2006, Ungersma *et al.* 2010). However, the low spatial resolution of these clinical imaging modalities does not make them suitable for a detailed morphological evaluation of the vascular network. X-ray micro computed tomography (micro-CT) has been acknowledged by a variety of authors (Duvall *et al.* 2004, Bolland *et al.* 2008, Nebuloni *et al.* 2013) as the most suitable imaging modality with a high resolution and reliability for the experimental assessment of vascular injuries.

Micro-CT is an advanced imaging modality that has been applied for high resolution visualisation between 1 and 100 μm (Guldberg *et al.* 2004, Zagorchev *et al.* 2010). The high resolution characteristics makes the micro-CT an accurate imaging modality, providing anatomical information in great detail particularly for hard tissue such as bone and its microstructure (Müller 2009). For instance, micro-CT is being used for 3D imaging and quantification of complex structures such as trabecular bone (Bouxsein *et al.* 2010), contrast-enhanced tissues and vasculature in animal models (Schambach *et al.* 2010).

Investigating the rat microvasculature injury following CSTT demands an accurate analysis of the vasculature network architecture during formation and remodelling. As the inner diameter of capillaries in rats' hindlimbs suggested to be less than 10 μm (Kindig *et al.* 1999), therefore, micro-CT with its high resolution can be more suitable for accurate visualisation of small capillaries in comparison with conventional imaging modalities. Furthermore, the accuracy of contrast enhanced micro-CT imaging for visualising and quantifying vascular structural parameters in 3D has been confirmed by other authors (Marxen *et al.* 2004, Jackowski *et al.* 2005, Bolland *et al.* 2008, Zagorchev *et al.* 2010).

In an X-ray image, the contrast and visibility of various tissue structures depends on their physical characteristics such as density and thickness.

This results in an attenuation spectrum of the X-ray image that allows for visualising structures of different contrast (Sprawls 1995, Bushberg *et al.* 2011). Since the density of soft tissue and blood vessels have small differences in contrast and also is much lower than bone, conventional X-ray imaging may not distinguish between the vasculature and tissues satisfactorily compared to the high contrasting bone. To increase the vascular contrast in the image, radio-opaque contrast agents are required to improve the visibility of the vascular network. Knowledge of contrast media and injection techniques becomes important for filling the microvasculature adequately in order to produce a high quality image. For example, a contrast agent with a high viscosity demands a higher pressure for infusion, which may cause the microvasculature to rupture. Depending on the contrast agent type, there are different methods to reduce the viscosity such as increasing the temperature or adding diluents (Voeltz *et al.* 2007). Available contrast agents for *in vivo* vascular imaging are divided into two categories. These are water-soluble media, which are used clinically, and blood-pool media that are currently only utilised for pre-clinical visualisations (Nebuloni *et al.* 2013).

Water-soluble media such as iohexol (Omnipaque, GE Healthcare) and iomeprol (Iomeron, Bracco) are iodine based with low toxicity but exhibit a high extracellular diffusion due to the small size of the iodine element leading to a lower resolution over prolonged imaging (Morcos *et al.* 1998, Hussain *et al.* 2012). To overcome this limitation, blood-pool contrast agents such as AuroVist 15 nm (Nanoprobes, Yaphank, NY) and ExiTron nano 12000 (Miltenyi Biotec, Berlin, Germany) were developed with a larger molecule size to remain within the blood at a higher concentration over a longer period (Hallouard *et al.* 2010, Annapragada *et al.* 2012). In a recent study, AuroVist 15 nm was identified as a suitable blood-pool media for *in vivo* visualisation of the vascular anatomical network because of its high X-ray attenuation and maximum concentration after prolonged imaging (Nebuloni *et al.* 2013). By using micro-CT and small animals for investigating the vascular network, there is a trade-off between *in vivo* and *ex vivo* imaging. *In vivo* imaging permits monitoring of the dynamics of the biological processes in real time. However, *in vivo* micro-CT can be challenging when it comes to the resolution and imaging time.

While high resolution imaging of up to 9 μm has been successfully used (Perilli *et al.* 2010), typically a lower resolution is chosen (e.g. 60-70 μm) to reduce imaging time and radiation exposure to the animal (Nebuloni *et al.* 2014). Hence, for detailed anatomical exploration of the vascular network, *ex vivo* imaging is preferred as it allows for a longer scanning duration and provides a higher resolution (e.g. up to 1 μm).

For *ex vivo* vascular imaging in rats, different contrast agents have been suggested to facilitate visualisation of the microvasculature using micro CT. These include water-soluble (Omnipaque/Iohexol) (Lu *et al.* 2010), insoluble in water (barium-sulphate) (Zagorchev *et al.* 2010) and blood pool (silicon rubber based microfil) contrast agents (Duvall *et al.* 2004). It is essential to evaluate the capability of each contrast agent for a stable and reproducible perfusion. A contrast agent should allow for the homogeneous X-ray attenuation to facilitate a better segmentation of the vascular network from surrounding tissues (Bouxsein *et al.* 2010). Therefore, contrast agents such as barium-sulphate which settles rapidly and affects the contrast homogeneity is not suitable for vascular perfusion (Marxen *et al.* 2004, Zagorchev *et al.* 2010).

The silicone rubber contrast agent (Microfil: MV-122 Microfil, Flow Tech, Carver, MA) has been used by several authors (Duvall *et al.* 2004, Bolland *et al.* 2008) due to its low viscosity (20 to 30 centipoises) and a satisfactory filling of the microvasculature (Duvall *et al.* 2004). This material is from the category of radio-opaque silicone rubbers, which are well known for their easy manipulation with limited variation of their physical properties. This makes microfil a good candidate for microvasculature visualisation. This material is also safe and simply polymerizes at room temperature after 90 minutes (Flow Tech Inc 1999). Consequently, microfil has been used in several studies as radio-opaque contrast agent for improving the visibility of the 3D vascular network in *ex vivo* research (Cheung *et al.* , Savai *et al.* 2009, Jia *et al.* 2010, Yeung 2011) as it fills both the arteries and veins completely (Zagorchev *et al.* 2010). These studies have confirmed that the methodologies using microfil allow for an accurate and reproducible characterisation of the vascular network.

It should be pointed out that other techniques for visualising the 3D architecture of vascular networks have been described in the literature, such as vascular corrosion casting. In this method, after replacing the vascular network with a polyurethane-based casting resin (e.g. PU4ii), the surrounding tissue is removed to reconstruct the vascular morphology (Krucker *et al.* 2006). However, since one of the goals of this project was to investigate the muscle injury, this technique was not deemed to be suitable for this research, as the muscle tissue was required to remain intact for the histological analysis.

In general, vascular imaging and analysis using micro-CT can be challenging requiring many choices such as determining a suitable voxel size, segmentation values (e.g. threshold) and volume of interest (Qin *et al.* 2007). Also, factors including animal preparation, quantification software and the property of the contrast agent (e.g. viscosity) may affect the image quality and the quantitative results obtained from micro-CT (Zagorchev *et al.* 2010).

Micro-CTs and their software packages were originally developed for the morphometric analysis of hard tissue such as trabecular bone structure. Due to the high resolution and accuracy, many authors have favoured micro-CT for the quantification of the vascular anatomical structure using contrast-enhanced techniques (Oses *et al.* 2009, Zagorchev *et al.* 2010, Nyangoga *et al.* 2011, Nebuloni *et al.* 2014). The morphometric parameters of the trabecular bone provided by micro-CT software such as Scanco (Scanco Medical, Switzerland) has been suggested to be interpretable for the vascular network (Bouxsein *et al.* 2010, Scanco Medical SCANCO Medical microCT systems: 3D analysis). For example, trabecular bone volume, number, and thickness have been translated as vascular volume, number and diameter (Duvall *et al.* 2004, Bouxsein *et al.* 2010, Zagorchev *et al.* 2010). However, a parameter such as the structural model index (SMI) has been developed specifically for trabecular bone characteristics of a plate or rod-like geometry of trabecular structures, which may not be directly used for the morphology vascular network (Birkenhäger-Frenkel *et al.* 1988). Furthermore, there are other geometrical properties within the vascular network that current micro-CT tools are not able to measure such as the length of blood vessels.

Due to this limitation, many authors have preferred using other software packages specifically developed for vascular geometrical exploration including; AngioTool (Zudaire *et al.* 2011), Rapid Analysis of Vessel Elements (RAVE) (Marc *et al.* 2011), AngioQuant (Niemistö *et al.* 2005), ImageJ (Fischer *et al.* 2010), AMIRA (Sider *et al.* 2010), and Winfiber3D (Edgara *et al.* 2012). However, many of these tools such as Angiotools, RAVE and AngioQuant have been developed for the characterisation of microvascular networks in tissue culture plates in 2D and are therefore not suitable for the evaluation of a 3D vascular network. In addition, each of these software packages only quantifies a limited number of morphometric parameters, and so far, none of them provides a complete set of anatomical parameters for characterising the vasculature completely. Therefore, combining the vascular parameters derived from a robust modality such as micro-CT with parameters provided by other 3D tools (i.e. AMIRA) may establish the most comprehensive assessment of the geometry for the vascular network.

2.5.2 Histological evaluation

Histology is the evaluation of tissue morphology at a microscopic level. Histological techniques have been used for the evaluation of muscle crush injury (Stratos *et al.* 2010), muscle contusion in a rat model (Khattak *et al.* 2010), the assessment of vascular density (Thompson *et al.* 2002) and also as an independent modality for the evaluation and validation of vascular morphometric parameters (e.g. vessel number) derived from other modalities such as micro-CT (Raines *et al.* 2011). Among several available histological procedures, the paraffin embedding method has been commonly used. The processing steps for this method include formalin fixation, dehydration, clearing, embedding, sectioning with a microtome, rehydration, staining, mounting on microscope slides, and finally visualising the specimen using a microscope. A variety of staining methods have been developed for the visualisation of various tissue components within histological sections. The most commonly used method of staining is haematoxylin (H) and eosin (E) staining (H&E staining technique).

Haematoxylin stains cell nuclei blue while eosin stains cytoplasmic components with a pink colour. Although histological visualisations provide high resolution insights into the microvasculature, they are limited to small 2D fields of view and are therefore not able to characterise the full three-dimensional structure of the vascular network.

Histological evaluation (e.g. histomorphometry) has been applied and acknowledged in the literature as a precise independent modality for validating micro-CT based characterisations of the vasculature including quantified vascular morphometric parameters (Boerckel *et al.* 2011, Tomlinson *et al.* 2013, Ehling *et al.* 2014). For example, in 2D validations of the vasculature, it has been shown that the vessel number obtained from microfil enhanced micro-CT images, is an accurate representation of the corresponding 2D histological sections (Bolland *et al.* 2008, Oses *et al.* 2009). Although micro-CT imaging can evaluate vascular morphometric parameters in 3D, the validation using 2D histomorphometrical analysis is limited to a few vascular morphometric parameters such as vessel number and diameter (Ehling *et al.* 2014, Nebuloni *et al.* 2014). Therefore, parameters such as vessel connectivity that can only be evaluated in 3D may not be validated using 2D histomorphometrical analysis.

ImageJ software is an image-processing tool, which has been successfully used by other authors for quantifying morphological parameters of the vascular network (Zhuang *et al.* 2006, Tomlinson *et al.* 2013). Using correlated 2D sections obtained from microfil-enhanced micro-CT and histology and with the aid of ImageJ, authors have provided a way for an acceptable unbiased correlation between these two independent modalities particularly for the vessel number parameter (Bolland *et al.* 2008, Raines *et al.* 2011).

2.6 CURRENT CLINICAL TREATMENT OF CSTT

Closed soft tissue injuries are clinically important, yet knowledge of an appropriate treatment is restricted and most current clinical treatments of CSTT are based on qualitative assessments. For example, immobilisation (Woodard 1954, Järvinen 1977, Khattak *et al.* 2010) and RICE principles (rest, ice,

compression and elevation) (Järvinen *et al.* 1993, Bleakley *et al.* 2004, Järvinen *et al.* 2005, Matharu *et al.* 2010, Takagi *et al.* 2011) are common approaches that are currently being used clinically as an immediate treatment for CSTT and haematoma.

Surgical interventions, such as fasciotomy, may be necessary for treatment of extensive CSTTs for relieving the muscle tissue pressure in compartment syndrome (Altizer 2004). The use of analgesic and anti-inflammatory medications represents another option, which requires more investigation regarding their side effects after long-term usage (Gierer *et al.* 2005, Schaser *et al.* 2005, Ochman *et al.* 2011).

Icing (cryotherapy) is commonly used for the treatment of CSTT, such as those resulting from sport injuries because it is assumed that this technique reduces inflammation through vasoconstriction (Smith *et al.* 1994, Deal *et al.* 2002, Bleakley *et al.* 2004, Bleakley *et al.* 2006). However, the effect of this technique on the healing of injured vasculature and muscle injuries following trauma has not been well investigated. Recent evidence suggests that muscle regeneration is delayed after cryotherapy (Takagi *et al.* 2011, Tseng *et al.* 2013).

2.6.1 Icing (cryotherapy)

Icing (cryotherapy) is defined as the use of cold modalities including ice packs, ice massages, cold baths, cold spray and cold compression for therapeutic purposes after trauma (Michlovitz *et al.* 2011). The immediate application of ice to the injured region has been adopted as a common practice for the general treatment of CSTT. While cryotherapy is being widely used in clinical applications, this method is mostly based on qualitative studies and the mechanism by which it is presumed to contribute to tissue healing is poorly understood. It is thought that cryotherapy induces vasoconstriction around the site of injury and through this mechanism restricts inflammation and microvascular permeability. Therefore, this leads to the reduction of inflammatory cell influx such as neutrophils and macrophages, which ultimately limits progressive swelling and pain (Smith *et al.* 1993, Smith *et al.* 1994, Deal *et*

al. 2002, Merrick 2002, Hubbard *et al.* 2004). Also it is assumed that this approach accelerates muscle regeneration (Merrick 2002) and tissue restoration resulting in faster functional recovery, shorter hospitalization and rehabilitation (Cohn *et al.* 1989). This implies that a reduction in local temperature, as it occurs in cryotherapy, decreases the oxygen demand and metabolic rate of hypoxic tissues (Merrick 2002) suggesting a reduction in repair responses to injury. Furthermore, it has been previously suggested that icing may reduce the amount of muscle degeneration following injury leading to a faster muscle repair (Merrick 2002). Overall, the benefits of local cooling for reducing the swelling and inflammation have mostly been attributed to vasoconstriction and suppression of immune reactions in the injured tissues. However, it is not well understood as to whether this treatment impacts the proliferative capacity of cells responsible for tissue revascularisation during the wound healing period (Bleakley *et al.* 2004, Collins 2008).

2.6.2 Adverse effects of cryotherapy and controversies

Contrary to studies which have claimed cryotherapy as an effective remedy for musculoskeletal injuries, clinical (Tseng *et al.* 2013) and experimental (Takagi *et al.* 2011) studies exist, suggesting that cryotherapy may slow down muscle recovery and tissue regeneration by inhibiting the local inflammatory response.

Tseng *et al.* explored the effect of clinical cryotherapy (using ice packs for 15 minutes at 0, 3, 24, 48, and 72 hours after exercise) for the recovery of muscle injuries due to the effect of elbow extensions as well as hemodynamic changes in eleven male subjects (aged 20-60 years). They have demonstrated that cryotherapy surprisingly elevated the creatine kinase-MB isoform (CK-MB) and myoglobin levels compared to the control group suggesting muscle damage. The subjective feeling of fatigue also increased 48–72 hours post injury, suggesting a delayed recovery (Tseng *et al.* 2013). Clinical problems resulting from exposure to very low temperatures may raise the complexity of the injury such as higher systemic blood pressure, an anaesthetic effect as well as ischemic necrosis leading to extensive skin loss or amputation (McMaster 1977).

Yet, the information obtained from the limited number of available clinical trials is not convincing enough to confirm that cryotherapy is necessarily beneficial for the improvement of acute tissue injuries or detrimental. Further clinical studies would be required to show evidence-based cryotherapy treatment was effective.

Takagi *et al.* experimentally investigated the effect of cryotherapy on muscle regeneration following a crush injury (Takagi *et al.* 2011). Crush injuries were induced by compressing the extensor digitorum longus (EDL) in rats' hindlimbs using forceps for 30 seconds. An ice pack (0.3-1.3°C at the surface) was applied for 20 minutes and then the results were evaluated at 6, 12 hours and 1, 2, 3, 4, 5, 6, 7 (n=3), 14 and 28 (n=6) days following the injury using histological analysis. The authors concluded that early cooling of the tissue delayed the macrophage influx into the skeletal muscles, causing the impairment of both muscle degeneration and regeneration. This means that the inflammatory response plays an important role during the early healing stages following injury. Evaluating the effect of cooling on the muscle injury at 11 time points has made this research one of the most detailed studies available in the field of cryotherapy. The necessity of macrophage activation after injury has been reported as key factors affecting the regulation of muscle regeneration (Honda *et al.* 1990, Takagi *et al.* 2011).

Takagi and Honda's findings disagree with earlier research which assumed that cryotherapy helps repair muscle faster through the reduction of inflammation and thus suppressing muscle degeneration following cryotherapy (Merrick 2002).

In other research, evidence was found that reducing the tissue temperature leads to blood flow reduction (Alexander *et al.* 1973, Smith *et al.* 1993, Dolan *et al.* 1997). However, the blood circulation may return after cessation of the therapy causing a local fluctuation in blood perfusion. It is still not well understood whether the disturbance in blood flow following the cryotherapy may aggravate muscle damage and influence the healing rate.

2.6.3 Cryotherapy application following CSTT

The goal of cryotherapy is to reduce the surface and core temperature of the injured region in order to decrease the inflammation, swelling and pain (Smith *et al.* 1993, Smith *et al.* 1994, Deal *et al.* 2002, Merrick 2002, Hubbard *et al.* 2004).

There are many external cryotherapy techniques described in the literature that use ice or iced-water and are typically referred to as “ice-therapy” which usually involves a low temperature near zero degrees Celsius (e.g. ice block, ice pack) (Bleakley *et al.* 2004, Algafly *et al.* 2007, Herrera *et al.* 2011). Also those at higher temperatures between 8°C - 22°C are referred to as “cold therapy” (e.g. the immersion in cold water or cold saline) (Schaser *et al.* 2006, White *et al.* 2013). It is shown that ice therapy is more effective regarding cooling the tissue faster (Mcmaster *et al.* 1978, Zemke *et al.* 1998, Kanlayanaphotporn *et al.* 2005) and to a lower temperature (Mcmaster *et al.* 1978, Swenson *et al.* 2007), when compared to cold therapy.

Following cryotherapy, the level of cooling is directly related to the cooling techniques, the temperature of the cooling component, the thickness of the fat under the skin and also the duration of the treatment (Bleakley *et al.* 2004).

Mars and colleagues have shown that during cryotherapy, tissue cooling is not uniform and different temperatures can be measured from the skin and muscles (Mars *et al.* 2006). They have studied the effect of cryotherapy on the skin surface (SK), subcutaneous fat (SC) and muscle (Ms) (rectus femoris to a depth of 1cm) in humans using an icepack, hypodermic needle-tip thermistors and a temperature probe (Mars *et al.* 2006). An icepack was placed on the skin for 15 minutes while the temperature was measured before, during, and for up to 45 minutes after cryotherapy. They found that after 5 minutes of cooling, the temperature of the skin, subcutaneous fat and muscle reduced from 37°C to 28.8 ± 1.4°C, 33.1 ± 1.1°C and 34.9 ± 1.2°C respectively. By continuing the icing therapy for 20 minutes, the temperature reached a minimum temperature of 8.1 ± 2.7°C (SK), 21.7 ± 2.2°C (SC) and 26.2 ± 3.5°C (Ms).

Although the temperature then increased 45 minutes after cryotherapy ceased, the temperature in different tissue layers still remained lower than the initial temperature prior to cryotherapy by approximately 5°C. Finally, the authors have suggested that the degree of inhomogeneity of the temperature at different tissue layers may be associated with a sympathetic response adjusting the local blood flow following cryotherapy (Mars *et al.* 2006, White *et al.* 2013). For an optimum cryotherapy including an efficient reduction in pain, cell metabolism and swelling, it has been suggested that the tissue temperature should be decreased within a range of 10-15°C (Rivenburgh 1992, Mac Auley 2001). However, prolonged cryotherapy is not recommended due to tissue damage and the impairment of the microcirculation caused by very low temperatures (Schaser *et al.* 2007, Collins 2008, Baoge *et al.* 2012). Also, it was indicated that a dramatic reduction of the tissue temperature to below 6° to 8°C causes serious damage to the microcirculation of the capillaries (Schaser *et al.* 2007).

In humans, a continuous and prolonged cryotherapy, even as short as 20-30 minutes, is not recommended to be a safe technique due to the risk of skin burns known as frostbite (Bleakley *et al.* 2004, Lee *et al.* 2007). For this reason, intermittent cryotherapy over short durations (e.g. 10 minutes) has been acknowledged for clinical applications (Bleakley *et al.* 2006, Knobloch *et al.* 2007).

Intermittent cryotherapy for 3×10 minutes has been shown to reduce the microcirculation of capillaries locally in Achilles tendon disorders by 71% measured by a laser Doppler spectrophotometry system while the oxygenation of the tendon has been facilitated by 2 minutes of rewarming within the cryotherapy sessions (Knobloch *et al.* 2007). Also, this technique has been suggested to diminish the pain and swelling caused by moderate ankle sprains in humans (Bleakley *et al.* 2006). However, the differences in skin structure between humans and rats should be taken into consideration. Human skin is attached to the tissue (Dorsett-Martin 2004) and a cooling temperature can quickly penetrate to the tissue beneath the skin (Knobloch *et al.* 2007).

However, rats are loose-skinned animals and their skin contains several thick cellular layers with a nonvascular structure on the surface and is not attached to the underlying tissue (Sanders *et al.* 1995, Dorsett-Martin 2004, Dorsett-Martin *et al.* 2008). This suggests that to transfer the cooling temperature of ice to the underlying tissue where the injury is located, more time may be required. Also, the severity of the CSTT models may not be comparable with mild or moderate injuries such as an Achilles tendon disorder (Knobloch *et al.* 2007) or ankle sprains (Bleakley *et al.* 2006).

In rats, one session of cryotherapy for a duration of 20 minutes appears to cool the muscle effectively (16°C) (Takagi *et al.* 2011) with no reported skin complications (Smith *et al.* 1994, Deal *et al.* 2002). In this regard, Takagi and colleagues examined the effect of cryotherapy on muscle regeneration following a crush injury induced by forceps for 30 seconds on the extensor digitorum longus (EDL) of rat's hindlimbs (Takagi *et al.* 2011). The authors applied an ice pack (0.3-1.3°C at the surface) onto the injured region for 20 minutes. The temperature of the muscle surface and the rectum (as a core temperature) were monitored using a thermometer during and after icing. The results were evaluated at 6, 12 hours and 1, 2, 3, 4, 5, 6, 7 (n=3), 14 and 28 (n=6) days following injury using histological analysis. The authors observed a linear reduction of temperature from 30°C (5 minutes before test) to 13.3±1.2 °C (20 minutes after icing) and indicated that the temperature raised to around 25°C, 20 minutes after cryotherapy ceased which was still 5°C lower than the initial temperature prior to cryotherapy (30°C). Investigating the effect of icing on the muscle injury at 11 time points has made their research one of the most detailed studies available in the field of cryotherapy.

2.7 STATISTICAL APPROACHES FOR VASCULAR MORPHOMETRIC ANALYSIS

The linear relationship between two vascular morphometric parameters within one modality (e.g. histology) is usually tested through a correlation coefficient (R) ranging between +1 (positive correlation) and -1 (negative

correlation) where 0 means no correlation. In addition, within one modality, the coefficient of determination (R^2) shows how well data fitted into the model. The quantitative validation between two modalities is commonly assessed using standard statistical criteria including an intra-class correlation coefficient (ICC) with a 95% confidence interval (CI) (Lee *et al.* 1989) and also with an agreement analysis (Bland-Altman plot) for measuring one particular morphometric parameter. The ICC is a reliability assessment indicating the degree of association between two or more quantitative measurements (Müller *et al.* 1994) and ranges between 0 and 1. Lee and colleagues have defined the principles of correlation and agreement between two independent methods measuring one parameter by demonstrating these criteria; no systemic bias, no statistically significant difference between the mean values obtained from the two techniques and also the ICC being greater than 0.75 for a 95% CI (Lee *et al.* 1989).

The Lee principles were completed by Bland-Altman suggesting the agreement assessment between two techniques based on the estimation of the mean and standard deviation (SD) of differences between measurements. In the Bland-Altman diagram where the scattered data of differences between two measurements are plotted versus the mean of differences, the agreement level between two independent methods lies between these two limits of agreement and given as mean \pm 1.96 SD.

The confidence interval (CI) is a range of defined values in which a specified probability is that the value of a parameter lies within it. A 95% confidence interval interprets that a range of values with a 95% certainty includes the true mean of the population (Webber 2013). It has been shown that for a CI of 95%, the ICC should be greater than 0.75 (Lee *et al.* 1989) which indicates good reliability.

2.8 GAPS IN KNOWLEDGE

Through this literature review, the following gaps in knowledge of vascular injury following CSTT were identified:

- ✚ Available experimental investigations regarding vascular injuries following CSTT have been mostly focused on the functionality changes of blood vessels (e.g. blood flow) and not morphology.
- ✚ Evaluation of current CSTT models is restricted to a highly localised and superficial regions and this may not provide comprehensive information regarding the morphology of the entire vascular network in 3D.
- ✚ Currently, there is no adequate experimental model that allows the study of morphological changes to the vasculature following trauma in 3D. Developing a 3D characterisation model using a reliable imaging modality with higher resolution and accuracy (Guldberg *et al.* 2004) is needed to quantify changes to the vascular morphometric parameters such as vessel volume, number and diameter following CSTT.
- ✚ Changes to the vascular morphology and the revascularisation mechanisms, including degradation of the injured capillaries, propagation of surviving endothelial cells and development of the new vasculature network remain only partially understood (Zhuang *et al.* 2006). This is due to the complexity of the processes requiring fundamental experimental research.
- ✚ More investigation is required regarding the influence of microvasculature damage due to CSTT on the mechanisms such as vasodilation, angiogenesis and arteriogenesis during the healing process.
- ✚ Systematic research into cryotherapy and its influence on muscle regeneration and revascularisation is currently lacking due to a limited knowledge of the processes involved of the structural changes caused by injuries to the vascular network.

2.9 FINDINGS AND SUMMARY

The findings from the reviewing of the literature are discussed from two perspectives; experimental and clinical. In general, clinical evaluations are limited regarding a precise characterisation and quantification of vascular injury after the CSTT. Clinical investigations of musculoskeletal trauma are restricted by several factors; lack of knowledge regarding vascular injury following CSTT, and limited non-invasive analytical tools for monitoring and assessing these complications.

Available clinical CSTT classifications are qualitative, based only on macroscopic observation leading to a challenging and subjective diagnosis. For example, CSTT monitoring with only systemic markers makes a definite diagnosis of vascular impairment non-specific and potentially inaccurate. Despite the existence of advanced imaging techniques such as MR and CT angiography, their resolutions are not high enough to be suitable for the detailed analysis of microvasculature changes following CSTT.

From an experimental view, evidence was found regarding changes to the vascular functionality (Schaser *et al.* 1999, Schaser *et al.* 2003, Claes *et al.* 2006) and morphology (Duvall *et al.* 2004) following injuries indicating the necessity of vascularisation for the healing of injured tissue and muscle fibre regeneration (Järvinen 1976, Bauer *et al.* 2005, Järvinen *et al.* 2005, Nauta *et al.* 2011).

It was shown that only a few experimental methods are available that allow for a sufficiently detailed characterisation of CSTT *in vivo* and *ex vivo*. The importance of capillaries and skeletal muscle perfusion to supply nutrients and oxygen for the cellular metabolism during tissue repair has been emphasised in the literature (Landry *et al.* 2000, Wolfard *et al.* 2002, Schaser *et al.* 2003, Zhang *et al.* 2003, Järvinen *et al.* 2005, Claes *et al.* 2006, Duda *et al.* 2008). In ischemia models, the vital role of changes to the vascular morphology such as vessel volume, number and diameter following injury and during the natural wound healing process has been highlighted through angiogenesis and arteriogenesis (Tonnesen *et al.* 2000, Scholz *et al.* 2002, Duvall *et al.* 2004, Lu *et al.* 2010).

This indicates that during the natural healing period, these changes to vascular morphology are necessary for adequate perfusion, providing sufficient oxygen and nutritional supply for successful tissue regeneration.

Regarding CSTT treatments, while cryotherapy is widely used, disagreements were identified with respect to the effectiveness of this therapeutic method on the damaged tissue following injuries. Several authors have recommended cryotherapy as a beneficial method for reducing inflammation and vascular permeability following CSTT thereby reducing the swelling (Smith *et al.* 1993, Smith *et al.* 1994, Deal *et al.* 2002, Merrick 2002, Hubbard *et al.* 2004). However, this was not supported by other studies which have shown clinically (Bleakley *et al.* 2004, Collins 2008, Tseng *et al.* 2013) and experimentally (Takagi *et al.* 2011) that there was not enough evidence to confirm that cryotherapy can be an effective remedy for soft tissue injuries. Evidence has shown that decreasing the early inflammatory reaction delays the muscle regeneration and consequently reduces the speed and efficiency of the repair outcome during the healing period (Takagi *et al.* 2011).

The limitation of current CSTT evaluations emphasises the necessity for the development of a quantitative 3D method to show a detailed exploration of the morphometric changes of the vasculature such as vessel volume, number and diameter following CSTT.

The shortcomings of localised and superficial methods can be overcome by using appropriate techniques that are available for vascular assessment and better suited for deeper injury investigation (e.g. micro-CT imaging system).

2.10 RESEARCH SIGNIFICANCE

This research is expected to bring a significant contribution to the field of orthopaedics and traumatology by improving our understanding of the impact of CSTT's on changes to the microvascular network, and furthermore, on the influence of these changes on tissue healing.

Since most previous experimental studies regarding CSTT have been using localised and superficial (*i.e.* two-dimensional) methods to characterise vascular injury following CSTT, it is anticipated that the standardised, quantitative characterisation of the vascular injury in 3D may increase the accuracy and reproducibility of experimental CSTT models that are currently being used.

Previously, in the absence of objective and quantitative methods for the characterisation of closed soft tissue injuries, the efficacy of many clinical treatment modalities, such as cryotherapy or hyperbaric oxygen therapy, has remained controversial. As a result of the improved accuracy in detecting changes to microvascular architecture caused by CSTT and during the healing, it will be possible to better evaluate the efficacy of treatment modalities on the healing of closed soft tissue injuries, which will enable the objective comparison of therapeutic measures and also drive the development of new treatment modalities.

Ultimately, if the methods developed in this research lead to new insights on the relationships between changes to microvascular architecture, CSTT severity and healing, it will be possible to develop objective, quantitative clinical CSTT classifications that are superior to the currently used qualitative and subjective classification methods (*e.g.* Tscherne and AO). This is important, as better classification systems allow for more accurate diagnosis and monitoring of CSTT, resulting in better-informed decision-making during the treatment of these injuries. As such, the invasive, experimental methods developed in this project to characterise changes to the microvascular architecture may aid in the validation of future non-invasive clinical assessment modalities for CSTT.

2.11 RESEARCH QUESTIONS

From the review of the literature, the following key questions were raised.

1. Does vascular morphology change following CSTT and during the healing period?
2. What is the effect of cryotherapy on CSTT and the injured vasculature?

2.12 RESEARCH HYPOTHESIS

In this research, it was hypothesised that CSTT and cryotherapy change the vascular morphology during the healing period.

2.13 KEY GOAL AND RESEARCH AIMS

To answer the research questions and address the hypothesis, the main goal of this research was to investigate the effects of both CSTT and cryotherapy on the vascular morphology in 3D as well as the effect of cryotherapy on the CSTT. This was achieved through the development of a characterised CSTT model in rats, using contrast-enhanced micro-CT imaging and also histological analysis.

To achieve the main goal, the specific aims of this research were:

- ✚ To develop and characterise a CSTT model.
- ✚ To characterise vascular morphological changes following CSTT by developing perfusion and micro-CT evaluation protocols
- ✚ To investigate the effect of cryotherapy on the injured vasculature following CSTT

Chapter 3: Development and characterisation of the CSTT model

3.1 INTRODUCTION

In order to study CSTT and to see whether there are any changes in vascular morphology following trauma, the development of a well-defined CSTT animal model was required. CSTT animal models using an impact device have been established previously and reported in the literature (Schaser *et al.* 1999, Claes *et al.* 2006) as an efficient way to create a defined and reproducible injury. In this research, this same method was applied to create a standardised and reproducible CSTT with a defined vascular injury. To confirm that the impact device creates a consistent injury, it was essential to characterise the device at first. The CSTT was also characterised through qualitative observations and quantitative evaluations. This was carried out by monitoring the symptoms and the size of the muscle injury at different time points. The changes to the muscle injury were also verified using histological assessments. The developed and characterised experimental model was then used to study the effect of cryotherapy on the healing process after CSTT as well as the injured vasculature.

3.2 METHODOLOGY

3.2.1 Structural design and the functionality of the impact device

The following figures illustrate the components of the impact device (Figures 3-1).

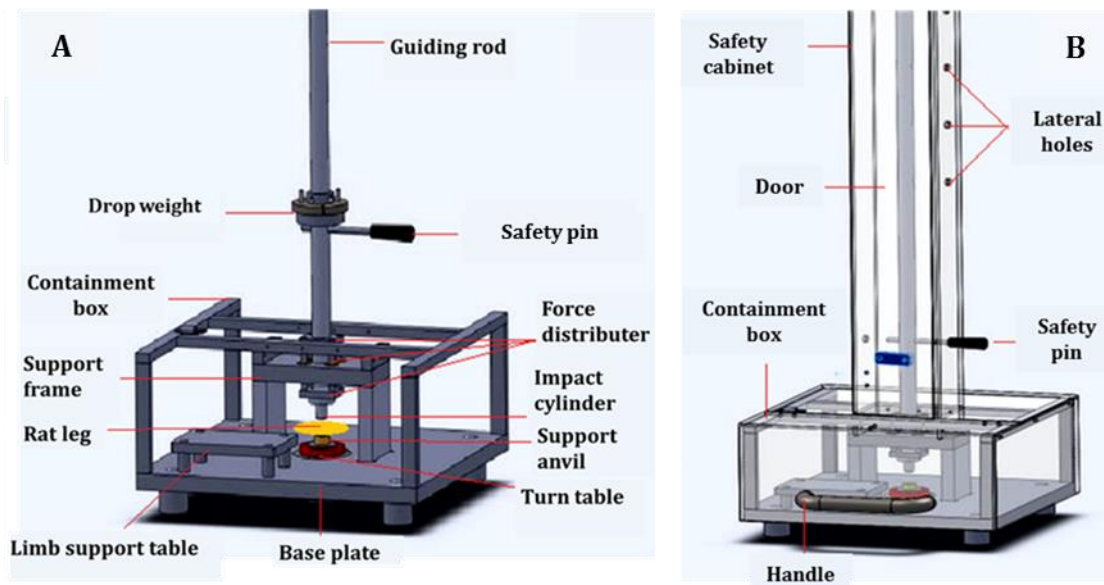


Figure 3-1: A schematic of the impact device's structure.

This schematic shows two views of the impact device's structure including the internal (A) and external (B) components. **A:** The top part of the impact device consists of a guiding rod, along which the drop weight slides down. The lower part of the device is comprised of a base plate, a support frame, an impact cylinder, and force distributors to transfer the force from the drop weight to the impact cylinder and a height-adjustable support anvil. Two safety pins were also used in the upper and lower parts of the device to secure the drop weight in its location. Since the height of the guiding rod was 1.66 m, here only the lower part of the device is shown. The positioning of the specimen (rat leg) between the impact cylinder and the support anvil is schematically exhibited. To reduce the risk of any injury to the researchers using this device, the entire impact device was encased by a frame made from Perspex panels, with lateral holes for locating the safety pins (**B**).

3.2.2 Characterising the impact device

To create a standardised and reproducible CSTT combined with a vascular injury, a previously manufactured impact device with a blunt impactor was used (Figures 3-1 and 3-2). The device was based on similar models reported in the literature where the authors had used a drop weight of 170g which fell freely from 1.8 m to create a CSTT of Grade 2, based on the Tscherne classification, on a rat's hindlimb (Claes *et al.* 2006). These authors presented the velocity of their drop weight as 6m/s at the impact surface producing an impact energy equal to 3.06 kg m²/s².

As indicated in Table 2-1, a Grade 2 injury according to the Tscherne classification is approximately equivalent to a Grade 4 in the AO classification, whereby both classifications describe a severe muscle and skin contusion.

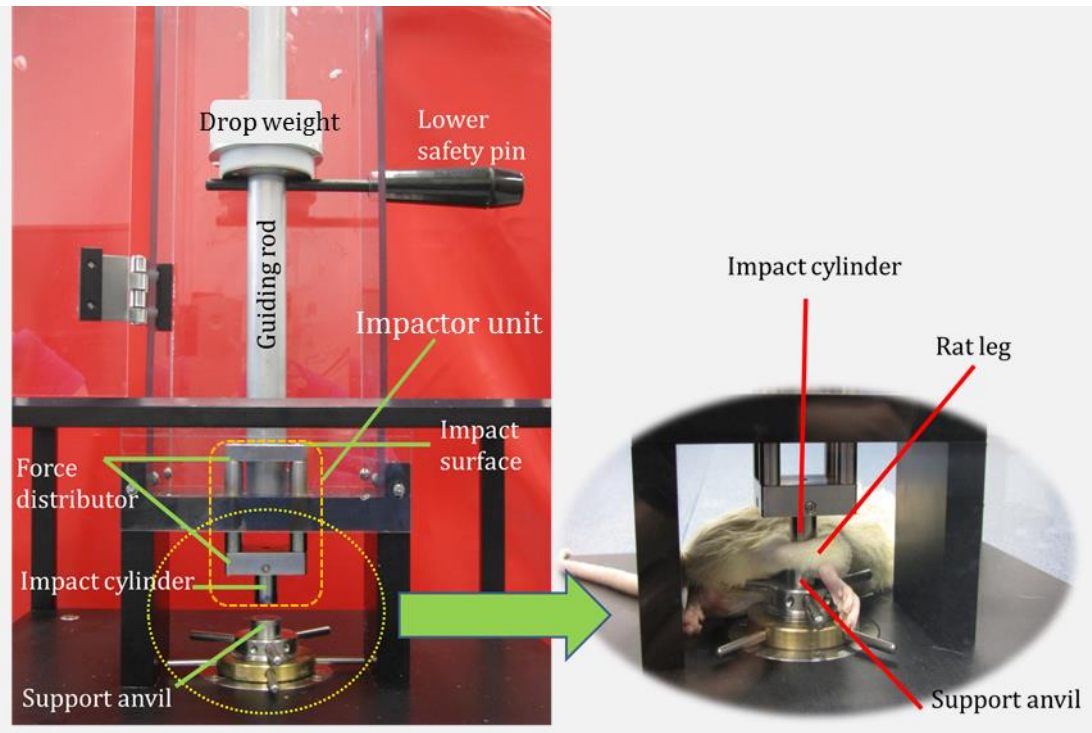


Figure 3-2: The structure and functionality of the impact device.

This image shows the impact device functionality in order to create an impact injury to a rat's hindlimb. The drop weight is positioned at its highest point (1.66m) where it is secured by the upper safety pin (for illustrative purposes only the lower safety pin is displayed here, as the upper safety pin at a height of 1.66m is outside the image area). The hindlimb of the rat is positioned between the impact cylinder and the support anvil. To begin the test, the lower and upper safety pins are removed to allow the drop weight to fall down along the guiding rod onto the impact surface, and onto the top part of the force distributor. The energy of this impact is thereby transferred to the impact cylinder and then onto the soft tissue of the hindlimb thereby creating the injury.

For this research, a suitable impact energy was desired to create a severe injury with no broken bone or skin perforation (equivalent to Grade 4 based on the AO classification). The impact energy is a function of the impact velocity and the mass of the drop weight. Therefore, to ensure that the impact device produced a consistent injury, it was characterised based on these two parameters; the weight and the velocity of the drop weight at the impact surface.

Determination of the impact velocity

Theoretical calculation of the impact velocity

Figure 3-3 shows the drop weight with mass m , at height h holding zero kinetic energy while it is resting in the starting position. By releasing the safety pins, the drop weight falls freely from its resting position in a vertical downward direction. This occurs under the influence of the force of gravity. The drop weight continues downward and after travelling the height h , it hits the impact surface where its kinetic energy is transferred to the impact cylinder and then absorbed by the muscle tissue.

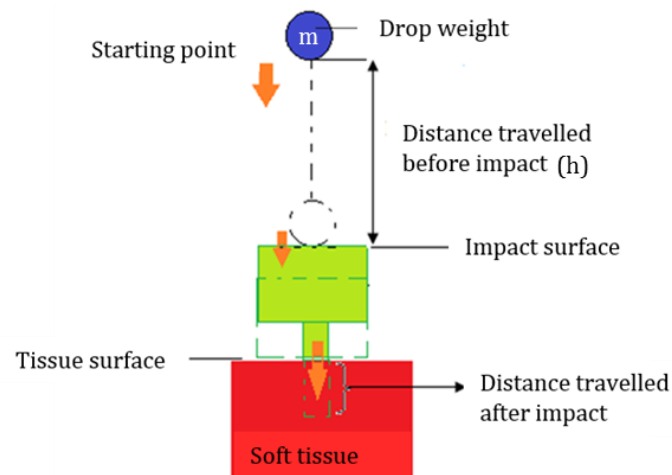


Figure 3-3: *A schematic of the mechanical functionality of the impact device. This schematic shows the penetrated distance of the impact cylinder through the tissue after a drop weight falls from a starting point towards the impact surface.*

According to the conservation of energy, the initial potential energy of the drop weight is equal to its final kinetic energy assuming an ideal system where the wasted thermal energy such as air resistance and the friction between the drop weight and guiding rod is zero. This is shown as:

$$mgh=1/2mv^2_f \quad (3-1)$$

The total height between the starting drop point and the impact surface was measured and then the final analytical velocity of the drop weight at the impact surface was calculated accordingly given as:

$$V_f = \sqrt{2gh} \quad (3-2)$$

The final impulse (I) of the drop weight at the impact surface was defined as:

$$I = mv_f \quad (3-3)$$

The information related to the starting point and the impact surface are summarised in Table 3-1.

Table 3-1: The initial and final conditions of the drop weight. The information related to the initial condition of the drop weight at starting point as well as at the impact surface (end point) is summarised in this table.

Initial condition at starting point	
Parameters	Descriptions and units
$h_i = h$	Initial height at starting point (m)
$PE_i = mgh$	Initial potential energy (J)
m	Mass of drop weight (kg)
$KE_i = 0$	Initial kinetic energy (J)
Conditions at impact surface	
$g = 9.8$	Gravitational acceleration (m/s^2)
$PE_f = 0$	Potential energy at impact surface (J)
$KE_f = 1/2mv_f^2$	Kinetic energy at impact surface (J)
$I = mv_f$	Impulse (kgm/s)

Velocity assessment using a high-speed camera (HSC)

The theoretical final impact velocity of the drop weight (v_f) (equation 3-2) was verified by applying a frame-by-frame analysis of the drop weight velocity measured with a high-speed camera (HSC: X-Stream XS4, Version 2.10.01) at the impact surface (Figures 3-4 and 3-5). The HSC was utilised as another independent method to visualise and analyse the drop weight's motion.

The drop weight velocity was recorded by tracking its motion using a HSC and an image acquisition processing software (IDT Motion Studio, DEL Imaging Systems, LLC. 1781 Highland Avenue, Cheshire, CT 06410). The camera was set up on a tripod and then connected to a laptop (Intel Core (TM) 2 Duo CPU, Windows 7). A 50 mm lens was calibrated at a distance of 1.36 m. The field of view was illuminated by using portable 1000 W LED lights (Figure 3-4).

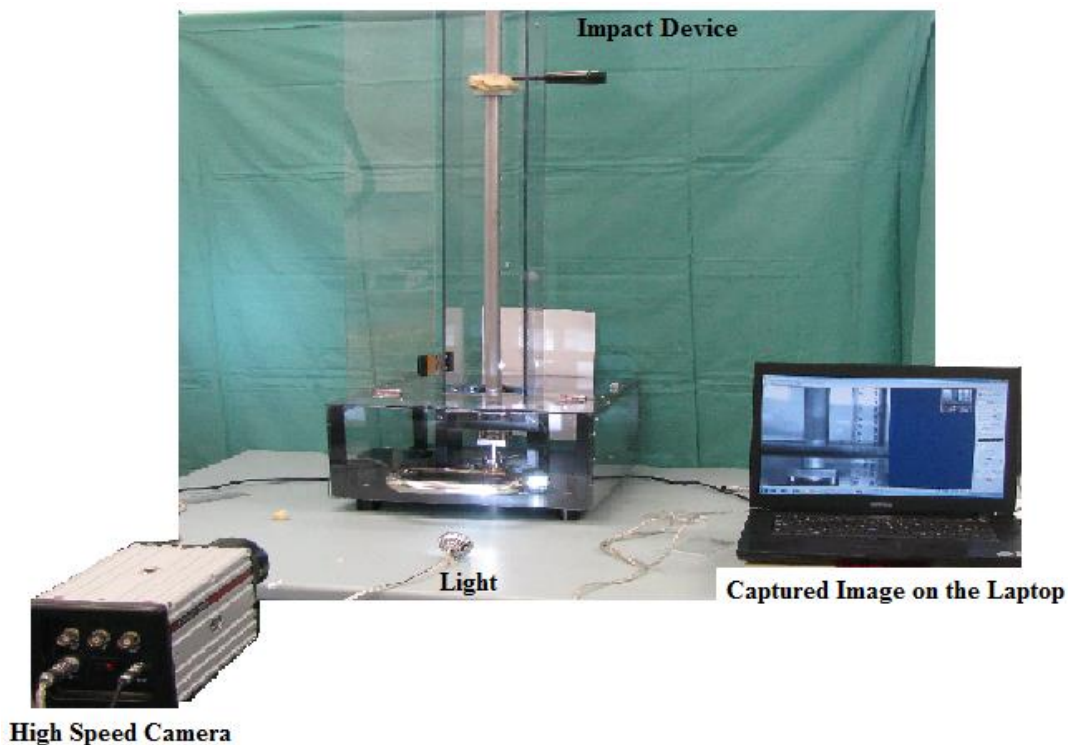


Figure 3-4: A set up for characterising the impact speed with a high-speed camera. The set up for characterising the impact speed using a high-speed camera, a laptop, the impact device and LED lights is shown. High-speed movies were captured from the impact area, where a frame-by-frame analysis of the drop weight position allowed for the calculation of the impact speed using a regression analysis performed in Microsoft Excel software.

An experimental study was conducted by releasing the drop weight to fall freely from the highest point (1.66 m) along the guiding rod. The frame rate for imaging (frequency) was adjusted to 1500 Hz. As the parameter 'time' is the inverse of the frequency, the time between two frames is $667\mu\text{s}$. By using the camera's frame rate, the time trace of the drop weight position was collected.

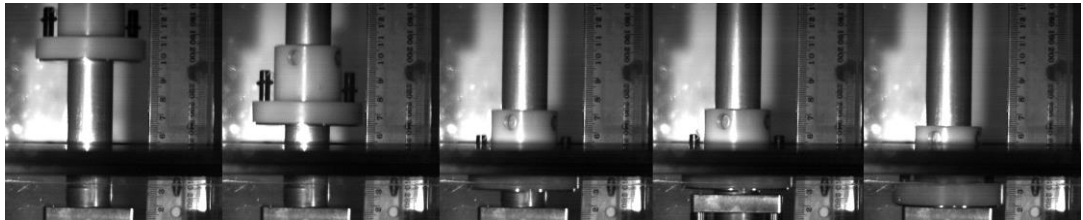
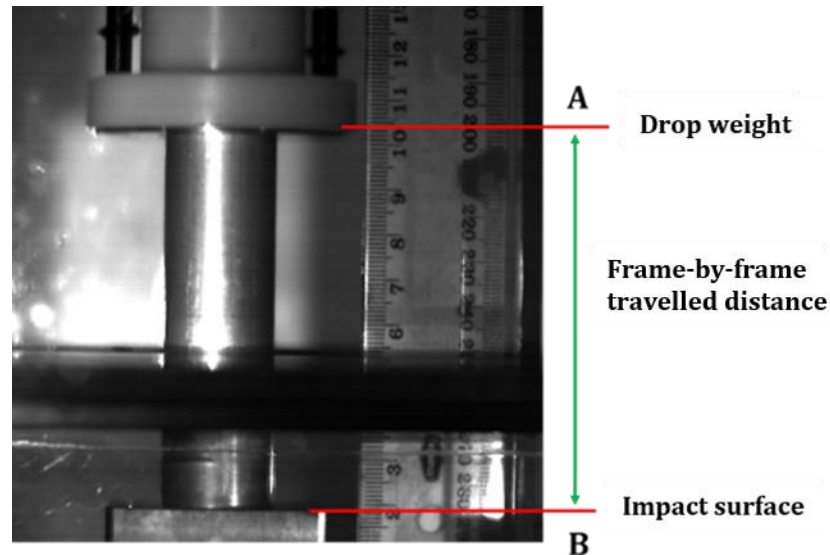


Figure 3-5: A representation of the captured images by the high-speed camera. The images exhibit the last sequences of a dropped weight while it is travelling from location A and approaching the impact surface (location B). The drop weight bounced back approximately 4 mm at its first impact, which is not shown here. The ruler shows the position of the drop weight from the starting point and the ending point at the impact surface. The positions of the drop weight between locations A and B (where visible) were recorded as well as the time between frames for measuring the velocity of the drop weight at different points and finally at the impact surface.

The velocity of the drop weight was measured at the impact surface using the HSC by applying a frame-by-frame analysis and by finding the position of the drop weight on each frame of the high-speed movie (Figure 3-5). By applying a regression analysis, the position of the drop weight as a function of time was determined and plotted.

The final drop weight velocity at the impact surface was derived by computing the derivative of the position-time function with respect to time. The impact experiments were repeated five times.

Determination of the appropriate impact weight

In Claes's research, the travelled distance by the drop weight (170g) was 1.8 m creating a velocity of 6 m/s (equation 3-2) and an impact energy of 3.06 kg m²/s² (equation 3-3) (Claes *et al.* 2006). In the impact device used for this research, the travelled distance by the drop weight was 1.66m; therefore, to achieve an equivalent impact energy as Claes *et al.*, the weight of the drop weight had to be increased. The first tested weight (n=5) was 180g which was obtained from equation 3-3, given the theoretical velocity of 5.7 m/s and the impact energy of 1.02 kg.m/s from the Claes study. However, by using this weight a severe injury was not achieved. Therefore, a variety of weights including 230g (n=7), 300g (n=4) and 400g (n=8) were tested for the drop weight in which the weight was increased sequentially by adding additional scaled plasticine on the drop weight until the desirable CSTT was achieved.

3.2.3 Development of a standardised CSTT model using the impact device

Animal ethics

All animal procedures were performed in accordance with the Australian National Health and Medical Research Council guidelines for laboratory animal use and were approved (approval number: 1100000318) by the 'University Animal Ethics Committee' at Queensland University of Technology (QUT), Brisbane, Australia.

Defining the region of interest

To create a standardised and reproducible injury using the impact device, a region of interest (ROI) was defined on the left hindlimbs of anaesthetised rats between the tibia-notch (TN) of the knee joint and tibia-fibula conjunction (TFC). This region contains the biceps femoris and gracilis muscles in the lateral and medial sides respectively (Figure 3-6).

The area of the ROI was measured for non-injured hindlimbs of all animals using ImageJ software (ImageJ 1.47v: Wayne Rasband, National Institute of Health, USA). This ROI was used for all experiments throughout this research.

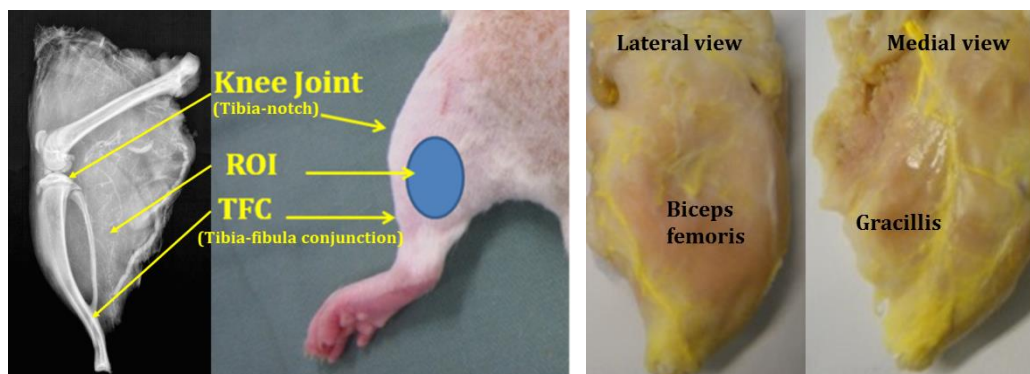


Figure 3-6: Defining a region of interest (ROI).

The ROI was defined between two anatomical markers; the tibia's notch of the knee joint (TN) and the TFC (tibia-fibula conjunction) (left images) and also on the biceps femoris and the gracillis muscles (right images).

Animal preparation

For this study, male Wistar rats (12 weeks) were provided from the Animal Resources Centre, Canning Vale, WA, Australia. The animal housing and welfare were based on the Australian code for the care and use of animals for scientific purposes (National Health and Medical Research Council 2013). Animals were accommodated in enclosed, safe and clean cages where they could freely have access to water and nutritious pellets as well as social and physical activity. Rats were anaesthetised prior to impact by inhaling isoflurane (2.5%) at a rate of 5 L/minutes mixed with oxygen at 4 L/minutes for induction and this was maintained with 2 L/minutes mixed with oxygen at 2 L/minutes. Prior to the initiation of the CSTT, the anaesthetised animals were injected with analgesic subcutaneously (Buprenorphine: 0.2 mg/ml, 0.05 mg/kg) and then transferred to the impact device. The left hindlimb was secured between the impact cylinder and support anvil. Care was taken to exclude the bone from the impact zone to prevent any bone fracture. Once the positioning of the animal was completed, the drop weight was released and it dropped along the guiding rod to create the desired CSTT.

After impact, animals were kept warm during recovery while their vital signs were monitored. The post-operative pain was managed by injecting one dose of Buprenorphine 12 hours after impact. The rats were euthanized 24 hours after impact according to the standard operating protocol (SOP) #261 of the Medical Engineering Research Facility (MERF) at QUT. Briefly, the rats were placed in a plastic container under a laboratory hood. The container was connected to CO₂ and had a sealed lid to prevent the gas leaking outside. A filling rate of 20% of the chamber volume per minute with 100% carbon dioxide was added to the existing air in the chamber to achieve a balanced gas mixture to fulfil the objective of rapid unconsciousness with minimal distress to the animals. After euthanasia, to ensure that the bone has not broken due to the impact, animals were placed inside a portable X-ray cabinet (Faxitron MX-20, Faxitron Bioptics LLC, USA) and imaged with an energy of 31 kVp for 83 seconds (Fouletier-Dilling *et al.* 2005).

3.2.4 CSTT and muscle injury characterisation using ImageJ software

To confirm the reproducibility of the model for creating a CSTT with a consistent injury grade, the severity of the created CSTT was determined qualitatively and quantitatively.

For qualitative assessments, one day after impact, animals were euthanised and then both lateral and medial views of the rat's hindlimb were visually observed. The CSTT was qualitatively evaluated based on macroscopic symptoms of the skin surface (tissue of epidermis side) and under the skin after dissection (subcutaneous tissue) and muscles (surfaces of the biceps femoris and gracillis). In addition, observations were made of the CSTT location and its symptoms such as bleeding (haematoma) and inflammation (redness, stiffness, and swelling). Finally, the CSTT observations were compared with the AO classification (Table 2-1) and then graded based on the muscle defect, contusion and segmental vascular injury.

For quantitative analysis, the inflamed areas of CSTT (haematoma) where the impact was induced were measured using ImageJ software.

The quantification of the CSTT (muscle injury) was carried out by measuring the total area of the inflamed region using the 'freehand selection' tool within ImageJ for each case (Figure 3-7).

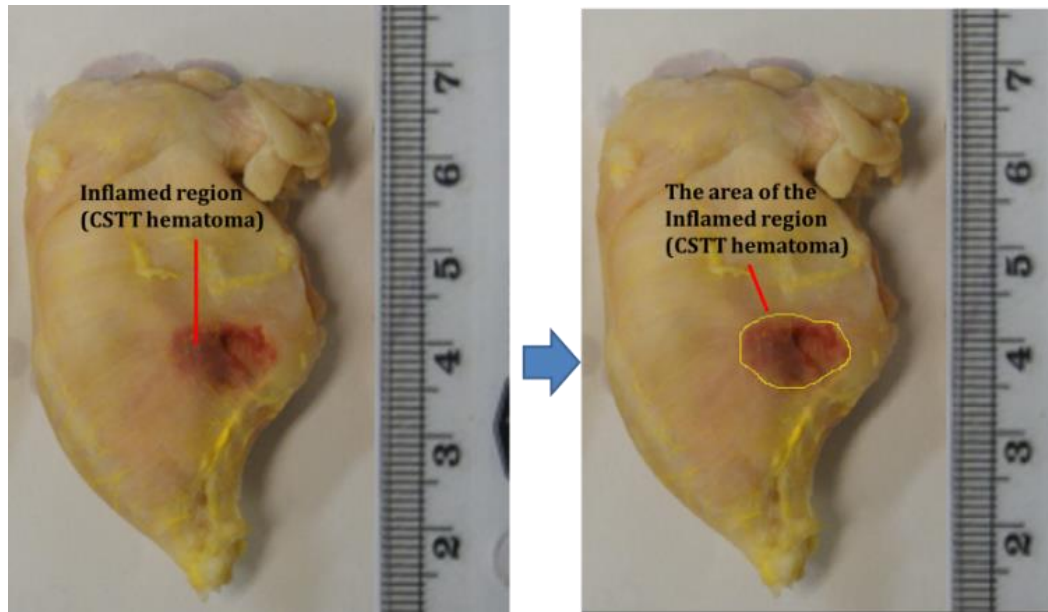


Figure 3-7: A configuration of the CSTT showing the inflamed area. This area of haematoma was used for the quantification of the size of the haematoma and the severity of the muscle injury.

3.2.5 Histology analysis

Biopsy samples

Corresponding biopsy samples were taken from both injured and non-injured contralateral hindlimbs using a biopsy punch for two reasons (Figure 3-8). One reason was for a detailed quantification of vascular morphology utilising contrast-enhanced micro-CT imaging, as described in Chapter 4.

The other reason was for evaluating the muscle injury and inflammation using histological techniques. Figure 3-8 shows a schematic diagram illustrating the geometrical technique that was designed to enable the collection of defined and reproducible biopsy samples from the same regions of rat's hindlimbs.

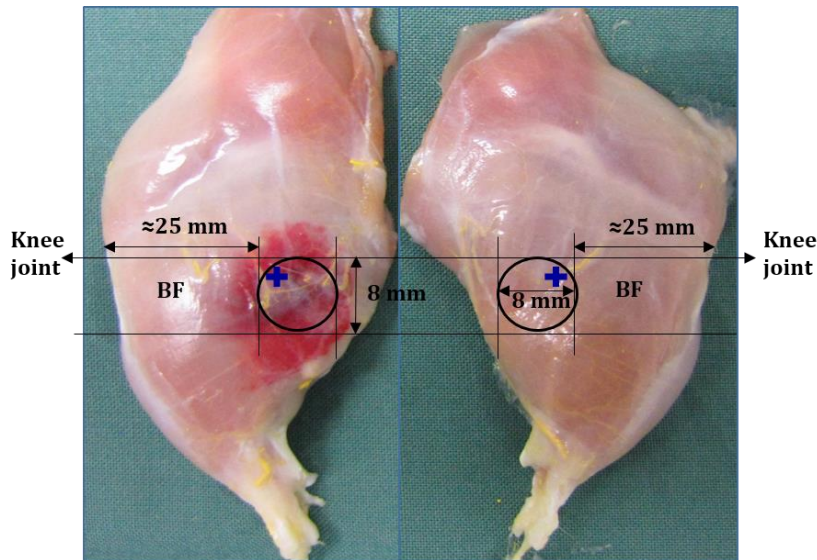


Figure 3-8: The geometrical technique for taking corresponding biopsy specimens. A schematic representing the geometrical design for taking two corresponding biopsy specimens from the CSTT location within the ROIs of injured and non-injured hindlimbs is shown. This method has been designed and applied to evaluate correlated areas in a consistent and standard manner for all samples throughout this research. After placing the paired hindlimbs side by side showing their lateral view where the injury was observed on the biceps femoris (BF). The knee joints (tibia notch) of both hindlimbs were used as anatomical markers and a straight line was drawn to connect them together. A circle was marked using the same diameter as a biopsy punch (8mm) on the tissue surface where the central region of the contusion was located. Straight parallel lines were then utilised to outline the circle to obtain the distance measurements required to reproduce the same region on the contra-lateral non-injured hindlimb. The blue cross within each circle, which is facing the corresponding knee joint, was utilised as an indicator for the biopsy sample's alignment.

Histological section preparation

The general section preparation for the histological analysis is based on the techniques previously reported in the literature (Tsivitse *et al.* 2003, Shireman *et al.* 2006). Briefly, the biopsy specimens were fixed in 10% neutral buffered formalin (NBF) for 24 hours to prevent tissue degradation.

The samples were treated using several different solutions using an automated tissue processor machine (Thermo Excelsior Tissue Processor and paraffin embedding station, Thermo Fisher Scientific, USA). The samples were dehydrated by increasing the ethanol concentration from 70% (30 minutes) to 90%, 95% and 100% for one hour respectively.

This was followed by incubation in a hydrophobic clearing agent (xylene for 2 hours) to remove the alcohol. Finally, the sample was embedded for 2 hours and 45 minutes into melted paraffin wax (the infiltration agent). After tissue embedding, the samples were placed on a freeze plate to allow the wax to harden into a block. Serial sections with a thickness of 5-um were then transversely sliced using a microtome (Leica Biosystems RM2235, Sydney, Australia) and mounted on Poly-L-lysine adhesion glass sections (Thermo Fisher Scientific, Brisbane, Australia). As tissue staining requires water and wax is hydrophobic, therefore, the wax needs to be removed from the tissue before staining. To achieve this, after the sectioning procedure, the wax was removed from the tissue samples using xylene for 12 minutes. This process was then followed by a rehydration procedure utilising serial ethanol with decreasing concentrations (100%, 90% and 70%, 3 minutes at each stage) and finally rinsing the sample in water for 3 minutes.

Haematoxylin and eosin (H&E) staining

The prepared tissue sections were stained using haematoxylin and eosin staining (H&E) (H&E, Sigma-Aldrich, NSW, Australia) in order to identify tissue components and to evaluate the degree of muscle injury and regeneration, as well as the level of the inflammatory cell influx and its location. The rehydrated tissue sections were rinsed with distilled water and then stained with Mayers haematoxylin for 5 minutes in order to stain the nuclei of the cells blue. The samples were then rinsed using running tap water for 10 minutes and stained with eosin for 10 seconds to colour the cellular cytoplasm and connective tissue pink.

Subsequently sections were then dehydrated again as explained previously and were mounted with menzel coverslips (Lomb Scientific, Australia) using a xylene based mounting medium (Eukitt: Kindler, Germany) and then dried overnight.

Imaging, analysis and quantifications of histological sections

The histology sections were scanned using a Leica SCN400 histology section scanner (Leica Microsystems Pty Ltd, NSW, AU) and visualised using a light microscope, Zeiss Axio Imager M.2 (Carl Zeiss, Gottingen, Germany). The histological images were captured using the Zeiss Axio Zen 2011 image analysis software and subsequently analysed qualitatively for evaluation of tissue morphology relating to the muscle injury, inflammation and muscle regeneration. Selecting random histological views and the quantitative analysis of the vascular morphometric parameters using histology and ImageJ software are explained in Chapter 4.

3.2.6 General statistics

The quantitative data obtained from experimental examinations is presented as a Mean \pm SD (standard deviation). Further calculations were performed using statistical tools available in SPSS (SPSS: IBM SPSS Statistics, Version 21), MedCalc software (MedCalc: Version 13.1.2.0, Microsoft Partner, Belgium) as well as Microsoft Excel (Microsoft Excel: Microsoft office professional 2010, Microsoft Corporation). For all statistical analysis, $p < 0.05$ was considered significant while comparing the differences between the mean values. The differences between two independent groups were analysed using a two-tailed Student t-test assuming equal variance. The reproducibility of the impact device was determined by finding the coefficient of variation (CV: $SD/mean \times 100\%$) for the velocity parameter. In this research, a CV less than or equal to 10% was determined to be an acceptable level of variability indicating the reproducibility of the described method (Jensen *et al.* 1994, Mitzner *et al.* 2001).

The criteria for detection and exclusion of an outlier value was defined based on determining a qualifying band for the measured values given in following formula (Thompson 2013):

$$\text{Mean} - (1.5 \times \text{SD}) < \text{Measured value} < \text{Mean} + (1.5 \times \text{SD}) \quad (3-4)$$

The SD is the standard deviation from the mean. The measured values outside the defined band were identified as outlier values and excluded.

3.3 RESULTS

3.3.1 Impact velocity characterisation

The theoretical results of the calculated velocities of the drop weight obtained from equation 3-2 are given as a function of different heights between the starting point at the top, where the drop weight is released, and the bottom point where the drop weight hits the impact surface (Figure 3-9 and Table A-1).

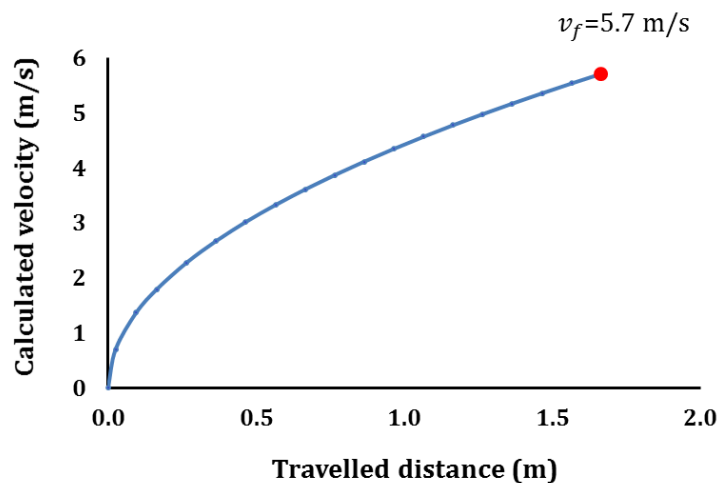


Figure 3-9: Calculated velocities of the drop weight versus various distances. The calculated velocities of the drop weight versus the distance travelled by the drop weight (drop height) between the starting point and the impact surface (ending point) is shown.

The final impact velocity v_{fc} at the impact surface was also calculated from this equation and presented below where the total travelled distance (drop height) by the drop weight was 1.66 m.

The data (Figure 3-9) showed that the velocity of the drop weight increased as it was approaching the impact surface.

$$v_{fc} = \sqrt{(2gh_i)} = \sqrt{(2 \times 9.8 \times 1.66)} = 5.7 \text{ m/s} \quad (3-4)$$

The calculated velocity validation using a high-speed camera (HSC)

As mentioned, to confirm that the theoretically calculated final velocity (v_{fc}) of the drop weight can accurately predict the actual velocity of the drop weight measured experimentally, v_{fc} was validated at the impact surface by a high-speed camera (HSC). The final drop weight velocity at the impact surface was obtained from the derivative of the position-time function with respect to time (Figure 3-10).

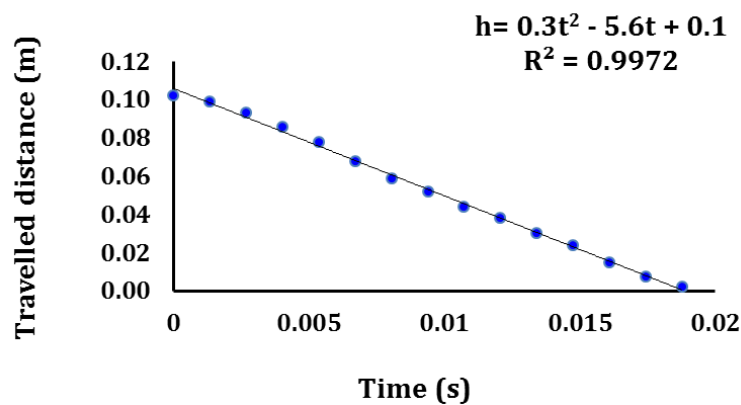


Figure 3-10: Measured velocities obtained from a high-speed camera (HSC).

One series of measurements observed for the distance travelled by the drop weight (drop heights) versus corresponding times captured by the HSC is shown. At the beginning of the test, the drop weight falls from the original starting point of 1.66m, which is the distance between the original point and the end point (impact surface). After travelling 1.56 m, the drop weight reaches the HSC field of view (FOV) where it begins to capture the images for the remaining distance (0.1m). This FOV distance (0.1m) was determined with a starting point of 0.1m (where the drop weight reaches the FOV and its position starts to be captured) and the ending point of 0.02m at the impact surface. The polynomial trend line (curve fitting) was set for the quadratic free fall equation where the R^2 (coefficient of determination) was computed as 0.99 indicating that the data fits well with the regression line.

The Mean \pm SD derived from the HSC was determined to be $v_{fm}=5.46$ (≈ 5.5) ± 0.15 m/s. This value was compared with the final theoretical velocity (5.7m/s). Comparisons between the final drop weight velocity derived from calculations using the formula (v_{fc}) (a single absolute value) and experimental measurements (v_{fm}) (mean value) utilising the HSC indicated no significant difference between these two methods (single Student t-test) for measuring the velocity at the impact surface (Figure 3-11).

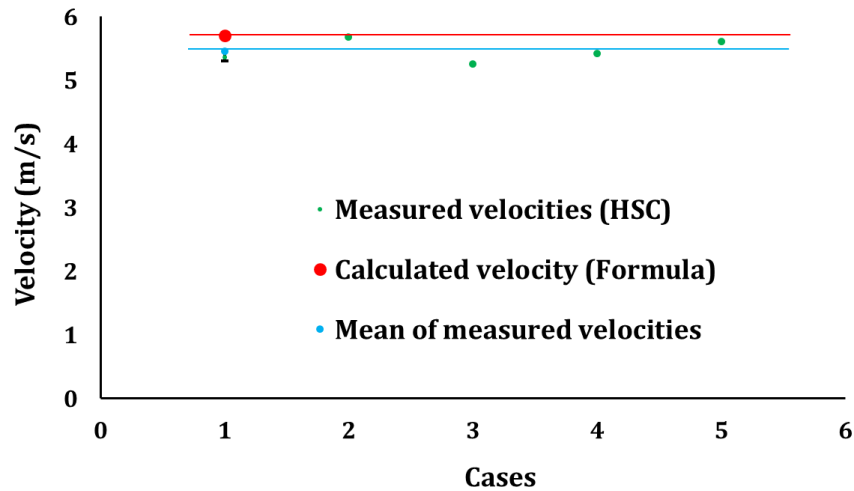


Figure 3-11: Comparisons between the calculated and measured velocities.

The comparison between the final calculated velocity using the formula (v_{fc}) (one absolute calculated value, $SD=0$) and the final velocity (Mean \pm SD, $n=5$) which was experimentally measured (v_{fm}) by using the high-speed camera (HSC). The measured velocity of case 1 was very close to the mean value therefore, it may not be clearly seen in this image. The $p > 0.05$ was obtained by statistical analysis using the “single Student t-test” for comparisons between the single value (calculated) and the mean value (measured) indicating that there is no significant difference between these two methods.

Impact velocity validation for reproducibility and accuracy

The relative error between final velocities derived from analytical calculation using the formula (v_{fc}) and experimental measurements (v_{fm}) utilising a high-speed camera is defined as:

$$\text{Relative error (\%)} = \frac{|v_{fc} - v_{fm}|}{|v_{fc}|} \times 100 \quad (3-5)$$

The numerator represents the absolute error (the absolute differences between the calculated and measured velocities). The relative error obtained from Equation 3-5 was as small as 3.5% and indicated that the final measured velocity (v_{fm}) produced by the HSC is very close to the final calculated velocity (v_{fc}) obtained from equation 3-2. Also, for the measured velocities (v_{fm}) obtained from experiments ($n=5$) using the HSC, a small coefficient of variation ($CV\% = SD/\text{Mean} \times 100$) of 2.8% was found. These results indicated that theoretical velocity is an accurate method to predict the velocity pattern of the drop weight in reality and therefore, it is reliable for creating a consistent injury.

The final theoretical velocity was used for calculating the energy of the impact to create the CSTT.

3.3.2 Impact weight characterisation

As discussed, the height of the impact device used in this research (1.66 m) was shorter than the one utilised by Claes and colleagues (Claes *et al.* 2006). Therefore, to achieve an equal impact energy the weight of the drop weight had to be increased to 180g. As the original weight of the drop weight was 130g, additional plasticine (50g) was added to the drop weight to obtain the weight of 180g. However, the drop weight of 180g, created a muscle injury of Grade 2 (n=5). Therefore, to achieve a CSTT of Grade 4, the weight of the drop weight was increased. The tested weights were 230g (n=7), 300g (n=4) and 400g (n=6) which produced a CSTT and muscle injuries of Grade 3, Grade 3 and Grade 4 respectively based on the AO classification (Figure 3-12).

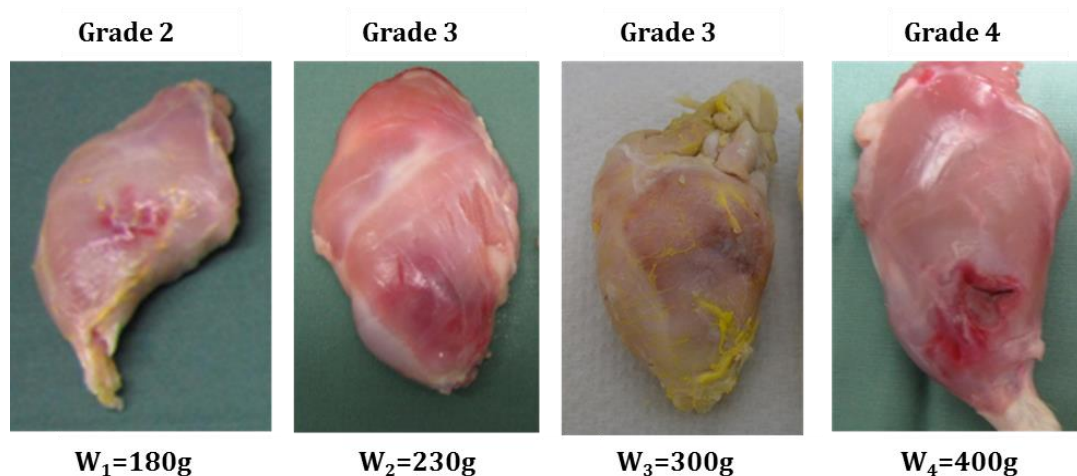


Figure 3-12: Determining the degree of CSTT and muscle injury.

The results of the muscle injury obtained from four different drop weights are shown. Various drop weights including 180g (n=5), 230g (n=7), 300g (n=4) and 400g (n=6) were applied to impact the biceps femoris muscle on the lateral side of the rat's hindlimb and also the gracilis muscle on the medial side. Here the results of the lateral side of the hindlimb are shown. These weights produced CSTTs of Grade 2, Grade 3, Grade 3 and Grade 4 respectively based on the AO classification. A severe CSTT with serious muscle injury (Grade 4) and defect (on the biceps femoris) was achieved using the drop weight of 400g.

By using a drop weight of 400g, a severe CSTT including extensive haematoma, inflammation and bleeding could be observed on the superficial muscles (biceps femoris and gracilis) of both lateral and medial sides of the rat's hindlimbs along with a muscle defect on the biceps femoris. These symptoms of the CSTT were defined as Grade 4 based on the AO classification (Figure 3-12). In addition, the skin evaluation showed no obvious haematoma or defect on the skin surface of the rat's hindlimbs utilising the drop weight of 400g, (Figure 3-13). Further investigation utilising an X-ray image (Faxitron DX V1, Faxitron Bioptics LLC, USA) revealed that there was no broken bone on the injured hindlimb where the drop weight of 400g was applied (Figure 3-14).



Figure 3-13: The evaluation of the skin surface of the rat's hindlimbs. The skin surface of the rat's hindlimbs from both lateral and medial sides is shown. No obvious haematoma or perforation could be seen on the skin surface of the injured hindlimb where CSTT was applied using the drop weight of 400g.

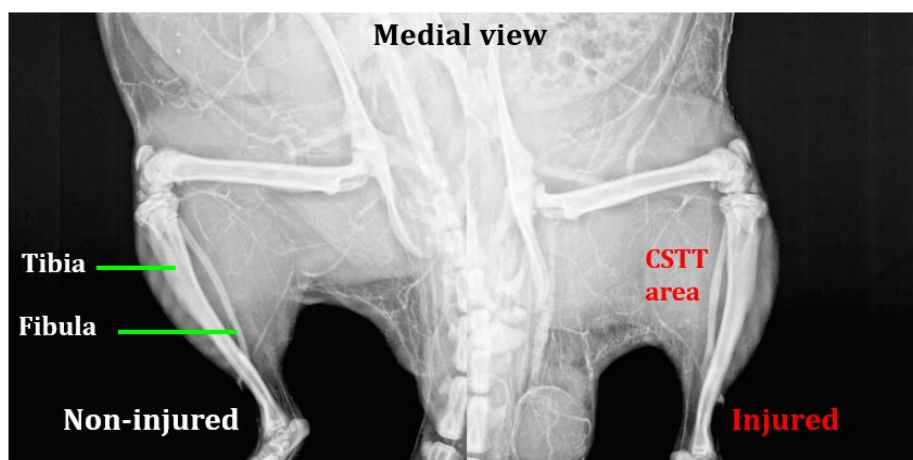


Figure 3-14: Bone fracture inspection following CSTT. An X-ray image from the medial view of both injured and non-injured hindlimbs is shown. No broken bone could be observed in the injured hindlimb where the CSTT was induced by the drop weight of 400g.

Therefore, the desirable CSTT of Grade 4 based on the AO classification including extensive muscle injury (Figure 3-12) with no skin perforation (Figure 3-13) and no broken bone (Figure 3-14) was achieved using the drop weight of 400g. This weight was chosen and kept constant throughout all experiments.

3.3.3 CSTT characterisation

One day after impact, the CSTT was qualitatively evaluated by taking photographs of the skin and muscle injury before and after skin dissection using a digital camera (Sony, DSLR-A330) for all animals. The symptoms were assessed before dissection of the skin surface (epidermis side) and after dissection to observe the injury under the skin (subcutaneous side). A mild to moderate swelling and stiffness could be palpated with no obvious haematoma on the skin surface where the CSTT was induced. Although the skin surface (epidermis side) showed no obvious sign of haematoma, a serious haematoma was observed under the skin (subcutaneous side) in the injured region after dissection (Figure 3-15). In addition, the CSTT was evaluated on the superficial muscles on both lateral (biceps femoris) and medial (gracillis) sides of the rat's hindlimb. To find whether CSTT had affected the deeper muscles, the biceps femoris on the lateral side of the rat's hindlimb, where a serious muscle defect could be observed, was dissected. The same symptoms as described for the superficial muscles could be observed on the deeper muscles as well (e.g. semimembranosus) (Figure 3-16).

The severity of the CSTT using the drop weight of 400g was also confirmed through histological analysis and observation of extensive muscle fibre destruction as well as the presence of inflammatory cells in the injured region (Figures 3-17). Furthermore, the reproducibility of the CSTT model was quantitatively verified to ensure that the model produced consistent muscle injuries with the same degree. This quantification was conducted by measuring the inflamed areas of the haematoma (n=6) of the hindlimbs where the CSTT was induced by the drop weight of 400g.

The Mean \pm SD of 5.2 ± 0.6 cm² was obtained from the results although an outlier value of 2.2 cm² was quantitatively detected (Figure 3-18).

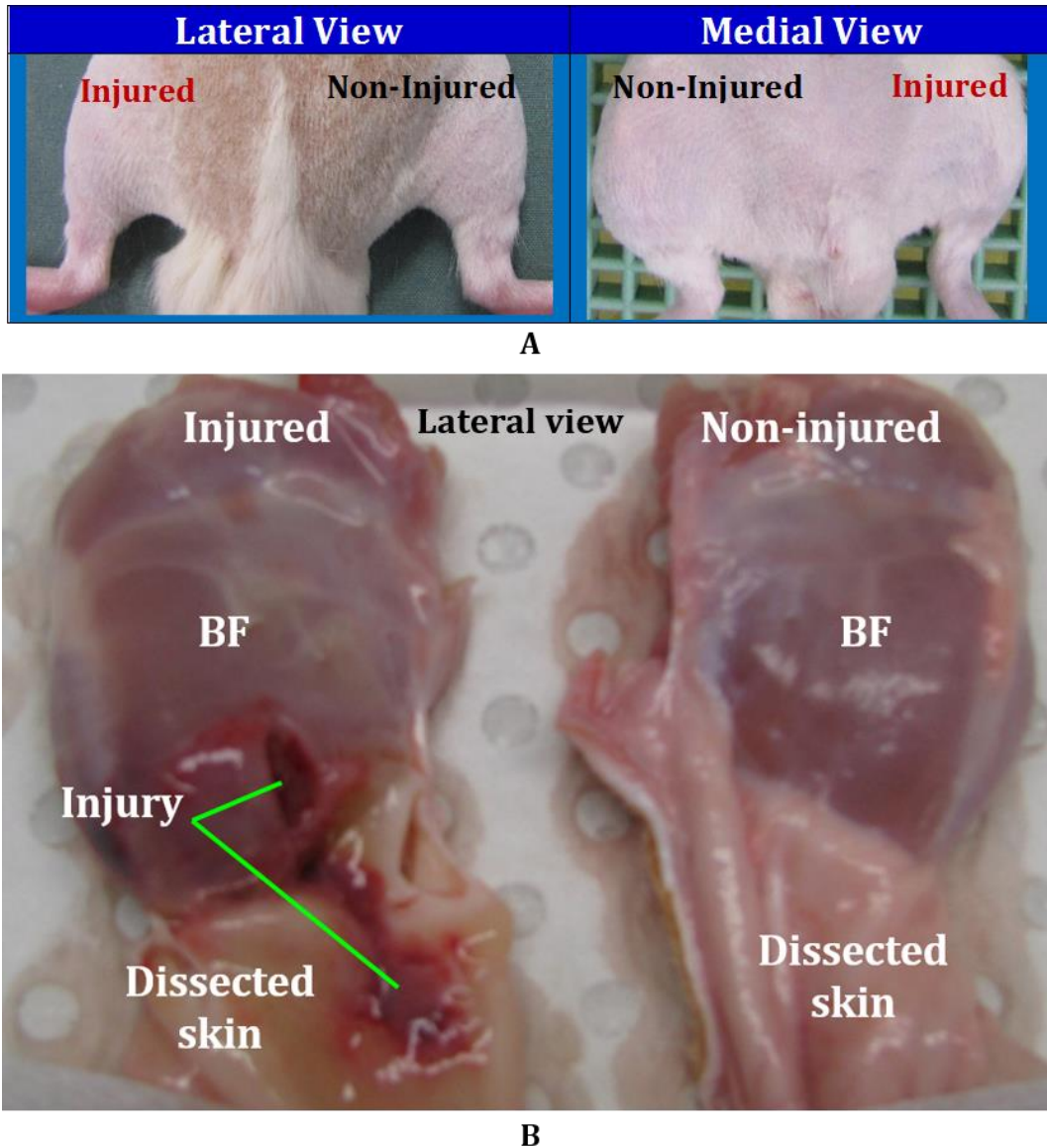


Figure 3-15: Skin evaluation after CSTT.

Skin inspection of both external and internal sides is shown after a CSTT created by the impact device using a 400g drop weight. **A:** The evaluation of the skin's surface showed no obvious haematoma on either lateral or medial sides of the injured hindlimb. **B:** This image exhibits that after skin dissection of the injured hindlimb, a severe haematoma could be observed under the skin (subcutaneous side) where it was attached to the biceps femoris muscle (BF) in the region that the CSTT was induced (green lines).

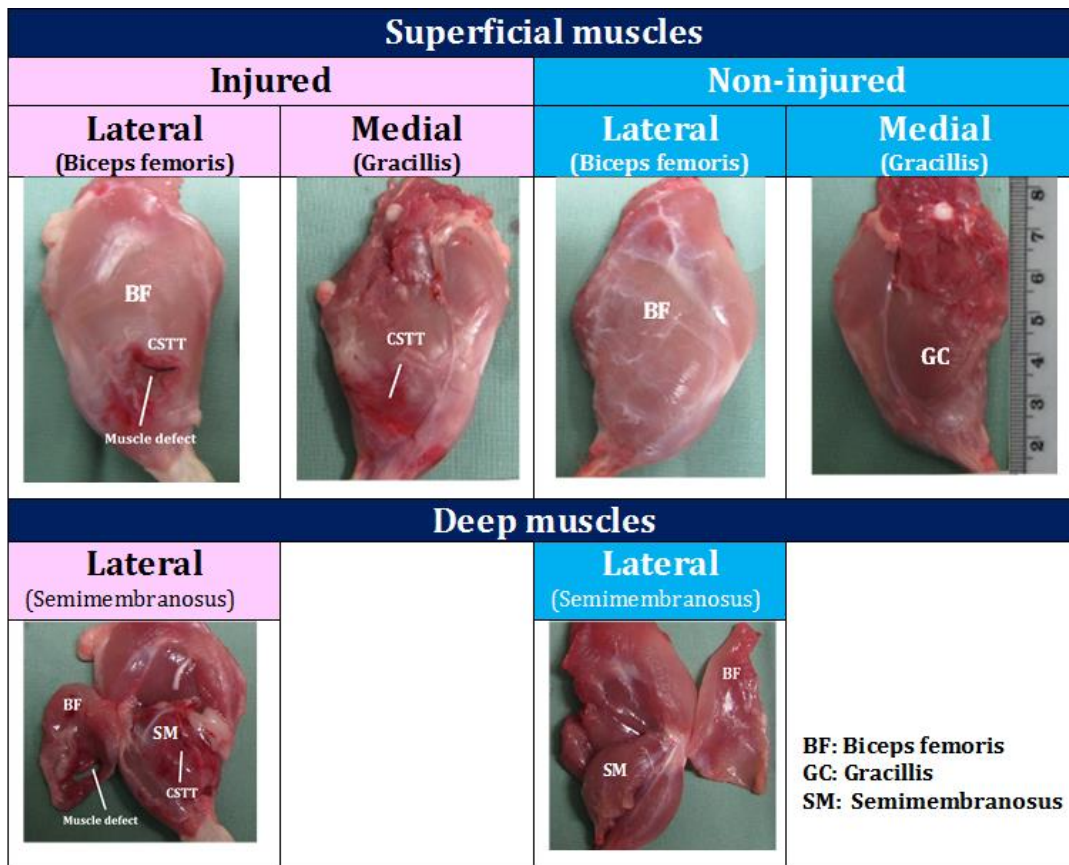


Figure 3-16: The CSTT and muscle injury evaluation following an impact. The CSTT and muscle injury inspection following CSTT using a drop weight of 400g is exhibited. The first row depicts the muscle injury and defect (Grade 4 based on the AO classification) on the superficial muscles of both lateral (biceps femoris) and medial (gracillis) views while the second row exhibits the deeper muscle injury of the lateral side (semimembranosus) after dissecting the biceps femoris. A severe muscle injury, haematoma, inflammation and bleeding resulted from the drop weight of 400g which could be observed in both superficial and deep muscles. This confirms the severity of the injury as well as the depth of the CSTT affecting several muscle compartments. These findings were consistent over all animals (n=6).

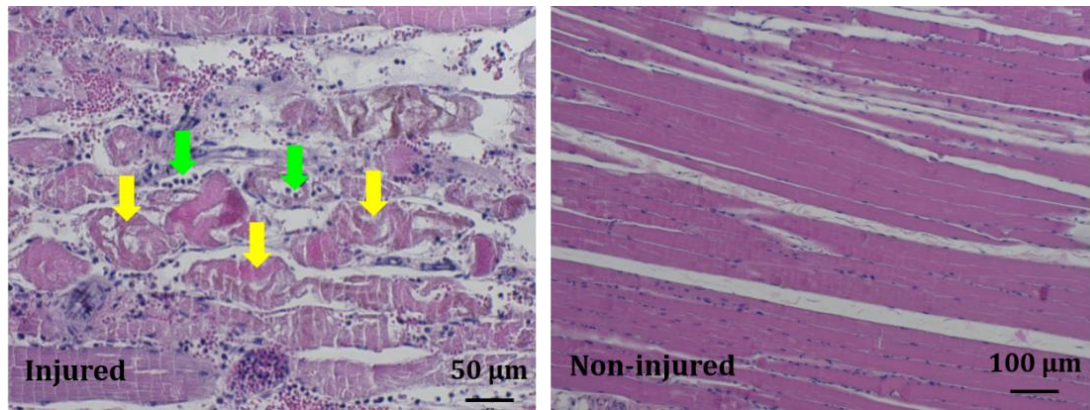


Figure 3-17: The histological analysis following CSTT.

The histological analysis (haematoxylin and eosin staining) of the injured and non-injured regions of the rat's hindlimbs (biceps femoris) is illustrated. The severity of the CSTT produced by a 400g drop weight was confirmed by observing extensive necrotic areas including destructed muscle fibres (yellow arrows) and the presence of inflammatory cells (green arrows) where the impact was induced. These findings were consistent over all animals (n=6).

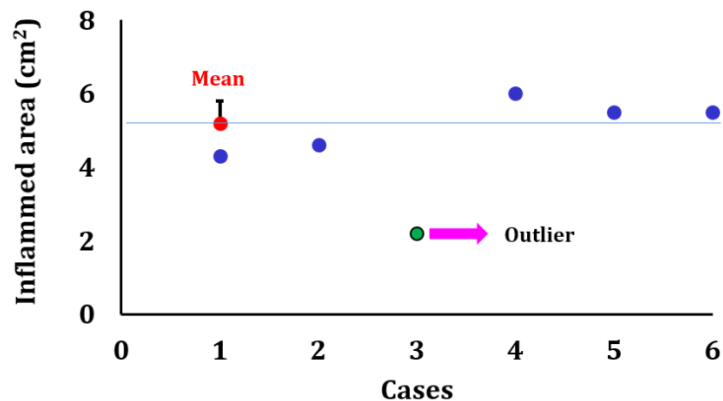


Figure 3-18: The quantitative analysis of inflamed areas due to CSTT.

The quantified inflamed areas of the CSTT (n=6) one day after impact where the injury was induced using a 400g drop weight. Regardless of the presence of an outlier value, which was excluded, the evaluation of the individual measurements with a Mean \pm SD of $5.2 \pm 0.6 \text{ cm}^2$ showed a small variation indicating the reproducibility of the CSTT model for producing the CSTT with the same degree of injury (Grade 4).

After exclusion of the outlier value based on the defined criteria (3.2.6), the variability reduced in data with a CV of 11.5% in the inflamed areas. This CV value was very close to the acceptable CV range ($\text{CV} \leq 10\%$) suggesting that the model was relatively reproducible for creating a consistent CSTT with the same degree (Grade 4).

The investigation regarding the characterisation of the impact device and the CSTT was finalised for this research by determining the standard operating procedures (SOP) for developing a severe and consistent injury using the impact device. These protocols can be used to create a CSTT with defined impact parameters including the weight (e.g. 400g) and velocity (e.g. 5.7 m/s) of the drop weight to produce a desirable injury within the ROI (e.g. Grade 4 based on the AO classification) (SOPs for the impact device, Appendix C).

3.4 DISCUSSION

3.4.1 The impact device characterisation

The goal of this study was to create a CSTT with serious muscle and vascular injury with no skin perforation and no broken bone. Such an injury has been described by the AO classification as Grade 4. The severity of the injury is primarily influenced by the energy of the impact, which was characterised based on two affecting parameters: the impact velocity and the weight of the drop weight.

To create a standardised and reproducible CSTT, a well-characterised impact device was required with a validated impact velocity as well as an appropriate weight for the drop weight at the impact surface. The impact velocity was characterised by analytical calculations and verified with respect to the reproducibility and accuracy using a high-speed camera. The small relative error of the measured velocity (v_{fm}) produced by the HSC was very close to the calculated velocity (v_{fc}) obtained from analytical calculations suggesting the accuracy of the HSC technique. In addition, a small coefficient of variation indicated that the impact device was a reliable system to produce precise and reproducible impacts with the same velocity thereby creating a consistent injury. One explanation for the small difference between the calculated and measured velocity can be the friction effect between the rod and the impactor.

A systematic characterisation of the impact velocity was not found in publications by other authors who also used an impact device to produce a defined CSTT, and only basic information such as the impact velocity was provided (Claes *et al.* 2006, Melnyk *et al.* 2008). Claes *et al.* reported that a CSTT of Grade 2 was created in their experiments, based on the Tscherne classification. However, a detailed description or images of the muscle injuries resulting from the CSTT to support this classification have not been provided in any of their research articles. In our experiments, even though the fundamental basis of the impact device, and initially also the impact energy for creating a CSTT was similar to the one applied by Claes *et al.*, we did not achieve the desired severity of muscle injury. It is unlikely that the difference in injury severity was caused by different animals in the experiments (we used male rats at 12 weeks of age, while Claes *et al.* used rats of unspecified gender at 11 weeks of age. But while we have no definitive explanation for the differences between Claes *et al.*'s and our findings, the discrepancy between reported injury severity may highlight the problems associated with the subjective injury classification systems of Tscherne and AO. Particularly for the injury assessment in rats, which do not exhibit any observable superficial bruising after CSTT (e.g. Figure 3-15) it is difficult to assess the degree of the muscle injury precisely from a superficial visual observation alone. Consequently, for the injury classification during the model development phase, we removed the skin and based our assessment on visual observation of the superficial muscles (Figure 3-12 and Figure 3-16). We then incrementally increased the weight of the drop weight to eventually achieve an injury that was classified as of Grade 4 based on the AO classification using the drop weight of 400g. This weight subsequently used throughout all experiments.

3.4.2 Characterisation of the CSTT model

A severe CSTT model (Grade 4 based on the AO classification) including extensive acute muscle injury, haematoma, inflammation with no skin perforation and no broken bone was achieved using the characterised impact device.

Based on the injury description given by the AO classification and the quantification of the inflamed areas, the established CSTT model for this research was consistently graded 4 using a drop weight of 400g with a velocity of 5.7m/s.

The muscle injury following CSTT was also verified by histological evaluations where serious muscle fibre destruction along with the presence of inflammatory cells were observed in the region that CSTT was induced. In the histological analysis, the CSTT region containing damaged muscle fibres and inflammatory cells potentially indicate necrosis as described in the literature (Radley *et al.* 2008). The skin observations indicated that while no obvious haematoma could be observed on the skin surface (epidermis side), there was substantial injury to the deeper layers (subcutaneous side). A reason why no obvious haematoma could be seen on the skin surface (epidermis side) may be explained by the nonvascular structure of the rat's skin.

In general, the structure of the skin's surface (epidermis side) is nonvascular with thick cellular layers that act as a barrier against mechanical loads (Sanders *et al.* 1995). Rats are loose-skinned animals and the skin is highly elastic with no strong structure to attach it to the underlying tissue (Dorsett-Martin 2004, Dorsett-Martin *et al.* 2008). This suggests that after a high-energy impact, the surface of the skin can slide on the deeper structures (subcutaneous fascia) and transfer this energy to the underlying tissue where the injury could be obviously seen.

However, the human skin is attached to the tissue (Dorsett-Martin 2004) and therefore, the CSTT can be obviously seen on the skin's surface since the energy of the impact can easily be passed on to the underlying soft tissue which is firmly attached to the skin. Although the skin results obtained from the CSTT model can be used for other loose-skinned animal models, these results may not be appropriate for humans.

In conclusion, the qualitative characterisation of the CSTT and muscle injury from the CSTT model developed for this research has confirmed and expanded on the previous efforts of other studies (Schaser *et al.* 1999, Claes *et al.* 2006).

The experimental model inflicted injuries that correspond with the description of qualitative CSTT symptoms in clinical classifications of CSTT (AO and Tscherne) (Table 2-1).

Chapter 4: Development of perfusion and micro-CT evaluation protocols for characterisation of the vascular injury following CSTT

4.1 INTRODUCTION

As discussed in Chapter 2, from CSTT models reported using a rat's hindlimb, evidence was found suggesting a reduction in blood flow during the first 24 hours after trauma (Claes *et al.* 2006). Also by using an ischemia model of mouse hindlimbs, changes to vascular morphology such as a decrease in the vessel volume, connectivity, number and diameter have been shown one day after injury (Duvall *et al.* 2004). Based on these findings, it was hypothesised that the vascular morphology changes after CSTT and this leads to a reduction of these parameters within the injured hindlimbs at day 1. To test this hypothesis, it was essential to visualise and then quantify the vascular morphometric parameters. These morphological parameters are vessel volume (VV), vessel connectivity density (VConn.D), vascular degree of anisotropy (DA), vessel number (VN), vessel diameter (thickness) (VD) and vessel spacing or separation (VSp). Briefly, VV is calculated based on the number of segmented voxels and the voxel size in the 3D micro-CT image after applying the thresholding technique (Jing *et al.* 2012). The parameter of vascular connectivity (VConn) which is defined per total volume (TV) (normalised by TV as $1/\text{mm}^3$) (Scanco Medical SCANCO Medical microCT systems: 3D analysis) is “the maximal number of branches that can be broken within a structure before it is divided into two separate parts” (Duvall *et al.* 2004). The vascular network orientation is analysed by the geometrical degree of anisotropy (DA) (1) and is quantified as the ratio between the maximum and the minimum radius of the ‘mean intercept length’ (MIL) ellipsoid. The DA varies from 1 for isotropy and greater than 1 for anisotropy (Bouxsein *et al.* 2010, Scanco Medical SCANCO Medical microCT systems: 3D analysis).

The VN, VD and VSp are determined based on a model-independent technique suggested for computing the thickness in 3D images (Hildebrand *et al.* 1997, Zagorchev *et al.* 2010). The inverse of the mean distance between the mid-lines of vessels (1/mm) gives the VN (Jing *et al.* 2012). The average of the local voxel (a volumetric pixel) thicknesses within the structure is calculated as the VD, and a similar calculation on the surrounding space of the voxels is computed as the VSp (Duvall *et al.* 2004).

Through the literature review performed in Chapter 2, it was found that the microfil contrast agent (Cheung *et al.*, Savai *et al.* 2009, Jia *et al.* 2010, Yeung 2011) and histomorphometry analysis (Boerckel *et al.* 2011, Tomlinson *et al.* 2013, Ehling *et al.* 2014) are accurate approaches for evaluating and quantifying vascular morphometric parameters. In addition, it was appeared that ImageJ software has been successfully used by other authors for quantifying morphological parameters of the vascular network (Zhuang *et al.* 2006, Tomlinson *et al.* 2013).

In a comprehensive systematic analysis, Nebuloni *et al.* (2014) have validated the accuracy of the vessel number produced by contrast-enhanced micro-CT using 2D histomorphometry and ImageJ software (Nebuloni *et al.* 2014).

Ehling and colleagues (2014) have correlated the microfil-enhanced micro-CT results with histology evaluation using ImageJ for the vessel number and diameter in tumour angiogenesis models (Ehling *et al.* 2014). They reported an excellent correlation and agreement between contrast-enhanced micro-CT utilising microfil, and histomorphometry for producing the vessel number and diameter in 2D correlated sections. Also, by using histomorphometrical evaluations, Jia and colleagues (2010) found significant positive correlations between 2D histology and 3D contrast-enhanced micro-CT for quantitative assessments of the vascular volume ratio and vessel number (Jia *et al.* 2010).

Therefore, in this research, a systematic characterisation method was established for a 3D vascular network through the development of protocols for perfusing and evaluating the vascular network of rat hindlimbs enabling us to visualise and quantify the vasculature using microfil enhanced micro-CT imaging.

The efficiency of the perfusion protocols developed for the vascular injury model to fill the vasculature and capillaries with contrast agent was verified using histomorphometrical analysis. Furthermore, ImageJ software was applied to compare micro-CT and histology images for possible vascular morphology changes as well as for testing the efficiency of the developed perfusion protocols.

The sensitivity of this characterised vascular model was tested for detecting the changes to the vascular morphometric parameter following injury. In addition, the reproducibility and accuracy of the vascular injury model obtained from micro-CT evaluation was confirmed using statistical and histomorphometrical analysis.

4.2 MATERIAL AND METHODS

4.2.1 Rat hindlimb injury model

In the previous chapter, a defined and reproducible experimental CSTT model including muscle injuries using rat's hindlimbs was developed and characterised. Here, a vascular injury, as a key element of a CSTT model, is characterised based on the standardised protocols for perfusion, visualisation and quantification of the vascular network.

4.2.2 Vascular perfusion protocol

To visualise the vascular network using micro-CT imaging in 3D, standard operating protocols (SOP, Appendix D) were developed to perfuse the blood vessels effectively with the microfil contrast agent. To achieve this, rats were anaesthetised and impacted on the left hindlimb (ROI) to create a standardized and reproducible vascular and muscle injury using an impact device (3.2.3). One day following trauma, animals were euthanised and prepared for perfusion with a contrast agent. Immediately after euthanasia, rats were laid in the supine position and the thoracic cavity was exposed.

A 22-gauge angio-catheter was inserted into the left ventricle and the vasculature was flushed with heparinised-saline (0.9% normal saline and heparin sodium (100 U/ml), Pfizer Ltd, NSW, Australia) through this catheter using a peristaltic infusion pump (Pump 1: Cole-Parmer, 6-600 RPM, Extech Equipment Pty Ltd, VIC, Australia). A vasodilating agent (Papaverine hydrochloride, 120mg/10ml, Hospira, VIC, Australia) was used to dilate the blood vessels and improve the subsequent contrast agent perfusion. The right atrium was punctured to facilitate the drainage of blood.

Once the flushing of the vasculature was completed and the fluid draining through the punctured right atrium appeared clear, the vascular perfusion was switched to microfil, a radio-opaque contrast agent (explained in 2.5.1). A compound-diluent ratio of 1:2 was used mixed with 10% curing agent by employing a second peristaltic pump (Pump 2: 505 U, 220 RPM, Watson Marlow Ltd, NSW, Australia) (Figures 4-1 and 4-2).

The microfil preparation protocols were carried out based on the manufacturer's instructions (Flow Tech Inc 1999). The pump flow rate was set to 20 ml/minutes to keep the perfusion pressure low enough to prevent any vasculature breakage or leakage. The perfusion continued for 15 minutes until the rat's organs, hindlimbs, feet and tail turned yellow (the colour of microfil) indicating a satisfactory perfusion (Figure 4-2). After perfusion, animals were stored at 4° Celsius overnight to facilitate the polymerization of the contrast agent. The next day, the hindlimbs were dissected and transferred to a 10% neutral buffered formalin fixative solution.

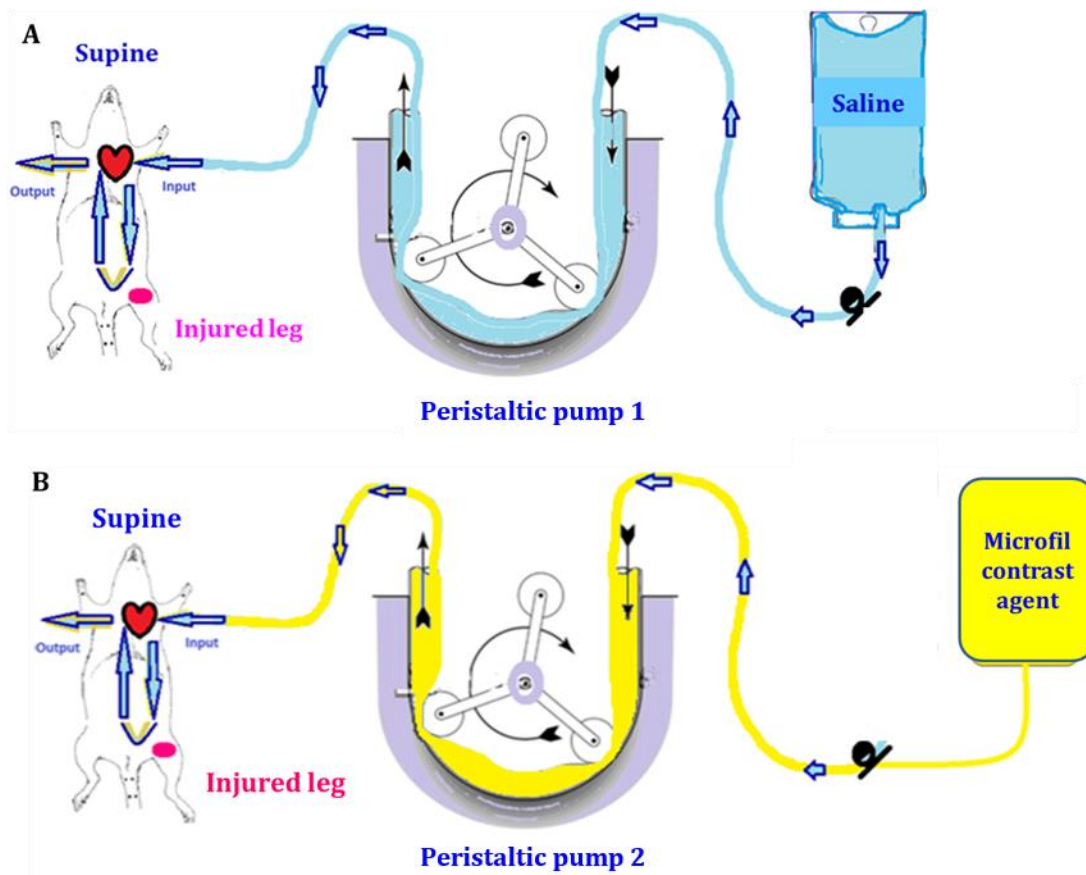


Figure 4-1: Two schematic views representing set ups for the perfusion protocol. Peristaltic pump 1 was used to flush the blood vessels by perfusing the heparinised saline (A) and peristaltic pump 2 was utilised for refilling the vasculature with the microfil contrast agent (B).

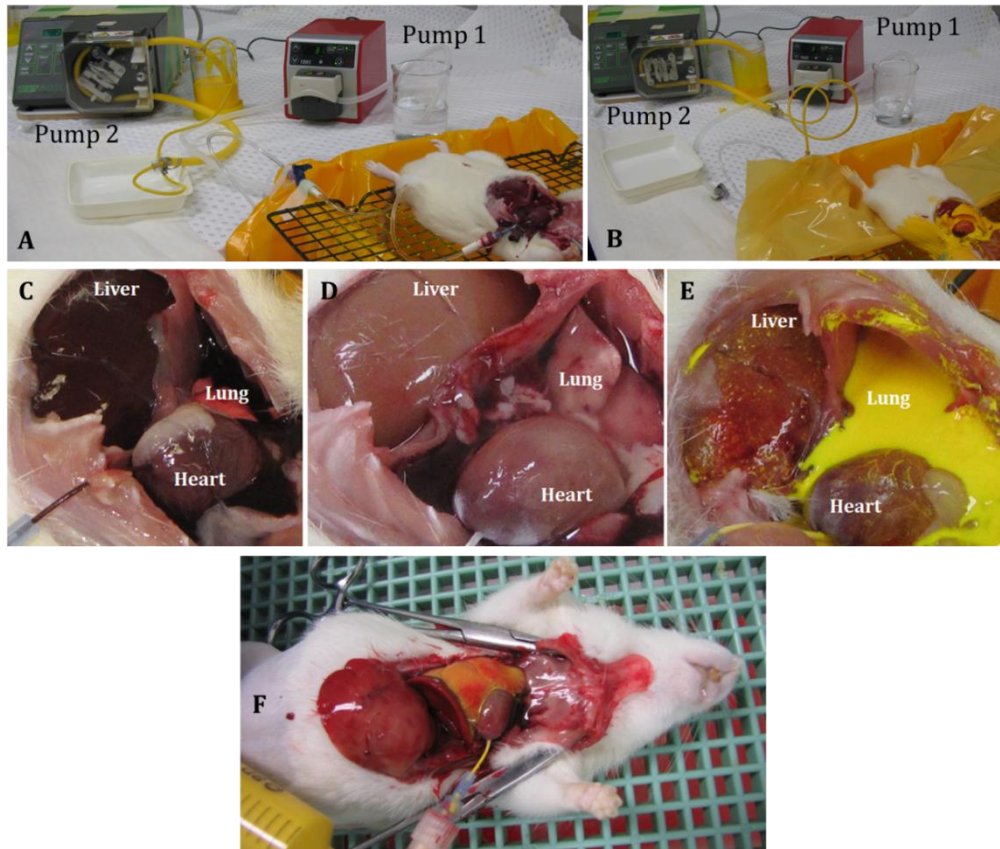


Figure 4-2: The designed set ups for perfusing the vascular network.

These images show the perfusion set-ups for flushing (A) and perfusing the blood vessels with the microfil contrast agent (B) using two peristaltic pumps. The organs in their natural state after euthanasia appear darker in colour due to the presence of blood within the vasculature (C). The perfused organs turned pale during cleansing since blood was flushed from the vasculature (D) and then yellow (the colour of microfil) (E) after microfil perfusion indicating that the microfil has filled the vasculature. The opened thoracic cavity and the microfil contrast agent perfused through the left ventricle and lungs are also shown (F).

4.2.3 Vascular visualisation and quantification using micro-CT

In order to evaluate the vascular network qualitatively and quantitatively, the analysis was divided into two steps. Firstly, the whole hindlimbs were scanned to observe the 3D vascular network particularly in the area where the injury was applied within the region of interest (ROI), which was defined as the tissue between the knee joint and the tibia-fibula conjunction. This was used for the visualisation of the macroscopic changes to the perfused vascular architecture, as well as for confirming the efficiency of the perfusion protocols for filling the major blood vessels.

Secondly, to visualise the vascular structural changes in more detail and for a quantitative assessment of the micro-vascular morphometric parameters, corresponding biopsy samples were taken (See 3.2.5) and scanned using micro-CT from the impacted region in the centre of the ROI.

Micro-CT imaging protocols for the hindlimb scan (ROI)

For a 3D visualisation of the entire vascular network within the ROI, the rat's injured and non-injured hindlimbs were scanned using a micro-CT imaging system (μ CT 40, Scanco Medical, Switzerland). Samples were scanned in a micro-CT sample tube (Figure 4-3) with an inner diameter of 37 mm at an energy of 55 kVp, intensity of 145 μ A, integration time of 250 milliseconds and at a maximum resolution (isotropic voxels¹ size) of 18 μ m. The energy and intensity values used for the scanning parameters were adapted from the literature (Duvall *et al.* 2004).

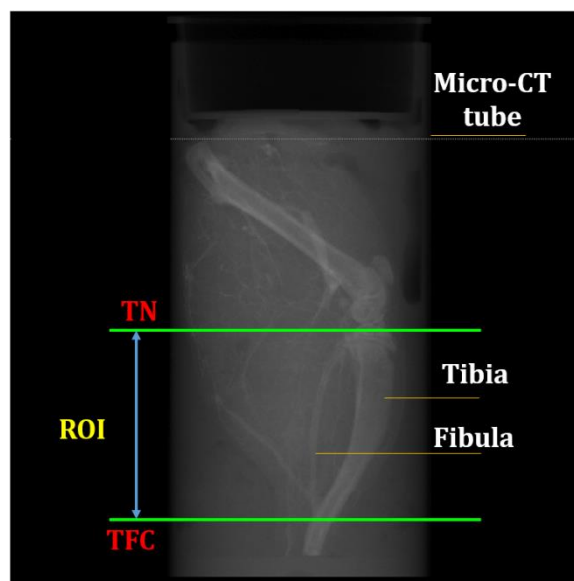


Figure 4-3: A scout view image of the rat's hindlimb inside the micro-CT tube. The position of the rat's hindlimb including the femur, tibia and fibula as well as the ROI is shown within the micro-CT tube.

¹ A voxel is a volumetric pixel, a basic element of 3D image.

For visualisation and quantification, the 3D image of the vascular network was segmented from the surrounding tissue using a threshold of 2072 Hounsfield units (HU: a standardised computed tomography attenuation coefficient) where a value of -1000 HU corresponds to air, 0 HU is assigned to water, and 2072 HU is for bone and microfil. In order to reduce noise, a low-pass Gaussian filter ($\sigma=0.8$, support=1) was utilised. The reconstructed images were evaluated using Scanco software (Scanco Medical AG, Version 4.05, Brüttisellen, Switzerland). In addition, the length of the ROI volume was assessed by multiplying the voxel size (isotropic, 18 μm) to the average number of micro-CT slices between the tibia notch and tibia-fibula conjunction and presented.

Vascular segmentation for the ROI evaluation

The scanned images contained the vascular network, as well as bone including the tibia and fibula. Since the x-ray attenuation of microfil is very similar to bone, it was not possible to distinguish the two structures using basic thresholding procedures alone. Therefore, for the 3D quantification of the ROIs, the entire hindlimb volume including bone and vasculature was scanned and evaluated (Figure 4-4). This volume within the ROI was defined as the “total segmented volume” (TSV) and is the summation of all segmented elements including bone volume (BV) and vessel volume (VV). The BV includes the summation of the reconstructed tibia and fibula volumes in the ROI micro-CT image. The VV is the total volume of blood vessels surrounding the tibia and fibula also segmented in the ROI micro-CT image. The TSV parameter was evaluated based on the assumption that the BV maintains a constant volume with negligible variations. The hypothesis was that if the BV variation is small between the injured and non-injured hindlimbs and also among the animals, then the TSV changes result from variations in the VV. To assess the BV variation between animals, the reconstructed bone was digitally extracted from the micro-CT image obtained from four rats. This was achieved by manually contouring the bone’s outer surface on some sections distributed along the length of the bone and then applying a ‘morphing’ tool available in the Scanco

evaluation software to interpolate the entire bone surface between two manually contoured sections. The vasculature was then eliminated using this contouring technique, leaving a 3D segment of bone.

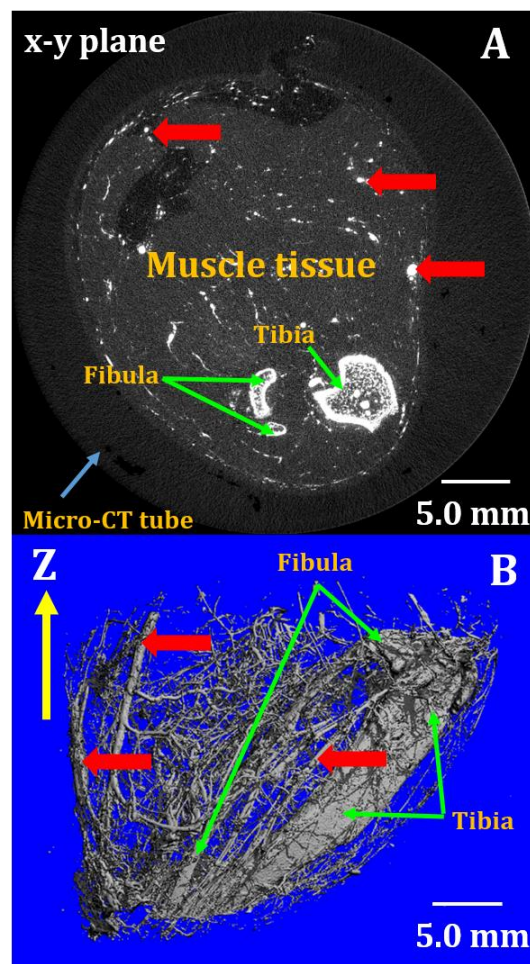


Figure 4-4: *Micro-CT images of the rat's hindlimb (ROI).*

A: *A greyscale cross-section image of the rat's hindlimb (ROI) including vascularised muscle tissue, tibia and fibula (green arrows) and microfil-filled blood vessels (red arrows) obtained from micro-CT in 2D (x-y plane, voxel size: 18 μ m). Since the grey-levels of microfil are very similar to bone, during thresholding, bone and vasculature were segmented as solids together (B).*

The BV values were recorded and presented as Mean \pm SD for the non-injured and injured hindlimbs. This was to ensure that there would not be a significant difference between the non-injured and injured hindlimbs and consequently, the TSV differences between the injured and non-injured hindlimbs are due to the VV differences.

The vascular network of the injured hindlimbs within the total ROI volume (TV) was quantified for the total vessel volume (TSV) which was compared to the non-injured contralateral hindlimbs. The TV parameter was selected as a cylinder comprising of the internal diameter of the micro-CT tube cross section (37 mm) where the hindlimb was located and also the length which was between two anatomical landmarks; the tibia-notch and tibia fibula conjunction. Since for each hindlimb, the diameter of the micro-CT tube and the distance between these two anatomical markers were constant, the TSV remained constant within this volume. Therefore, in this research, the ratio of the TSV/TV was not used.

Micro-CT quantification of vascular morphometric parameters (biopsies)

Since the resolution (voxel size) used for the whole hindlimb (ROI) imaging was limited to 18 μm , any capillaries smaller than 18 μm diameter were not visualised. Therefore, for a detailed analysis of the microvasculature architecture, corresponding smaller biopsy samples were taken from both injured and non-injured hindlimbs using a biopsy punch (8 mm diameter) (See 3.2.5). These smaller biopsy samples could be scanned with the smallest micro-CT tube providing the highest available resolution (the smallest isotropic voxel size) of 6 μm . This method facilitated the visualisation and quantification of small micro-vessels and capillaries down to 6 μm diameter. The scanning parameters (energy, intensity and the integration time) for the biopsy samples were kept the same as the ROI scans, with the exception of the threshold, which was adjusted to 1434 HU for better visualisation of capillaries and ultra-small blood vessels. To quantify the vascular morphometric parameters, 250 sections (1.5 mm) from the biceps femoris region, which was the most affected muscle by the injury, were processed using the morphometric evaluation scripts in the Scanco software. In the "Scanco evaluation window", the 250 sections were selected from where the vascularised muscle tissue within the cross section of the full circular biopsy began (x-y plane where 'z' direction indicates the length of biopsy sample) (Figure 4-5).

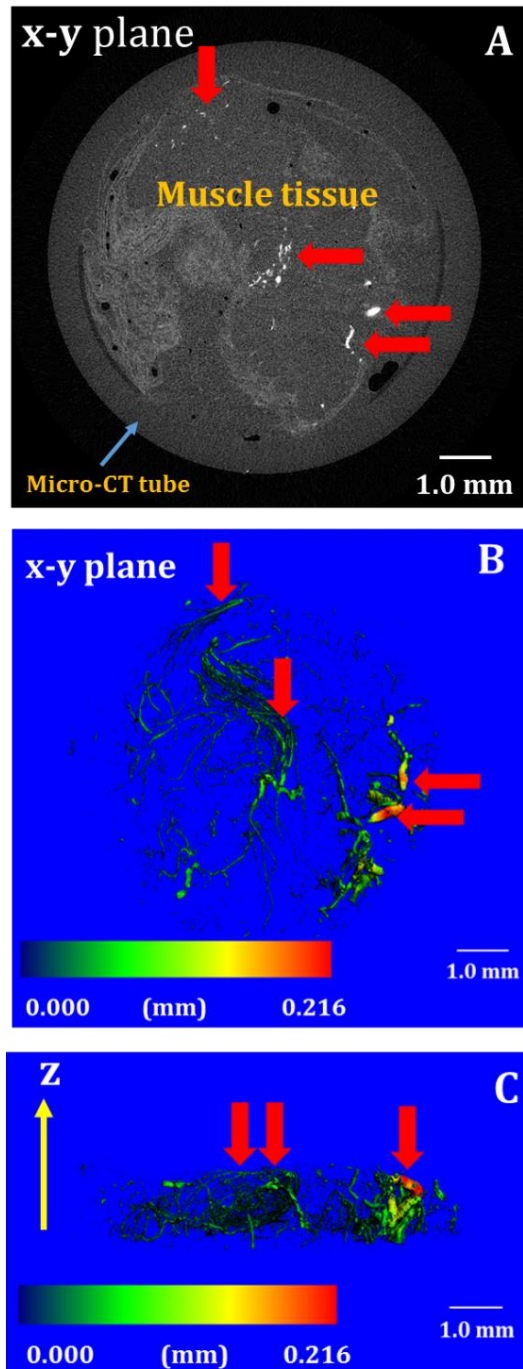


Figure 4-5: Selection of a biopsy stack for micro-CT imaging.

An example showing the selection of the 250 slices from the top section of a biopsy sample including the vascular network for quantifying the vascular morphometric parameters using micro-CT (voxel size: 6 μm). **A:** A cross-section of a biopsy stack in 2D showing the first selected slice where the vascularised muscle tissue (red arrows) can be seen within the x-y plane. **B:** The cross section of the 250 slices are exhibited in 3D (x-y plane where 'z' direction indicates the length of biopsy stack) with corresponding vascularised regions (red arrows) derived from Image A. **C:** A 3D image of the 250 slices in the 'z' direction (the length of the biopsy sample) with corresponding blood vessels (red arrows) derived from image A is illustrated.

4.2.4 Validation of the vascular injury model following CSTT

Selecting random histology views

The histology sections obtained from biopsy samples were prepared and H&E stained according to 3.2.5. The H&E histology images were then visualised and a grid was superimposed on the image using the Leica Biosystem software (Leica Biosystem, NSW, Australia). Each grid was divided into smaller $300\mu\text{m} \times 300\mu\text{m}$ fields of view and numbered along the 'x' and 'y' axis. Six randomly generated numbered pairs were selected by using Microsoft Excel software (2013, Microsoft Corporation, USA) (Figure 4-6). The first number of each pair was plotted on the 'x' axis of the grid and the second number was plotted on the 'y' axis (Figure 4-6). These six randomly selected fields of view were used for histological analysis.

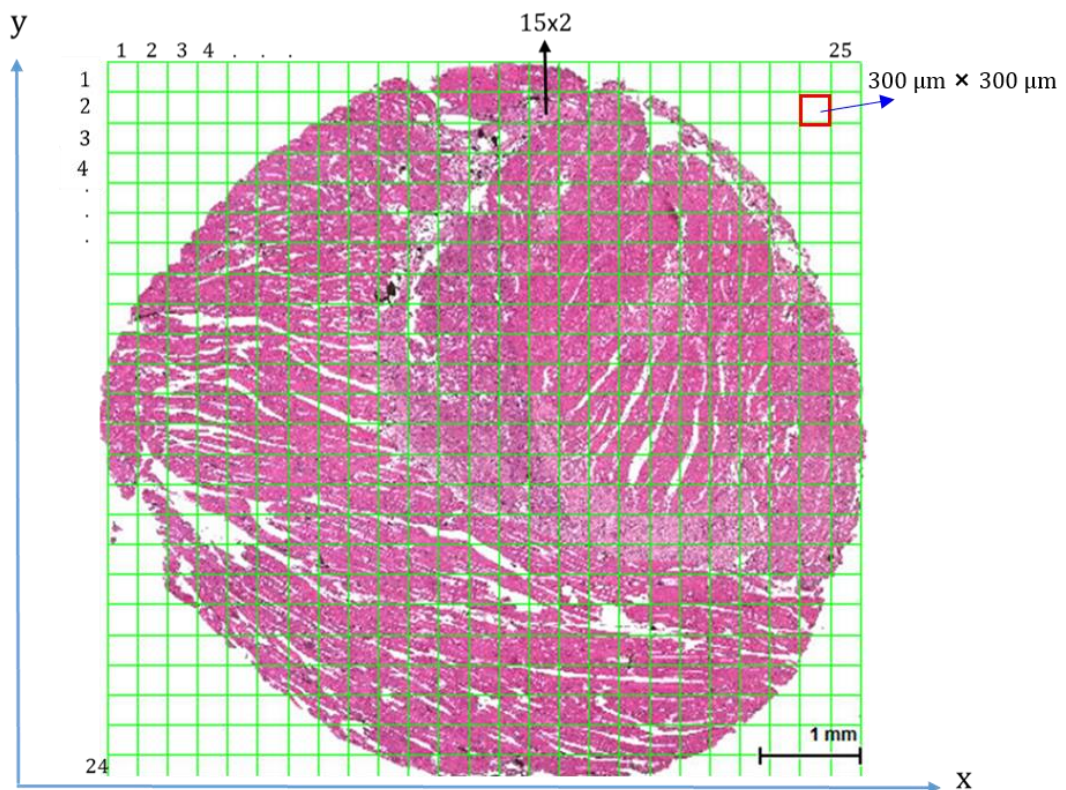


Figure 4-6: A gridded histology image and a randomly generated section.

A gridded histology image (25×24) captured from an injured hindlimb at day 1 is shown. A randomly selected field of view ($300\mu\text{m} \times 300\mu\text{m}$) was chosen by using the 'random number generator function' within the Microsoft Excel software ($x=15, y=2$) and is exhibited by a black arrow in the image. This method was used throughout this research to randomly select each section for histological analysis.

It should be pointed out that only the fields of view fully filled with tissue were quantified and therefore, the randomised fields of view with no tissue or partially filled with tissue were not taken into account.

Determination of the perfusion limit for small blood vessels using VD

The efficiency of the developed perfusion protocols was tested by measuring the smallest diameter capillaries that were filled with microfil. In a given histology section, the diameter of the smallest detected capillary per field of view was directly measured using ImageJ software (freehand line tool) and then the results were presented as Mean \pm SD per square millimetre of tissue area.

Verification of the perfusion efficiency using VN

In the micro-CT scans, it is only possible to observe the vessels perfused with contrast agent (microfil) and not the total number of blood vessels. Therefore, the quantified VN within the micro-CT slices is actually the perfused vessel number (PVN). In a histology section, both perfused (filled) and non-perfused (non-filled) vessels can be identified, making up the total number of blood vessels (TVN).

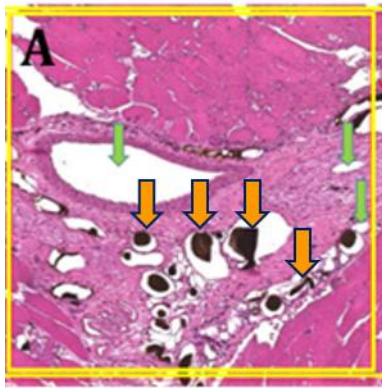
In this study, the PVN parameter per area of tissue was used for two purposes. Firstly, to determine the correlation between the micro-CT and histology-derived values. Secondly, to test the efficiency of the developed perfusion protocols as a better perfusion means more blood vessels are perfused with the contrast agent. Besides the PVN, an additional parameter was defined for testing the efficacy of the vascular perfusion protocols. This parameter was named the “relative vascular perfusion” (RVP) and was defined as a percentage of the PVN over the total number of blood vessels (TVN) (summation of filled and non-filled vessels) counted per square millimetre of tissue area ($RVP = PVN/TVN \times 100$).

In a histology section, the PVN can be measured manually by directly counting the filled vessels, or automatically using tools available for contrast-enhanced images within the ImageJ software. The automatic measurement of the PVN per area of tissue in a randomised histology view is explained in the following section.

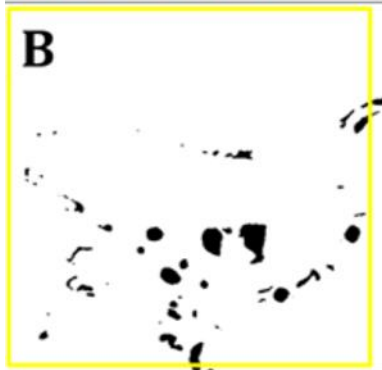
Automatic PVN measurement using ImageJ

After transferring the image (JPEG format) into ImageJ, the threshold was adjusted (87) to separate the perfused blood vessels from the background. The background noise was reduced using the 'analyse particles' tool by selecting the smallest pixel size to be removed and by applying the 'de-speckle' tool.

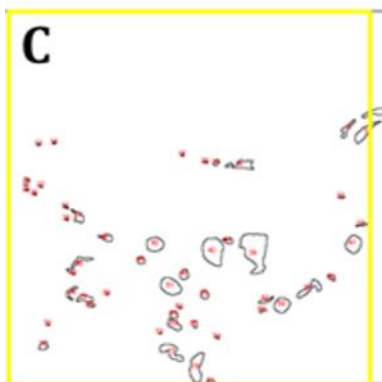
The image was then converted to a binary image to facilitate other image processing such as filling the partially filled vessels. The reason for this was to ensure that during de-speckling, partially filled small vessels were not removed from the image. If two or more blood vessels were attached to each other, they were separated using the 'watershed' tool for precise counting. The image was then converted to 'mask' and then the PVN counted using the 'analyse particles' tool (Figure 4-7).



Reading a randomly selected image in ImageJ. These non-perfused vessels (green arrows) and perfused vessels (red arrows) are shown.



The segmented perfused vessels are highlighted from the background using an adjusted threshold.



The quantified measurements of perfused vessels.

Figure 4-7: Counting the perfused vessel number using ImageJ.

The image processing techniques for counting the perfused blood vessels (orange arrows) are illustrated in the images A-C. **A:** H&E image shown using ImageJ which includes tissue structures, perfused blood vessels (red arrows) and non-perfused vessels (green arrows). Although the non-filled vessels are called here 'non-perfused vessels' for simplicity, there is a possibility that they may have been perfused earlier and the microfil has been washed away from the vessels due to extensive rinsing. As the microfil contrast agent within the blood vessels (black spots) has a higher intensity compared to the surrounding tissue, the blood vessels can be separated from the tissue structure. This was carried out by applying a threshold to the image to separate the perfused vessels from the background. The image was then converted to a binary image to show the blood vessels as black against a white background (**B**). The image processing continued for de-speckling to reduce the level of noise, filling the vessels that are partially filled and then separating those that are attached to each other. The image was then converted to 'mask' to facilitate quantification of the vessel number counted per total area using the 'analyse particle' tool (**C**). Although a general microfil shrinkage can be observed within the blood vessels, this may not affect the blood vessel count as even a small spot is taken into account.

Collecting correlated sections between micro-CT and histology

Correlated sections between micro-CT and histology results were needed for validating the PVN parameter. To confirm that correlated sections from biopsy samples were collected from the same regions, the first step was to find the variability in the biopsy length by averaging the height of the biopsy samples (biopsy length) between injured and non-injured hindlimbs. This was then followed by collecting the correlated sections from biopsy samples used for micro-CT and histological analysis (Figure 4-8).

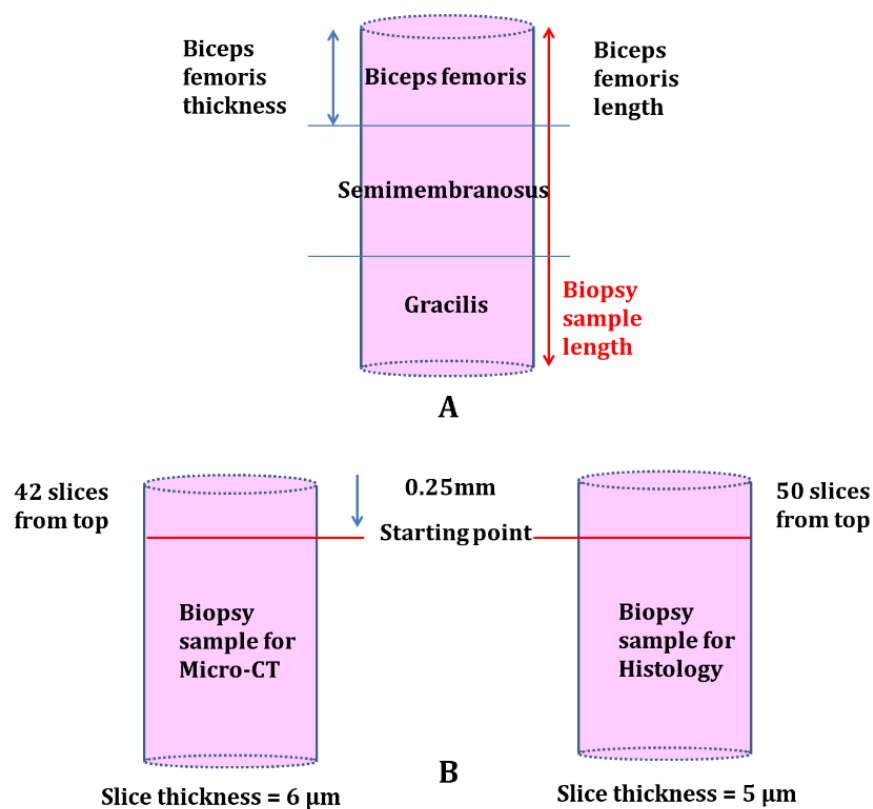


Figure 4-8: *Correlating the micro-CT and histological slices.*

Image (A) exhibits three main muscle compartments of a biopsy including biceps femoris on top, semimembranosus in the middle and gracilis at the bottom (See Figures 2-3 and 2-4). Image (B) depicts the starting point where the correlated sections have been taken from biopsy samples for both histology and micro-CT evaluations. The length of 0.25mm (250 μm) was discarded from the top of each sample to ensure the tissue sample filled the entire cross section of the image. This length was equivalent to 42 slices with a thickness of 6 μm ($250\mu\text{m}/6\mu\text{m}=42$ slices) for the micro-CT samples and 50 sections with a thickness of 5 μm for the histology biopsy samples. In this research, for the micro-CT quantification, 250 sequential digital slices were taken from the starting point where the biceps femoris was located.

Validation of the micro-CT using histology for producing the PVN

The PVN parameter determined by micro-CT was validated using histological assessments by calculating the PVN using ImageJ software between two correlated sections obtained from these two modalities (Figure 4-9).

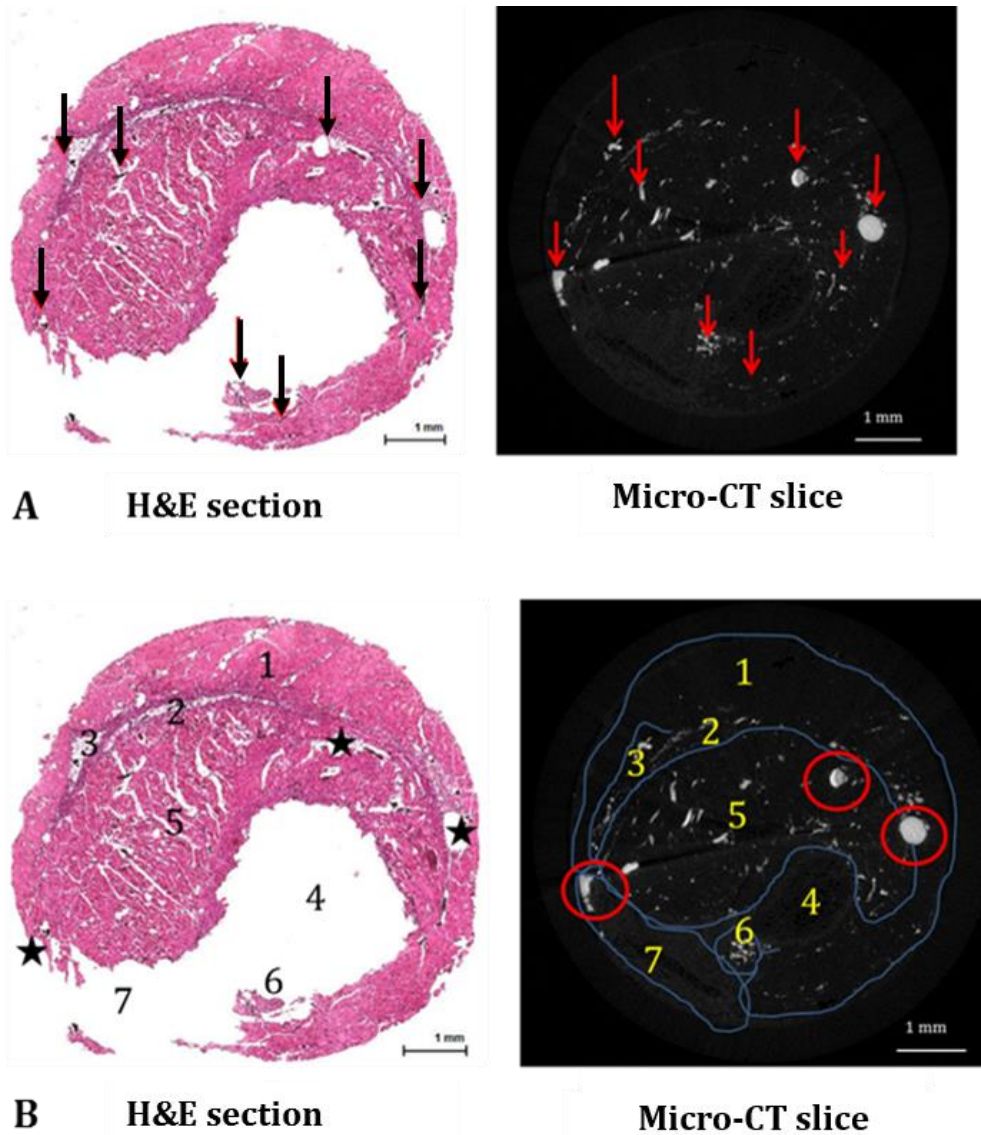


Figure 4-9: The correlated cross sections of a biopsy sample captured from micro-CT and histological analysis (H&E).

The correlated blood vessels (histology: black arrows and micro-CT: red arrows) (A) as well as the correlated locations of the muscle compartment which have been identified by numbers (B) are illustrated. In the H&E sections (B), the stars indicate a few blood vessels that were filled with microfil previously as they could be seen in the micro-CT slice (red circles). The microfil in these few vessels may have been washed away during the histological process.

4.2.5 Statistical analysis for the reproducibility and validity of the vascular injury model

As well as the general statistical analysis explained in 3-2-6, statistical approaches were applied for the quantitative validation of the vascular injury model following CSTT. These analyses were undertaken to verify the reproducibility of the characterised vascular injury model. The sensitivity of the vascular injury model to detect vascular morphometric changes was assessed based on the significant differences ($p < 0.05$) between the non-injured and injured hindlimbs where the mean values were compared using the two tailed Student's paired t-test for means. However, there are influencing parameters that may affect the p value such as sample size and variability in the data. Therefore, in these situations, utilising the effect size (ES) within the evaluated population can be useful. The ES is defined as the degree of a phenomenon occurrence within the evaluated population in which the null hypothesis can be rejected. The ES is a non-zero value in which a greater ES value will indicate a higher effect of a phenomenon within a population (Cohen 2013). The ES is calculated as the difference between two independent mean values of a parameter (e.g. the mean values of the injured and non-injured hindlimbs for vessel volume) divided by the average of the standard deviations given for two independent mean values. The ES is classified into three categories: small, medium, and large with given values of .20, .50, and .80 respectively representing the degree of effectiveness of a phenomenon or a method (Cohen 1992). For example, the effect size of 0.8 represents that a method or a phenomenon has been highly effective and the effect size of 0.2 shows a small effect.

In this research, the level of correlation and agreement between vascular morphometric parameters determined by micro-CT and histological techniques was validated according to the approaches described by Lee (Lee *et al.* 1989) and Bland-Altman (Bland *et al.* 1990) using ICC and the Bland-Altman plot. The coefficient of variation was also calculated to determine the reproducibility of the vascular injury model following CSTT.

The accuracy of the micro-CT based vascular injury model was also validated using histomorphometry to determine the correlation and agreement between the results obtained from these two independent modalities for producing the PVN parameter.

4.3 RESULTS

In the presentation of the results, the following colour coding has been used consistently in bar charts throughout this chapter:

Table 4-1: The colour coding and symbols used for presenting the results.

Colour coding	Translation
Red	The values for the injured hindlimbs
Blue	The values for the non-injured hindlimbs
Symbols	Translation
*	P values between injured and non-injured pairs ($p < 0.05$)
**	P values between injured and non-injured pairs ($p < 0.01$)
***	P values between injured and non-injured pairs ($p < 0.001$)

4.3.1 Characterisation of the vascular injury model

Using micro-CT analysis, the visualisation and characterisation of the vascular morphology changes following trauma are presented for the injured and non-injured hindlimbs (n=6) one day after trauma.

Visualisation of the total vascular architecture (ROI)

The 3D vascular anatomy was scanned at a resolution of 18 μm to visualise the perfused blood vessels located within the ROI of the hindlimbs where the length of the ROI was measured as 23.6 ± 0.9 mm based on the method described in 4.2.3. Well-perfused hindlimbs within micro-CT images were identified by observing the tree of vascular network including the major blood vessels. Perfused hindlimbs with only a few individual perfused vessels with microfil indicated a poor perfusion, which caused variability within the data.

The vascular network including the main arteries (e.g. arteria poplitea) could be visualised in the rat's hindlimb suggesting that the vascular perfusion protocols developed for perfusing the blood vessels with microfil contrast agent were optimally performed (Figure 4-10).

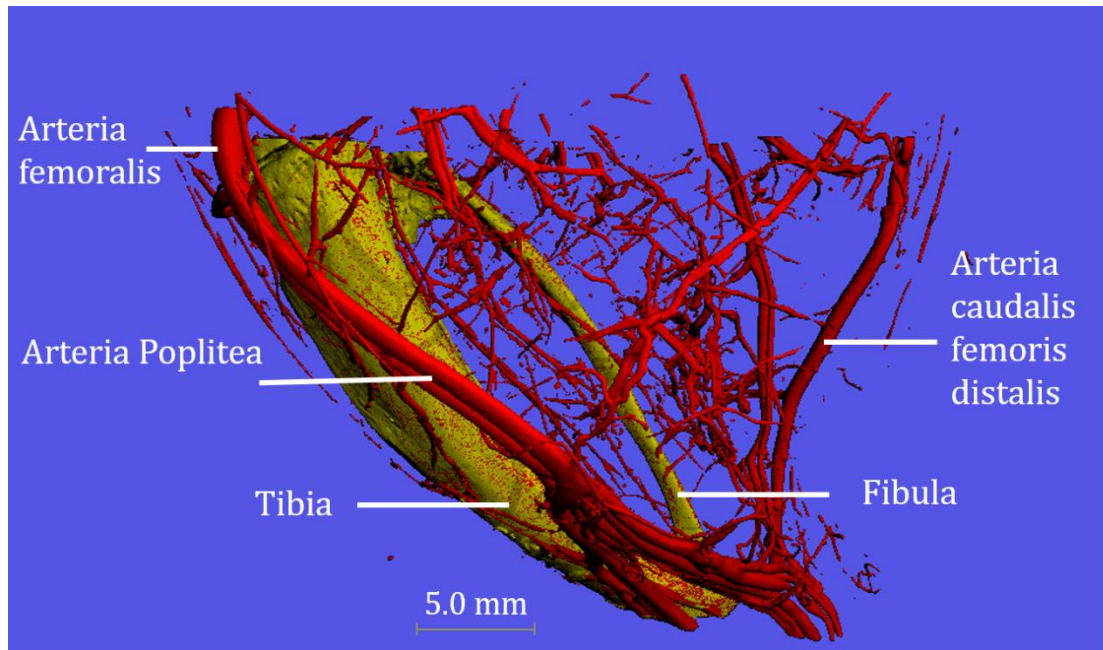


Figure 4-10: Micro-CT visualisation of the vascular network.

The 3D micro-CT reconstruction of the vascular network is shown for non-injured hindlimbs (medial view, voxel size: 18 μm). Three main arteries including the arteria femoralis, arteria poplitea, and arteria caudalis femoris distalis are highlighted.

The 3D reconstructed results of the ROI (Figure 4-11) obtained from six rats exhibited a satisfactory perfusion in most cases. However, there were a few cases (e.g. Figure 4-11-I) that showed a lower number of perfused vessels that may be due to a delay in perfusion. In the ROI evaluation, less perfused cases (e.g. Figures 4-11, I, J, K and L) caused a variation within the data and this effect could be observed in the non-injured hindlimb of one of these cases (Figure 4-11-I).

For this research, the values that caused variability within the data due to a known reason (e.g. experimental obstacles) were excluded after a quantitative assessment confirmed that their values were defined to be outliers. The data was then presented with and without these outlier values to investigate the effect of the excluded values on the final results.

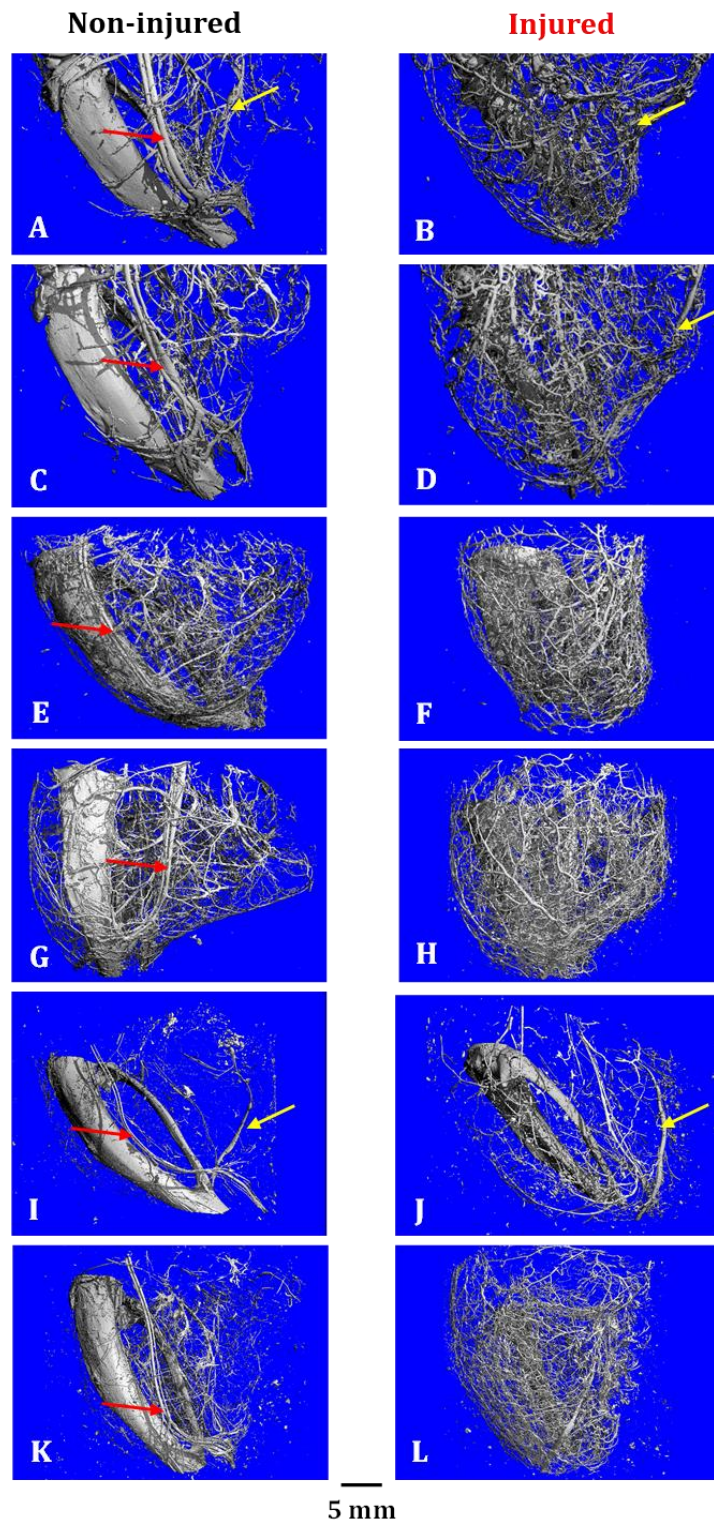


Figure 4-11: A 3D micro-CT visualisation of the vascular architecture. A 3D micro-CT visualisation of the vascular network is shown for the paired hindlimbs (ROIs) one day after CSTT (voxel size: $18\ \mu\text{m}$). A few identified major vessels including 'arteria poplitea' (red arrows) and 'arteria caudalis femoris distalis' (yellow arrows) are highlighted. Images I and K suggest there are less perfused vessels compared to the others. The results obtained from the injured hindlimbs appear to show more blood vessels compared to those from the non-injured hindlimbs.

The evaluation of Figure 4-11-I suggests that except for a few individual large vessels including 'arteria poplitea' and 'arteria caudalis femoris distalis', a connected vascular network can hardly be observed. In addition, while more blood vessels and the connected vascular network could be seen in Figure 4-11-K, the 'arteria caudalis femoris distalis' was barely visible. Although the injured hindlimbs of these cases indicated more blood vessels (e.g. Figure 4-11-L), during the exclusion process of these inconsistent cases, both non-injured and injured hindlimbs had to be removed since they were assessed as paired hindlimbs.

Overall, the 3D segmented results of the total vascular network within the ROI suggested that more blood vessels could be observed in the injured hindlimbs compared to the non-injured hindlimbs one day post trauma (Figure 4-11).

Quantification of total vessel volume obtained from ROI's

As explained, the total segmented volume (TSV) parameter was defined as the summation of bone volume (BV) and vessel volume (VV). By assuming that BV does not change over time as a result of injury or during healing, it was hypothesised that if the BV variation would be small enough among the samples, then the TSV may represent the VV changes. The comparisons between the extracted BV values obtained from injured and non-injured hindlimbs (using methods described in 4.2.3: Vascular segmentation for the ROI evaluation) showed no significant differences between these two groups with very small values for the coefficient of variation (Table 4-2). This indicates that the TSV variations represent the total vessel volume changes within the ROI model, as the BV variations are very small. Therefore, the mean value of the BV was calculated between the injured and non-injured hindlimbs and presented as one value $BV=297.6\pm 10$ (mm³) for comparisons with the TSV parameter (Figure 4-12). The absolute and normalised results are presented (scattered and Mean \pm SD) for the TSV captured from the ROIs of the injured and non-injured hindlimbs (Figure 4-13 and Appendix A-2).

In this research, six animals was used for the TSV analysis and four animals were utilised for the extracted BV values.

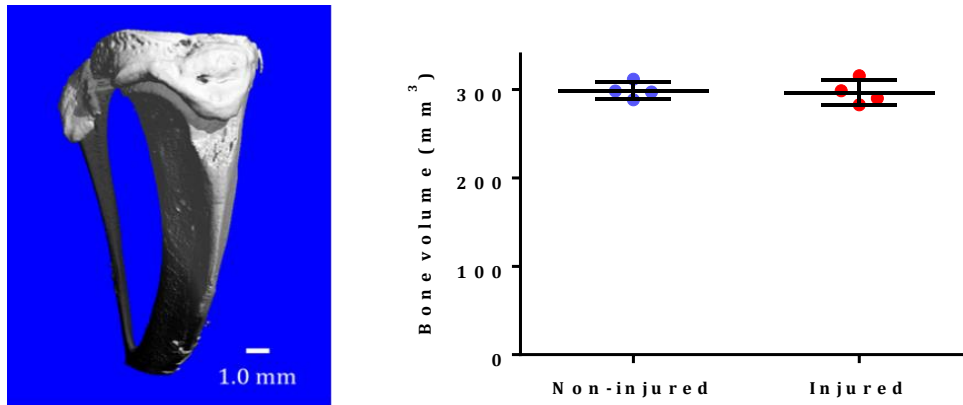


Figure 4-12: Bone volume evaluation.

The comparisons between the extracted BV values ($n=4$) obtained from injured and non-injured hindlimbs (ROI region) (showed no significant differences (Student paired t-test).

The averaged results obtained from original data indicated significantly higher TSV values for the injured hindlimbs compared to the non-injured hindlimbs (Figure 4-13-A). To investigate the changes between individual paired hindlimbs, the results are also exhibited as scattered data (Figure 4-13-B). A variability could be observed within the absolute TSV values as particularly two cases (5 and 6) (Figure 4-13-B) corresponded to Figures 4-11-I, J, K and L indicating lower values compared to the other hindlimbs. One possible way to reduce this variability was to present the data as normalised values (injured/non-injured $\times 100$) (Figure 4-13-C). The data obtained from the absolute values of the TSV indicated some variation for both non-injured and injured hindlimbs. After normalising the TSV data, the coefficient of variation reduced to an acceptable level suggesting that the normalised model is reproducible (Table 4-2). The data of the non-injured hindlimb of case 5 that was less perfused compared to other hindlimbs was assessed to detect whether this case met the quantitative criteria of an outlier value explained in 3.2.6. The investigation indicated that the TSV value of the non-injured hindlimb of case 5 (304.1 mm^3) was outside the defined band ($317\text{-}486.1 \text{ mm}^3$). Therefore, this case was excluded and the results of the five cases were evaluated.

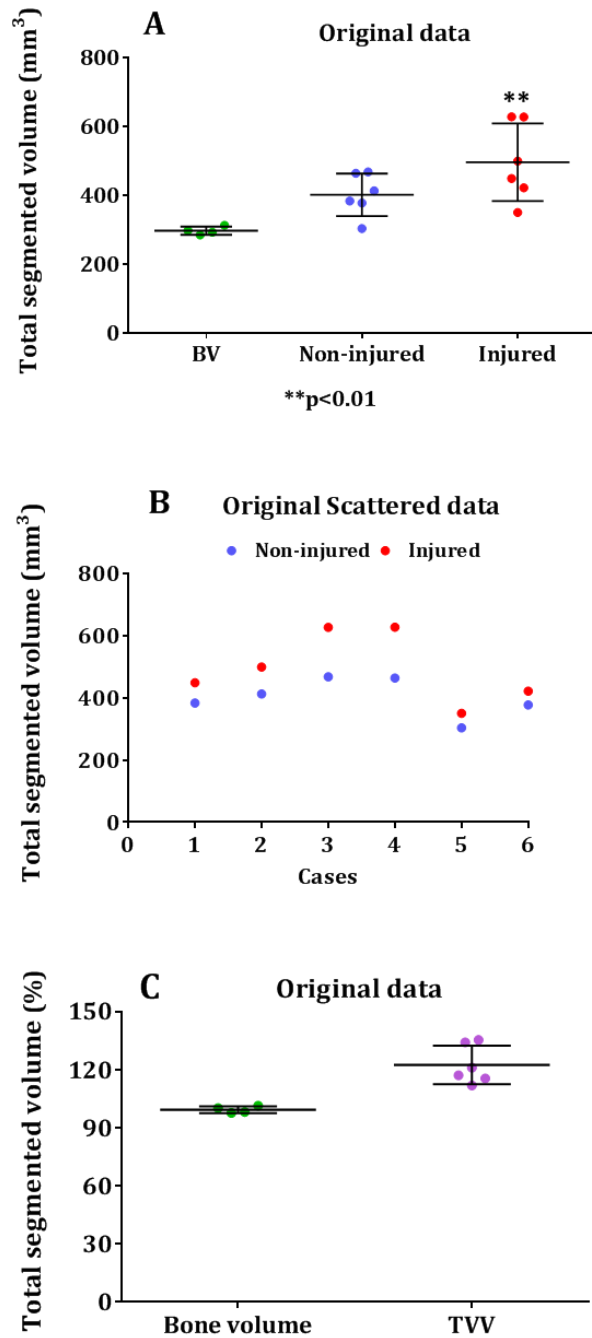


Figure 4-13: The quantitative analysis of the TSV.

The comparisons of the total segmented volume (TSV) results obtained from the ROIs at day 1 following CSTT are shown. The TSV results are presented ($n=6$) as absolute values (scattered data and Mean \pm SD) between the non-injured and injured hindlimbs (A) and (B) and normalised values (injured/non-injured \times 100) (C). The bone volume (BV, $n=4$) is illustrated as an average between the non-injured and injured hindlimbs. The TSV results suggest significantly higher values in the injured hindlimbs compared to the non-injured hindlimbs ($p < 0.01$, Student paired t-test) (A). Image C indicates that by normalising the injured data over non-injured values, the variability in the data has been reduced.

The normalised and absolute mean values of the TSV increased after the exclusion of the outlier values for the non-injured and injured hindlimbs respectively. In addition, after excluding the outlier value, lower CV values indicated that the variability within the data reduced (Table 4-2). This suggests that this method has reduced the error value since the non-injured hindlimbs represented an acceptable level of reproducibility after exclusion. The BV parameter with very small CV values indicated a good level of reproducibility. The TSV and VV showed to be reliable with acceptable CV values after normalising the data. The TSV were also exhibited acceptable CV values after exclusion of an outlier value (Table 4-2).

Table 4-2: The evaluation of the coefficient of variation (CV).

A comparison between the coefficient of variation (CV) obtained from the ROI is presented for the original and normalised data as well as the results with outlier excluded values collected from the BV, TSV and VV parameters.

CV (%) for the ROI	BV	TSV	VV
Original data			
Non-injured	2.7	13.9	53.73
Injured	4.1	20.7	51.7
Outlier excluded			
Non-injured	N/A	9.1	16.6
Injured	N/A	31.0	38.3
Normalised with no outliers			
(Injured/ Non-injured) × 100	1.5	7.4	8.5

The differences between the mean values and CVs obtained from the normalised data with and without an outlier value were not significant suggesting that normalising the data is a robust method for reducing the variability of the data. Overall, the TSV results suggest that CSTT has significantly induced a higher perfused volume in the ROI of the injured hindlimbs compared to the non-injured hindlimbs. As the BV variation was small, another alternative to this particular study was to subtract the mean BV from each TSV and present the remaining value as VV by assuming that the BV does not change over time (after one day).

The VV values indicated significantly higher values in the injured hindlimbs compared to the non-injured hindlimbs including the outlier value. After excluding the outlier value, the results showed less variability for the injured hindlimbs compared to the non-injured hindlimbs. The normalised VV results were $285.0 \pm 236.5\%$ and $179.4 \pm 15.3\%$ before and after the outlier value was excluded. The CV values also reduced after exclusion of the outlier value (Table 4-1). The normalised mean value results presented for the VV indicated significantly higher values compared to the normalised TSV mean values after omitting the outlier data (Figure 4-14).

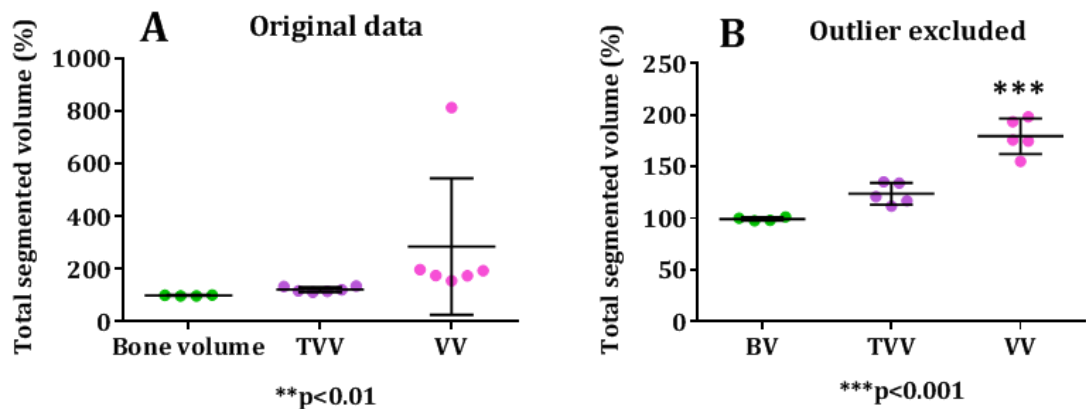


Figure 4-14: The comparisons between the total segmented volume (TSV) and vessel volume (VV).

The comparisons of results between the normalised values (Mean \pm SD) of the TSV and VV obtained from the ROIs at day 1 following CSTT are shown with (A, n=6) and without (B, n=5) the outlier value. The bone volume (BV, n=4) is illustrated as an average between the non-injured and injured hindlimbs. The VV results suggest significantly higher values compared to the TSV after excluding the outlier value (B, $p < 0.001$, Student t-test).

4.3.2 Microvascular injury visualisation (biopsies) using micro-CT

The 3D vascular network that was analysed at a high resolution of 6 μm obtained from biopsy samples indicated a highly detailed structure including capillaries (Figure 4-15) compared to the images obtained from the ROI with resolution 18 μm (Figure 4-11).

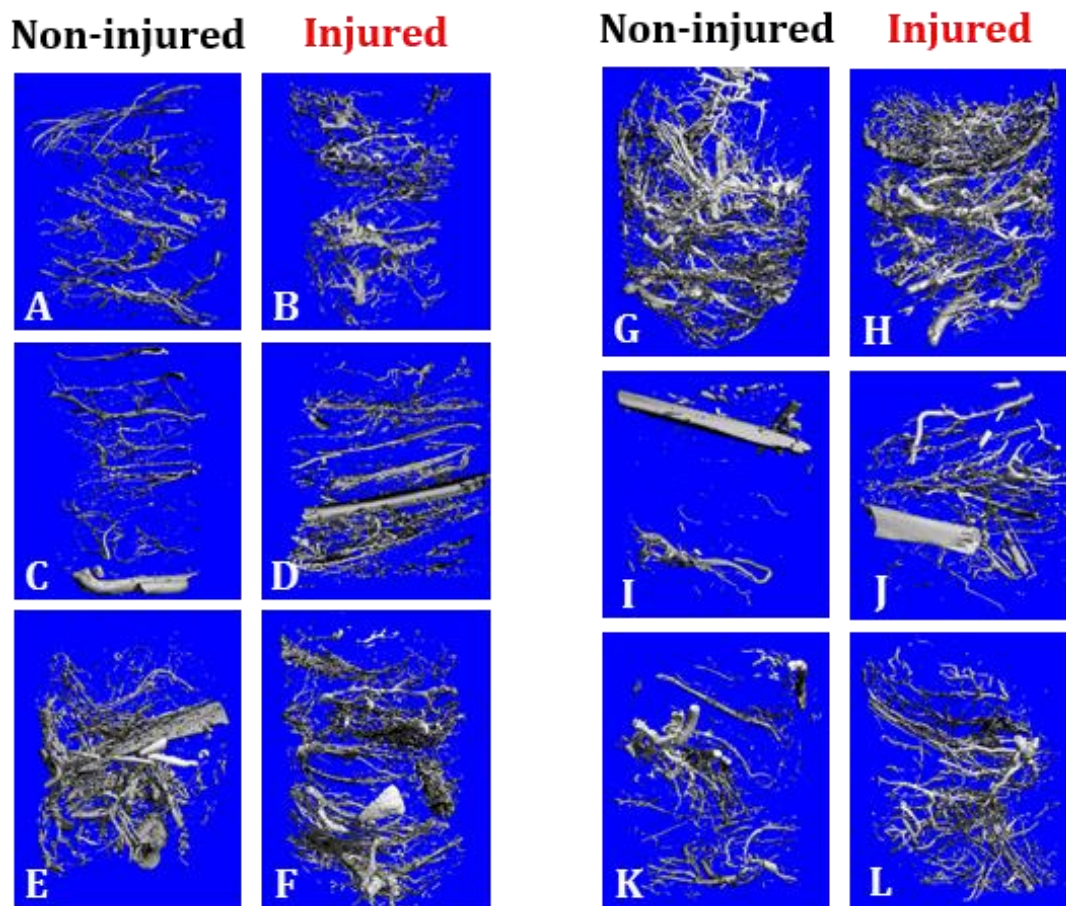


Figure 4-15: The microvascular visualisation obtained from biopsy samples. The visualisation of the microvascular structure obtained from 3D cylindrical biopsy samples (longitudinal view) using the micro-CT imaging system one day after trauma ($n=6$, voxel size: 6 μm). The left (A, B, C, D, E and F) and right (G, H, I, J, K and L) panels indicate paired hindlimbs of three cases which the left column of each panel (A, C, E and G, I, K) shows the non-injured hindlimbs and the right columns (B, D, F and H, J, L) exhibit the injured hindlimbs. Overall, the qualitative assessments suggested there were more blood vessels in the injured hindlimbs compared to the non-injured hindlimbs. However, Image I obtained from a non-injured biopsy indicates a lower number of captured blood vessels compared to other non-injured biopsy images.

4.3.3 Optimising the quantification by defining a cut-off diameter

In a few micro-CT images obtained from biopsy samples, a small number of large blood vessels were noticed that appeared to overshadow the results of these samples particularly for the VV and the VD parameters. Although the biopsy samples were collected in a defined manner, these large vessels randomly appeared in the micro-CT images. Large blood vessels observed in the biopsy images could also be identified in the corresponding 2D micro-CT slices (Figure 4-16). To reduce this effect, a method was developed as a possible way to remove the effect of the large blood vessels on the VV and VD results. To achieve this, a vessel diameter “cut-off point” was determined, whereby vessels with a diameter larger than this point were removed from the calculations.

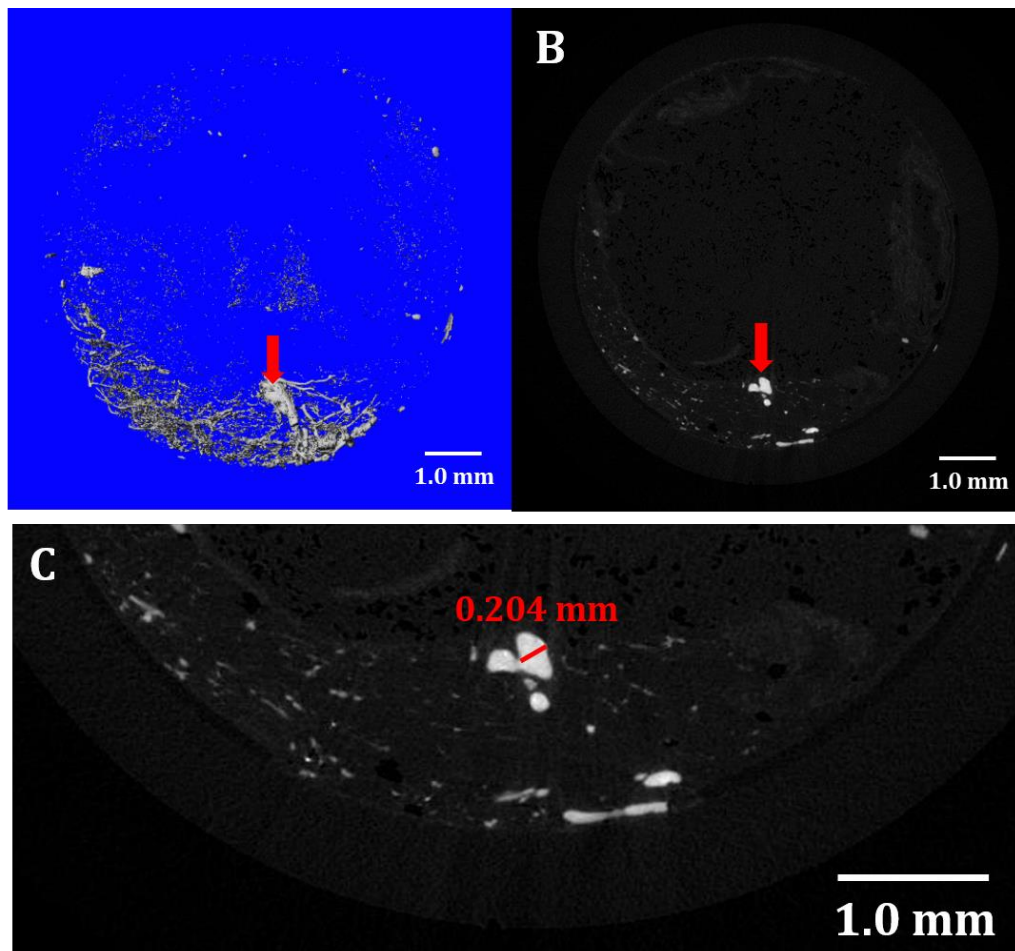


Figure 4-16: Identifying the largest blood vessels in the micro-CT images. This example shows a large blood vessel (red arrow) identified in a 3D biopsy image (A) and the corresponding vessel detected in a 2D micro-CT slice (voxel size: 6 μm) (B). The diameter of this vessel was 204 μm (C).

To find a suitable cut-off diameter, two criteria were addressed. One criterion was to determine an appropriate cut-off diameter where the vasculature below this point would indicate an acceptable coefficient of variation for the VD and VV parameters. Another criterion was to determine the techniques for recalculating the VD and VV after applying the cut-off method and removing the large vessels. The first stage to find a suitable cut-off diameter was to identify the diameter range of the large blood vessels. To determine this, histograms of the vessel diameter distributions versus their relative populations (blood vessels with given diameter as a percentage of entire blood vessel population) were plotted for the non-injured hindlimbs (Figures 4-18).

It should be pointed out that only the non-injured hindlimbs were taken into account for this evaluation, since the diameter of the blood vessels in the injured hindlimbs may have been affected by the injury (e.g. possible vasodilation).

For simplicity in analysis and comparisons, the vessel diameters of this particular histogram were divided into various categories: small, medium, large and very large vessels (Figure 4-17). For example, vessels with diameters ranging between 6-72 μm that accounted for more than half of the microvasculature population (54.5%) were categorised as “small” blood vessels. The diameter of 72 μm that was approximately in the middle of the frequency distribution was chosen as the midpoint diameter. The next group ranging between 72-144 μm ($72 \mu\text{m} \times 2 = 144 \mu\text{m}$) which accounted for 16.5% of the vascular population was categorised as medium sized blood vessels. The “large” vessels ranging between 144-216 μm ($72 \mu\text{m} \times 3 = 216 \mu\text{m}$) had a population of 13.8% and the “very large” vessels ranging between 216-294 μm had a population of 15.2%. This showed that the small and medium groups together contributed towards the majority of vasculature within the biopsy samples (71% of the vascular population) while the “large” and “very large” vessels together accounted for 29% of the population. The graph shows that the vessel population is skewed towards the small microvasculature.

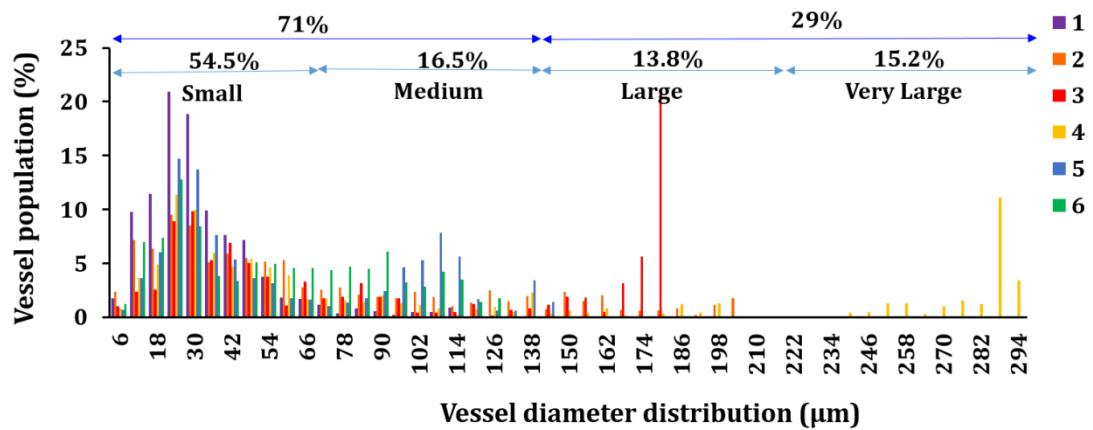


Figure 4-17: The vessel diameter distribution versus their population. The vessel diameter distribution plotted versus their population is shown for the non-injured hindlimbs (n=6) at day 1 post trauma (12 week old rats). The categories of the vessel diameters along with their populations are also exhibited.

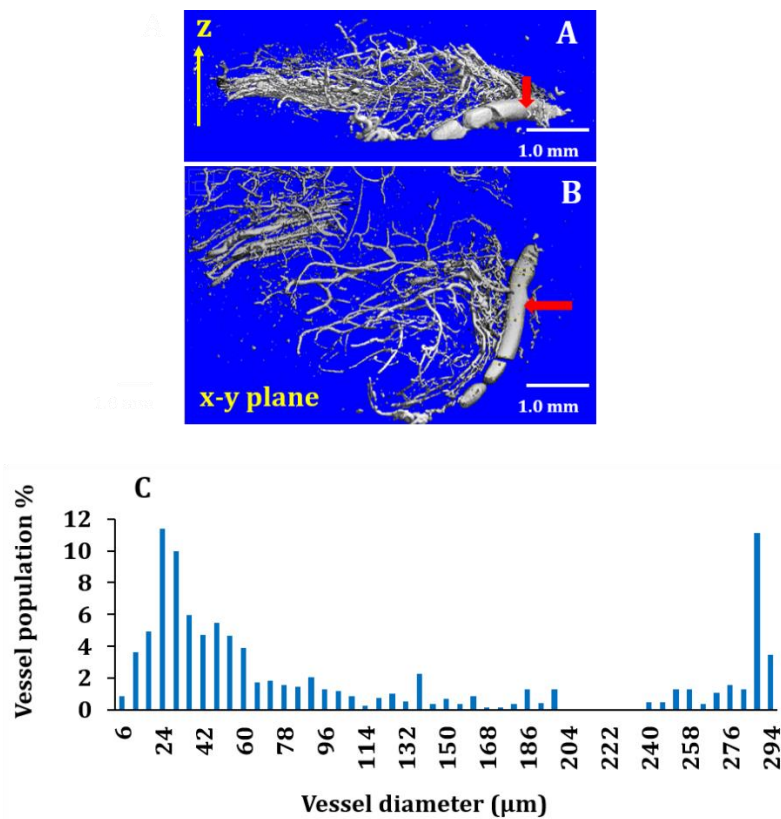


Figure 4-18: Identifying the largest blood vessels in the micro-CT images. An example of a biopsy stack (250 slices) exhibiting two 3D views of the vascular network in 'z' direction (A), x-y plane (B) and the corresponding histograms of the vessel diameter distributions versus their populations (C) (voxel size: 6 µm). The major segment of the largest blood vessel (red arrow) ranged between 240-294 µm that indicates that this vessel belongs to the category of very large blood vessels (216-294 µm). The images and the histogram show that this vessel has a small concentration within the biopsy stack compared to other vessel diameters.

After applying the cut-off technique and removal the values of the large blood vessels from the VV and VD, these parameters were required to be recalculated again to obtain their new values without large blood vessels. The recalculated VD distributions were obtained through the ‘weighted mean value’ of the VD distributions and given as:

$$X = \frac{\sum_{i=1}^n w_i x_i}{\sum_{i=1}^n w_i}$$

where X, is the weighted mean, x_i is each individual VD (bin diameter) in the distribution range and w_i is the non-negative weight. Here the ‘weight’ means a constant value representing the quantity of x_i within the distributed range. The VV parameter was also recalculated as the summation of the distributed voxel volumes above the cut-off diameter (Table 4-3).

Table 4-3: The recalculation methods for the VV and VD parameters. The micro-CT quantitative results obtained from a non-injured hindlimb one day after CSTT are shown.

A

Voxel size 0.006 (mm)			
Bin diameter (mm)	Bin counts	Bin volume (mm ³)	Bin population (n %)
0	0	0	0
0.006	11852	0.00256	0.59
0.012	57344	0.012386	2.853
0.018	74060	0.015997	3.685
0.024	179459	0.038763	8.928
0.030	185529	0.040074	9.23
0.036	122158	0.026386	6.077
0.042	123992	0.026782	6.169
0.048	156157	0.03373	7.769
0.054	89208	0.019269	4.438

Cut-off

↓
Total VV=Sum (bin volumes)

B

Voxel size 0.006 (mm)			
Bin diameter (mm)	Bin counts	Bin volume (mm ³)	Bin population (n %)
0	0	0	0
0.006	11852	0.00256	0.59
0.012	57344	0.012386	2.853
0.018	74060	0.015997	3.685
0.024	179459	0.038763	8.928
0.030	185529	0.040074	9.23
0.036	122158	0.026386	6.077
0.042	123992	0.026782	6.169
0.048	156157	0.03373	7.769
0.054	89208	0.019269	4.438

Cut-off

bin diameter × bin count ←

Sum (bin diameter × bin count) Sum (bin counts)

Total VD=sum (bin diameter × bin count)/sum (bin counts)

In Table 4-3, the 'bin' means vessel and 'bin diameter' shows the distribution of the vascular diameter ranges within the biopsy sample. The 'bin count' represents the frequency distribution of vessels within each diameter range and the 'bin volume' indicates the volume of the vessels in a diameter range within the biopsy sample. Based on these definitions, Table 4-3 shows the distribution of the vessel diameter (VD) ranges versus their corresponding count, volume, and population (%). This example shows the techniques for recalculating the total vessel volume (VV) and VD after applying the cut-off technique. The techniques for recalculating the VV (Table 4-3-A) and VD (Table 4-4-B) after applying the cut-off method are also explained.

Here, a suitable cut-off diameter was determined to be the largest vessel diameter (bin diameter) which was within an acceptable CV level ($CV < 10\%$) for the recalculated VD and VV parameters. Diameters larger than the cut-off diameter had a $CV > 10\%$.

In the example shown in Figure 4-17, various diameters were chosen from the defined categories. Since the category of small vessels had the highest population, more diameters were selected from this group. These diameters were 72 μm (the midpoint diameter and the diameter between the small and medium groups), 144 μm (the diameter between the medium and large groups), 216 μm (the diameter between the large and very large groups) and 294 μm (the largest diameter in the frequency distribution). Also, the two diameters of 50 μm and 100 μm were found from the literature (Bemelmans *et al.* 2009) to be within the microvascular range (the small category). In the frequency distribution (Figure 4-17), the closest diameters to 50 μm and 100 μm were 48 μm and 102 μm so these were selected. The diameter of 78 μm (the midpoint between 48 and 102 μm) was also used. The results of the recalculated VD and VV parameters obtained from six biopsy samples were compared at cut-off diameters 48 μm , 72 μm , 78 μm , 102 μm , 144 μm , 216 μm and 294 μm (Figures 4-19 and 4-20).

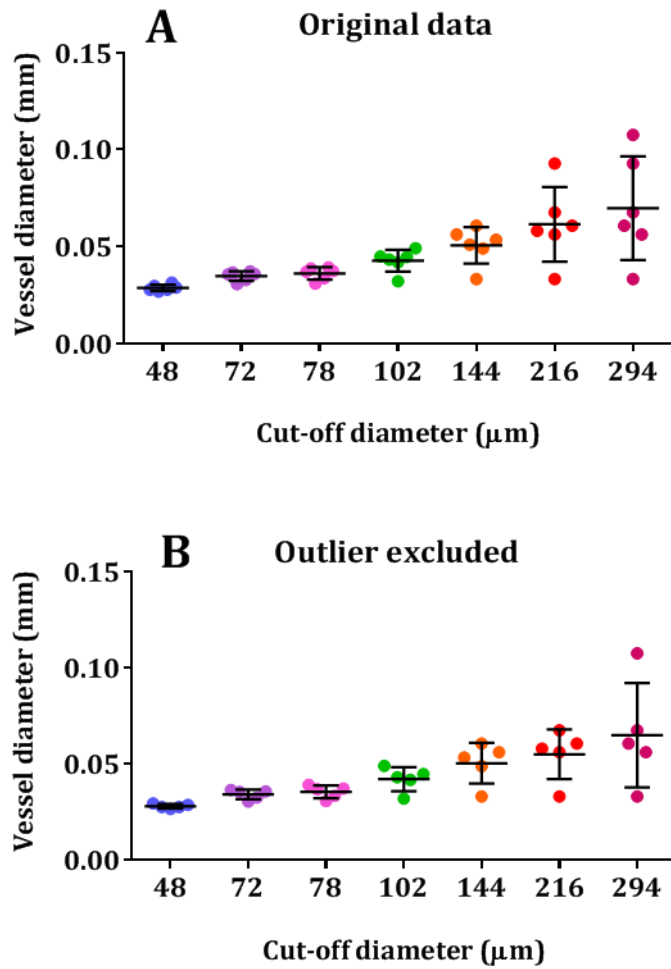


Figure 4-19: Determining the cut-off diameter for the vessel diameter (VD). The recalculated values for the vessel diameter (VD) parameter are illustrated with (A) and without (B) the outlier value at various cut-off diameters (Mean \pm SD) at day 1. The data suggests that the VD values less than 78 μm indicate considerably lower variations compared to the larger cut-off diameters and the exclusion of the outlier value has no significant effect on the reduction of the VD variations.

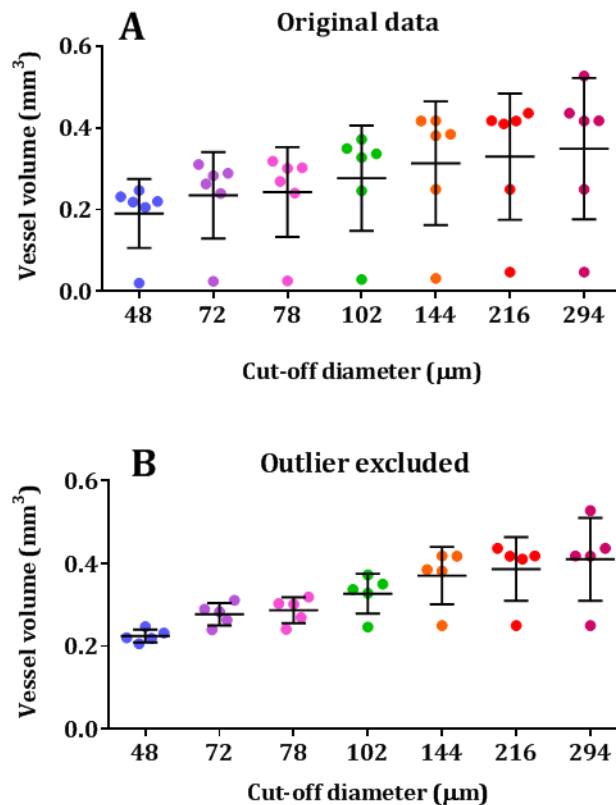


Figure 4-20: Determining the cut-off diameter for the vessel volume (VV). The recalculated values for the vessel volume (VV) parameter are shown for the original (A) and outlier excluded (B) data at various cut-off diameters (Mean \pm SD). The variability within the data has notably reduced after removal of the outlier value (B) particularly for the VV values less than 78 μm .

The results indicate that the VD parameter was not affected by the outlier value regarding the VV. Therefore, exclusion of this value did not have a significant effect on the VD. The cut-off point of 78 μm showed an acceptable level of variability before and after excluding the outlier value compared to other cut-off points and the cut-off diameters higher than 78 μm increased the CV values. While the mean values for the cut-off points at 144 μm and 216 μm showed very close values, the error was smaller at 144 μm (Figures 4-19 and 4-20, Table 4-4). As the cut-off results suggested that the diameter of 78 μm includes most vasculature with an acceptable CV for both VV and VD parameters (Figures 4-19 and 4-20, Table 4-4), this cut-off diameter was chosen to be used throughout this research. By selecting this cut-off diameter, the evaluations for the VV and VD were within the range of microvasculature with a population of 56%.

Table 4-4: Reproducibility of the VD and VV at various cut-off diameters.

A comparison between the coefficients of variation is presented comparing the original data to the results that exclude the outlier values at various cut-off diameters one day post trauma. Except for the original VV (real data), the cut-off points of 78 μm and under, showed an acceptable level of variability before and after excluding the outlier value.

CV for vascular parameters (%)	VV (Original)	VV (Outlier excluded)	VD (Original)	VD (Outlier excluded)
Cut-off diameter (μm)				
48	0.40	0.06	5.24	3.57
72	41.14	8.67	6.67	6.58
78	41.42	9.78	8.18	8.42
102	41.56	10.71	12.15	13.23
144	42.06	12.21	17.01	18.65
216	42.50	13.15	28.66	21.05
294	44.17	16.81	35.01	37.20

Also, the results indicated that except for the VV values presented for the microvasculature smaller than 48 μm with a small CV of 0.4%, the VV values obtained from other cut-off diameters indicated a high variability (CV > 10%). It appeared that the existence of an outlier value as well as the presence of large blood vessels have significantly influenced the variation of the VV data which resulted in high CV values. Although applying either the cut-off technique or excluding the outlier value reduced the CV for all vascular diameter ranges, the CV was still higher than 10%. Using the cut-off point of 78 μm along with excluding the outlier value reduced the CV to an acceptable level (CV < 10%) compared to other cut-off points. After this point, the CV showed higher values (CV > 10%). While the cut-off point of 144 μm and 216 μm reduced the variability within the data, the CV values were not within an acceptable level (CV < 10%). Although the VV mean values at the cut-off points 144 μm , 216 μm and 294 μm showed very close values, the error was smaller at 144 μm .

The suggested cut-off technique was applied to reduce the variations of the VV and VD results. These results were then compared to the VV and VD values given by the original data.

Since the VV and VD parameters were calculated independently from other vascular morphometric parameters (e.g. the VN), applying the cut-off point may not significantly affect the analysis of the other vascular morphometric parameters. The data showed that the effect of the outlier value was more notable on the VV compared to the VD. This may be due to the existence of various diameter ranges (bin sizes) distributed within the vascular network which has been taken into account for the calculation of the VD parameter. However, the VV is calculated as the summation of the voxels allocated to the to the diameter distribution (bins). Therefore, the count (weight) of these voxels is important as it allocates more volume of voxels within these bins.

Here, the cut-off diameter of 78 μm was obtained from the non-injured hindlimbs of 12-week-old rats at day 1 post trauma. To confirm whether the CV values obtained for the VV and VD remains in an acceptable range for other independent experimental groups after applying the cut-off point of 78 μm , the results attained from day 1 were compared with another independent group; the non-injured hindlimbs of 16 week old rats 28 days post injury (Figure 4-21). The results collected from the rats at day 28 verified an acceptable CV range for both VV and VD parameters using the cut-off diameter of 78 μm .

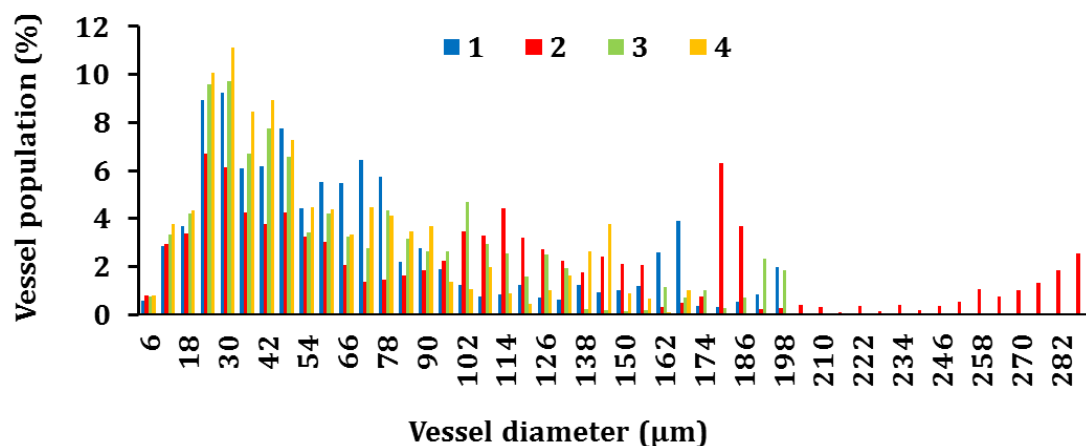


Figure 4-21: The frequency distribution of the vessel diameter at day 28. The vessel diameter distribution plotted versus their population is exhibited for the non-injured hindlimbs ($n=4$) at day 28 post trauma (16 week old rats). The graph shows that the vessels are skewed towards the small and medium size vessels (e.g. microvasculature less than 150 μm) with a higher population compared to the larger vessels.

The cut-off evaluation using this group of rats (16 week old at day 28) with no outlier value indicated that the maximum cut-off diameter could be increased to 120 μm for the VV and to 150 μm for the VD diameter (Figures 4-22 and 4-23, Table 4-5). Consistent with the cut-off diameter of 78 μm proposed for 12 week old rats at day 1, the results for the cut-off diameter of 78 μm obtained from the 28 day group exhibited an acceptable CV for the VV and the VD parameters (Table 4-5).

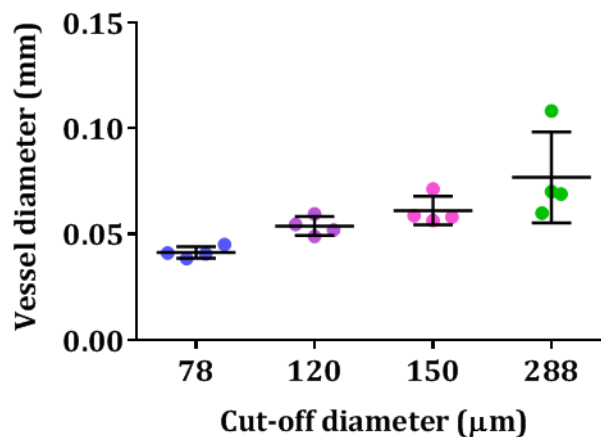


Figure 4-22: The recalculated vessel diameter (VD) at various cut-off diameters. The recalculated VD values are shown for the non-injured hindlimbs of 16-week-old rats at various cut-off diameters (Mean \pm SD) 28 days post trauma. The data suggests that the VD values less than 150 μm indicate considerably lower variation compared to the larger diameters (288 μm).

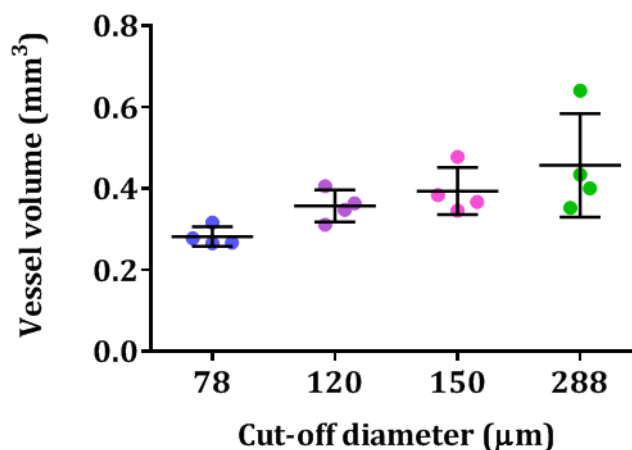


Figure 4-23: The recalculated vessel volume (VV) at various cut-off diameters. The recalculated values for the VV parameter are presented for the non-injured hindlimbs of 16 week old rats 28 days post trauma at various cut-off diameters (Mean \pm SD). The variability within the data increased for the cut-off diameters larger than 120 μm .

Table 4-5: Comparisons of coefficient of variations at various cut-off diameters. The values for the coefficient of variation are presented as a percentage for the original values of the vessel volume (VV) and vessel diameter (VD) parameters at various cut-off diameters at day 28 post trauma. The CV values were within an acceptable range (CV < 10%) for the cut-off diameter less than 120 μm for the VV and less than 150 μm for the VD.

CV for vascular parameters (%)	VV (original data)	VD (original data)
Cut-off diameter (μm)		
78	7.30	5.83
120	9.53	7.25
150	12.80	9.70
288	24.06	24.14

4.3.4 Quantification of microvascular morphometric parameters (biopsy)

The quantitative results for vascular morphometric parameters obtained from the biopsy samples including the vessel volume (VV), diameter (VD), number (VN), vessel space (VSp), connectivity density (VConn) and degree of anisotropy (DA) are presented (Figures 4-24 to 4-29 and Appendix A-3).

The vascular morphometric results obtained from biopsy evaluations suggest that CSTT induces notably higher values for the VV, VD and VConn in the injured hindlimbs compared to the non-injured hindlimbs one day after trauma. The CSTT effect was not significant for the VSp, VN and DA parameters although the VN was lower and the VSp was higher in the injured hindlimbs at day 1 post injury.

It appeared that case 5 of the non-injured hindlimbs was not well perfused compared to other hindlimbs and created outlier values for a few parameters including the VV, VN and VSp. For example, the VV variability was due to the presence of an outlier value that was quantitatively identified as being 0.05 mm^3 that was outside the qualifying band of 0.11-0.63 mm^3 based on the defined criteria (3.2.6) so was excluded. However, the variability of the VD parameter was due to the presence of large blood vessels.

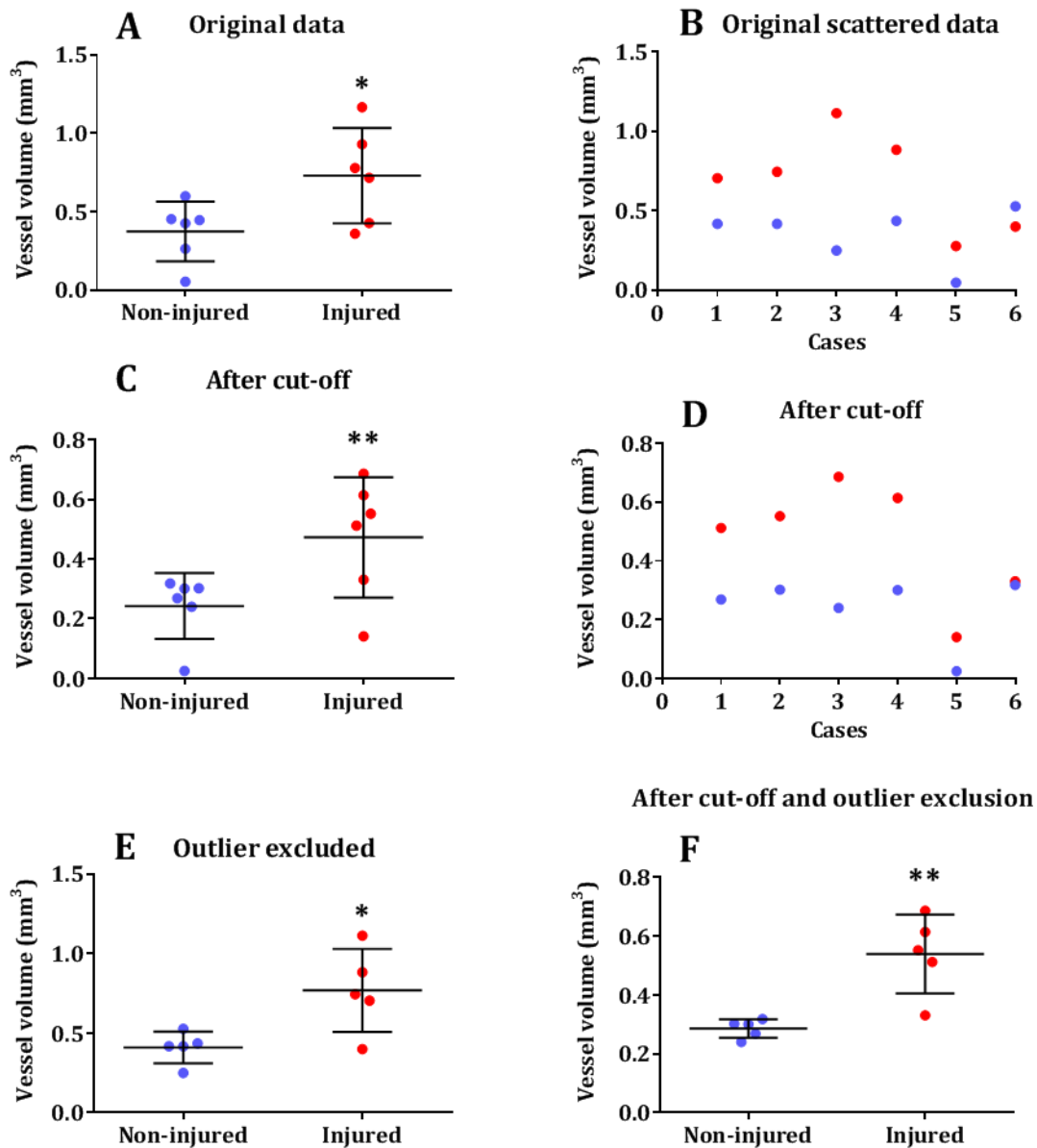


Figure 4-24: Comparisons for the vessel volume (VV) parameter.

The quantitative VV collected from biopsy samples ($n=6$) are presented for non-injured and injured hindlimbs one day after trauma. The original absolute values (Mean \pm SD) (A) as well as the corresponding scattered data (B) suggested significantly higher values for the injured hindlimbs compared to the non-injured hindlimbs ($p < 0.05$, paired Student t -test). The variability in the data that can be observed is due to an outlier value (case 5). The absolute VV values are also presented after applying the cut-off technique (Mean \pm SD) (C) and the corresponding scattered data is showing (D). This indicates that the VV values obtained from the vessel less than $78 \mu\text{m}$ exhibit significantly higher values for the injured hindlimbs compared to the non-injured hindlimbs ($p < 0.01$). After the exclusion of the outlier value from both the original (E) and the cut-off data (F), the variability notably reduced particularly for the non-injured hindlimbs. The results show that the variability of the VV reduced by removing the outlier value from the data while the injured hindlimbs still indicated significantly higher values compared to the non-injured hindlimbs.

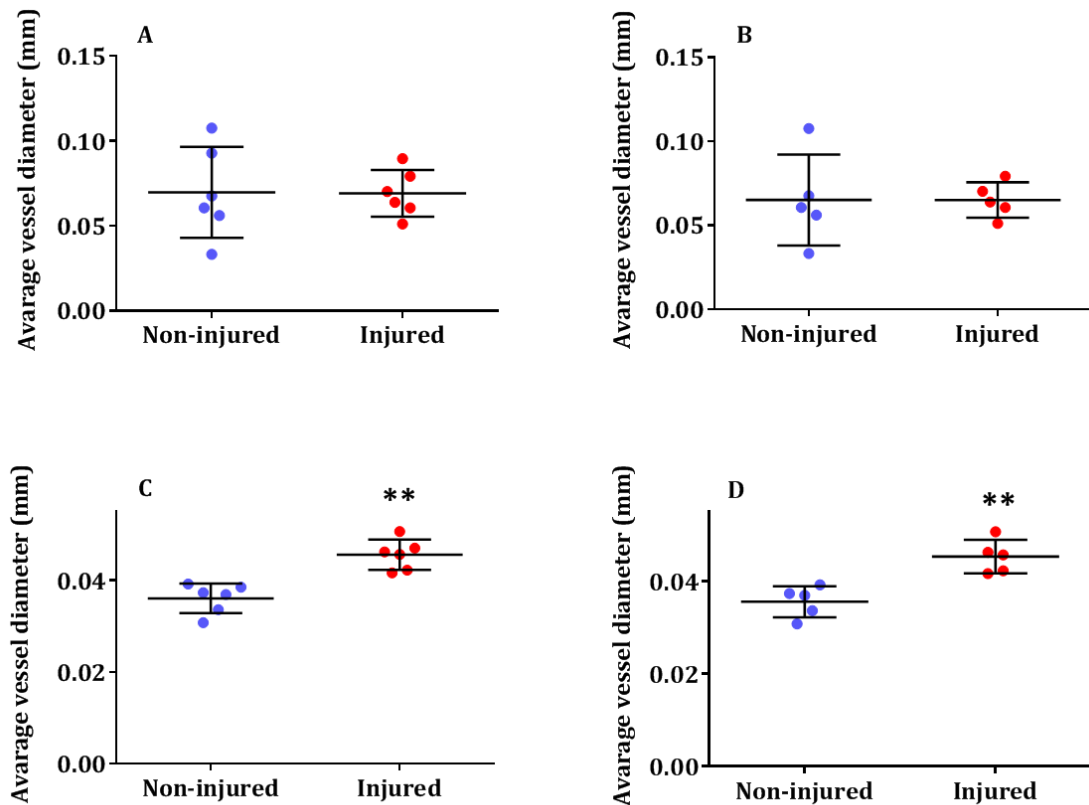


Figure 4-25: Comparisons for the vessel diameter (VD) parameter.

The quantitative VD obtained from biopsy samples ($n=6$) are shown for non-injured and injured hindlimbs one day after trauma. The absolute values for the VD collected from the original data (Mean \pm SD) (A) as well as the corresponding scattered data (B) suggested no significant differences between the non-injured and injured hindlimbs. The variability in the data can be observed particularly in the non-injured hindlimbs. The absolute VD values are also presented after applying the cut-off technique as (Mean \pm SD) (C) and the corresponding scattered data is showing (D). This indicates that the VD values obtained from the vessels less than 78 μm illustrate significantly higher values for the injured hindlimbs compared to the non-injured hindlimbs ($p < 0.01$, paired Student *t*-test). The data variability reduced considerably after applying the cut-off technique.

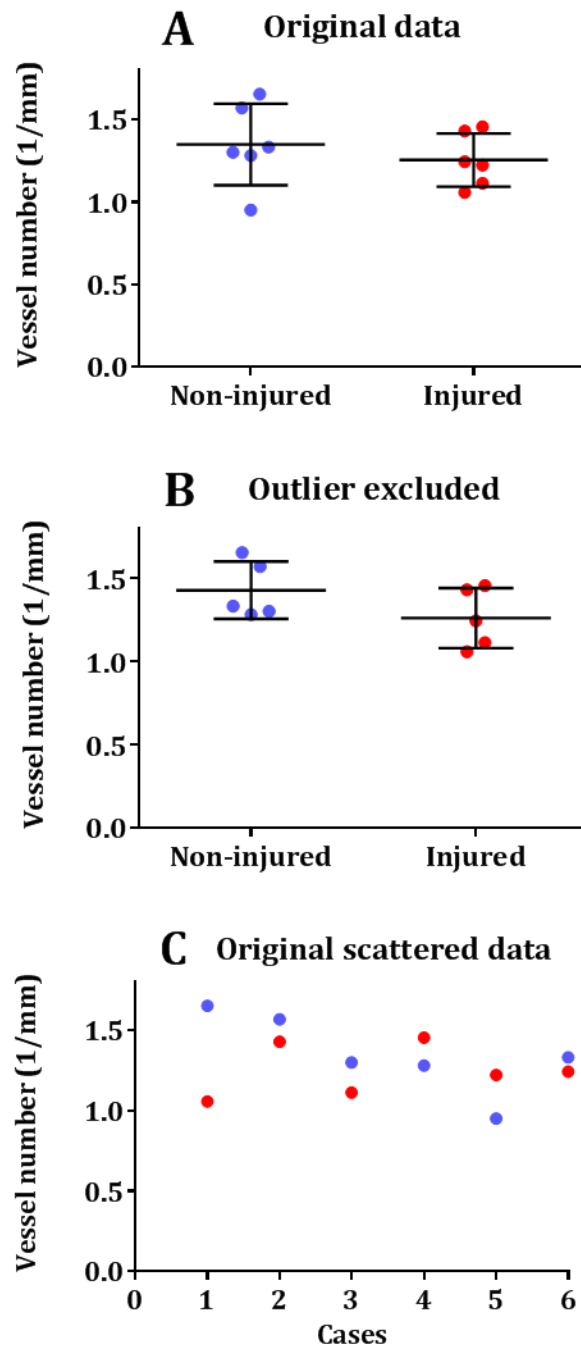


Figure 4-26: Comparisons for the vessel number (VN) parameter. The quantitative VN obtained from biopsy samples ($n=6$) is exhibited for non-injured and injured hindlimbs one day after trauma. The absolute values for the VN obtained from the original data (Mean \pm SD) (A) as well as the corresponding scattered data (C) showed lower values for the injured hindlimbs compared to the non-injured hindlimbs. The variability in the data reduced notably after excluding the outlier value (non-injured hindlimbs of case 5) from the original data ($p = 0.1$, $ES > 0.8$) (B).

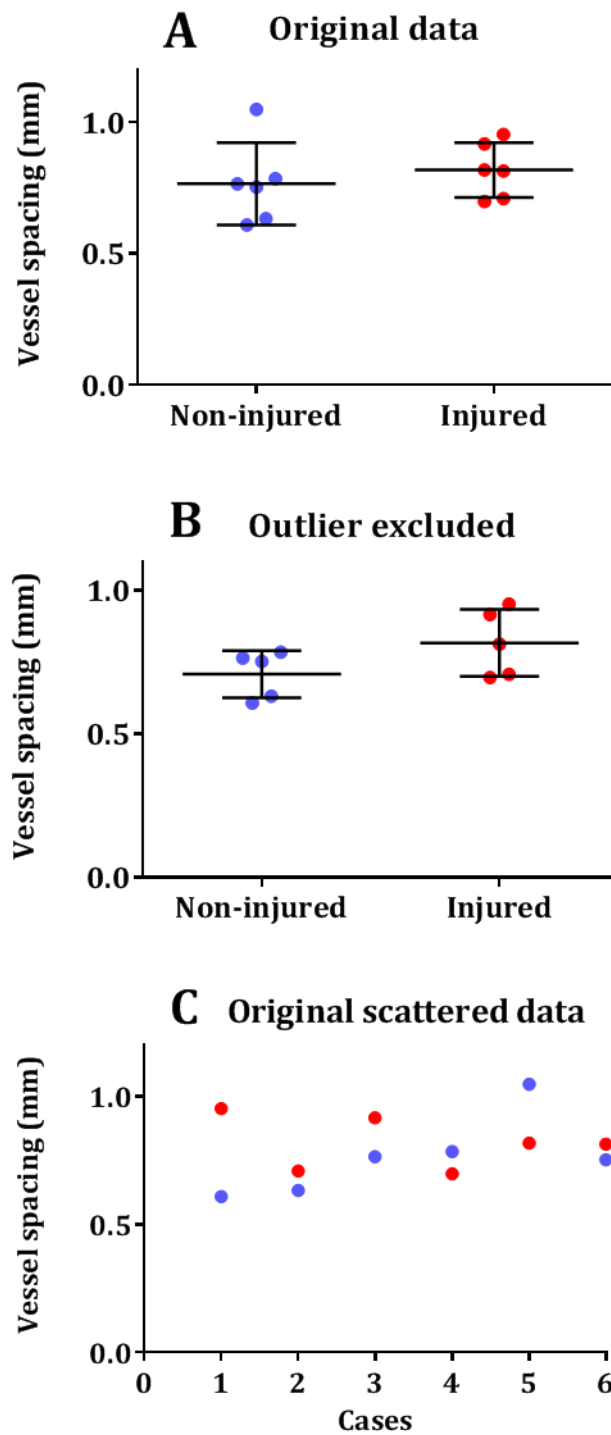


Figure 4-27: Comparisons for the vessel spacing (VSp) parameter. The quantitative VSp captured from biopsy samples ($n=6$) is illustrated for non-injured and injured hindlimbs one day after trauma. The absolute values ($n=6$) for the VSp obtained from the original data (Mean \pm SD) (A) as well as the corresponding scattered data (C) indicated no significant differences between the non-injured and injured hindlimbs ($p = 0.27$). The variability reduced notably after excluding the outlier value (the non-injured hindlimb of case 5) from the original data (B). The injured hindlimbs displayed higher VSp values compared to the non-injured hindlimbs after excluding the outlier value ($p = 0.098$).

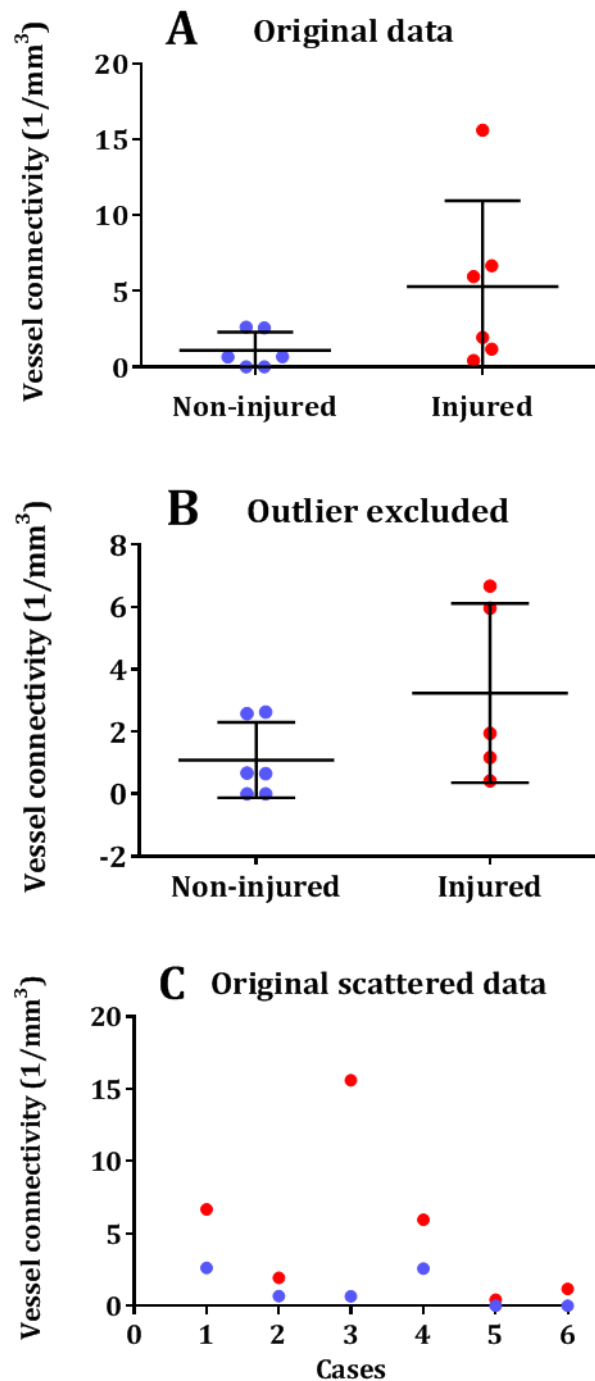


Figure 4-28: Comparisons for the vessel connectivity (VConn) parameter. The quantitative VConn collected from biopsy samples ($n=6$) is shown for non-injured and injured hindlimbs one day after trauma. The absolute values ($n=6$) for the VConn obtained from the original data (Mean \pm SD) (A) as well as the corresponding scattered data (C) suggested notably higher values for the injured hindlimbs compared to the non-injured hindlimbs ($p = 0.058$, effect size of 1.2) although this was not statistically significant. A high variability could be observed within the data obtained from both non-injured and injured hindlimbs. Here, the outlier value was a very well perfused hindlimb (case 3) rather than case 5 and by removing this value, the variability within the data reduced although this was not significant ($p = 0.062$) (B).

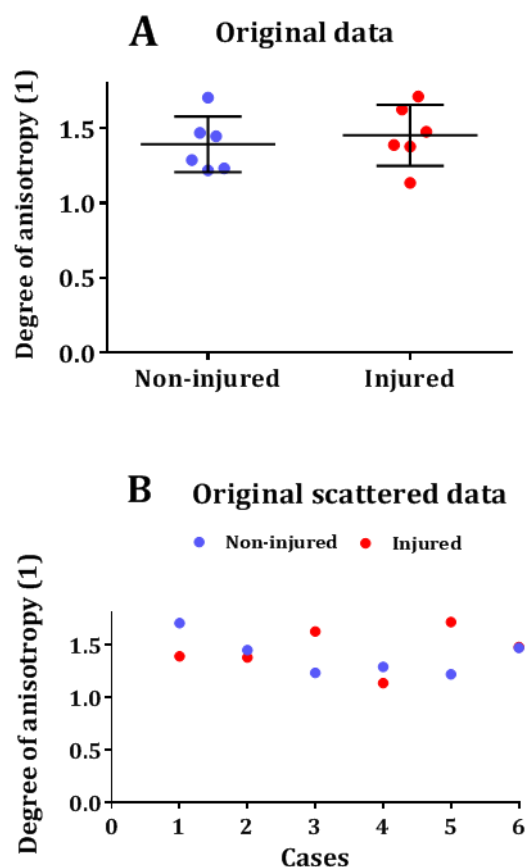


Figure 4-29: Comparisons for the vascular degree of anisotropy (DA) parameter. The quantitative DA captured from biopsy samples ($n=6$) is displayed for the non-injured and injured hindlimbs one day after trauma. The absolute values ($n=6$) for the DA obtained from the original data (Mean \pm SD) (A) as well as the corresponding scattered data (B) showed no significant differences ($p = 0.33$) between the non-injured and injured hindlimbs. The variability in the data was minimal for both non-injured and injured hindlimbs.

4.4 VERIFICATION AND VALIDATION

4.4.1 The reproducibility of the vascular injury model (biopsy)

In general, some variability was observed in the actual values of the vascular morphometric parameters obtained from the biopsy evaluation. After, data processing including the exclusion of outlier values and by using the cut-off technique, the variability was reduced. The CV values obtained from the original and processed data were computed for each vascular morphometric parameter and presented in Table 4-6.

For example, after data processing, the VV and VD indicated an acceptable level of reproducibility (defined in the terminology and applications section) with a CV of 9.7% and 8% respectively (Table 4-6). Removing outliers reduced the CV for parameters such as VN and VSp to 12% and 11.5% respectively. Normalising the data did not significantly reduce the variability of the results.

Table 4-6: The CV values for all vascular morphometric parameters. The acceptable values of the CV (red) as well as the values with small variation (blue) are shown.

CV (%)	Absolute values	Absolute values after outlier exclusion	Normalised values	Normalised values after outlier exclusion	Absolute values after cut-off	Absolute values after cut-off and exclusion
Parameter						
VV	46	24	71	58	41	9.7
VD	38	41	50	52	8	8
VN	18	12	21	17	N/A	N/A
VSp	20	11.5	22	19	N/A	N/A
VConn	110	92	144	169	N/A	N/A
DA	13	13	20	17	N/A	N/A

4.4.2 Perfusion of the smallest capillaries

One way to test the degree to which the vascular perfusion was successful, was to determine the smallest capillary diameter that could be filled with the contrast agent (microfil) (4.2.4). The smallest filled capillary that could be detected from the histology sections (n=10) had a diameter of approximately 2 μm , while the average diameter of the ten smallest filled vessels in each histological section was $2.96 \pm 0.57 \mu\text{m}$ (Figure 4-30). Considering that the smallest capillary diameter in a rat's hindlimb was reported to be in the order of 2 μm (Kano *et al.* 2000), this finding suggested that there is no minimum limit to the vessel diameter for a capillary to be filled by contrast agent.

Therefore, capillaries much smaller than the micro-CT resolution (6 μm) could be perfused using these methods.

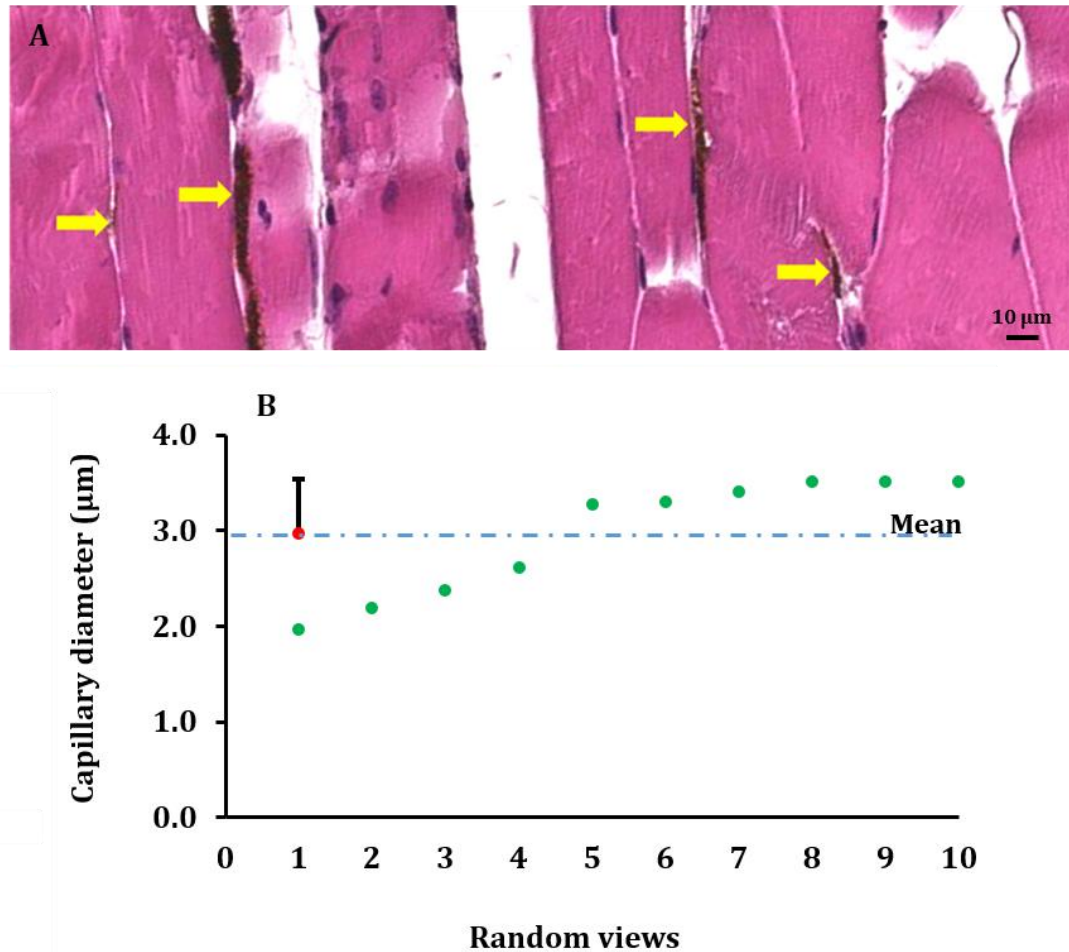


Figure 4-30: The smallest capillary filled with microfil contrast agent.

The assessment of finding the smallest capillary filled with microfil contrast agent to test the perfusability of the perfusion protocols. The capillary bed filled with microfil contrast agent (dark brown stain) captured from histological sections (haematoxylin and eosin staining) is shown with yellow arrows (A) within the random histology fields of view of the non-injured hindlimb tissue one day after CSTT. The individual diameter values of the smallest perfused capillaries with microfil contrast agent as well as the average value (Mean \pm SD) are presented per area of tissue (B). To determine the smallest capillary filled with microfil, the scattered data was sorted from smallest to largest.

Qualitative verification for the efficiency of the perfusion protocols

As well as being identified in the micro-CT images, the microfil-perfused blood vessels could also be identified in histology sections captured from biopsies (Figure 4-31).

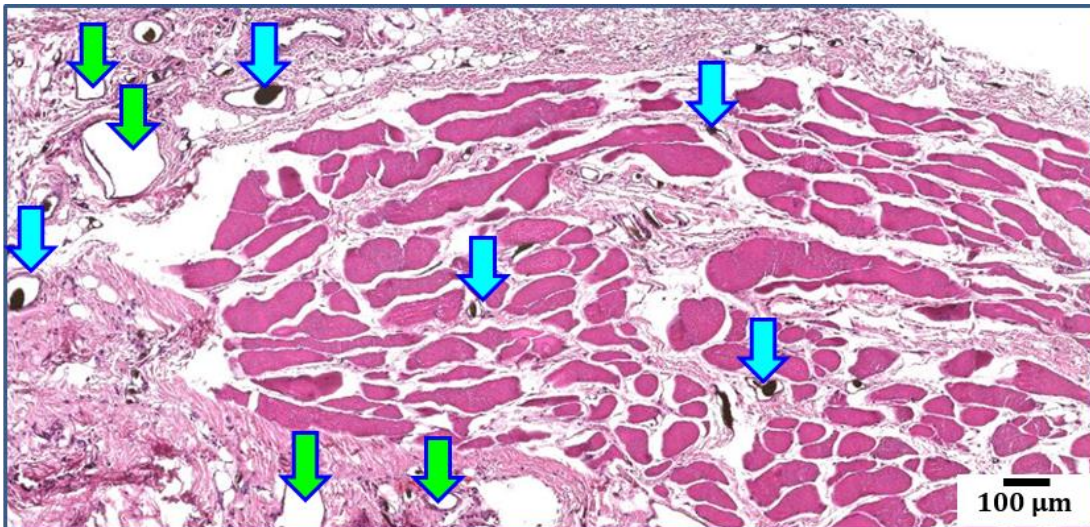


Figure 4-31: Perfused vessels with microfil in a histology image.
 An example of a histology image (haematoxylin and eosin) exhibiting the perfused vessels with microfil is presented from a non-injured hindlimb tissue one day after CSTT. This image indicates the perfused blood vessels (blue arrows) with the microfil contrast agent (dark brown/black spots) and non-perfused vessels (green arrows). The observation of perfused vessels qualitatively confirmed that the perfusion protocols were able to fill a large number of the blood vessels and the microfil could still be observed within the blood vessels after the histological process. However, a general shrinkage of the microfil contrast agent could be seen within all perfused blood vessels.

4.4.3 Validation of the micro-CT analysis using histology (biopsies)

Collecting correlated sections between micro-CT and histology

Correlated sections between micro-CT and histology modalities were needed for validating the PVN parameter. To ensure that correlated sections from biopsy samples were collected from the same regions, the average depths of the biopsy samples (biopsy length) between injured and non-injured hindlimbs was measured (Mean \pm SD) and compared (n=18). The calculated average depths of the biopsy samples were derived from the non-injured and injured hindlimbs and these were calculated as 10.92 ± 1.3 mm and 10.88 ± 1.3 mm respectively that were not significantly different (Figure 4-32).

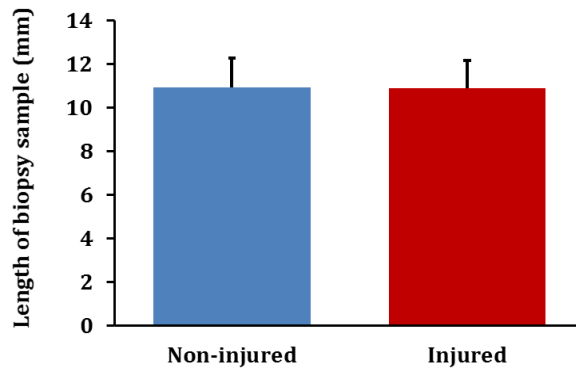


Figure 4-32: Evaluation of the length (depth) of the biopsy samples. The length comparisons between the mean values (Mean \pm SD) of biopsy samples (n=18) of the non-injured and injured hindlimbs has shown no significant difference between these two groups (Paired student t-test).

Quantitative validation between the micro-CT and histology

To ensure that the results of the perfused vessel number (PVN) per tissue area (mm²) obtained from biopsy samples using the micro-CT technique is correct, the PVN values were validated using histomorphometrical analysis by comparing the PVN results obtained from two modalities (Figure 4-33). The correlation and agreement between the micro-CT and histology for producing PVN were analysed using the Intra-class correlation coefficient (ICC) (Table 4-7) and the Bland-Altman plot (Figure 4-34).

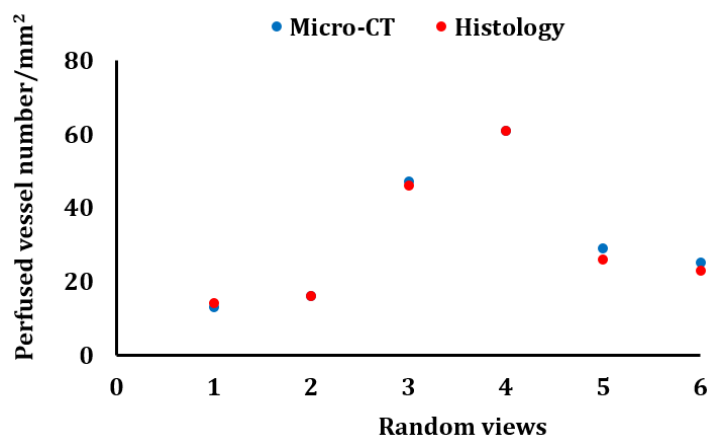


Figure 4-33: Validations between micro-CT and histomorphometry for the PVN. The comparisons between the individual values of the perfused vessel number per tissue area (PVN/mm²) as determined by the micro-CT imaging system and histomorphometry for six fields of view showed no significant difference between these two modalities ($p > 0.05$) (Student t-test).

Table 4-7: Validations between micro-CT and histomorphometry for the PVN.

The validation factors for the perfused vessel number (PVN/mm²) determined by micro-CT and histology (H&E). The two modalities have shown significant correlation ($p < 10E-5$) with a 95% confidence interval and an ICC value of 0.988 indicating the accuracy of these two modalities for the PVN parameter.

Modalities		Micro-CT and IHC				
Parameter	N	Mean ± SD (Micro-CT)	Mean ± SD (Histology)	ICC	CI _{95%} ICC	P
PVN /mm ²	6	31.8±17	31±16	0.998	0.988-1.0	<10E-5
Descriptions						
N	Sample size					
ICC	Intra-class correlation coefficient					
CI	Confidence Interval					
P	Significance level of correlation coefficient					

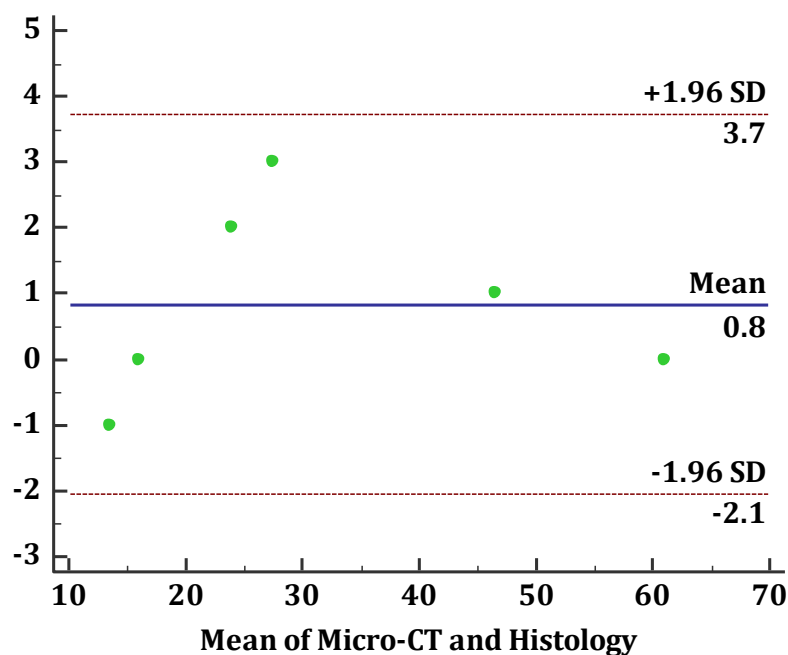


Figure 4-34: Validations between micro-CT and histomorphometry.

The Bland-Altman plot of differences between micro-CT measurements versus histology (H&E) for the perfused vessel number per tissue area (PVN/mm²) obtained from MedCalc software. The vertical axis shows the difference between the PVN values produced by micro-CT and histology. The horizontal axis exhibits the mean (0.8) of the individual measurements for the PVN produced by the two modalities. The blue solid line indicates the mean difference, and the red dashed lines show the 95% confidence intervals that have been defined as $1.96 \times SD$ confirming the level of agreement between the two techniques. All measurements have fallen between the two lines of agreement indicating a good level of agreement between these two modalities for producing the PVN.

4.4.4 Verification of the PVN and RVP using histomorphometry

To verify the VN results obtained from micro-CT using histomorphometry, the blood vessels perfused with microfil contrast agent were quantified in the histological sections obtained from biopsy samples. More blood vessels could be observed per tissue area in the injured regions at day 1 (Figure 4-35). The variation within the data points suggests that the distribution of the PVN was not uniform across the histology section.

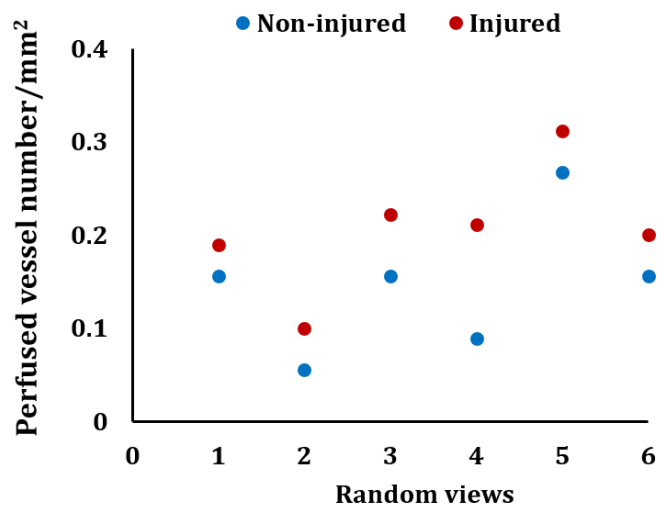


Figure 4-35: The perfused vessel number (PVN) from histological analysis. The individual PVN per tissue area (PVN/mm²) of two biopsy samples obtained from a rat's non-injured and injured hindlimb (six random histological fields of view for each biopsy sample). The results indicated higher PVN values for the injured hindlimbs compared to the non-injured hindlimbs one day after trauma.

In order to determine the efficiency of the developed perfusion protocols to fill the vasculature, we determined the “relative vascular perfusion” (RVP). This parameter was calculated as the percentage of the total number of blood vessels filled with contrast agent divided by the total number of blood vessels (filled and non-filled) counted per tissue area (mm²). The average RVP obtained from the analysis of six random views of one histological section revealed that $72 \pm 11\%$ (Mean \pm SD) of the vasculature within the non-injured hindlimbs could be perfused where the values were within a range of 55.6-89% (Figure 4-36). This suggests that the perfusion technique developed for this research successfully filled a majority of the blood vessels (72%) within the six field of views that

were perfused with the microfil contrast agent. In addition, the data suggests that the RVP distribution within one biopsy section is not uniform and there may be regions that are highly perfused (89%) compared to areas with a 33.4% reduction in the RVP (55.6%).

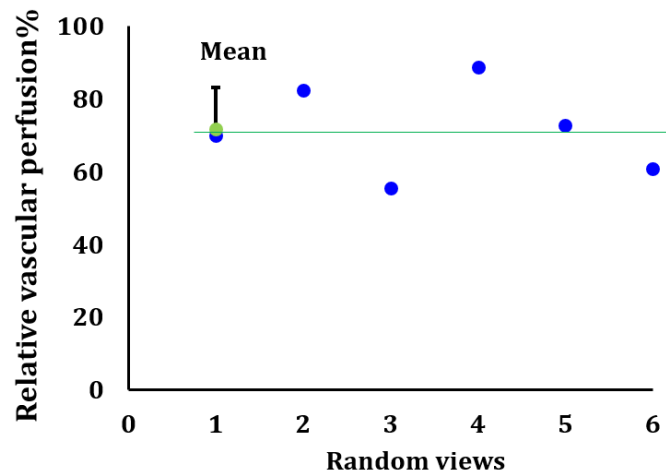


Figure 4-36: The relative vascular perfusion (RVP) parameter per tissue area (mm²).

The RVP parameter was defined for testing the efficiency of the developed perfusion protocols for filling the vasculature obtained from the non-injured hindlimbs. The RVP parameter was calculated as the percentage of the total number of blood vessels filled with contrast agent divided by the total number of blood vessels (filled and non-filled) counted within random field of views (n=6) of a histological biopsy section. The results suggest that the perfusion technique developed for this research was successful as the majority of the blood vessels with an average RVP of $72 \pm 11\%$ (Mean \pm SD) were perfused with the microfil contrast agent within the field of views where the values were within a range of 55.6-89%.

Verification of vasodilation using histomorphometry and the VD

The micro-CT results have suggested a significantly higher VD in the injured hindlimbs compared to the non-injured hindlimbs one day after trauma (Figures 4-24). The micro-CT results raised the hypothesis that at day 1, the higher VD in the injured hindlimbs may be due to vasodilation.

To verify this hypothesis, 10 micro-vessels with the largest diameters were measured within the histological sections (n=6 per group) of the non-injured and injured hindlimbs at day 1 (Figure 4-37, Appendix A-4).

The reason for choosing the largest vessels was because vasodilation is a mechanism that mainly occurs within the large blood vessels (Dodd *et al.* 1993, Williamson *et al.* 2004).

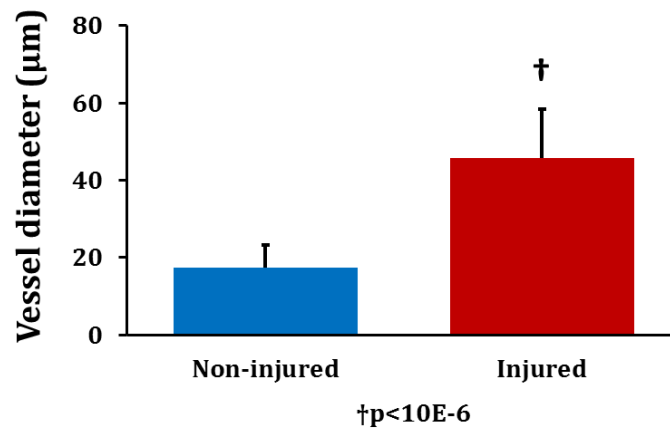


Figure 4-37: Vasodilation one day after trauma using histomorphometry.

The diameter of the 10 largest blood vessels (VD) captured from random views of histological sections (n=6) obtained from biopsy samples of the non-injured and injured hindlimbs of rats are presented (Mean \pm SD). These results suggest significantly higher VD values for the injured hindlimbs (2.6 times) compared to the non-injured hindlimbs ($p < 10E-6$) (Student t-test) that may be due to the effect of vasodilation.

4.4.5 Evaluation of the microfil shrinkage

During evaluation of the histological sections, a general shrinkage of the microfil contrast agent could be observed in all blood vessels (Figure 4-30). To quantify this shrinkage in the histology images, the microfil diameter (MD) filling the blood vessels was measured as well as the actual diameter of the corresponding perfused blood vessels (VD). The shrinkage percentage of the microfil was then calculated as $100 - MD/VD \times 100$ and presented versus the actual vessel diameter (Figure 4-38). The results indicated that regardless of the diameter of the blood vessel, shrinkage has occurred in all blood vessel diameter ranges and that the amount of shrinkage is not dependent on vessel diameter. This was confirmed through a comparison of different correlations, whereas all resulted in small R^2 values (linear correlation: $R^2 = 0.0202$; logarithmic: $R^2 = 0.0652$; power: $R^2 = 0.0493$; 2nd and 3rd order polynomials: $R^2 = 0.0618$ and $R^2 = 0.2813$, respectively).

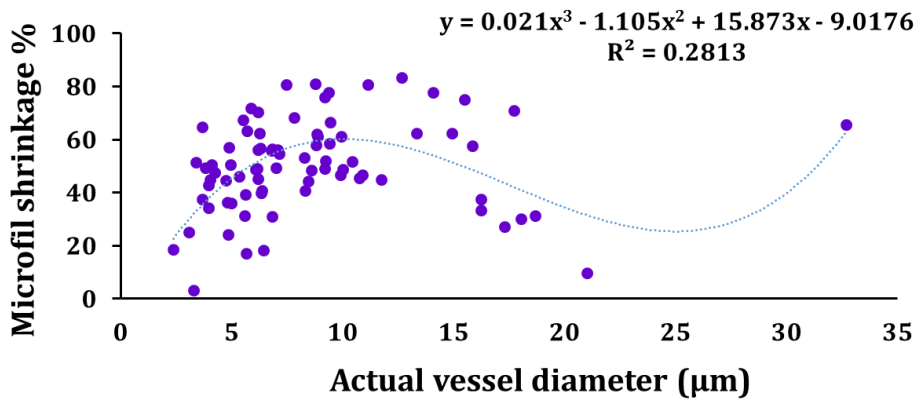


Figure 4-38: The microfil shrinkage.

The microfil shrinkage values (%) versus the actual vessel diameter (VD) for the non-injured hindlimbs is shown. Regression analysis has shown a small R^2 indicating no relationship between the VD and the microfil shrinkage.

4.5 DISCUSSION

Characterisation of the vascular morphology changes following CSTT

The characterisation of the vascular injury following CSTT was performed at two levels. One evaluation was taken from the ROIs that was defined to visualise the 3D vascular anatomy of the perfused blood vessels in the whole hindlimb where the CSTT was located. Another assessment was made from biopsies that were taken from the central areas of the CSTT and scanned with a higher resolution for a more detailed analysis of the vascular structure particularly at the capillary level.

In general, the 3D images of the vascular network captured from the ROI exhibited a satisfactory perfusion in most cases. The qualitative evaluation of the vascular architecture in both the ROI (Figure 4-11) and biopsy images (Figure 4-15) revealed notable changes in the vascular network suggesting more perfused blood vessels in the injured hindlimbs compared to the non-injured hindlimbs one day post trauma. The general vascular network including the main arteries (e.g. arteria poplitea) obtained from the ROI images were comparable with the anatomy of the blood vessels of a rat's hindlimb as presented in the literature (Duvall *et al.* 2004, Zhuang *et al.* 2006, Oses *et al.* 2009).

The 3D quantitative results for total segmented volume (TSV) obtained from the ROI has illustrated higher values in the injured hindlimbs compared to the non-injured hindlimbs one day following trauma. The TSV parameter is mainly comprised of the BV and only a small portion of VV. Therefore, since the BV variation was small, to highlight the volume changes of the vasculature, the VV was also analysed by subtracting the BV from the TSV. This was demonstrated by the small CV where it was assumed that the BV does not change over time (after one day).

Another, physical method to remove the bone from the samples, by decalcifying the bone using a mixture of formic acid and formalin has been reported previously (Nyangoga *et al.* 2011). However, due to the susceptibility of microfil to exposure of ethanol and solvents (resulting in shrinkage) we did not think this was a suitable option for our purposes.

The VV results also demonstrated significantly higher values for the injured hindlimbs compared to the non-injured hindlimbs. These results contradicted with the findings from a mouse ischemic model where the authors have indicated a reduction in the vessel volume of the injured hindlimbs one day after injury (Marks *et al.* 2013). The reason for differences between the findings of this research with those of Marks *et al.* 2013 may be explained through the fundamental differences between the CSTT and ischemia models. In ischemia models, the main vessel (arterial femoralis) which is responsible for the main VV is completely disconnected and is therefore no longer able to provide blood supply to regions more distally from the point of ligation. Therefore, until alternative vasculature has been developed that can compensate for the loss of perfusion capacity, a lower VV is expected after one day. In contrast, in a CSTT model, our results have shown that this vessel remains mostly intact and functional, therefore no immediate loss in perfusion capacity is expected.

In this research, the exclusion of an outlier value for the ROI evaluation was based on the quantitative assessment of the ROIs.

Potentially, poorly perfused hindlimbs including those with major blood vessels that have not been filled with microfil (e.g. arteria popliteal and arteria caudalis femoris distalis) can be suggested as another possible criterion for qualitative exclusion along with quantitative assessments.

In agreement with the ROI results, the biopsies have also shown a significantly higher VV in the injured hindlimbs compared to the non-injured hindlimbs one day after CSTT. This may be interpreted that the response of the vasculature to trauma was to increase the perfused vessel volume in the injured hindlimbs.

In general, the quantitative assessments of the biopsies suggest that the vascular morphology changes one day following CSTT. CSTT caused significantly higher values for the VV, VD and VConn in the injured hindlimbs compared to the non-injured hindlimbs one day after trauma. Although the CSTT effect was not statistically significant for the VSp, VN and DA parameters, the effect size was large for both VN and VSp after exclusion of the outlier value. The VN was lower and the VSp was higher in the injured hindlimbs at day 1 post injury as expected since the VSp is directly correlated to the inverse of the VN.

In agreement with the VN results, lower capillary density has been reported in the injured hindlimbs of a mouse ischemia model one day after injury (Couffinhal *et al.* 1998).

The changes to the VD derived from micro-CT images may be attributed to the effect of vasodilation one day after CSTT (Williamson *et al.* 2004). The vasodilation effect was confirmed at day 1 post injury by further histomorphological evaluation suggesting a statically significant increase in the VD values of the injured hindlimbs compared to the non-injured hindlimbs. This suggests that the vasodilation effect in the injured hindlimbs may have allowed a higher perfused volume (VV) through the vasculature of the injured hindlimbs.

Within a one day difference, a significant increase in the VD along with a notable decrease in the VSp have also been shown in the injured hindlimbs of a mouse ischemia model 2 days after injury (Nebuloni *et al.* 2014).

These findings aligned with the VD results and contradicted the VSp values presented for this research one day after CSTT.

The developed cut-off technique was found to be an effective method for reducing the variability caused by large blood vessels within the evaluation volume. Similar patterns of vascular diameter distributions shown in this study have been reported in the literature before, confirming a large proportion of blood vessels with diameters below 100µm (Boerckel *et al.* 2011, Uhrig *et al.* 2013).

It should be pointed out that there are other techniques available in the literature such as vascular corrosion casting for visualising the 3D of blood vessels. In this method, after replacing the vascular network with a polyurethane-based casting resin (e.g. PU4ii), the surrounding tissue is removed to reconstruct the vascular morphology (Krucker *et al.* 2006). However, since one of the goal of this project was to investigate the muscle injury, none of these technique could be used in this research as for the histological analysis, the muscle tissue was required to remain intact.

The reproducibility of the injured vascular model

The capability of the microfil enhanced micro-CT imaging system to characterise the vascular network morphology accurately and consistently has been demonstrated previously (Duvall *et al.* 2004, Bolland *et al.* 2008, Savai *et al.* 2009, Ehling *et al.* 2014). The reproducibility of the vascular injury model with two evaluation methods (ROI and biopsy) was tested. In general, both models indicated some degree of variability.

The CVs obtained from the mean absolute values presented for the TSV and VV indicated variability for both non-injured and injured hindlimbs. Normalising the data along with excluding the outlier value appeared to increase the level of reproducibility to an acceptable level for both TSV and VV within the ROI.

The vascular injury model obtained from the ROI evaluation was found to be reliable and presenting the results as normalised without outlier values was shown to be an effective measure to reduce inter-individual variability.

In addition, the evaluation of the vascular morphometric parameters captured from biopsies indicated a high reproducibility of the results after data processing including normalising, exclusion of outlier values and application of a cut-off technique, particularly for the parameters VV and VD, which had an acceptable coefficient of variation. While VN, VSp and DA indicated a small variation after data processing, the VConn parameter was highly variable even after data processing and therefore, may not be a reliable parameter for the characterisation of the vascular injury model.

Validation of the micro-CT accuracy using histomorphometry

The accuracy of the vascular injury model (biopsies) derived from micro-CT scans was validated based on the perfused vessel number (PVN) through qualitative and quantitative histology in the correlated regions. This was aligned with the literature where micro-CT has been acknowledged for producing accurate vessel number parameter through correlation with histomorphometric results (Savai et al. 2009, Boerckel et al. 2011, Ehling et al. 2014, Nebuloni et al. 2014). In this research, the PVN was validated as a common key parameter between micro-CT and histology because both modalities have independently showed higher PVN for the injured hindlimbs. The accuracy of the vascular injury model captured from biopsy samples was validated by demonstrating a significant correlation between micro-CT and histomorphometry for producing the PVN.

This validation was also confirmed by Bland–Altman’s limits of agreement indicating that the measurements have not been affected by systemic bias since there were no significant differences between the mean values obtained from micro-CT and histology for the PVN parameter, as it had been shown previously (Savai *et al.* 2009, Ehling *et al.* 2014, Nebuloni *et al.* 2014).

Verification of the perfusion protocols' efficiency

Qualitatively, the functionality of the perfusion protocols was verified for the vascular injury model (ROI and biopsy) through the identification of the vascular network in the micro-CT images.

The anatomy of the connected vascular network including the main arteries (e.g. arteria popliteal) could be also confirmed by comparison with corresponding reports in the literature (Duvall *et al.* 2004, Zhuang *et al.* 2006). The established perfusion protocols were able to fill the vascular network successfully so the changes between the injured and non-injured hindlimbs could be visually detected one day after trauma.

Quantitatively, the efficiency of the perfusion methods was confirmed using histological biopsy sections through two approaches. In the first approach, the “relative vascular perfusion” (RVP) was calculated to determine the perfusability of the microfil through the vascular network. The analysis of the RVP obtained from histomorphometrical assessments confirmed that the perfusion protocols developed for this research were successful to fill a majority of the blood vessels (72%) within the non-injured hindlimbs with the microfil contrast agent.

The second approach was to test the efficiency of the perfusion protocols by finding the smallest capillaries that could be filled with the contrast agent. In this research, the smallest capillary that could be detected as being filled with microfil contrast agent in the histology sections was approximately 2 µm in diameter. This was in agreement with the smallest capillary diameter of 2 µm from a range of 2-10 µm previously reported in rat's hindlimbs (Kano *et al.* 2000).

4.5.1 Limitation of the vascular injury model

In the development and characterisation of the vascular injury model following CSTT, limitations were found in both ROI and biopsy evaluations. In the ROI evaluation, extracting the bone from the surrounding vascular network appeared to be very time consuming and computationally extensive in practice.

Due to the large micro-CT file size (25-27 GB for each hindlimb) and lack of memory space within the micro-CT system, this technique was not found to be logistically feasible for this project.

Although 3D micro-CT images indicated a satisfactory perfusion for most of the blood vessels, there were a few cases that showed a lower number of perfused vessels compared to others. A reason for this was a delay in perfusion after euthanasia that may be due to blood sampling taken from the left ventricle that was conducted prior to starting the perfusion in some of the experiments. This experience showed that the time between euthanasia and perfusion is crucial and any delay in perfusion can cause a poor perfusion due to the blockage of blood vessels with blood clots.

In general, some variability could be observed in both ROI and biopsy assessments. One reason for this was the existence of an outlier value due to a delay in perfusion. However, by excluding the outlier value, the results improved particularly for the VV. While normalising the results appeared to be useful for reducing the variability, there were cases (e.g. VConn) which were irresponsive to this technique and consequently could not be represented as reproducible values. A small sample size can be another reason that makes the model sensitive to any variation. While collecting the biopsy samples was conducted in a defined and reproducible manner, large blood vessels within the biopsy samples were randomly captured.

For a better evaluation of the microvasculature, the assessment of either more slices, whole biopsy samples or the completely affected muscle component (e.g. biceps femoris muscle) is required. However, this was technically not possible due to limitations in memory size and computing power of our micro-CT system, which prevented the quantitative analysis of larger volumes. Furthermore, the vascular injury model developed was restricted due to a general shrinkage of the microfil contrast agent that was observed in all blood vessels during microscopic evaluation of histological sections. The investigation for the comparisons between the diameter of the correlated blood vessels obtained from the micro-CT (microfil diameter) and histology sections (actual vessel diameter) showed a considerable shrinkage of the microfil.

Therefore, the vessel diameter parameter may not be accurately represented in the micro-CT scans, and consequently other parameters related to the VD will be affected (e.g. absolute values of the VV). However, there are vascular morphometric parameters such as PVN, RVP, VConn and DA that are independent from the VD and therefore, are not being influenced by the microfil shrinkage. In addition, the VSp parameter obtained from the non-injured hindlimbs at day 1 indicated that this parameter is 10.9 times larger than the VD. Consequently, the VSp parameter may not be significantly affected by the VD variations that are too small compared to the VSp and therefore, the shrinkage effect on the VSp is negligible.

Finally, further analysis revealed that the microfil shrinkage has occurred in all diameter ranges of the blood vessels independent of the vessel size. Therefore, the comparison results of this research were presented as normalised values to reduce the effect of the microfil shrinkage on the findings.

4.5.2 Concluding remarks

Overall, by establishing the perfusion and micro-CT protocols, the vascular injury model following CSTT was developed and characterised to fulfil one of the aims of this research. The developed vascular injury model showed the ability to detect the changes to the vascular morphometric parameters following CSTT one day after trauma. This was confirmed through sensitivity tests to identify the differences between the injured and non-injured hindlimbs post trauma. Through histomorphometrical analysis and data processing, the reproducibility of this model was confirmed.

As discussed in 4.1, based on the literature (Duvall *et al.* 2004), it was hypothesised that the vascular morphology changes following CSTT and this leads to a reduction of these parameters within the injured hindlimbs one day after injury. The results of this research confirmed the changes to the morphology of the vascular network one day after CSTT.

However, the findings of this research suggests that the values of a few parameters such as VV, VD and VConn increased following CSTT which contradicted the results of similar vascular morphometric parameters reported for an ischemia model (Duvall *et al.* 2004).

It was expected that this model would be able to distinguish the vascular morphometric changes over a longer period of time following CSTT and during treatments. Therefore, the next step was to apply the developed methods and the results of the vascular injury model to a therapeutic modality (e.g. cryotherapy). This was conducted to test the sensitivity of the model for identifying the changes to the anatomy of the vascular network in response to treatment at various time points that are explained in Chapter 5.

Chapter 5: The effect of cryotherapy on CSTT and injured vasculature

5.1 INTRODUCTION

In the previous chapter, it was demonstrated that contrast-enhanced micro-CT imaging is capable of detecting differences in the vascular network architecture one day following CSTT. The findings from the literature review performed in Chapter 2 (Duvall *et al.* 2004, Oses *et al.* 2009) and also results presented in Chapter 4 raised a question whether the changes to the vascular morphology shown one day after CSTT will continue during the healing period, and whether a treatment will affect these changes?

Therefore, it was hypothesised that the vascular morphology changes after CSTT during the healing period and during treatment. To confirm this hypothesis and to determine whether the developed methods for the vascular injury model would be sensitive enough to detect differences in the effect of treatment modalities, the model was tested using cryotherapy for two reasons. Firstly, this technique has been acknowledged in the literature (2.6.1) as the most commonly used therapy for CSTT treatment (Smith *et al.* 1993, Smith *et al.* 1994, Deal *et al.* 2002, Schaser *et al.* 2006, Swenson *et al.* 2007). Secondly, controversies exist regarding the effect of cryotherapy on CSTT healing (Takagi *et al.* 2011) (2.6.2).

Therefore, the aim was to investigate the effect of CSTT and cryotherapy on the vascular morphology over time in rats using contrast-enhanced micro-CT imaging.

5.2 METHODOLOGY AND STUDY DESIGN

5.2.1 Sample size analysis

The sample size was calculated for this research based on the equation below where 'n' is the sample size, Z_{α} is a constant based on the α error (e.g. for error of 5%, Z_{α} is 1.65), $Z_{1-\beta}$ is also a constant depending on the power of the study (e.g. for a power of 95%, $Z_{1-\beta}$ is 1.64), σ is the estimated standard deviation and $\mu_0 - \mu$ is the mean difference (effect size) between the known mean value (μ_0) and the estimated mean value (Kadam *et al.* 2010, Rosner 2010).

$$n = \frac{2(z_{\alpha} + z_{1-\beta})^2 \times \sigma^2}{(\mu_0 - \mu)^2} \quad (5-1)$$

For example, the sample size for the ratio of the TSV/TV (%) parameter with the known mean value of 1.2 from the literature (Oses *et al.* 2009) and the estimated mean value of 1.9 ± 0.3 (non-injured hindlimb in the ROI) gives a sample size of 4.

$$n = \frac{2(1.65 + 1.64)^2 \times (0.3)^2}{(1.2 - 1.9)^2} = 3.9 \approx 4$$

Consequently, for micro-CT quantifications including the ROI and biopsy evaluations the sample size of $n=4$ was chosen. Also, the sample size of $n=2$ was determined for verification purposes of the micro-CT results using histological analysis. Therefore, in this study, the sample size of $n=6$ was applied per group at each time point (Moding *et al.* , Melnyk *et al.* 2008).

5.2.2 Animal preparation and treatment groups

For this research, 54 male Wistar rats (12 weeks) from the Animal Resources Centre, Canning Vale, WA, Australia were used. The experimental groups contained a pre-injury group (control group: $n=6$, day 0) and two post-injury groups which were randomly divided into sham and icing groups ($n=6$ per time point, time points 1, 3, 7 and 28 days).

Except for the control group, all rats were anaesthetised and impacted to induce a standardized and reproducible CSTT and vascular injury on the left hindlimbs within the ROI (e.g. biceps femoris) using an impact device (3.2.3).

In the icing group, cryotherapy was applied onto the CSTT region based on the methodologies described in the literature (Zemke *et al.* 1998, Jutte *et al.* 2001, Takagi *et al.* 2011). Cryotherapy was carried out five minutes after the impact injury was induced while the rats were still anaesthetised. A cylindrical ice block (5-cm diameter) was created, by freezing water in a paper cup, and was gently applied without compression where the only pressure was the weight of the ice block. The ice block was applied for one session to the skin's surface surrounding the CSTT for 20 minutes in a circular motion to ensure that ice block covered the entire injured region.

In the sham group, a 50-ml flat-bottomed beaker comparable with the ice block was gently applied to the injury area without compression where the only pressure was the weight of the beaker. The beaker was applied at room temperature for 20 minutes in the same manner as the ice block to simulate the icing method with no cooling. The control group and also the non-injured hindlimbs of both sham and icing groups received no injury or treatment.

Animals were euthanized at days 0 (n=6, uninjured control group), 1, 3, 7, and 28 (n=6 for each time point and treatment). For a three-dimensional vascular morphological assessment, the blood vessels of euthanised rats were flushed with heparinised saline and then perfused with the microfil contrast agent using two peristaltic pumps (4.2.2).

After perfusion, both hindlimbs were dissected, and then the injured and non-injured hindlimbs were imaged using a micro-CT scanner for quantifying the vascular morphometric parameters including TSV, VV, VD, VSp, VN, VConn and DA (4.2.3). The biopsies were then analysed histologically to confirm the results derived from contrast-enhanced micro-CT imaging (4.2.4). For this study, the histological processes including the section preparation and H&E staining were carried out based on the methods described in 3.2.5.

Since the developed vascular injury model indicated vasodilation in the injured hindlimbs one day after trauma, the effect of icing on the diameter of the blood vessels following CSTT was also investigated. The VD was measured one day after trauma in both sham and icing groups and then compared according to the histomorphometrical analysis. The PVN parameter was also measured within the histological sections using the histomorphometrical technique (4.2.4) as an indication of angiogenesis and presented as the Mean \pm SD for both sham and icing groups at different time points.

Qualitative CSTT assessments

The CSTT was qualitatively evaluated by taking photographs of the skin before and after dissection using a digital camera (Sony, DSLR-A330). The epidermis and subcutaneous sides of the skin as well as muscles including the biceps femoris and gracilis surfaces were assessed for signs of injury and presented for all time points.

5.2.3 Statistical analysis

The statistical approaches applied for this study have already been explained in 3.2.6 and 4.3.5. In addition to these statistical techniques, one-way analysis of variance (ANOVA) was used for comparisons of each vascular morphometric parameter across the time points. ANOVA analysis was followed by a post-hoc test called the Fisher's Least Significant Difference (LSD) to identify the significant differences across the five time points for each parameter within the different groups.

The differences between the two treatment groups (sham and icing) were analysed using a two-tailed Student T-test assuming equal variances. The sensitivity of the vascular injury model to detect vascular morphometric changes was assessed based on the significant differences ($p < 0.05$) between the sham and icing groups over time.

5.3 RESULTS

The table below shows the colour coding that was used for presenting the quantitative results of this research.

Table 5-1: The colour coding and symbols used for presenting the results.

Colour coding	Translation
Pink	The values for the sham group
Blue	The values for the icing group
Green	The values for the control group
Symbols	Translation
*	P values between the sham and icing groups ($p < 0.05$)
**	P values between the sham and icing groups ($p < 0.01$)
***	P values between the sham and icing groups ($p < 0.001$)
+	P values between the sham and icing groups ($p < 0.0001$)

5.3.1 CSTT qualitative and quantitative assessment

Observation of the epidermis and subcutaneous sides of the skin

The observations of the skin surface (epidermis side) showed no obvious haematoma in either sham or icing groups for all time points. Since the appearance of the skin's surface for all hindlimbs was similar, only one example is exhibited here (Figure 5-1).



Figure 5-1: Skin evaluation.

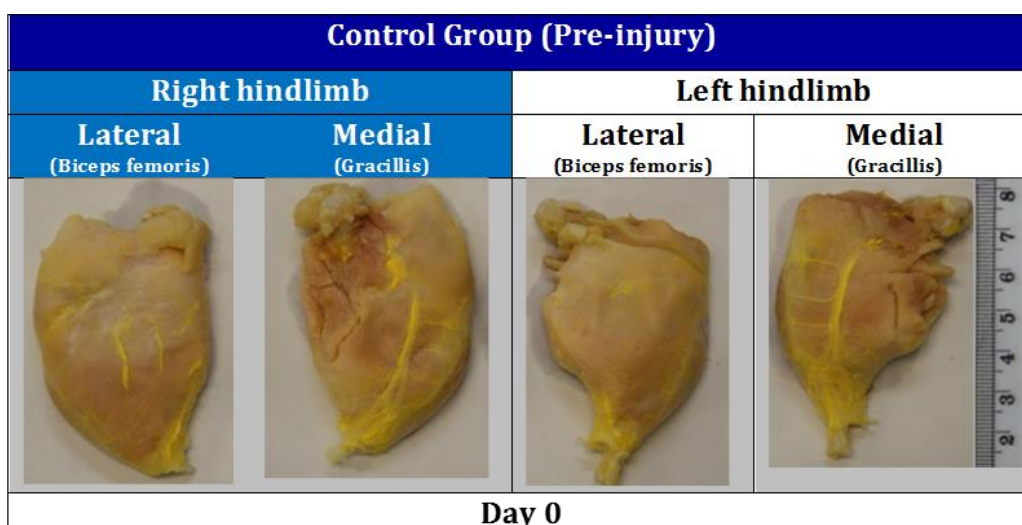
The observation of the skin (epidermis) from the lateral and medial views exhibited no obvious haematoma. The presented images are from day 1 of the sham group.

A mild to moderate swelling and stiffness was palpated in the region that the CSTT was induced at day 1 in all groups. Following skin dissection, it was observed that unlike the skin surface, the subcutaneous side of the skin exhibited extensive haematoma, inflammation and bleeding in all animals at day 1 post injury. These symptoms reduced in size progressively towards day 3, 7 and 28 in all groups (Figure 5-2).

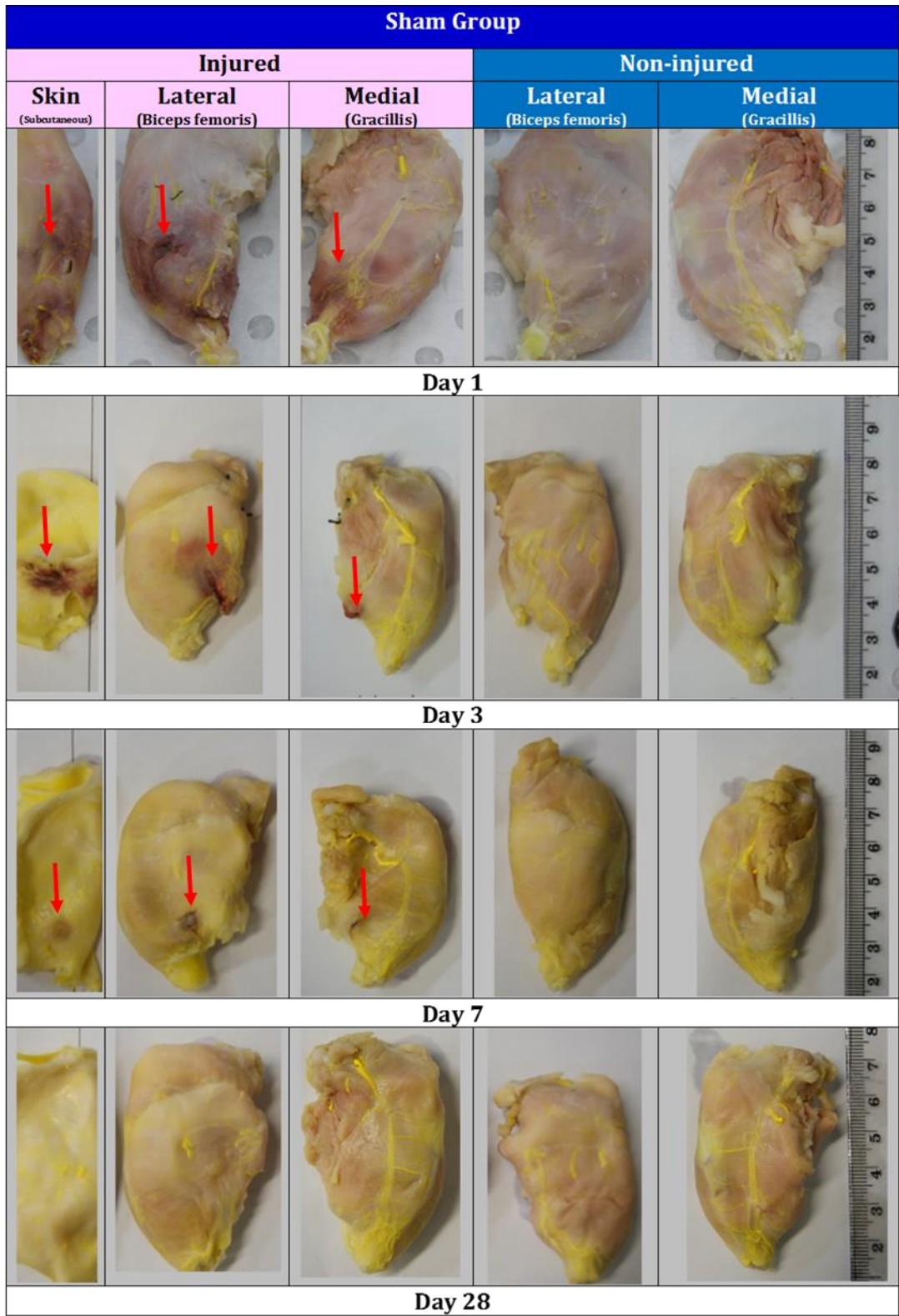
Muscle observation after dissection of the skin

Observations of the traumatised muscle tissue revealed an extensive haematoma, bleeding and inflammation, located in the region where the CSTT was induced compared to the non-injured hindlimbs. The CSTT was observed on the lateral side of the hindlimb on the biceps femoris muscle (BF) and on the medial side of the hindlimb on the Gracilis muscle (GC).

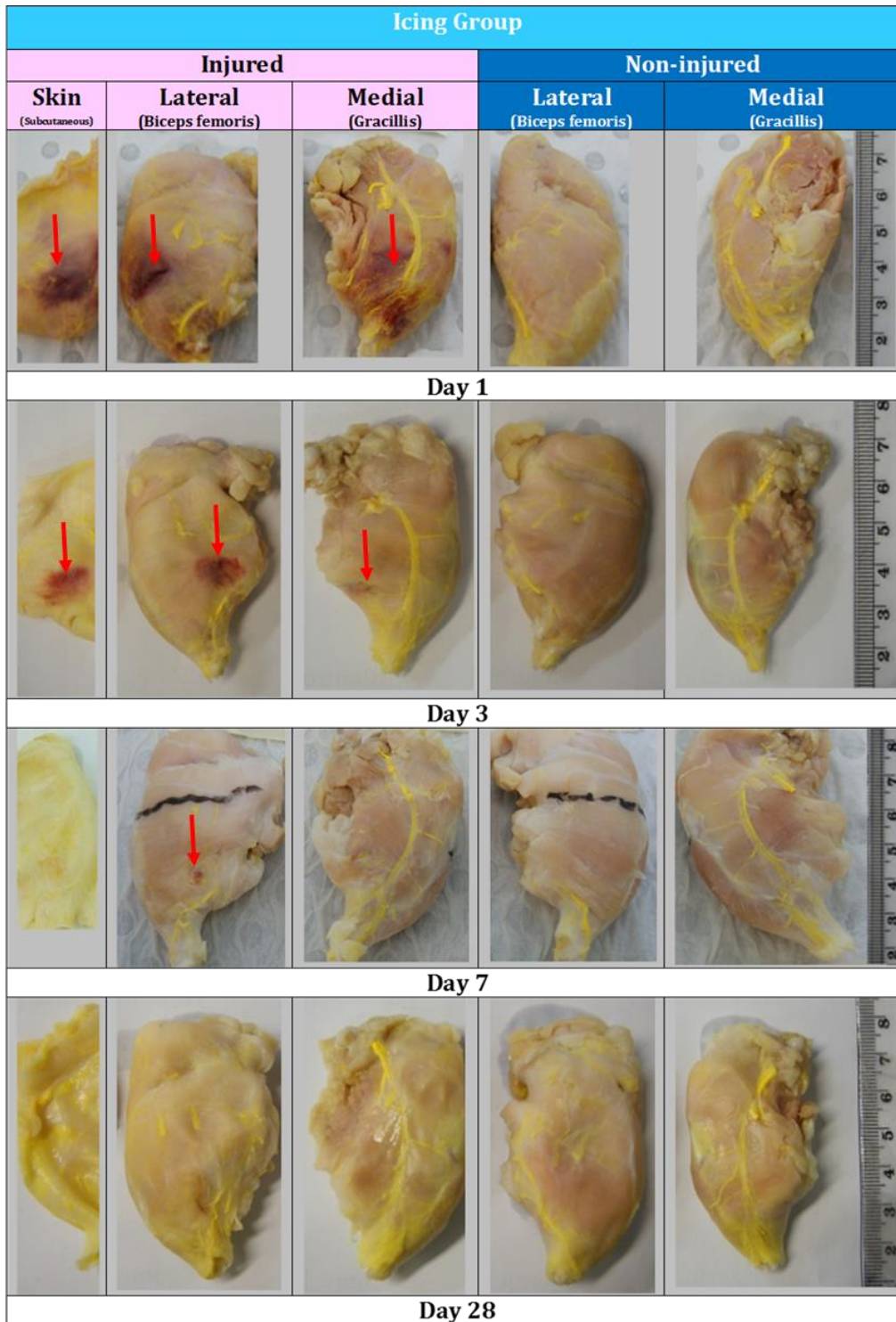
The injury was severe particularly at day 1 (Grade 4 based on the AO classification) in the lateral and medial sides of all hindlimbs for both sham and icing groups. Contusions and swelling symptoms decreased in size from day 3 to day 28 post trauma in the lateral and medial sides of all hindlimbs for both sham and icing groups (Figure 5-2).



A



B



C

Figure 5-2: Muscle injury evaluation.

The muscle injury (red arrow) is qualitatively exhibited for the sham (B) and icing (C) groups compared to the non-injured (control) group (A). The images of the sham and icing groups show the skin (subcutaneous tissue (SC)) and the traumatised muscles including biceps femoris (BF, lateral side) and Gracilis (GC, medial side). Extensive haematoma and inflammation could be observed at day 1 post injury (grade 4 based on the AO classification) which then reduced in size towards day 3, 7 and 28. The yellow colour indicates the presence of the microfil in the vasculature.

The CSTT was qualitatively graded 4, 3, 2 and 1 at day 1, 3, 7 and 28 respectively based on the symptoms described in the AO classification (Table 5-2).

Table 5-2: CSTT and muscle injury descriptions.

This table represents a comparison between the observed CSTT symptoms at different time points and the graded symptoms of the soft tissue injury described by the AO classification. CSTT observations confirmed the information given by the AO classification and also provided additional information regarding the CSTT symptoms.

The AO description of the muscle and vascular injury		Additional CSTT symptoms observed in this research	
Grade	Symptoms	Time points	Symptoms
4	Muscle defect, tendon laceration, extensive muscle contusion, extensive segmental vascular injury	Day 1	Extensive haematoma in muscle tissue and subcutaneous side of the skin, muscle laceration, inflammation, bleeding, swelling, stiffness
3	Considerable muscle injury, two compartments, localized vascular injury	Day 3	Localised haematoma and inflammation in muscle tissue and subcutaneous side of the skin, possible muscle laceration
2	Circumscribed muscle injury, one compartment only, isolated nerve injury	Day 7	Small haematoma located mostly on one muscle and subcutaneous side of the skin
1	No muscle injury, no neurovascular injury	Day 28	The injury was healed, no obvious haematoma or symptoms

The quantitative analysis of the CSTT area

A quantitative assessment was carried out to determine the changes in the inflamed area of the haematoma during the natural healing period and during ice treatment over time. The quantitative data obtained from measurements of the area of the inflamed regions illustrated a healing trend from day 1 to day 7 through a reduction in size of the inflamed areas (Figure 5-3, Appendix A-5). In addition, the results suggest that icing has significantly reduced the inflamed area at day 1. By day 7, the sham group indicated a smaller inflamed area compared to the icing group.

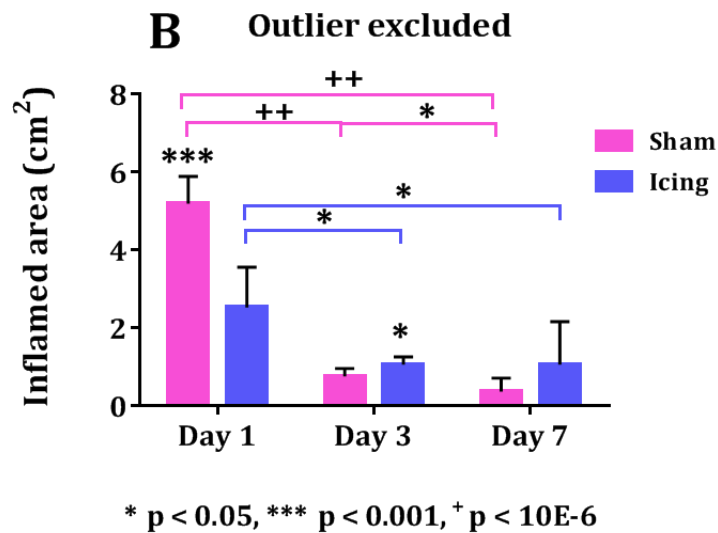
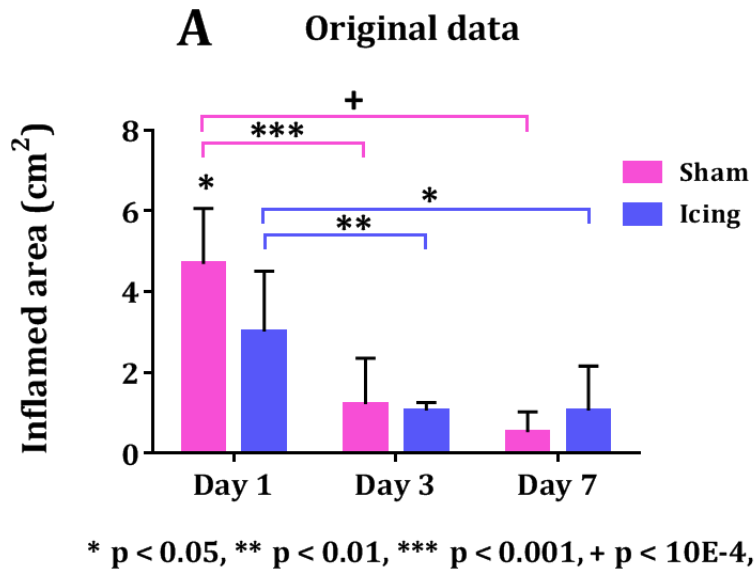


Figure 5-3: Quantitative evaluation of the CSTT area.

The quantified changes to the size of the CSTT and muscle injury (inflamed regions) over time for both sham and icing groups are shown (Mean \pm SD, $n=6$). **A:** The evaluation of the inflamed regions obtained from the original data (Mean \pm SD, $n=6$) suggested that icing has significantly decreased the inflammation at day 1 compared to the sham group ($p < 0.05$) (Student *t*-test). The size of the inflamed areas significantly reduced from day 1 to day 7 in both sham and icing groups. **B:** The variability within the data reduced after excluding the outliers from both sham and icing groups. While the size of haematoma significantly reduced in the sham group from day 3 to day 7 ($p < 0.05$), the icing group indicated an increase in the size of the haematoma at day 3 ($p < 0.05$) and day 7 ($ES > 0.8$) compared to the sham group (**B**). Since the haematoma was healed at day 28, the quantification of the inflamed areas was conducted up to day 7.

Several outlier values could be quantitatively detected causing a variability within the data at days 1, 3 and 7 in the sham group as well as day 1 in the icing group.

After exclusion of the outlier values i.e. from the sham group at days 1 (2.2 cm² which was outside the qualified band of 2.8 – 6.5 cm²) based on the defined criteria explained in 3.2.6 and equation 3-4, the data variability reduced (e.g. CV reduced from 27% to 12%).

5.3.2 CSTT and muscle injury verification using histology

Haematoxylin and eosin (H&E) stained sections were utilised to evaluate the level of muscle damage and regeneration, as well as the degree and location of the inflammatory cell influx. The infiltration of inflammatory cells appeared in the injured regions (Figure 5-4), possibly indicating macrophages (large mononuclear cells) and neutrophils (cells with a complex, lobulated shape nucleus) (Tsivitse *et al.* 2003, Shireman *et al.* 2006). The degenerated muscle fibres were distinguished by a faded staining of the sarcoplasm and reduction of nuclei, presence of inflammatory cells in the site of the injury, broken sarcoplasm which in some cases was hardly visible, irregular shape and disorientation (Grounds *et al.* 2004, Rüegg *et al.* 2011). Also, the non-injured myofibres were identified by their regular and orientated shape (polygonal shape in cross-sections), peripheral nuclei, intact sarcolemma and sarcoplasm.

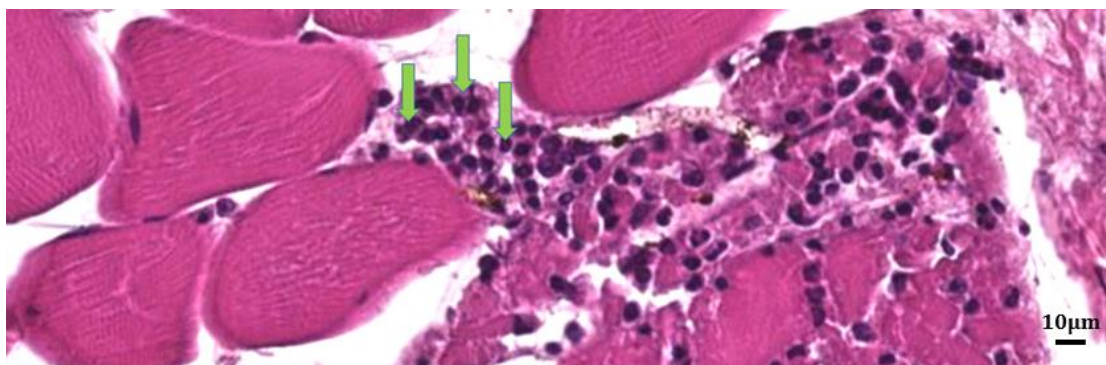


Figure 5-4: Inflammatory cell influx in a histology image (H&E). A configuration of the inflammatory cell influx (green arrows) within the haematoma is shown for the injured hindlimb of the sham group at day 1.

Extensive injury of muscle fibres along with the inflammatory cells was observed at day 1 post trauma in both the sham and icing groups (Figures 5-5).

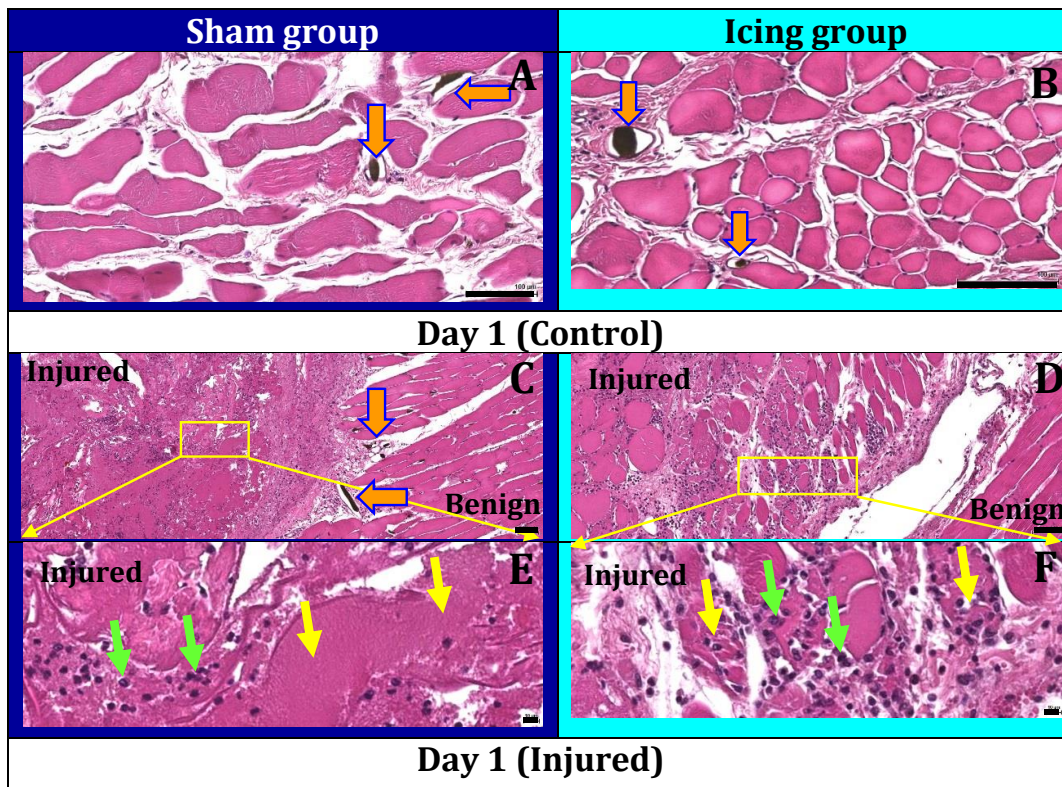


Figure 5-5: Histological evaluation of the CSTT at day 1.

Histological cross-sectional images (H&E) of the rat's muscle following CSTT are shown at day 1. The sham group is shown in the left column of the table while the icing group is located in the right column. The first row (A, B) shows the non-injured hindlimbs. The second row (C, D) shows comparisons between the muscle injury area (left hand side of each section) and the benign region (right hand side of each section). The third row (E, F) shows magnified images of the second row's highlighted areas (yellow boxes). Serious muscle fibre damage (yellow arrows) in the injured regions was observed at day 1 (E, F) compared to the regular and oriented muscle fibres in the benign areas and the control hindlimbs of both sham and icing groups. Arrows: (orange: blood vessels, green: inflammatory cells, yellow: destroyed muscle fibre). The scale bars of the first and second rows of each table are 100 μm and those in the third row of each table are 10 μm .

The presence of the inflammatory cells in the site of the injury increased particularly at day 3 in the sham group and at day 7 in the icing group (Figures 5-6 and Figures 5-7). The regenerated muscle fibres could be observed at day 7 in the sham group while this was delayed in the icing group (Figure 5-7).

The tissue was healed in both sham and icing groups at day 28 as a large number of matured muscle fibres could be observed with peripheral nuclei (Figures 5-8). A few newly regenerated muscle fibres were also detected at this time with a centrally located nuclei within the myofibres (Myburgh *et al.* 2012) immigrating to the peripheral sides of the myofibres during maturation.

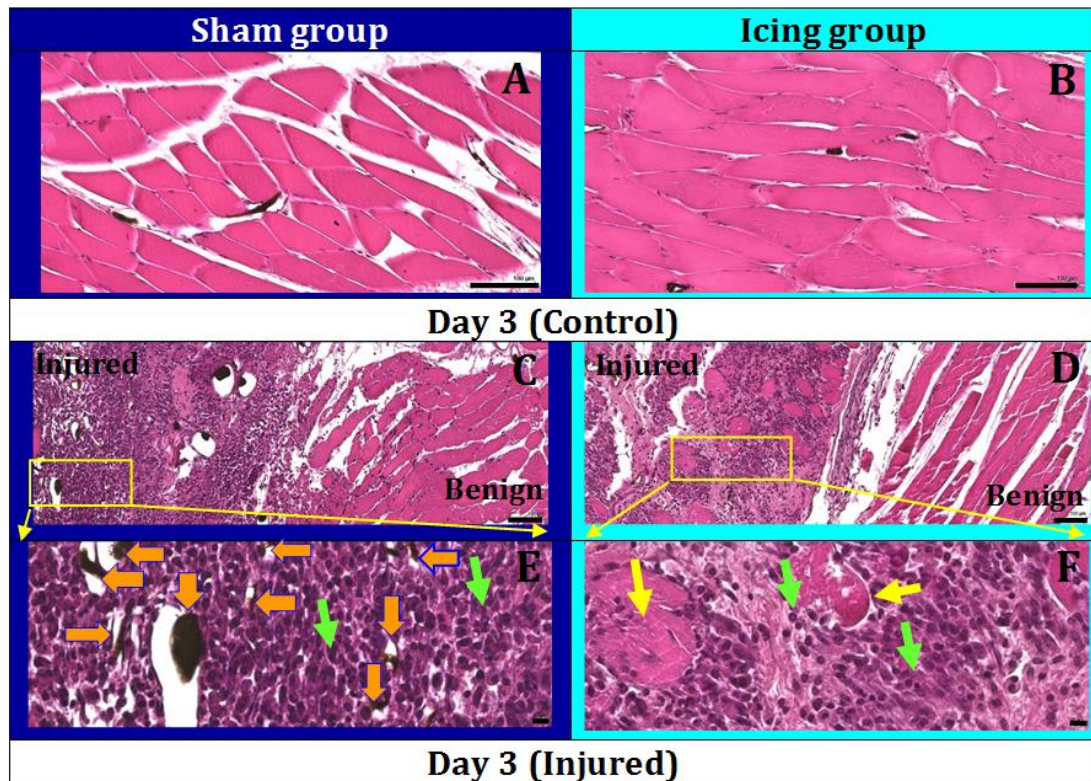


Figure 5-6: Histological evaluation of the CSTT at day 3.

Histological cross-sectional images (H&E) of the rat's muscle following CSTT are shown at day 3. The sham group is shown in the left column of the table while the icing group is located in the right column. The first row (A, B) shows the non-injured hindlimbs. The second row (C, D) shows comparisons between the muscle injury area (left hand side of each section) and the benign region (right hand side of each section). The third row (E, F) shows magnified images of the second row's highlighted areas (yellow boxes). At day 3, the injured muscle fibres had almost cleared in the sham group (C, E) but these could still be observed in the icing group (D, F). Also, at day 3, more inflammatory cells could be seen in the injured regions of the sham group (C, E) compared to the icing group (D, F). Arrows: (orange: blood vessels, green: inflammatory cells, yellow: destroyed muscle fibre). The scale bars of the first and second rows of each table are 100 μm and those in the third row of each table are 10 μm .

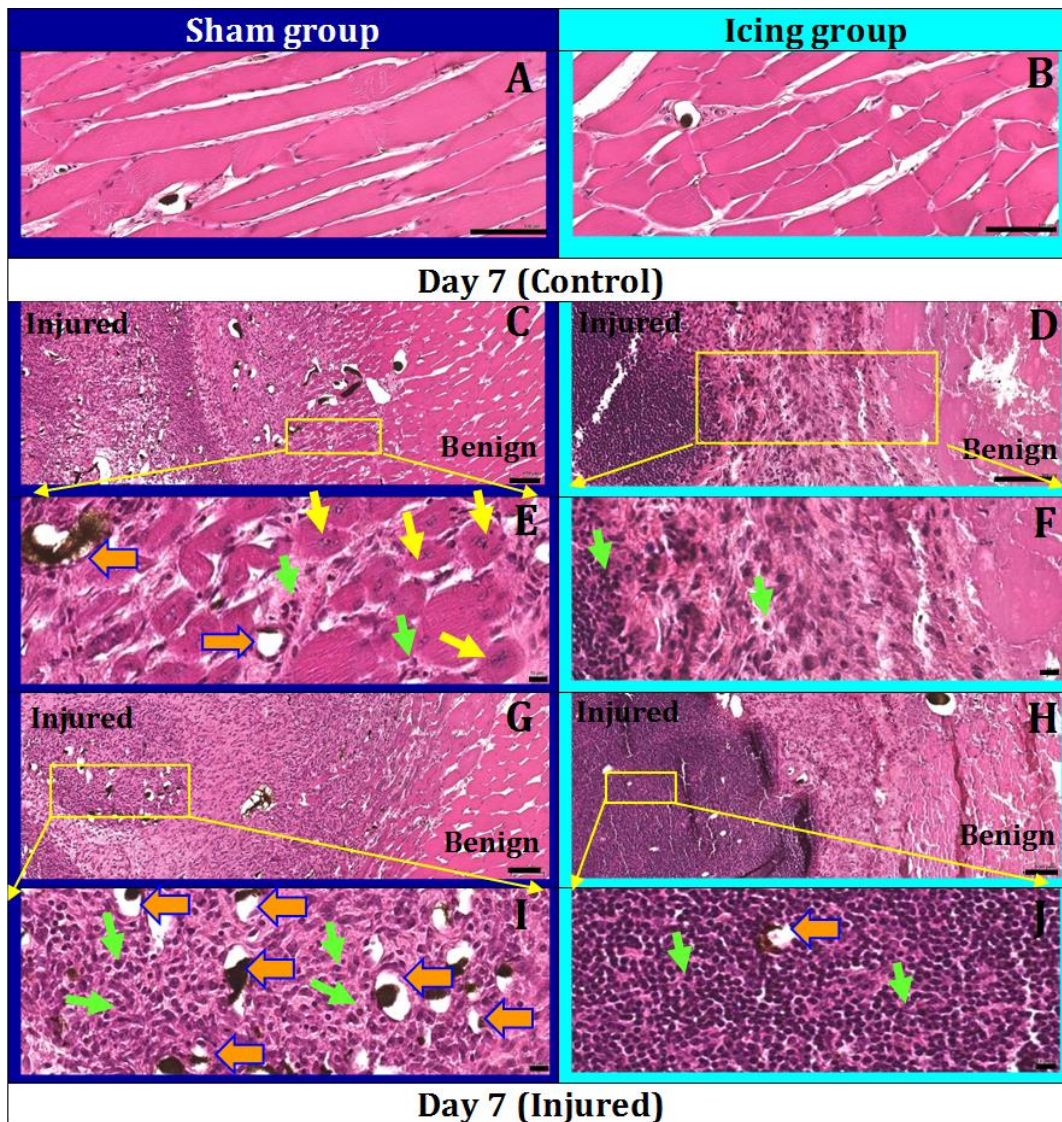


Figure 5-7: Histological evaluation of the CSTT at day 7.

Histological cross-sectional images (H&E) of the rat's muscle following CSTT are shown at day 7. The sham group is shown in the left column of the table while the icing group is located in the right column. The first row (**A**, **B**) shows the non-injured hindlimbs. The second and fourth rows (**C**, **D**, and **G**, **H**) show comparisons between the muscle injury area (left hand side of each section) and the benign region (right hand side of each section). The third and fifth rows (**E**, **F** and **I**, **J**) show magnified images of the second and fourth row's highlighted areas (yellow boxes). In general, at day 7, a decrease in inflammatory cells (green arrows) and an increase in the blood vessels (orange arrows) (**G**, **I**) were exhibited in the injured areas of the sham group. Here, the regenerated muscle fibres with central nuclei were mostly observed in the boundary region between the injured and benign areas (yellow arrow) (**C**, **E**). However, the icing group showed a large number of inflammatory cells and less blood vessels (**H**, **J**) within the necrotic areas at day 7 where hardly any regenerated muscle fibres could be seen (**D**, **F**) within either the necrotic region or the boundary between the injured and benign areas. The scale bars of the first, second and fourth rows are 100 μm and those in the third and fifth rows are 10 μm .

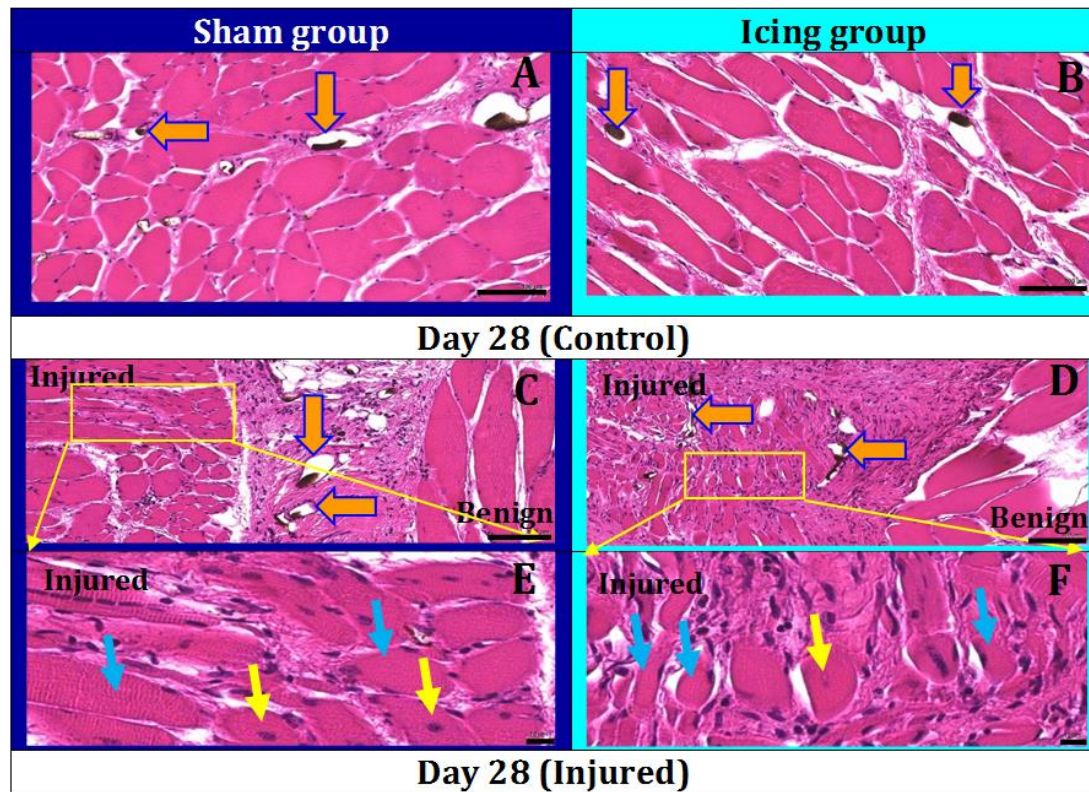


Figure 5-8: Histological evaluation of the CSTT at day 28.

Histological cross-sectional images (H&E) of the rat's muscle following CSTT are shown at day 28. The sham group is shown in the left column of the table while the icing group is located in the right column. The first row (A, B) shows the non-injured hindlimbs. The second row (C, D) shows comparisons between the muscle injury area (left hand side of each section) and the benign region (right hand side of each section). The third row (E, F) shows magnified images of the second row's highlighted areas (yellow boxes). At day 28, a large number of matured muscle fibres with many peripheral nuclei could be observed in the injured regions along with a very few regenerated muscle fibres in both sham and icing groups indicating tissue has healed at this time point (C, D, E, F). Arrows: (orange: blood vessels, yellow: regenerated muscle fibre, light blue: matured muscle fibre). The scale bars of the first and second rows of each table are 100 μm and those in the third row of each table are 10 μm .

5.3.3 Vascular injury following CSTT and cryotherapy

Visualisation of the total vascular architecture (ROI)

The qualitative observation of 3D images obtained from the ROI suggested more blood vessels in the injured hindlimbs compared to the non-injured hindlimbs in both sham and icing groups at various time points post trauma (Figure 5-9).

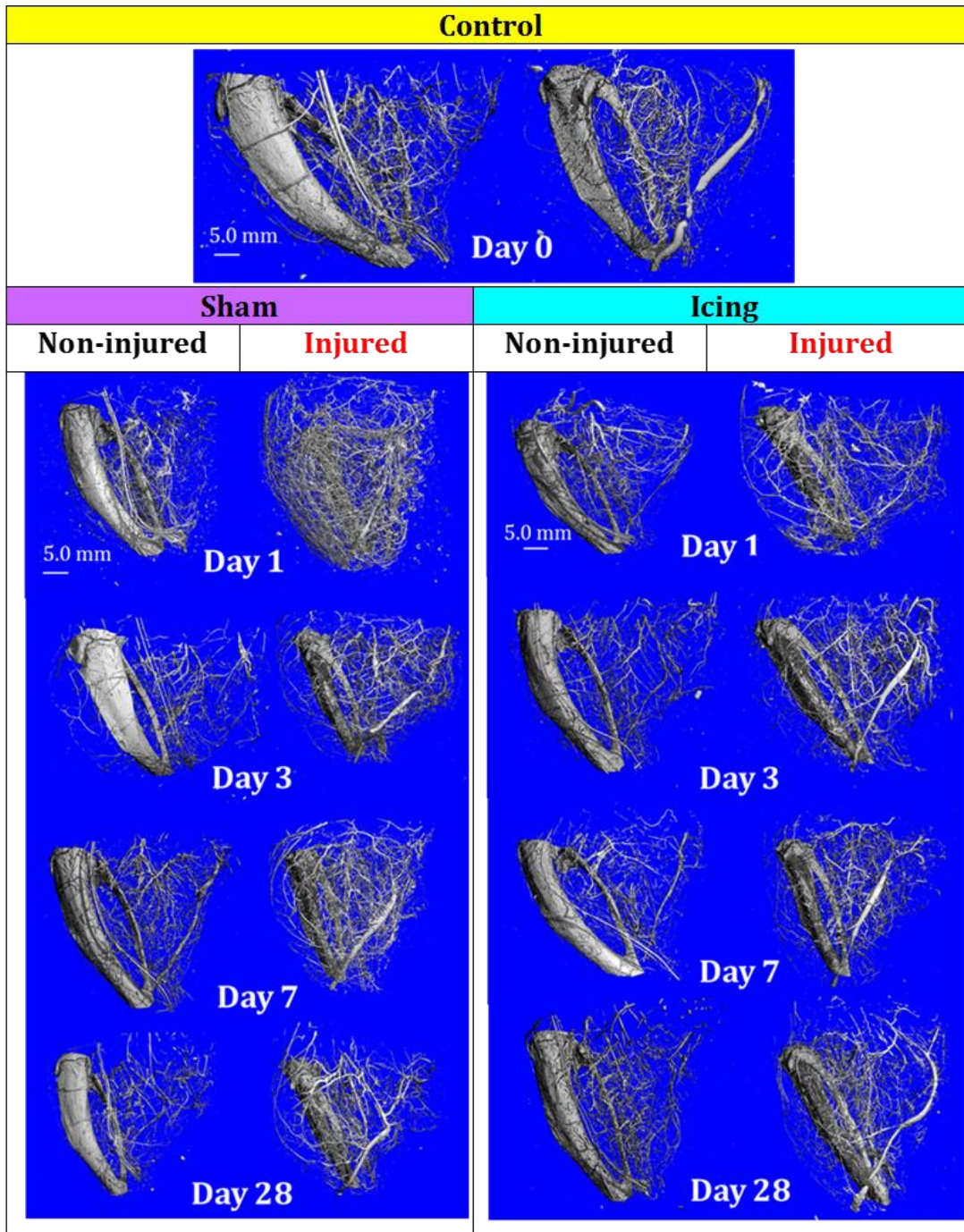


Figure 5-9: 3D visualisation of the vascular network using micro-CT. 3D micro-CT visualisation of the vascular architecture is shown for the ROI of the control, sham and icing groups at different time points (voxel size: 18 μm). The images of the injured hindlimbs appear to have more blood vessels compared to those from the non-injured hindlimbs. Also, more blood vessels could be observed in the injured hindlimbs of the sham group at days 1 and 7 post injury compared to the injured hindlimbs in the icing group.

Quantification of the total vessel volume ratio obtained from the ROI's

The TSV normalised results (Mean \pm SD) obtained from the ROI evaluation suggest notably higher values for the sham group compared to the icing and control groups at days 1, 3 and 7 although these were not statistically significant (Figure 5-10, Appendix A-6). The mean values of the TSV for both sham and icing groups fell from day 1 towards day 3 and were at the same level at day 28. A significant difference between the TSV mean values of the control group and both sham and icing groups at day 28 suggested the TSV did not return to pre-injury values within this time frame. Although the difference in TSV values for the injured hindlimbs of the sham group compared to the icing group were not statistically significant, the large effect sizes were measured at days 1 (ES > 0.8) and 3 (ES > 0.8) as well as a medium effect size at day 7 (ES > 0.5). Also, while the TSV values in the sham group reduced from day 1 to day 3 (ES > 0.8) and remained steady towards day 28, these values decreased from day 1 to day 7 followed by an increasing trend towards day 28 (ES > 0.5) in the icing group.

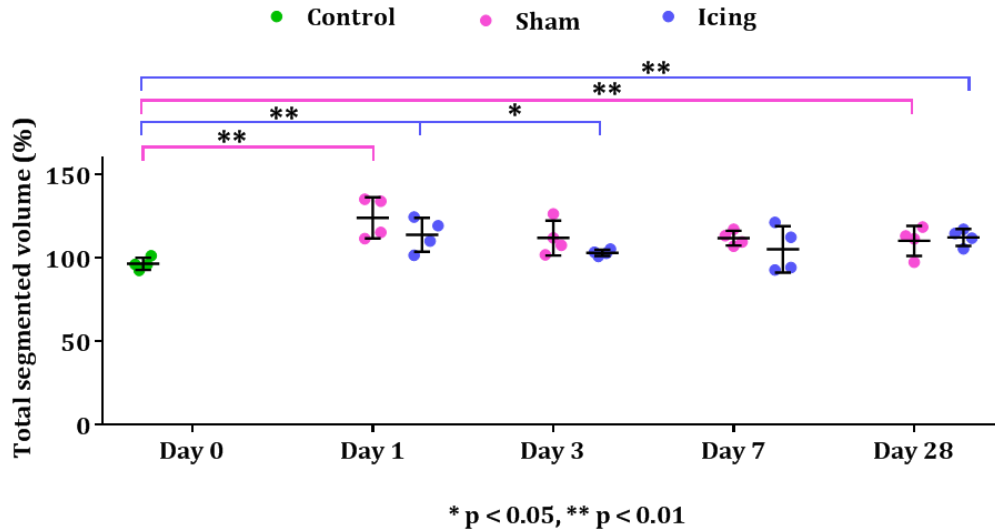


Figure 5-10: Total segmented volume (TSV) results obtained from the ROI. Normalised values of the TSV obtained from the ROI are presented (n=4) for comparisons between both sham and icing groups (TSV%=injured/non-injured×100) at various time points. The results suggest that icing has significantly reduced the TSV values at days 1, 3 and 7 compared to the sham group (Paired Student t-test). Both sham and icing groups indicated significantly (p < 0.01) higher TSV values at day 1 compared to the control group followed by a notable decrease at day 3 where this was significant for the icing group (p < 0.05). Both sham and icing groups showed considerably higher values (p < 0.01) compared to the control group at day 28 suggesting these did not return to the original values prior to injury (ANOVA).

5.3.4 The reproducibility of the micro-CT results obtained from the ROI evaluation

The CV values presented for the TSV parameter obtained from the micro-CT based ROI evaluation indicated that nearly 89% of all results (100% for the sham group and 75% for the icing group) exhibited either a good or acceptable level of reproducibility for both sham and icing groups at days 1, 3, 7 and 28 (Table 5-3).

Table 5-3: The CV results for the TSV parameter.

The CV values are presented for the TSV parameter obtained from the ROI evaluation. The acceptable values of the CV (red) as well as the values with a small variation (black) are shown.

CV (%) ROI (Real data)	Day 0	Day 1	Day 3	Day 7	Day 28
Control	3.0				
Sham		8.5	8.0	3.0	7.0
Icing		7.7	1.7	13.0	3.8

5.3.5 Microvascular injury visualisation (biopsies) using micro-CT

The 3D vascular network which was studied at a high resolution of 6 μm for the biopsy samples displayed a highly detailed structure capturing more capillaries compared to those obtained from the ROI with a resolution of 18 μm (Figure 5-11).

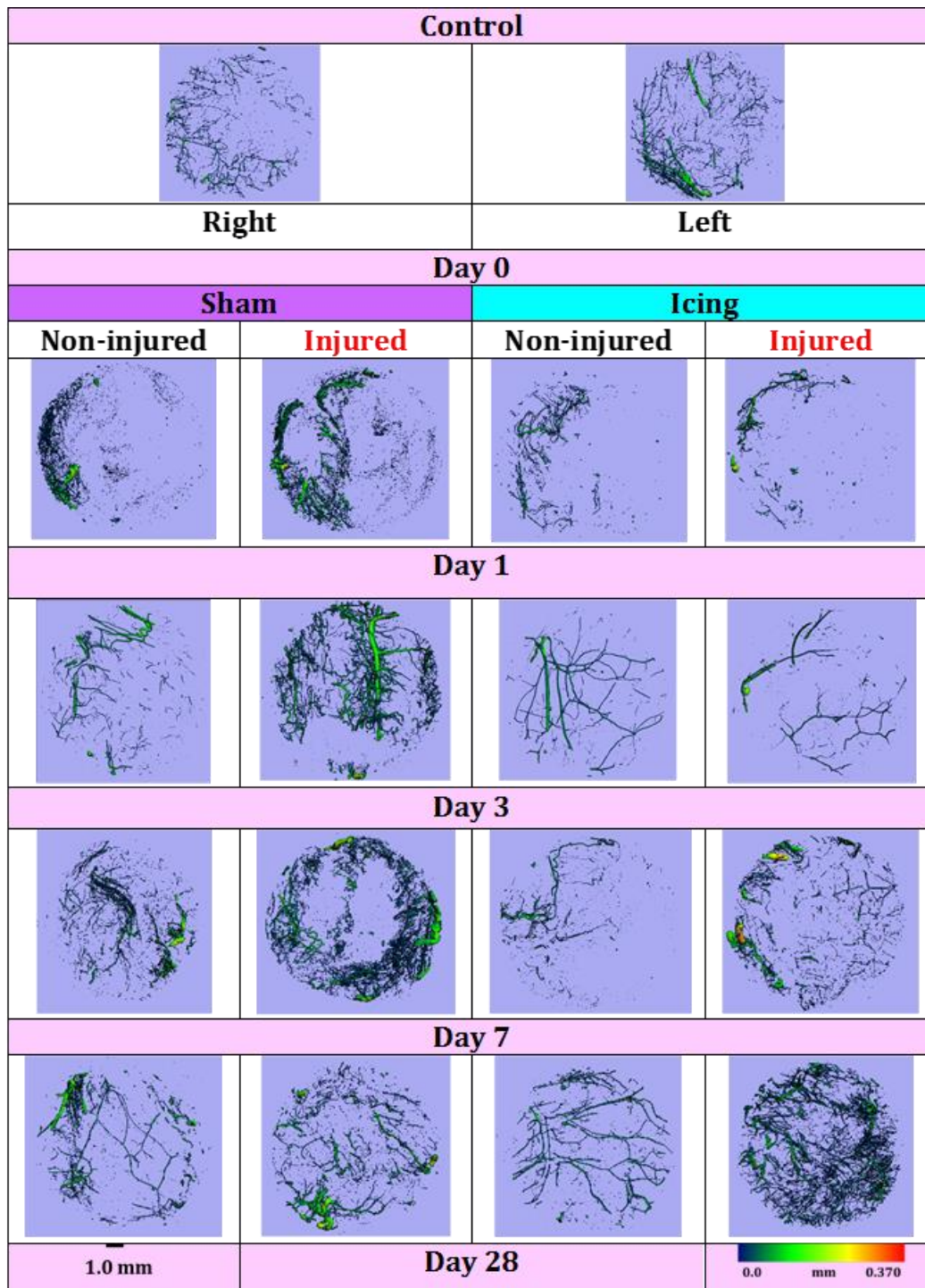


Figure 5-11: Micro-CT visualisation of the microvascular morphology.

The microvascular structure of 3D biopsy stacks (transversal view) was visualised using the micro-CT imaging system and is shown for three groups (control, sham and icing) at different time points ($n=4$, voxel size: $6\ \mu\text{m}$). Overall, the qualitative assessments suggested more blood vessels in the injured hindlimbs compared to the non-injured hindlimbs. Also more blood vessels could be observed at day 1, 3 and 7 in the sham group and surprisingly in the icing group at day 28. The colour coding shows that most of these vessels have a dark blue to black colour suggesting that these vessels are within the range of very small blood vessels and capillaries.

5.3.6 Quantifications of microvascular morphometric parameters (biopsy)

The micro-CT results for the quantified vascular morphometric parameters obtained from biopsy samples are presented (Mean \pm SD, n=4) as normalised values (non-injured/injured \times 100) (Figure 5-12 to 5-17 and Appendix A-8). It should be pointed out that although both sham and icing groups at various time points indicated a satisfactory perfusion, there were a few cases from days 1, 3 and 7 that appeared to be poorly perfused due to a delay in perfusion. These cases were excluded from data after they were quantitatively identified to be outliers. The data was then presented with and without the outlier values to assess the effect of these values on the results.

Vessel volume (VV)

The original normalised values of the VV indicated some variability due to the presence of outlier values and large blood vessels. The results improved after the data processing and notable effect sizes could be seen between the groups at various time points even though the differences between mean values were not statistically significant. After exclusion of the outlier values, not only did the data variability reduce but also the differences between the sham and icing groups exhibited a notable effect size (e.g. ES > 0.8 at day 1, sham group). For instance, after excluding the outlier value of 2278.9% which was outside the qualified band of -605.8-2073.1%, based on the defined criteria (3.2.6, equation 3-4) from day 7 of the sham group, the CV reduced from 121% to 20%. Although the differences between and within the sham and icing groups were not statistically significant, the effect size was large. For example, while the sham group showed a large effect size (ES > 0.8) compared to the icing group at day 7, this reversed at day 28 (ES > 0.8). Both sham and icing groups showed notably higher VV values at day 1 compared to the control group (ES > 0.5 and ES > 0.8 respectively). The VV values reduced from day 1 towards day 3 (ES > 0.8) which was followed by an increasing trend from day 3 to day 7 (ES > 0.8) and then again towards day 28 (ES > 0.5).

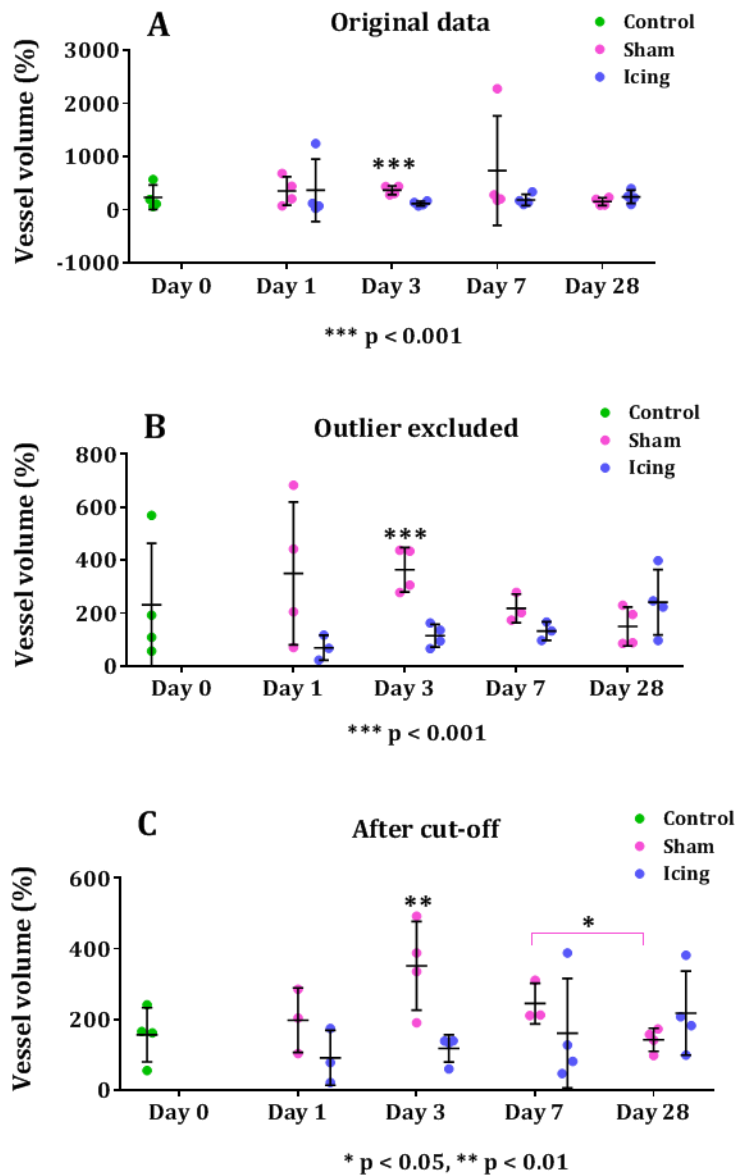


Figure 5-12: The results for the vessel volume (VV) parameter.

The normalised values for the VV parameter captured from biopsy samples are presented ($n=4$) for the sham, icing and control groups at various time points. A: The normalised values of the VV obtained from the original data (Mean \pm SD) indicated significantly ($p < 0.001$) higher VV values for the sham group compared to the icing group at day 3 (A). The VV values reduced from day 1 towards day 3 which was followed by an increasing trend from day 3 to day 7 and then again towards day 28. After exclusion of the outlier values (e.g. day 7 of the sham group) the data variability reduced (B). Also, a reduction in the VV from day 3 to day 7 could be observed in the sham group. The variability due to the presence of the large blood vessels within the biopsy samples was also reduced by applying the cut-off technique to the data with the excluded outliers (C). Overall, the results suggest an increasing trend from day 1 to day 7 for the VV values followed by a decreasing pattern towards day 28 in the sham group (C). However, the icing group indicated an increasing trend from day 1 to day 28. After data processing, while the icing group indicated lower VV values compared to the control group at day 1, this was considerably higher in the sham group (C) (Student *t*-test and ANOVA).

However, the VV increase at day 1 remained steady in the sham group until day 7 which was followed by a decrease towards day 28 (ES > 0.8). In addition, by applying the cut-off technique to the data with the excluded outliers, the variability due to the presence of large blood vessels within the biopsy samples was also reduced (e.g. CV reduced from 65% to 20% at day 28).

Vessel diameter (VD)

The original normalised values for the VD parameter indicated some variability due to the presence of large blood vessels within the biopsy sample affecting the VD results. This variability was reduced considerably after applying the cut-off technique (e.g. CV reduced from 45% to 8.5% at day 28) where different results could be observed between the original and cut-off data. For example, the VD results showed slightly higher values for the icing group compared to the sham group at day 1 (ES > 0.2), however, after applying the cut-off technique this outcome was reversed. The original data illustrated higher VD values in the sham group at days 3 (ES > 0.8) and 7 (ES > 0.5) compared to the icing group. Compared to the control group, the original data showed that the VD values of the sham group reduced at day 1 (ES > 0.5) followed by an increase towards day 7 (ES > 0.5) where again the VD decreased to the values below the control group at day 28 (ES > 0.8). In addition, in the icing group, the VD reduced from day 1 to day 3 (ES > 0.8) followed by an increase towards day 7 (ES > 0.8) and again a decrease in the values below the control group at day 28 (ES > 0.5).

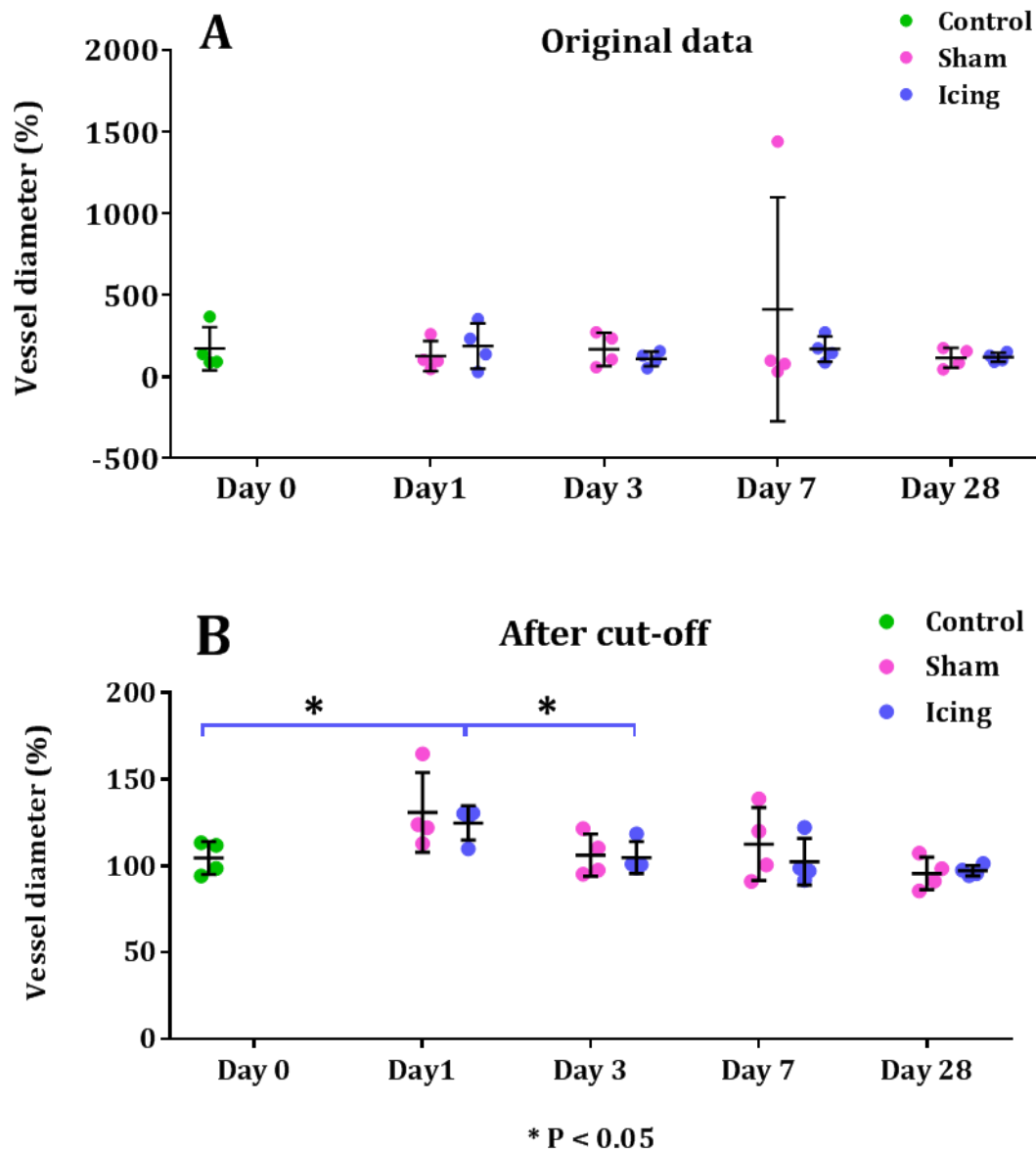


Figure 5-13: The results for the vessel diameter (VD) parameter.

The normalised values for the VD parameter from biopsy samples are illustrated ($n=4$) for the sham, icing and control groups at various time points. While the normalised data of the VD captured from the original data (Mean \pm SD) indicated slightly higher values for the icing group compared to the sham group at day 1 ($ES > 0.2$), this was higher in the sham group at days 3 ($ES > 0.8$) and 7 ($ES > 0.5$) (A). However, a variability within the data was reduced after applying the cut-off technique (e.g. at day 7 in the sham group) (B). B: The cut-off results suggest higher VD values for the sham group at days 1 ($ES > 0.2$) and 7 ($ES > 0.5$) compared to the icing group where no significant differences could be detected at days 3 and 28. Both sham ($ES > 0.8$) and icing ($P < 0.05$) groups indicated significantly higher VD values compared to the control group at day 1. The VD values of the sham ($ES > 0.8$) and icing ($P < 0.05$) groups notably decreased from day 1 to day 3 followed by an increase from day 3 towards day 7 ($ES > 0.2$). The VD values of both sham ($ES > 0.8$) and icing ($ES > 0.5$) groups reduced from day 7 towards day 28 where these values were lower than the control group (Student t -test and ANOVA).

Vessel number (VN)

The normalised results of the VN collected from the original data indicated higher values for the sham group at days 1 and 3 (ES > 0.8) and for the icing group at day 28 (ES > 0.8). The comparisons with the control group revealed that the VN values in the icing group notably reduced at days 1 (ES > 0.8) and 3 (ES > 0.5) followed by an increasing trend towards day 7 (ES > 0.8) and then to higher values than the control group at day 28 (ES > 0.5). In the sham group, the VN values increased to higher values than the control group at day 28 (ES > 0.8).

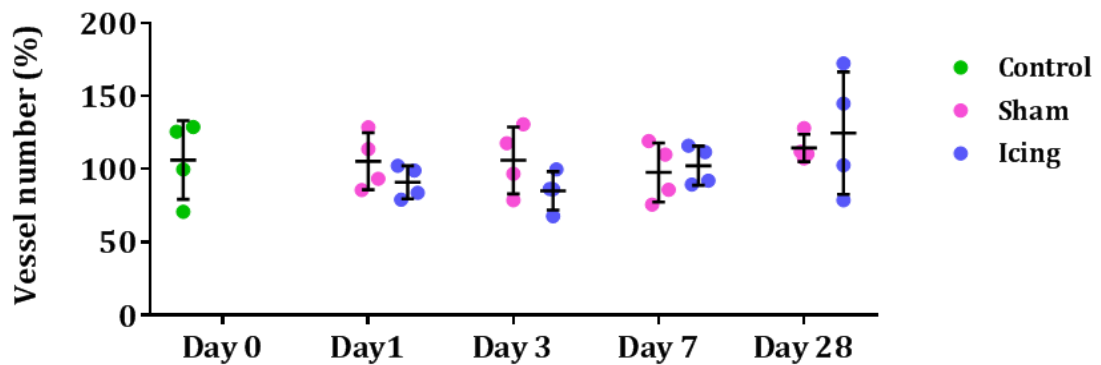


Figure 5-14: The results for the vessel number (VN) parameter.

The normalised original values (Mean \pm SD) for the VN parameter from biopsy samples are shown (n=4) for the sham, icing and control groups at various time points (Student t-test and ANOVA).

Vessel spacing (VSp)

The normalised results of the VSp obtained from the original data indicated higher values for the icing group compared to the sham group at days 1 and 3 (ES > 0.8). The comparisons with the control group exhibited that the VSp values notably increased for the icing group at days 1 and then 3 (ES > 0.5) followed by a decreasing trend towards day 7 (ES > 0.8) and then to lower values than the control group at day 28 (ES > 0.5). In the sham group, the VSp values did not show significant changes compared to the control group at earlier time points until day 7 where the VSp reduced to lower values than the control group at day 28 (ES > 0.8).

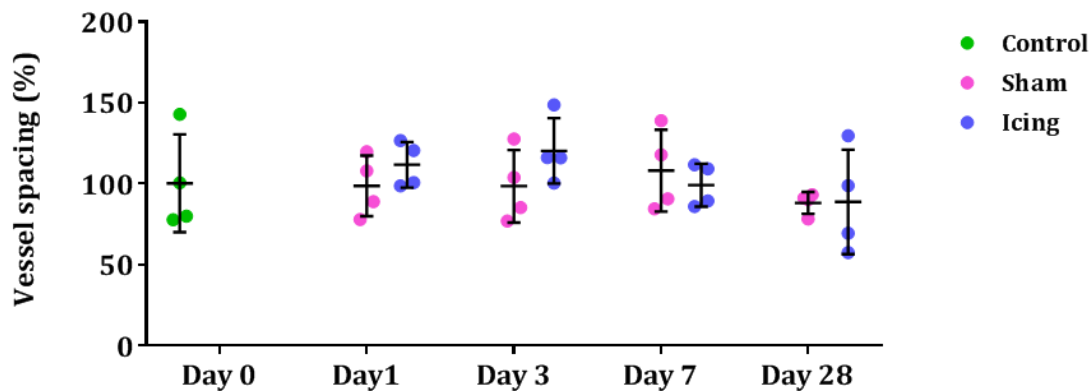


Figure 5-15: The results for the vessel spacing (VSp) parameter. The normalised original values (Mean ± SD) for the VSp parameter from biopsy samples are displayed (n=4) for the sham, icing and control groups at various time points (Student t-test and ANOVA).

Vessel connectivity (VConn)

The normalised original values of the VConn indicated a high variability due to the presence of three outliers that could be observed within the data particularly in the sham group at days 1, 3 and 7 (e.g. 22154.7% which was outside the qualifying band of -4796.7 - 20867.0 % at day 1) based on the defined criteria (3.2.6, equation 3-4).

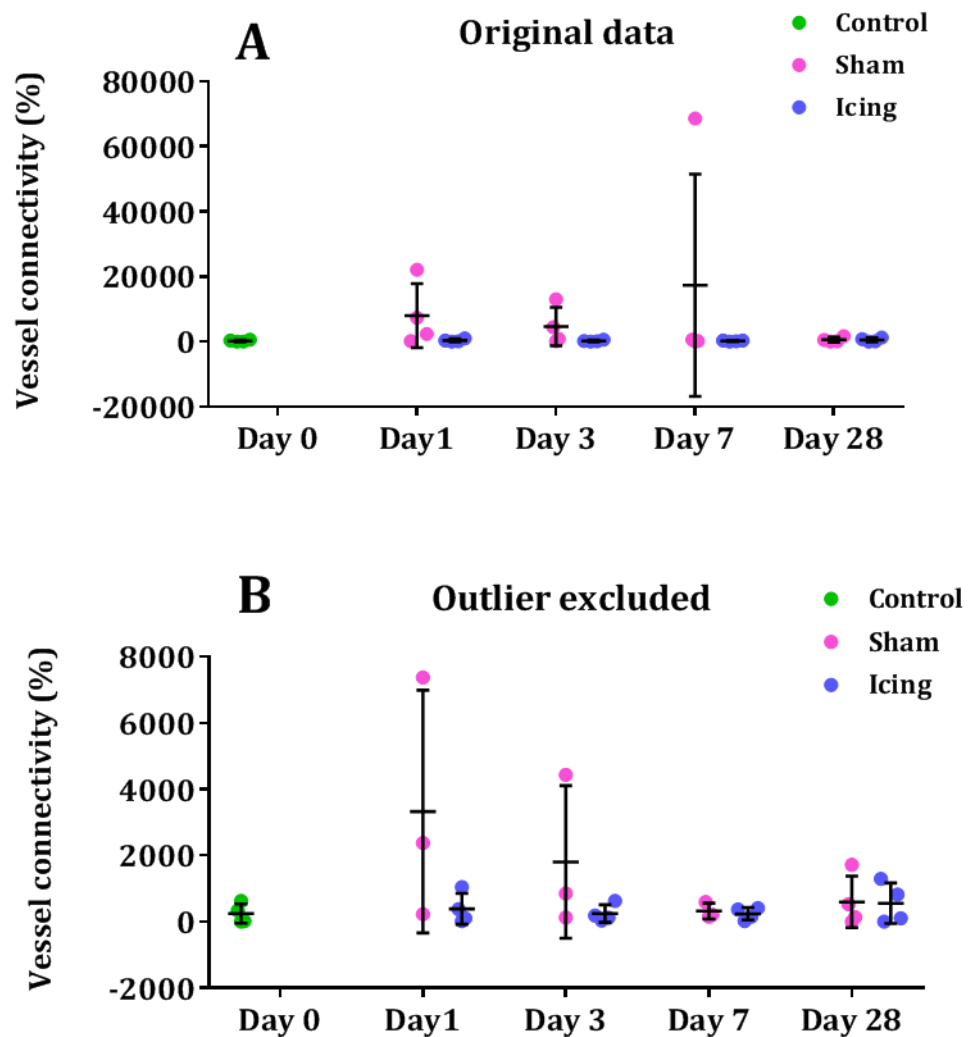


Figure 5-16: The results for the vessel connectivity (VConn) parameter.

The normalised original values for the VConn parameter captured from biopsy samples are presented ($n=4$) for the sham, icing and control groups at various time points (A). After exclusion of the outlier values, the normalised values of the VConn (Mean \pm SD) indicated higher values for the sham group compared to the icing group at days 1 ($ES > 0.8$), 3 ($ES > 0.8$) and 7 ($ES > 0.2$) (B). The increased VConn values at day 1 reduced over time towards day 7 and then gradually increased towards day 28 for both sham and icing groups (Student t -test and ANOVA).

Degree of anisotropy (DA)

The normalised values of the DA collected from the original data suggested significantly higher values for the sham group compared to the icing group at days 1 (ES > 0.8) and 3 (p < 0.05) post trauma. However, the icing group indicated higher DA values compared to the sham group at day 28 (ES > 0.8). While the icing group indicated a decrease in the DA values from day 1 to day 3 (ES > 0.8), this increased towards day 7 (ES > 0.8) but then reduced again at day 28 (ES > 0.8). In the sham group, the DA values indicated a dramatic increase compared to the control group at day 1 (ES > 0.8) followed by a decrease towards day 3 (ES > 0.5). The DA values increased again at day 7 in the sham group and then significantly reduced at day 28 (p < 0.001). Although a small variation could be observed with the data particularly at day 1, no outlier value could be detected.

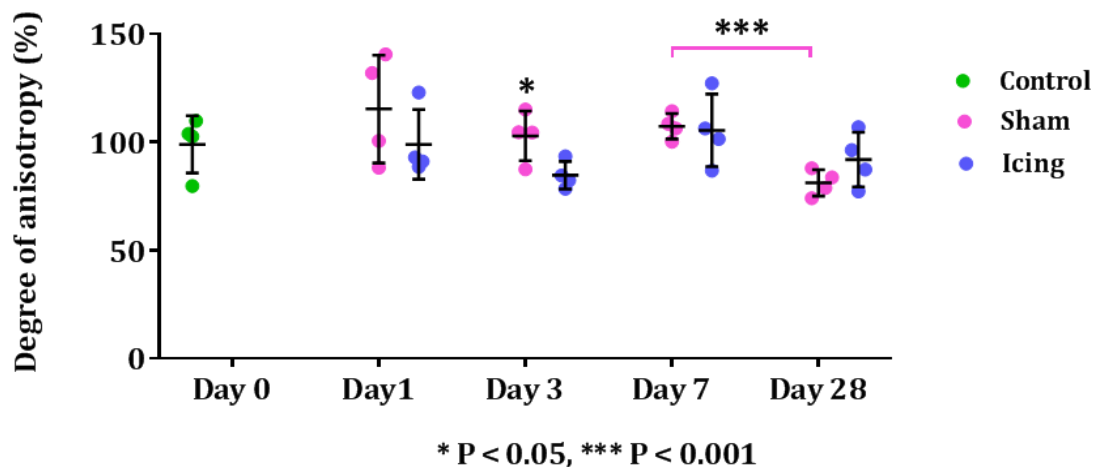


Figure 5-17: The results for the vascular degree of anisotropy (DA) parameter. The normalised values (Mean ± SD) for the DA parameter obtained from biopsy samples are illustrated (n=4) for the sham, icing and control groups at various time points (Student t-test and ANOVA).

5.3.7 The reproducibility of the results obtained from the biopsy evaluation

The data showed that the DA, VN and VSp were robust parameters compared to the other vascular morphometric parameters as their variations were small and no outlier value could be detected within the data. In addition, it was confirmed that the DA parameter was the most reliable parameter since the CV results indicated that 60% of the measurements were in an acceptable range (CV < 10%) and 20% of the results exhibited a low level of variability (CV = 11.5%). The VD after applying the cut-off technique and excluding the outlier value showed an acceptable range of reproducibility in most cases (60%). However, the VV and VConn were more sensitive than the other vascular morphometric parameters particularly the VConn that illustrated a high level of variability even after excluding the outliers. Overall, the CV results suggest a significant improvement towards day 28 (Table 5-4).

Table 5-4: The CV results for the vascular morphometric parameters.

The CV values are presented for the vascular morphometric parameters obtained from the normalised processed results of the biopsy evaluation after excluding the outliers and large blood vessels in the sham group at various time points. The acceptable values of the CV (red) as well as the values with small variation (blue) are shown.

CV (%)	Day 0	Day 1	Day 3	Day 7	Day 28
Parameter					
VV	42.2	37.5	30.9	19.0	19.7
VD	7.8	15.2	9.9	16.2	8.5
VN	22.0	16.0	18.7	18.0	7.0
VSp	26.0	16.4	22.8	31.3	6.6
VConn	103.3	89.9	104.2	62.0	113.0
DA	11.5	18.7	9.6	4.7	6.4

5.4 VERIFICATIONS

Verification of vasodilation using the VD

The micro-CT results have suggested a higher VD in the injured hindlimbs of the sham group compared to the icing group (Figures 5-14). Through the developed vascular injury model, the effect of vasodilation was confirmed one day after trauma after comparisons between the injured and non-injured hindlimbs.

To investigate whether the vasodilation effect is influenced by cryotherapy, the VD was measured in the non-injured and injured hindlimbs of the sham and icing groups and at day 1 using histology images (n=10) according to the methodologies described in 4.5.4. The VD values were then normalised to the non-injured limb and presented (Mean \pm SD) (Figure 5-18 and Appendix A-7).

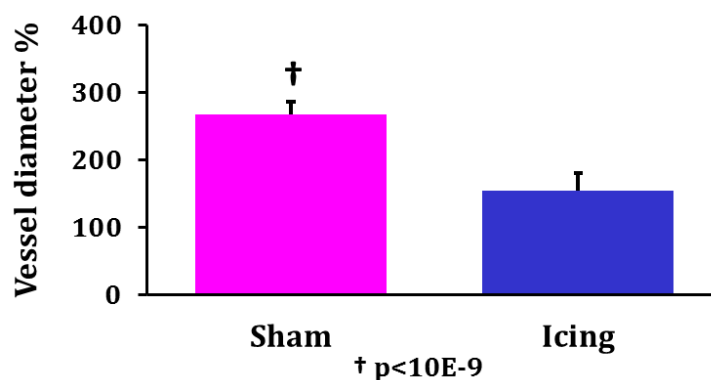


Figure 5-18: Indications of vasodilation using the VD.

The effect of icing on the diameter of the large blood vessels (VD) captured from random histology sections (n=10) of the biopsy samples is presented (Mean \pm SD). These normalised VD results represent the comparisons between the sham and icing groups at day 1. This image suggests that cryotherapy following CSTT has significantly decreased the vasodilation effect through the reduction in VD values (1.7 times) in the icing group compared to the sham group ($p < 10E-9$) (Student t-test).

The comparisons between the sham and icing groups for the VD indicated that icing has significantly reduced the vasodilation effect following CSTT.

5.4.1 Angiogenesis indication using the PVN over time

The blood vessels perfused with the microfil contrast agent were identified and quantified in histological sections obtained from biopsy samples of both sham and icing groups. More blood vessels could be observed per tissue area in the injured regions of the sham group compared to the icing group at each time point (Figure 5-19 and Appendix A-9).

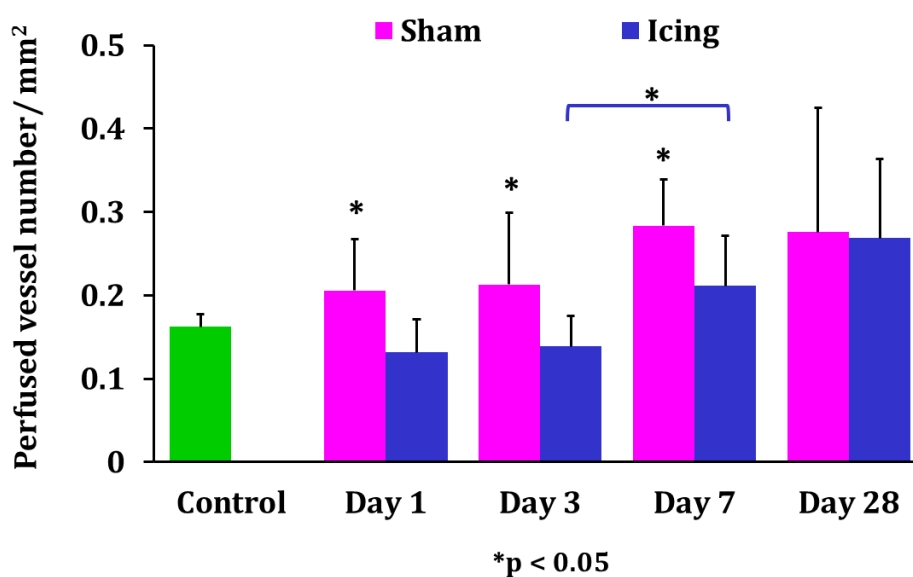


Figure 5-19: The perfused vessel number (PVN) per tissue area (mm^2).

The PVN captured from 2D histological sections of the biopsy samples ($n=6$) (Mean \pm SD) for the non-injured (control) and injured hindlimbs of both sham and icing groups. The results indicated higher values for the injured hindlimbs of the sham group compared to those in the icing group that was significant at days 1, 3 and 7 ($p < 0.05$). Since the differences between the mean values of the control hindlimbs were not significant ($p > 0.05$), only an average of these mean values is presented (Student *t*-test and ANOVA).

Another angiogenesis indication using vWF

In addition to this research, the von Willebrand Factor (vWF) which is a commonly used angiogenesis marker (Starke *et al.* 2011) was investigated through immunohistochemistry (IHC) analysis. vWF is an endothelial cell marker synthesized by endothelial cells of both pre-existing and newly formed blood vessels and is used for studying angiogenesis/neovascularisation (Starke *et al.* 2011). The methodologies for vWF staining are given in Appendix B.

The initial results of the vWF expression are presented in Figure 5-20 suggesting more blood vessel (capillaries) at day 3 and 7 in the sham group compared to the icing group. While initial results for vWF expression were promising, further optimisation is required to suppress the non-specific background staining. Even though the vWF staining was accompanied with background artefacts, the initial results have shown more blood vessels stained with the vWF at day 3 and 7 following CSTT, which seemed to support the occurrence of angiogenesis.

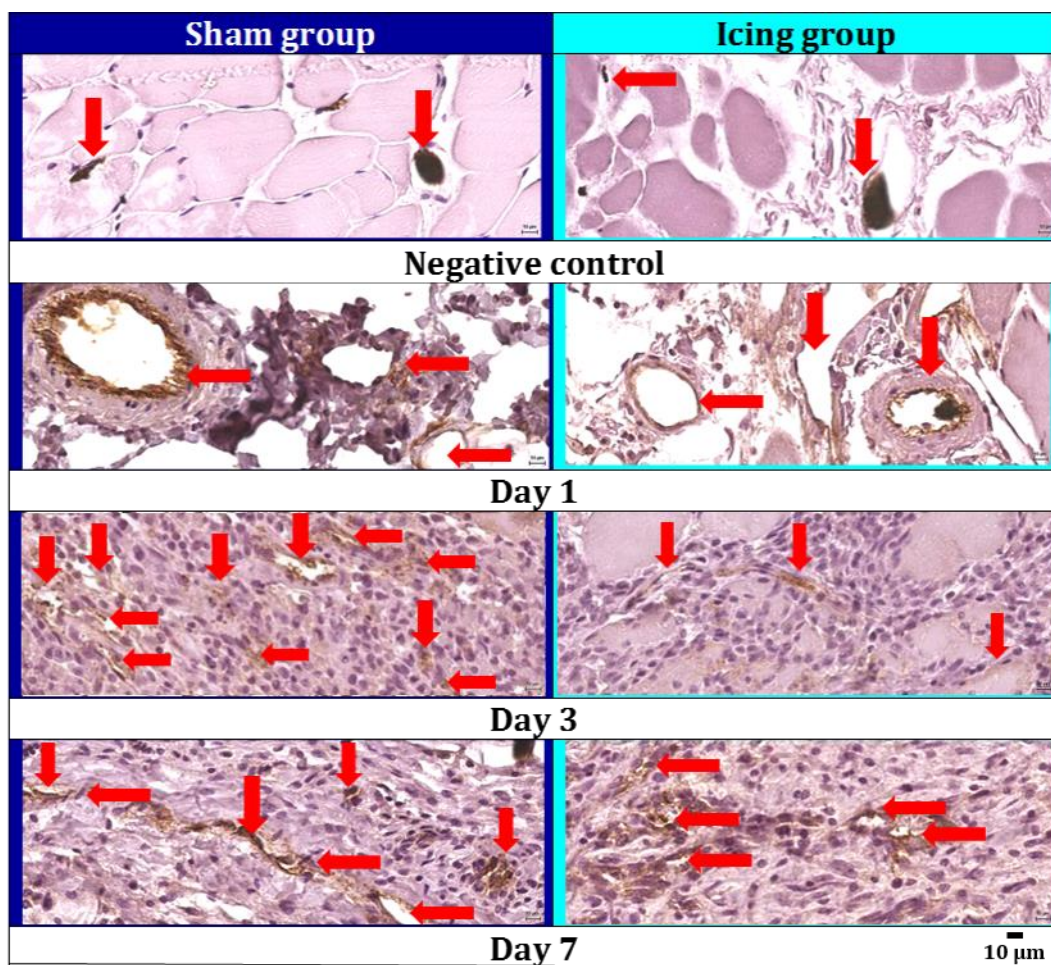


Figure 5-20: The positively stained blood vasculature with the vWF antibody

The positively stained blood vessels and capillaries with the vWF antibody (red arrows) using immunohistochemistry staining are presented for the negative control and injured hindlimbs. Images are from muscle samples collected from the sham (left column) and icing (right column) groups at 1, 3 and 7 days post injury. More blood vessel (capillaries) could be detected at day 3 and 7 in the sham group compared to the icing group. The scale bar for all images is 10 μm.

5.5 DISCUSSION

5.5.1 The effect of cryotherapy on muscle injury following CSTT

While icing may reduce the swelling (Deal *et al.* 2002) and haematoma (Swenson *et al.* 2007), the results of this research suggest that this therapeutic modality may delay healing of the injured tissue at earlier time points. Regarding muscle injury, the delay in tissue healing following cryotherapy is supported by another study on the effect of icing on CSTT reported by Takagi and colleagues (Takagi *et al.* 2011). The authors have concluded that as muscle temperature was reduced by more than 15°C due to cryotherapy, there was a delay in the degeneration of the necrotic muscle fibers for 12 hours following injury. The authors also concluded that early cooling of the tissue delayed the macrophage influx into the skeletal muscles, causing the impairment of both muscle degeneration and regeneration in the injured region of the icing group compared to the sham group.

Contrary to their results indicating the initiation of muscle fibre regeneration in rats at days 3 and 4 (sham group), this research could hardly find any regenerated muscle fibres at day 3, but they were present at day 7. Furthermore, in a rat's trauma induced hindlimb, the temperature difference between the cooling object and the skin has been shown to be small (2°C) (Schaser *et al.* 2006). For example, the rat's skin temperature was reported to be 10°C after superfusing cold saline at 8°C through the skin for 20 minutes using a needle probe (Schaser *et al.* 2006). Also, the results of a recent clinical study did not support the application of cryotherapy for muscle recovery after damaging exercise since icing was found to be ineffective in reducing the muscle soreness (Crystal *et al.* 2013).

The time points chosen for this research were based on the critical events following CSTT during the healing phases of muscle injury including destruction, regeneration and remodelling (Järvinen *et al.* 2005, Claes *et al.* 2006, Smith *et al.* 2008).

For example, the initiation of angiogenesis at day 3 (Orbay *et al.* 2013) and muscle fibre regeneration at day 7 (Desgranges *et al.* 1999) have been identified as important events that occur following ischemic muscle injuries.

The visual macroscopic observation of the muscle injury suggested that the CSTT created extensive acute symptoms such as haematoma and inflammation at earlier time points (destruction phase). These symptoms decreased in size from day 1 to 28 with no obvious haematoma at day 28 for both sham and icing groups (repair and remodelling phase). These results aligned with other reports verifying early acute symptoms such as inflammation and swelling in the first few days (destructive phase), muscle regeneration at day 7 (repair phase), and healing of the necrotic tissue at day 28 (repair and remodelling phases), with no more visible swelling (Huard *et al.* 2002, Winkler *et al.* 2011).

Quantitative analysis has confirmed the qualitative findings regarding the reduction in size of the injury from day 1 to day 7 for the sham and icing groups suggesting healing after CSTT. These findings were aligned with the wound healing process of the muscle injury and the time course (Huard *et al.* 2002). In addition, the quantitative results suggested that icing had notably reduced the haematoma at day 1 compared to the sham group. This finding supported other reports in the literature regarding cryotherapy decreasing the inflammatory reactions after soft tissue injury and also delays in haematoma formation (Swenson *et al.* 2007). However, at days 3 and 7, the reduction in the size of the haematoma was more pronounced in the sham group compared to the icing group. Since no obvious haematoma could be observed at day 28, the quantitative evaluations were only conducted up to day 7.

The findings from the CSTT observations were qualitatively verified with microscopic assessments using histology (Shireman *et al.* 2006). This evaluation was carried out by the identification of inflammatory cells as well as the level of muscle injury and its progressive improvement from day 1 to 28.

Similar to the descriptions reported for traumatised muscles in a rat crush injury model (Winkler *et al.* 2011), the histological analysis of the muscle injury following CSTT has confirmed the underlying serious damage to the muscle

fibres in the regions where the haematoma was originally located. The injured regions appeared in the histological images displaying extensive muscle damage along with the presence of inflammatory cells that potentially indicate necrosis as described in the literature (Radley *et al.* 2008) at day 1 and 3 following CSTT in both sham and icing groups. The histological observations suggest that the acute CSTT symptoms may be due to extensive muscle injury and tissue destruction following trauma. The muscle injury was accompanied by inflammatory cell influx that may explain the reason for inflammatory reactions and swelling (Järvinen *et al.* 2005). The damaged muscle fibres had mostly disappeared by day 7 and were replaced with regenerated muscle fibres with centred nuclei (Winkler *et al.* 2011) in the sham group whereas this procedure was delayed in the icing group. The healing of the muscle injury was identified by maturation of the regenerated muscle fibres (central nuclei) (Carlson 1973) into the larger muscle fibres with a peripherally located nuclei (Novak *et al.* 2014) 28 days post trauma. In the sham group, the mature muscle fibres were more organised, larger and closer together (remodelling phase) (Järvinen *et al.* 2007) compared to the icing group.

Overall, the outcomes of the CSTT characterisation over time suggest a trend of injury improvement for the sham group while icing appeared to delay the healing process.

5.5.2 The effect of CSTT and cryotherapy on the vascular injury

The evaluation of the vascular injury following CSTT and cryotherapy (at two levels) allowed a 3D assessment of the vascular network for the whole hindlimb where the CSTT was located (ROI), as well as a detailed analysis at the capillary level (biopsy) over time. As it was hypothesised, the qualitative and quantitative evaluation of the vascular architecture from both ROI and biopsy samples revealed notable changes to the vascular network following CSTT and cryotherapy for all time points. These findings supported the results reported for ischemia models indicating vascular morphometric changes such as the VV, VD, VN, VSp and DA following injury at various time points (Duvall *et al.* 2004, Oses *et al.* 2009).

The 3D quantitative results obtained from the ROI suggested that CSTT induces higher TSV values at days 1, 3, 7 and 28 compared to the uninjured control group. These findings were also aligned with the higher VV values in the injured hindlimbs compared to the control groups at days 3, 7 and 28 described for ischemia models (Duvall *et al.* 2004, Oses *et al.* 2009).

This increase was reduced by ice therapy at days 1, 3 and 7 compared to the sham group; however, by day 28 after injury, no significant differences could be seen between these groups. The TSV results presented for day 28 did not suggest a return to the original values prior to CSTT as the values were still significantly higher than those for the control group. Since day 28 was the latest time point in these conducted experiments, it is unknown whether after 28 days the TSV values would have reduced back towards the original values prior to injury.

In agreement with the ROI results, data for the biopsies also showed that CSTT has caused a higher VV in the sham group compared to the control group at day 1, 3, and 7 while icing has significantly induced a lower VV on these days. On the other hand, the quantified biopsy results suggest that cryotherapy has significantly reduced the VD at days 1 and 7. This was also confirmed by histomorphometrical analysis that cryotherapy significantly reduced the effect of vasodilation at day 1. In humans, it has been shown that brachial artery vessel diameter increase leads to a post occlusion blood flow increase after whole body resistance exercise training (Rakobowchuk *et al.* 2005). This finding can be further supported by reports in the literature where the capillary constriction as well as a reduction in capillary permeability and blood flow due to cold-water application has been suggested (Eston *et al.* 1999, Howatson *et al.* 2005).

The differences between the control group with either sham or icing group were not significant for VV values at day 28 suggesting a return to the original values prior to CSTT. However, in a CSTT model, authors have shown higher values for blood flow (about 20%) compared to a baseline at day 28 (Claes *et al.* 2006).

In addition, the results suggested that the pattern of vascular morphometric changes over time can be varied by the choice of treatment. For example, the sham group exhibited an increase in the VV from day 1 to day 7 followed by a decrease towards day 28 while the icing group showed a constant increase in the VV from day 1 towards day 28.

Similar to the VV results obtained from biopsy samples in the sham group (after cut-off) where higher VV values exhibited at days 1, 3 and 7 compared to the control group as well as a decrease trend of the VV towards day 28, Claes and colleagues reported an increasing trend in blood flow from day 1 to day 7. Also, the authors have shown that blood flow increases until the maximum values were reached at day 14, then they decreased towards day 28 (Claes *et al.* 2006).

On the other hand, cryotherapy has reduced the Vconn at days 1, 3 and 7 as well as the VN and DA values at days 1 and 3 post injury compared to the sham group. This may be due to a delay in angiogenesis at days 3 and 7 in the icing group. These results did not support other reported CSTT assessments using fluorescent microscopic regarding cryotherapy for 20 minutes (Schaser *et al.* 2006) and 6 hours (Schaser *et al.* 2007) following injury significantly restores the decreased functional capillary density due to CSTT to the level of non-injured hindlimbs and also increases tissue perfusion after injury.

At earlier time points, a reduction in acute CSTT symptoms such as haematoma in the icing group (Swenson *et al.* 2007) may be explained by a decrease in the VD and VN causing a delay of the perfused vessel volume in the injured region. TSV

However, the VN was significantly higher in the icing group compared to the sham group at day 28 leading to a considerable lower VSp compared to the control group since the VN is correlated with the inverse of the VSp. The elevated VN in the icing group at day 28 compared to the sham group may be due to delayed angiogenesis. Furthermore, the biopsy results suggest that icing has led to a notable decrease in the VN values only at earlier time points (days 1 and 3) compared to the sham and control groups.

The VN increased after day 3 towards day 28 in the icing group where the values at day 28 were surprisingly higher than the control group.

While species and injury model were different, the results of this study were consistent with those of previous micro-CT studies for a mouse ischemia model (Duvall *et al.* 2004). Both studies measured higher values for the VV and VConn parameters as well as lower values for the VSp at day 3 (Duvall *et al.* 2004). At day 7, the elevated values of the VV and VConn of the sham group supports the results of the same parameters reported by other authors in the injured hindlimbs of mice subjected to an ischemia model and compared to the control group (non-injured) (Oses *et al.* 2009).

5.5.3 Verification of vasodilation

After applying the cut-off technique, the micro-CT results showed higher VD values at day 1 for the sham and icing groups compared to the control group. However, the VD values were slightly reduced in the icing group. To confirm these findings, further histomorphological evaluation of day 1 post injury revealed a significant increase in the VD for the injured hindlimbs of both sham and icing groups compared to the non-injured hindlimbs. However, the histomorphological comparisons between the sham and icing groups indicated that cryotherapy has significantly reduced the VD compared to the sham group.

The vasodilation effect at earlier days following injury has been acknowledged in the literature (Stadelmann *et al.* 1998, Williamson *et al.* 2004, Li *et al.* 2007), therefore, the increase in the VD at day 1 may be attributed to vasodilation mechanism.

Vasoconstriction has been reported leading to a lower blood flow rate as well as a reduction in inflammation and swelling soon after the cooling of the traumatised muscles in rats by either cooling the tissue utilising ice pellets for 20 minutes (Smith *et al.* 1994), or superfusing cold saline at 3°C for 10 minutes (Lee *et al.* 2005), or superfusing cold saline at 8°C for 20 minutes (Schaser *et al.* 2006).

The results of this research suggest that vasoconstriction due to icing may be a short term effect and is replaced with vasodilation one day after trauma although this mechanism was reduced in the icing group compared to the sham group. The VD reduced from day 1 to day 3 for both sham and icing groups towards values close to the control group suggesting that vasodilation is an effect that occurs at very early time points and lasts for a few days. However, an increase in the VD at the later time points (e.g. at day 7 in the sham group) may be related to another mechanism such as arteriogenesis (Scholz *et al.* 2002). The effect of arteriogenesis has been reported as a dramatic increase in the diameter of pre-existing vessels 7 days after arterial occlusion in a rat ischemia model (Scholz *et al.* 2002). Both vasodilation and arteriogenesis mechanisms are necessary an adequate perfusion in the injured regions as shown by other studies (Hershey *et al.* 2001, Hoy *et al.* 2009).

This was also supported by the results of this research as higher VD values at day 1 and 7 post injury were attributed to higher VV values at the same time points in the sham group although this effect was delayed in the icing group. However, controversies were found regarding changes to the diameter of the blood vessels after cooling. While vasoconstriction has been reported following cold therapy (Lee *et al.* 2005), other authors have reported an increase in the diameter of veins although the diameter of the arteries remained the same (Smith *et al.* 1993). This may require further histomorphometrical evaluation to investigate the response of the veins and arteries to cryotherapy over time.

5.5.4 Indications of Angiogenesis

Angiogenesis has been demonstrated previously as the measurement of an increase in vascular density (the vessel number per tissue area) (Couffinhal *et al.* 1998, Hershey *et al.* 2001). The vessel number has also been applied to validate angiogenesis using micro-CT by histomorphometry (Bolland *et al.* 2008, Raines *et al.* 2011, Nebuloni *et al.* 2014). Although the micro-CT results did not indicate significant changes to the VN in the sham group compared to the control group at early time points (days 1, 3 and 7), the VN notably increased from day 7 towards day 28.

However, in the H&E images obtained from histological evaluations, more perfused blood vessels and capillaries could be qualitatively observed at day 3 and 7 post trauma in the injured hindlimbs of the sham group compared to the non-injured hindlimbs and the icing group. Quantitative histomorphometrical analysis has also verified a higher PVN at day 3 and 7 in the injured hindlimbs of the sham group compared to the non-injured hindlimbs and the icing group (Couffinhal *et al.* 1998, Hershey *et al.* 2001).

In agreement with qualitative and quantitative histological results presented for this research, previous studies have also confirmed that angiogenesis occurs mostly at the capillary level between days 3-10 after an ischemic injury in a rat's hindlimb (Schaser *et al.* 1999, Orbay *et al.* 2013).

The increase in the capillary density and angiogenesis at day 3 following injury has been also demonstrated earlier by *in vivo* microscopy of rat hindlimbs after application of a CSTT (Schaser *et al.* 1999). Newly formed capillaries need time to mature for perfusion functionality (Hershey *et al.* 2001). In addition, our micro-CT's highest available resolution (6 μm) does not allow capillaries less than 6 μm to be visualised. However, in this project, capillaries as small as 2 μm could be identified by histomorphometrical analysis. Therefore, based on findings from the literature, the increase in the PVN at day 3 and 7 shown in the histomorphometrical analysis may be attributed to angiogenesis in response to the vascular injury although this could not be detected with our micro-CT at earlier time points. As expected the newly formed blood vessels at earlier time points combined with the vascular network leading to an increase in the VN as shown by the micro-CT at the latest time point (day 28) for both sham and icing groups.

Although vWF was initially investigated outside the scope of this research, this marker is known to stain all blood vessels including pre-existing and newly formed blood vessels and may not be a specific marker to identify angiogenesis (Akagi *et al.* 2002, Legan 2005). CD105 (endoglin) has been introduced in the literature as a specific angiogenesis marker which is mostly expressed on endothelial cells of newly formed capillaries and is absent in pre-existing blood vessels (Valeria *et al.* 2008).

This immunohistochemistry marker (CD105) has been successfully used for demonstrating angiogenesis following a hindlimb ischemia in a rat model (Orbay *et al.* 2013). Using this marker, the authors could confirm that angiogenesis activation occurs between day 3 and 10 post injury in rats (Orbay *et al.* 2013). As the PVN results obtained from histomorphometrical analysis suggested higher values at days 3 and 7, this can be further investigated using CD105 marker in future research.

5.5.5 Alternatives for cryotherapy application

A variety of cryotherapy techniques using ice have been discussed in the literature such as using an ice pack without additional compression (where the weight of the ice pack was the only pressure), and with additional compression using adhesive tape on the ice pack (Barlas *et al.* 1996, Oliveira *et al.* 2007). Using a temperature probe inserted into the muscle it was shown that application of an ice pack with compression on a dog's thigh for 1 hour has reduced the intramuscular temperature by 2.5°C more than cryotherapy without compression (Barlas *et al.* 1996).

The effect of cryotherapy combined with compression for reducing the intramuscular temperature has also been confirmed in humans which leads to a 4°C lower temperature compared to cryotherapy alone (Merrick *et al.* 1993). Although cryotherapy with additional compression increases the cooling effect (Barlas *et al.* 1996) as well as restricting swelling of the tissue by locally decreasing the blood flow using a mechanical force (Levin *et al.* 1996), this method has its limitations. The overcooling of the tissue may increase the risk of damage to the tissue due to freezing, prolonged vasoconstriction and hypoxia (Wilke *et al.* 2003). Two common cryotherapy techniques have been compared by investigating the cooling of deep tissue by using an ice pack containing ice cubes and a solid ice block made in a cup (Zemke *et al.* 1998). This experiment was conducted in humans by measuring the muscle temperature using a hypodermic needle microprobe inserted through the skin into the medial side of the gastrocnemius muscle (n=7) for 15 minutes.

It was confirmed that the muscle cooled faster after application of an ice block (17.9 ± 2.4 minutes) compared to an ice pack (28.2 ± 12.5 minutes). Therefore, for this research, the cryotherapy technique was conducted by gently applying a block of ice over the injured muscle with no additional compression except for the weight of the ice block. Furthermore, since this research focused on the vascular morphometric changes following traumatic injury, the goal was to avoid any other influencing factors on the vasculature and muscle tissue such as compression. In general, cryotherapy using a block of ice was inexpensive and simple. The small blocks of ice were made and applied directly onto the CSTT region. However, based on the results presented here, cryotherapy using an ice block for 20 minutes is not recommended for a fast recovery of the injured tissue and vasculature following CSTT in rats.

While intermittent cryotherapy over a short duration (e.g. 3×10 minutes) has been suggested to be efficient for relieving the pain of ankle sprains (Bleakley *et al.* 2006) and Achilles tendon disorders in humans (Knobloch *et al.* 2007), this treatment regime has been tested in rats over a longer duration of 3×30 minutes for each session.

Although the results of the extended intermittent cryotherapy in rats has been shown to be effective for reducing the size of the injury area (Oliveira *et al.* 2007), this may cause more internal damage to the muscles and vasculature due to the prolonged exposure to cold temperatures (Wilke *et al.* 2003, Schaser *et al.* 2007). At the other end of the cryotherapy spectrum, the immersion of the rat's impacted hindlimbs in cold water ($12-15^{\circ}\text{C}$) for 30 minutes has shown to restrict swelling after soft tissue trauma (Dolan *et al.* 1997).

Finally, another possible treatment regime is the application of alternating 'cold and hot' water, which has been suggested to reduce acute sports injuries in humans through alternating vasoconstriction and vasodilation and consequently, stimulating the blood flow and decreasing the swelling (Cochrane 2004).

More research is still required for an objective conclusion regarding the effect of cryotherapy alternatives on the healing of the vascular and muscle injury following trauma.

5.5.6 Limitations of the icing study

Although both sham and icing groups at various time points indicated a satisfactory perfusion, there were a few cases from days 1, 3 and 7 that appeared to be poorly perfused due to a delay in perfusion causing a variability within the data of a few vascular morphometric parameters.

A reason for this delay was that the inserted catheter popped out of the left ventricle during perfusion. To perfuse the rats, a catheter was inserted through the left ventricle and secured by a liquid adhesive glue (UHU All Purpose Glue Adhesive 7 ml). However, a proper adhesion was not achieved by using this glue, and this caused the catheter to pop out of the left ventricle during perfusion in a few cases. Although this problem improved by replacing the adhesive with a superior glue (Loctite Super Glue 5g), the catheter still popped out of the left ventricle in a few cases due to the wet tissue surface. This issue was finally resolved for the later groups by gently drying the heart's surface using a small paper towel before inserting the catheter and applying the super glue. However, the removal of the catheter in the middle of the perfusion procedure led to a delay and consequently a reduction of the perfusion in a few cases. Since the data was normalised, which reduced the inter-individual differences, and as the qualified outliers were removed from the analysis, the final results were not significantly affected by this problem.

A high variability in the biopsy results may also be due to the small sample size. The sample size of 4 calculated for this study was based on the TSV/TV parameter obtained from the ROI with comparable values found from the literature. Throughout this research, it was shown that the ROI evaluations exhibited a lower CV compared to the biopsy samples. Therefore, by increasing the sample size the high variability within the biopsy samples may be reduced.

Current methods described for this study have used micro-CT evaluation and histological analysis (H&E and vWF) to show an increase in the number of blood vessels following CSTT particularly at days 3 and 7 in the injured hindlimbs. However, this study was unable to distinguish between pre-existing and newly formed blood vessels.

More immuno-histological assessments using markers specifically for newly formed blood vessels (e.g. CD105) (Orbay *et al.* 2013) are still required to provide further evidence confirming angiogenesis. Furthermore, for better detection and quantification of different inflammatory cells including macrophages and neutrophils, immunohistochemistry analysis using specific markers such as CD68 to identify macrophages and HIS48 to detect neutrophils can be suggested for future studies.

5.5.7 Concluding remarks

In order to fulfil another aim of this research, the CSTT was characterised qualitatively and quantitatively over time and after cryotherapy. A trend of healing along with a reduction of haematoma was found from day 1 towards day 28. While cryotherapy significantly reduced acute CSTT symptoms such as the size of the haematoma only one day after trauma, this caused a delay in healing over a longer period (days 3 and 7). Histological evaluations also suggested that cryotherapy delays the presence of inflammatory cells and regenerated muscle fibres in the injured regions at days 3 and 7.

The developed vascular injury model allowed us to investigate the effect of CSTT and cryotherapy on structural elements of the vascular network over time. The assessment of the vascular morphometric parameters suggested that cryotherapy delays the early mechanisms (e.g. vasodilation and perfused vessel volume) which are necessary for healing the injured vasculature and tissue particularly at earlier time points from day 1 to 7. The values of the vascular morphometric parameters in the sham group did not return to the values prior to injury (control group) in most cases suggesting that the healing period may not be complete at day 28. This finding supports other studies where the authors have shown in a CSTT model that blood flow did not return to the control values at day 28 (Claes *et al.* 2006).

The effect of vasodilation was also confirmed one day after CSTT while this was reduced due to cryotherapy in the icing group.

Furthermore, indications of angiogenesis were found in the histomorphometrical analysis at days 3 and 7 which was in agreement with previous reports (Orbay *et al.* 2013).

The normalised results obtained from the ROI over time suggested a good level of reproducibility by indicating small CV values at different time points. However, the normalised results collected from the biopsy samples exhibited degrees of variability for the vascular morphometric parameters. The variability within the normalised results was significantly reduced in most cases by applying different strategies such as excluding outlier values and by applying the cut-off technique.

In addition, by refining the methods presented in this research for perfusing the animals over time, the results improved at the later time points particularly at day 28, which exhibited small CV values. The reproducibility comparisons confirmed that the DA was the most reproducible parameter and the VConn with a high level of variability even after excluding the outliers was the most sensitive parameter. Investigation through the literature also confirmed that the VConn shows more variability compared to other vascular morphometric parameters (Duvall *et al.* 2004, Oses *et al.* 2009). This suggests that the VConn parameter obtained from the micro-CT software (Scanco) may not be suitable for future vascular analysis.

Chapter 6: Discussion and conclusions

6.1 GENERAL DISCUSSION

The focus of this research was to characterise changes to the vascular anatomy following a closed soft tissue trauma (CSTT) and to determine whether it is affected by a therapeutic method, such as cryotherapy.

Therefore, the first aim of this research was to develop a validated CSTT model using an impact device. To achieve this, the first step was to characterise and validate the impact device to ensure that it created a controlled and reproducible CSTT and vascular injury.

The reproducibility of the CSTT model based on the impact device was demonstrated and the optimal weight and velocity of the drop weight for producing a reproducible CSTT with the same grade of severity was determined. Furthermore, by using a high-speed camera, it was confirmed that the drop weight motion and its velocity pattern could be accurately predicted using theoretical analysis. This means that the impact energy transferred to the tissue to create the injury can also be anticipated accurately using theoretical calculations. Using the characterised impact device, a reproducible CSTT model including a vascular injury of Grade 4 based on the AO classification was developed. This model was characterised quantitatively for changes to the vascular morphology following CSTT using contrast-enhanced micro-CT imaging. The model was then verified through histological and histomorphometrical assessments. This was to confirm the vascular morphometric results derived from the micro-CT evaluations, as well as to assist in the interpretation of the micro-CT results, indicating physiological processes during the healing period, such as vasodilation at day 1 and efficiency of the perfusion protocols. Three phases of CSTT healing including destruction, repair and remodelling mechanisms have been identified by microscopic observations of the injured areas (Järvinen *et al.* 2005, Hodde *et al.* 2007, Enoch *et al.* 2008, Smith *et al.* 2008).

These observations showed destructed muscle fibres and blood vessels, disoriented muscle fibres and the presence of inflammatory cells at the earlier time points particularly at days 1 and 3 (destruction phase). The destructed injured regions were eventually replaced with newly regenerated muscle fibres at the later time points initiating at day 7 along with the presence of capillary clusters in the injury site (regeneration and repair phase).

Consistent with the literature (Cízková *et al.* 2009, Myburgh *et al.* 2012), the results of this research confirmed regenerating skeletal muscle fibres which were detected as myofibres with a central nuclei in the histological assessments along with more blood vessels that appeared in the injured regions at day 7 post injury. Muscle observations at the latest time point (day 28) showed a large number of matured muscle fibres with migrated nuclei onto the periphery of the myofibres in tissue regions where trauma was induced in both sham and icing groups.

The next goal of this research was to investigate the vascular morphology changes following CSTT and during icing treatment through a standardised vascular injury model in 3D. Using high-resolution contrast-enhanced micro-CT images and histological analysis, the developed model enabled us to characterise the vascular morphometric changes following CSTT qualitatively and quantitatively. A 2-stage evaluation of whole hindlimb and localised sub-region characterisation of the microvasculature allowed for detection of detailed architectural changes of the vascular network. The evaluation methods were shown to be sensitive enough to detect structural changes in the vascular network following injury and during the healing period in treated (cryotherapy) and untreated animals. The reproducibility of this model was confirmed by indicating a small coefficient of variation for the normalised TSV results obtained from the ROI evaluation. Furthermore, after data processing biopsy samples suggested an acceptable level of reproducibility for a few vascular morphometric parameters such as VD and DA at three time points including day 28. After improvement of the perfusion methods at later time points (day 28), the VN and VSp also indicated an acceptable level of reproducibility.

The accuracy of the model was also verified through validation of the micro-CT results by using histomorphometrical analysis, particularly for the parameter vessel density (vessel number per area), using an intra-class correlation coefficient and Bland-Altman plot. The efficiency of the perfusion protocols for filling the blood vessels with contrast agent (microfil) was determined through the calculation of an average relative vascular perfusion rate of 72%, which was independent of vessel diameter. This suggested that the contrast agent also filled vessels below the detection limits of the micro-CT scanner.

The developed CSTT model indicated significant changes in the vascular morphometric parameters following trauma in the injured hindlimbs compared to the non-injured hindlimbs. The model suggests that CSTT causes a higher TSV and VV, VD, VConn, VSp and a lower VN in the injured hindlimbs compared to the non-injured hindlimbs one day post trauma. These morphological changes at day 1 may be explained through the events that occur during the destructive phase. For example, the destruction of the blood vessels due to trauma, which causes early blood flow deficiency (Claes *et al.* 2006) may have resulted in a higher demand for more oxygen supply and nutrition for the injured tissue (Järvinen *et al.* 2005). The response by the surviving vasculature surrounding the necrotic region to this demand may be to widen the blood vessel diameter through vasodilation to increase the blood perfusion rate and vessel volume (VV) in the injured regions.

In addition, the results obtained from the icing study suggested that not only CSTT changes the vascular morphometric parameters soon after injury and over time but also the recovery of the vascular network may vary by the choice of treatment. For example, the results of this research suggested that cryotherapy has reduced the vasodilation at day 1 as well as the VV, VN and VConn following CSTT and at earlier time points.

Together, the results suggest the effect of vasodilation at day 1 following injury as well as arteriogenesis and indications of angiogenesis at later time points may indicate the restoration of the perfused vessel volume (VV) at the injury site.

Signs of angiogenesis were qualitatively evaluated through histological analysis by observing the large number of capillaries in the injured region. This was also quantitatively shown by histomorphometrical analysis of the perfused vessel number (PVN) indicating higher values in the injured hindlimbs compared to the non-injured hindlimbs. Based on the results presented for the PVN parameter, it appears that icing treatment significantly delays angiogenesis at days 3 and 7.

Throughout this research, it was demonstrate that by early interference with the natural healing process using ice treatment; vasodilation at day 1 may be reduced, resulting in a decrease of the perfused volume. This may also cause a retardation of arteriogenesis and angiogenesis at later time points. While icing reduces acute CSTT symptoms such as swelling and pain post trauma, the findings of this research suggest that it may delay the recovery of the injured vasculature and tissue at earlier time points. The delay in tissue healing and muscle fibre regeneration following cryotherapy is supported by other CSTT models reported in the literature (Takagi *et al.* 2011). However, it was also found that the differences of the measured vascular morphometric parameters between sham and icing groups were not statistically significant at the latest time point (day 28) although the VV and DA were notably higher in the icing group. Furthermore, it appeared that healing period of the CSTT and injured vasculature may take longer than 28 days since most vascular morphometric parameters did not show a return to the original values prior to injury.

6.1.1 What is novel?

To the best knowledge of the author, this research has for the first time provided a systematic characterisation of vascular injury following CSTT and during healing, with or without treatment using ice therapy. New strategies and methods were developed to answer relevant research questions. The novel aspects of this research are:

- ✚ The systematic characterisation and validation of the weight and velocity of the drop weight at the impact surface of an impact device to ensure a standardised and reproducible CSTT including vascular injury.
- ✚ To date, all available 3D vascular injury characterisations reported in the literature have been based on ischemia injury models, but for the first time this was conducted for a CSTT model through this research.
- ✚ The application of ice for CSTT treatment is not new and this therapeutic method has been studied qualitatively (Hubbard *et al.* 2004) and quantitatively in 2D (Schaser *et al.* 2006, Takagi *et al.* 2011). However, this research represents the first 3D characterisation of the effect of icing on the recovery of the damaged vascular network.
- ✚ A new method was developed to verify the efficiency of the perfusion protocols for filling the vascular network with contrast agent (microfil). This method was based on the measurements of the relative vascular perfusion parameter (RVP) and the smallest perfused capillary that could be detected. This approach can be applied for any contrast-enhanced imaging system.
- ✚ A geometrical technique was designed to collect correlated areas in a defined, consistent and standardised manner for all biopsy samples throughout this research.
- ✚ Although the shrinkage of microfil has been qualitatively reported in the literature (Nyangoga *et al.* 2011), this has been quantified for the first time in this research using histological sections.

6.1.2 Limitations and recommendations

1. One of the major challenges for this research was a general shrinkage of the microfil contrast agent that was observed in all blood vessels during microscopic evaluation of histological sections. The comparisons between the diameter of the correlated blood vessels obtained from the

micro-CT (microfil diameter) and histology sections (actual vessel diameter) showed a considerable shrinkage of the microfil. Therefore, in the micro-CT scans, the absolute values of the vessel diameter may not be a precise representation of actual vessel diameter as was observed in the histological images. Subsequently, other parameters related to the VD such as absolute values of the VV will be affected. Further analysis revealed that the microfil shrinkage of about 50% has occurred in all diameter ranges of blood vessels and this was independent of vessel size. A strategy to overcome the shrinkage problem could be to present the results as comparisons between and within the groups as well as normalising the quantitative values of the injured hindlimbs over the non-injured hindlimbs instead of using absolute values. Therefore, the comparison results between the sham and icing groups across the time points were presented as normalised values to reduce the effect of the microfil shrinkage on the findings in this research. Additionally, there are vascular morphometric parameters such as PVN (related to the VN), RVP (related to the VN), VConn (related to the vascular connections) and DA (related to the vascular orientation) which are independent from VD and therefore, are not influenced by the microfil shrinkage. The biopsy results of the vascular injury model presented for the VSp parameter obtained from the non-injured hindlimbs at day 1 indicated that this parameter is 14.4 times larger than the VD (both parameters have the same unit (mm)). Therefore, the VSp may not be significantly affected by the VD variations because the VSp values are too large compared to the very small VD variations and consequently, the shrinkage effect on the VSp is negligible. As discussed, previous studies have recommended the microfil contrast agent as a superior material for a high quality image *in vitro*. These authors scanned their samples while they were stored in formalin with no mention of shrinkage (Bentley *et al.* 2002, Duvall *et al.* 2004, Yeung *et al.* 2011). In this study, the samples were transferred to ethanol after fixation with formalin and scanned while they were stored in ethanol. Recently, microfil shrinkage in vascular imaging due to ethanol has been discussed in the literature (Nebuloni *et al.* 2014).

Unfortunately, this article was published after the experimental studies were finished. The relaxation of the vascular smooth muscle 24 hours after death (Ebner *et al.* 2011) can be another possible cause for an increase in the discrepancy between diameters of the microfil and the vessels which requires further investigation.

2. While leakage of the microfil contrast agent outside the broken blood vessels has also been reported in the literature (Downey *et al.* 2012), in this research, leakage was not observed. Although the presence of a haematoma is a sign of vascular breakdown and subsequently internal bleeding within the tissue, the vascular tear may have been sealed by blood clots soon after the impact. Therefore, after the microfil perfusion at 1, 3, 7 and 28 days following trauma, a leakage of microfil was not observed within the tissue. Furthermore, this may indicate that the perfusion flow rate used for microfil infusion utilising the peristaltic pump had been adjusted appropriately and this has facilitated a fluid pressure that prevented vascular rupture and microfil leakage.
3. Further limitations were faced during the micro-CT evaluation, due to the relatively large file size caused by the high resolution scanning of both intact hindlimbs (n=108, around 25-30 GB for each hindlimb) and biopsy samples (n=108, around 7-10 GB for each biopsy sample).
4. Due to the limited memory of our micro-CT system, the quantitative evaluations of vascular morphology had to be limited to biopsy samples only, and within those, to the region of the most affected muscle (biceps femoris) which was located in the top 250 image slices sections of the biopsy specimens.
5. During the perfusion experiments, a high sensitivity of the perfusion protocols with respect to timing of the perfusion was also noticed. After euthanasia, a delay in starting the perfusion and flushing the blood

vessels appeared to cause blockages in blood vessels that may be due to blood clot formation leading to variability of the results. Furthermore, although the RVP percentage (72%) indicated a satisfactory perfusion, the blockage of the blood vessels due to a delay in perfusion may have reduced the perfusability level of the vasculature causing 28% of blood vessels not to be filled with microfil. In this research, due to animal welfare concerns, blood vessels were flushed using heparinised saline immediately after euthanasia, once death was confirmed. It has been described (Lu *et al.* 2010) that perfusion may be initiated on the anaesthetised animal, ultimately causing the animals death by excessive blood loss during anaesthesia. In this procedure, since the animals are still alive, the pumping of the heart assists the drainage of the remaining blood. This may reduce the blockage of blood vessels due to blood clots, and therefore will increase the number of perfused blood vessels. In addition, as the RVP parameter was measured in the histological sections (72%), there is a possibility that the microfil was washed away from a few vessels due to extensive rinsing during the histological processing. This suggests that the effective number of blood vessels filled with microfil during micro-CT scanning may have been higher than the RVP presented for the histomorphometrical results. In the histological sections, microfil had washed away from a few blood vessels that was found by comparing corresponding sections from micro-CT. Therefore, to prevent this, another histological process that does not require extensive washing such as the cryosectioning technique is suggested. This method uses frozen tissue for sectioning allowing for less tissue processing (Herzog *et al.* 2002, Brey 2003). On the other hand, the microfil contrast agent is a viscous material and therefore, a higher flow rate may allow perfusing more blood vessels. However, the concern was that a higher flow rate may also increase the chance of rupturing blood vessels due to super-physiological pressures.

6. Another limitation was that current methods described for this study have used micro-CT evaluation and histological analysis (H&E and vWF) to show an increase in the number of blood vessels following CSTT in the injured hindlimbs. However, this study was unable to distinguish between pre-existing and newly formed blood vessels. More immunohistological assessments using markers specific to newly formed blood vessels (e.g. CD105) are still required to provide further evidence confirming angiogenesis. In addition, this research was limited to precisely detect and quantify different inflammatory cells including macrophages and neutrophils. The immunohistochemical analysis using specific markers for identifying the inflammatory cells can be suggested for future research.

6.2 RESEARCH IMPLICATIONS AND CONTRIBUTIONS TOWARDS KNOWLEDGE

A standardised CSTT model was developed based on real clinical conditions such as sports injuries or accidents that can improve the guidelines for current clinical classifications (e.g. Tscherne and AO). For example, the quantitative measurements of the inflamed areas (haematoma) can be added to qualitative observations by applying the methods established in this research to monitor the healing trend over time using a particular treatment (e.g. cryotherapy). The CSTT quantification procedure based on the measurements of the haematoma area is inexpensive providing valuable information in a non-invasive manner for clinical applications.

The methodologies developed for characterising the impact device and creating a controlled CSTT can be useful for other experimental orthopaedic research including musculoskeletal injuries. The findings of this research based on the characterisation of CSTT and the pattern of changes to the vascular morphology following CSTT provides a framework that may be applied as a fundamental basis for future wound healing and therapeutic modalities to monitor the effect of a treatment over time, such as cryotherapy.

For example, the results of this experimental study indicated that icing may cause secondary tissue damage through a reduction in vasodilation and the perfusion volume at earlier time points.

These findings not only encourage clinical and experimental studies on other therapeutic alternatives but also question the efficiency of these traditional treatments that have no convincing evidence and should be re-examined using a scientific basis.

Furthermore, a cut-off technique was developed throughout this research that can be beneficial for the study of microvasculature within various diameter ranges or to reduce the variability of results due to the presence of large blood vessels for the VV and VD parameters. While the perfusion methods used in the literature have been described qualitatively, we have also developed new quantitative measures to determine the smallest capillary diameter that was filled with contrast agent, and to determine the efficiency of the perfusion protocols based on the calculation of the RVP . These methods can be beneficial for characterising the perfusability of any contrast agent throughout the vascular network. In addition, the quantitative assessment of the microfil shrinkage may be useful for future studies using this contrast agent for perfusing vasculature.

The main contribution of this research to knowledge is to provide a scientific framework for the quantitative characterisation of changes to the vascular architecture in preclinical studies of CSTT. This allows for the objective diagnosis and monitoring of CSTT, and for the evaluation of the impact of treatment on the progression of healing. Eventually, the methods developed in this project may serve as a validation tool during the development of future non-invasive clinical assessment modalities for CSTT.

6.3 FUTURE DIRECTIONS

In this research, the quantitative framework was developed for vascular morphometric assessments using contrast enhanced micro-CT imaging.

To extend this model, an investigation into the vascular functionality following CSTT is suggested. Open questions remain on the long-term effect of icing on the healing of injured muscles. Also, practicing different icing protocols and using heat for the injury treatment rather than icing are other alternatives requiring further research.

This research investigated the effect of icing on the vascular and muscle injuries during 28 days following CSTT where the destructive and repair phases as well as the early remodelling phase were discussed. However, our knowledge regarding the effect of icing on the healing of vascular and muscle injury during the remodelling phase is limited. For example, a few vascular morphometric parameters such as the VN showed significantly higher values at day 28 in the icing group. In this regard, the unanswered questions are whether the values of this parameter will increase further or eventually decrease and if it decreases, when does the decline occur? A long-term study may allow for a better judgment regarding the outcome of the muscle injury using cryotherapy.

Different cryotherapy alternatives were also discussed in Chapter 5. Although some of these methods such as intermittent cryotherapy with shorter duration were reported to be efficient for humans, this still needs to be assessed in rats.

Application of low-level heat wrap therapy has been reported to significantly reduce the muscle soreness and lower back pain in humans (Mayer *et al.* 2006). This treatment can be an option for future investigation on the effect of low-level heat on the vascular injury following CSTT.

Using electromyogram (EMG), a clinical study on healthy ankles has proposed that icing influences the pain threshold where a 10°C decrease in skin temperature has been shown to result in a 33% reduction of nerve conduction velocity as well as an increase in pain threshold and pain tolerance (Algaflly *et al.* 2007). With respect to the vascular morphometric changes, the relationship between the injured and non-injured muscle activity following trauma as well as between the sham and icing treatments may be worthy of future assessments. This research was limited to quantitatively measuring the activity level of the muscles following CSTT and cryotherapy.

For future research, the examination of other available therapeutic methods for CSTT such as hyperbaric oxygen therapy (HBOT) can be explored. The benefits of this non-invasive method which uses a high concentration of oxygen for wound healing has been discussed in the literature (Babul *et al.* 2003, Buettner *et al.* 2007).

The literature shows that HBOT has been advocated for increasing tissue oxygenation, thereby improving the collagen deposition and angiogenesis (Gill *et al.* 2004, Hopf *et al.* 2005, Rodriguez *et al.* 2008).

However, the direct effect of HBOT on the healing of the vascular injury following CSTT has not yet been quantitatively evaluated.

For better verification of the muscle injury and its regeneration, microscopic evaluations can be utilised through immunohistochemistry using the nestin antibody (Cízková *et al.* 2009) which has been recently introduced for identifying newly formed myofibres. As mentioned, the vWF marker has been commonly used confirming angiogenesis activation (Starke *et al.* 2011). This marker was also applied in the methodology of this research to confirm the increase in the number of blood vessels that may be due to angiogenesis. However, vWF stains all blood vessels including pre-existing and newly formed ones.

Recently, the CD105 antibody has been suggested as a marker to specifically identify newly formed endothelial cells of capillaries indicating angiogenesis (Orbay *et al.* 2013). Therefore, this research can be continued using the CD105 marker to distinguish between pre-existing and newly formed capillaries to provide stronger evidence confirming angiogenesis particularly at days 3 and 7.

It has been shown that inflammatory cells such as macrophages stimulate angiogenesis (Li *et al.* 2007), therefore, another future direction can be to determine the relationship between the inflammation and angiogenesis following CSTT through the evaluation and quantification of the inflammatory cells such as macrophages using immunohistochemistry analysis (Tsivitse *et al.* 2003).

On the other hand, micro-CT software packages were originally developed for the morphometric analysis of hard tissue such as trabecular bone structures and have been modified for vascular morphological investigation. However, there are geometrical parameters that further describe the vascular network, such as vessel length, that the standard micro-CT software was not able to measure.

Therefore, combining the vascular parameters derived from a robust modality such as the standard micro-CT evaluation software with other morphometric parameters provided by other software tools (i.e. AMIRA) may allow for an even better interpretation of the micro-CT results.

Initial evaluations were conducted to assess the vascular morphometric parameters more comprehensively through AMIRA software and the preliminary results of a pilot study are presented in Figure 6-1.

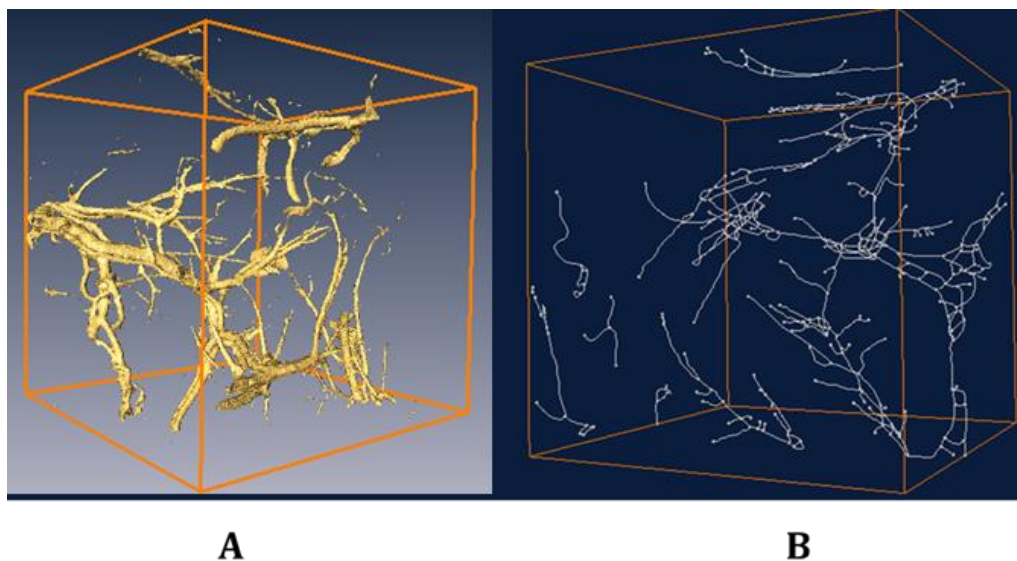


Figure 6-1: 3D of the vascular network using AMIRA software. Initial results obtained from a pilot study using AMIRA software are presented for the vascular network of a non-injured hindlimb of the sham group. Image (A) shows a 3D reconstruction of the vascular network morphology and image (B) illustrates a skeletonised image of the same vascular network where the vascular connections are exhibited as nodes.

6.4 CONCLUSION

This research was primarily aimed to develop a new, standardised trauma model in rats and methods to investigate the changes of the vascular morphology following CSTT in 3D at different time points.

In order to characterise the experimental model, its reproducibility and accuracy were verified through comparisons with histomorphometrical assessments.

The sensitivity of this experimental framework was also tested by comparing the vascular morphology after trauma and during healing in untreated and treated rats using cryotherapy. The sensitivity of this framework was confirmed through the detection of the significant differences between the injured and non-injured hindlimbs regarding the muscle injury size and the vascular morphometric parameters following trauma, over time (sham group) as well as between treatment groups (sham and icing groups).

The key findings of this characterised experimental model and its application to study the effect of cryotherapy on CSTT were:

- ✚ The vascular morphology changed significantly after trauma, and its recovery varied between untreated animals and those treated with ice.
- ✚ CSTT increases the perfused vessel volume in the injured region at earlier time points while cryotherapy delays this mechanism.
- ✚ One day after trauma, the diameter of the injured blood vessels increased significantly compared to the non-injured vessels due to vasodilation, which perfused more blood to the injury site during healing. However, cryotherapy reduces the effect of vasodilation through decreasing the diameter of the blood vessels leading to a reduction in the vessel volume perfusion one day after trauma.
- ✚ The early disorientation (degree of anisotropy) in the vascular network due to the CSTT reduces significantly at the latest time points (day 28) suggesting more organised network in the remodelling phase.

- ✚ Despite the fact that icing reduces the size of the haematoma in the early stages of injury recovery, the evaluation of the vascular injury suggests that it also delays the restoration of the vascular network.
- ✚ Practically, normalising the data, excluding the qualified outlier values and using the cut-off technique were found to be effective ways for reducing the variability within the data obtained from the vascular network quantitatively.

Bibliography

- Akagi, K., Y. Ikeda, Y. Sumiyoshi, Y. Kimura, J. Kinoshita, M. Miyazaki and T. Abe (2002). "Estimation of angiogenesis with anti-CD105 immunostaining in the process of colorectal cancer development." *Surg* 131(1, Supplement 1): S109-S113.
- Akimau, P., K. Yoshiya, H. Hosotsubo, H. Takakuwa, Tanaka and H. Sugimoto (2005). "New experimental model of crush injury of the hindlimbs in rats." *J Trauma* 58: 51-58.
- Alexander, G., A. W. Bell and J. R. Hales (1973). "Effects of cold exposure on tissue blood flow in the new-born lamb." *J Physiol* 234(1): 65-77.
- Algafly, A. A. and K. P. George (2007). "The effect of cryotherapy on nerve conduction velocity, pain threshold and pain tolerance." *Br J Sports Med* 41(6): 365-369.
- Altizer, L. (2004). "Compartment syndrome." *J Orthop Nurs* 23(6): 391-396.
- Anderson, J. E. and A. C. Wozniak (2004). "Satellite cell activation on fibers: modeling events in vivo--an invited review." *Can J Physiol Pharmacol* 82(5): 300-310.
- Annapragada, A. V., E. Hoffman, A. Divekar, E. Karathanasis and K. B. Ghaghada (2012). "High resolution blood pool vascular imaging with nano scale vectors." *J Methodist Debaque Cardiovasc* 8(1): 18-22.
- Australian Institute of Health and Welfare. (2012). "Australia's health." 13 AUS 156. AIHW. Canberra. from <http://www.aihw.gov.au/WorkArea/DownloadAsset.aspx?id=10737422169>
- Babul, S., E. C. Rhodes, J. E. Taunton and M. Lepawsky (2003). "Effects of intermittent exposure to hyperbaric oxygen for the treatment of an acute soft tissue injury." *J Clin Sport Med* 13(3): 138-147.
- Badiru, A. B. (2013). "Handbook of industrial and systems engineering." CRC Press ISBN:1-4665-1504-X, 978-1-4665-1504-8.
- Baoge, L., E. Van Den Steen, S. Rimbaut, N. Philips, E. Witvrouw, K. F. Almqvist, G. Vanderstraeten and L. C. Vanden Bossche (2012). "Treatment of skeletal muscle injury: A review." *ISRN Orthop* 2012: 7.
- Barlas, D., C. S. Homan and H. C. Thode Jr (1996). "In vivo tissue temperature comparison of cryotherapy with and without external compression." *Ann Emerg Med* 28(4): 436-439.
- Bartlett, J. W. and C. Frost (2008). "Reliability, repeatability and reproducibility: analysis of measurement errors in continuous variables." *Ultrasound Obstet Gynecol* 31(4): 466-475.
- Bauer, S. M., R. J. Bauer and O. C. Velazquez (2005). "Angiogenesis, vasculogenesis, and induction of healing in chronic wounds." *Vasc Endovascular Surg* 39(4): 293-306.
- Bemelmans, R. H. H., E. C. Boerma, J. Barendregt, C. Ince, J. H. Rommes and P. E. Spronk (2009). "Changes in the volume status of haemodialysis patients are reflected in sublingual microvascular perfusion." *Nephrol Dialysis Transplant* 24(11): 3487-3492.

- Bentley, M. D., M. C. Ortiz, E. L. Ritman and J. C. Romero (2002). "The use of microcomputed tomography to study microvasculature in small rodents." *Am J Physiol Regul Integr Comp Physiol* 282(5): R1267-R1279.
- Birkenhäger-Frenkel, D. H., P. Courpron, E. A. Hüpscher, E. Clermonts, M. F. Coutinho, P. I. Schmitz and P. J. Meunier (1988). "Age-related changes in cancellous bone structure. A two-dimensional study in the transiliac and iliac crest biopsy sites." *Bone mineral* 4(2): 197-216.
- Bismarck Public School. (2014). "Rat dissection, Bismarck, North Dakota, USA." from http://www.bismarckschools.org/uploads/resources/21460/rat_dissection.pdf
- Blaisdell, F. W. (2002). "The pathophysiology of skeletal muscle ischemia and the reperfusion syndrome: a review." *J Cardiovasc Surg* 10(6): 620-630.
- Bland, J. M. and D. G. Altman (1990). "A note on the use of the intraclass correlation coefficient in the evaluation of agreement between two methods of measurement." *Comput Biol Med* 20(5): 337-340.
- Bland, J. M. and D. G. Altman (2010). "Statistical methods for assessing agreement between two methods of clinical measurement." *Int J Nurs Stud* 47(8): 931-936.
- Bleakley, C., S. McDonough and D. MacAuley (2004). "The use of ice in the treatment of acute soft tissue injury: a systematic review of randomized controlled trials." *Am J Sports Med* 34: 251-261.
- Bleakley, C. M., S. M. McDonough and D. C. MacAuley (2006). "Cryotherapy for acute ankle sprains: a randomised controlled study of two different icing protocols." *Br J Sports Med* 40(8): 700-705.
- Boerckel, J. D., B. A. Uhrig, N. J. Willett, N. Huebsch and R. E. Guldberg (2011). "Mechanical regulation of vascular growth and tissue regeneration in vivo." *Proc Natl Acad Sci*.
- Bolland, B. J. R. F., J. M. Kanczler, D. G. Dunlop and R. O. C. Oreffo (2008). "Development of in vivo μ CT evaluation of neovascularisation in tissue engineered bone constructs." *J Bone* 43: 195-202.
- Bouxsein, M. L., S. K. Boyd, Christiansen B.A., R. E. Guldberg, K. J. Jepsen and R. Müller (2010). "Guidelines for assessment of bone microstructure in rodents using micro-computed tomography." *J. Bone Miner Res.* 25(7): 1468-1486.
- Bouxsein, M. L., S. K. Boyd, B. A. Christiansen, R. E. Guldberg, K. J. Jepsen and R. Müller (2010). "Guidelines for assessment of bone microstructure in rodents using micro-computed tomography." *J Bone Miner Res* 25(7): 1468-1486.
- Boylan, J. E., P. Goodwin, M. Mohammadipour and A. A. Syntetos (2015). "Reproducibility in forecasting research." *Int J Forecasting* 31(1): 79-90.
- Brancaccio, P., F. M. Limongelli and N. Maffulli (2006). "Monitoring of serum enzymes in sport." *Br J Sports Med* 40(2): 96-97.
- Brey, E. M. (2003). Quantitative three-dimensional analysis of vascular microstructure in tissue engineering. 3090794 Ph.D., Rice University.
- Buettner, M. F. and D. Wolkenhauer (2007). "Hyperbaric oxygen therapy in the treatment of open fractures and crush injuries." *Emerg Med Clin North Am* 25(1): 177-188.

- Bushberg, J. T., J. A. Seibert, E. M. Leidholdt Jr and J. M. Boone (2011). *The essential physics of medical imaging*. r. edition. PA, USA, Wolters Kluwer/Lippincott Williams & Wilkins: 1030.
- Canadian Society of Diagnostic Medical Sonography. (2008). "Professional practice guidelines and policy statements for Canadian sonography." from http://www.sonographycanada.ca/Apps/Sites-Management/FileDownload/DataDownload/6945/CSDMS_ProfessionalPractice_E/pdf/1/1033
- Carlson, B. M. (1973). "The regeneration of skeletal muscle — a review." *Am J Anatomy* 137(2): 119-149.
- Casey, D. P. and M. J. Joyner (2012). "Influence of α -adrenergic vasoconstriction on the blunted skeletal muscle contraction-induced rapid vasodilation with aging." *113(8): 1201-1212.*
- Cheung, W. H., M. H. Sun, Y. P. Zheng, W. C. W. Chu, A. H. C. Leung, L. Qin, F. Wei, Y., and K. S. Leung "Stimulated angiogenesis for fracture healing augmented by low-magnitude, high-frequency vibration in a rat model—evaluation of pulsed-wave doppler, 3-D power doppler ultrasonography and micro-CT microangiography." *Ultrasound Med Biol* 38(12): 2120-2129.
- Cízková, D., T. Soukup and J. Mokřý (2009). "Nestin expression reflects formation, revascularization and reinnervation of new myofibers in regenerating rat hind limb skeletal muscles." *Cells, tissues, organs* 189(5): 338-347.
- Claes, L., N. Maurer-Klein, T. Henke, H. Gerngross, M. Melnyk and P. Augat (2006). "Moderate soft tissue trauma delays new bone formation only in the early phase of fracture healing." *J Orthop Res*: 1178-1185.
- Clark, R. (1996). *The molecular and cellular biology of wound repair*. Springer Science & Business Media. NY, USA: 611.
- Cochrane, D. J. (2004). "Alternating hot and cold water immersion for athlete recovery: a review." *Phys Ther Sport* 5: 26–32.
- Cohen, J. (1992). "A power primer." *Psychol Bulletin* 112(1): 155-159.
- Cohen, J. (2013). *Statistical power analysis for the behavioral sciences*. Taylor and Francis Oxon, UK: 567.
- Cohn, B. T., R. I. Dreager and D. W. Jackson (1989). "The effects of cold therapy in the postoperative management of pain in patients undergoing anterior cruciate ligament reconstruction." *Am J Sports Med* 17: 244–249.
- Collins, N. C. (2008). "Is ice right? Does cryotherapy improve outcome for acute soft tissue injury?" *Emerg Med J* 25(2): 65-68.
- Couffinhal, T., M. Silver, L. P. Zheng, Kearney, M. Witzembichler, B., and J. M. and Isner (1998). "Mouse model of angiogenesis." *Am J Pathol* 152(6): 1667–1679.
- Creative Commons. (2007). "Chapter 3: Rat external anatomy." Attribution-NonCommercial 3.0 Unported License, [Biologycorner.com](http://www.biologycorner.com/worksheets/rat_external.html). from http://www.biologycorner.com/worksheets/rat_external.html

- Crystal, N. J., D. H. Townson, S. B. Cook and D. P. LaRoche (2013). "Effect of cryotherapy on muscle recovery and inflammation following a bout of damaging exercise." *Eur J Appl Physiol* 113(10): 2577-2586.
- Deal, D. N., J. Tipton, E. Rosencrance, W. W. Curl and T. L. Smith (2002). "Ice reduces edema: A study of microvascular permeability in rats." *J Bone Joint Surg* 84(9): 1573-1578.
- Desgranges, P., C. Barbaud, J. P. Caruelle and J. Gautron (1999). "A substituted dextran enhances muscle fiber survival and regeneration in ischemic and denervated rat EDL muscle." *The FASEB J* 13(6): 761-766.
- Dodd, L. R. and P. C. Johnson (1993). "Antagonism of vasoconstriction by muscle contraction differs with alpha-adrenergic subtype." *Am J Physiol* 264(3): H892-H900.
- Dolan, M. G., R. M. Thornton, D. R. Fish and F. C. Mendel (1997). "Effects of cold water immersion on edema formation after blunt injury to the hind limbs of rats." *J Athl Train* 32(3): 233-237.
- Dorsett-Martin, W. A. (2004). "Rat models of skin wound healing: A review." *Wound Repair Regen* 12(6): 591-599.
- Dorsett-Martin, W. A. and A. B. Wysocki (2008). *Rat models of skin wound healing. Sourcebook of Models for Biomedical Research*. P. M. Conn, Humana Press: 631-638.
- Downey, C. M., K. S. Arvind, L. V. Michelle, R. B. Helen, K. B. Steven and R. J. Frank (2012). "Quantitative ex-vivo micro-computed tomographic imaging of blood vessels and necrotic regions within tumors." *PLoS One* 7(7): e41685.
- Driessen, N. J. B., G. W. M. Peters, J. M. Huyghe, C. V. C. Bouten and F. P. T. Baaijens (2003). "Remodelling of continuously distributed collagen fibres in soft connective tissues." *J Biomech* 36(8): 1151-1158.
- Duda, G. N., W. R. Taylor, T. Winkler, G. Matziolis, M. O. Heller, N. P. Haas, C. Perka and Schaser K.D. (2008). "Biomechanical, microvascular, and cellular factors promote muscle and bone regeneration." *Exercise Sport Sci Rev* 36(2): 64-70.
- Duvall, C. L., R. Taylor, W. D. Weiss and R. E. Guldberg (2004). "Quantitative microcomputed tomography analysis of collateral vessel development after ischemic injury." *Am J Physiol* 287: 302-310.
- Ebner, A., B. Zatschler and A. eussen (2011). "Evaluation of cold storage conditions for vessels obtained from donor rats after cardiac death." *J Vasc Surg* 54(6): 1769-1777.
- Edgara, L. T., S. C. Sibolea, C. J. Underwooda, J. E. Guilkeyb and J. A. Weissa (2012). "A computational model of in vitro angiogenesis based on extracellular matrix fibre orientation." *Computer Methods in Biomech Biomed Eng* 1(1): 1-12.
- Ehling, J., B. Theek, F. Gremse, S. Baetke, D. Möckel, J. Maynard, S. A. Ricketts, H. Grüll, M. Neeman, R. Knuechel, W. Lederle, F. Kiessling and T. Lammers (2014). "Micro-CT imaging of tumor angiogenesis: Quantitative measures describing micromorphology and vascularization." *Am J Pathol* 182(2): 431-441.
- Enoch, S. and D. J. Leaper (2008). "Basic science of wound healing." *J Surg (Oxford)* 26(2): 31-37.

- Eston, R. and D. Peters (1999). "Effects of cold water immersion on the symptoms of exercise-induced muscle damage." *J Sports Sci* 17(3): 231-238.
- Fastol (2012). Rat leg superficial muscles dissection. A & P Course Objectives. MA, USA, Harvard University Medical School.
- Feinberg, M. (2007). "Validation of analytical methods based on accuracy profiles." *J Chromatography A* 1158(1-2): 174-183.
- Fischer, M. J. M., S. Uchida and K. Messlinger (2010). "Measurement of meningeal blood vessel diameter in vivo with a plug-in for ImageJ." *Microvas Res* 80(2): 258-266.
- Flow Tech Inc. (1999). "MICROFIL®, Massachusetts, USA." from <http://www.flowtech-inc.com/microfil.htm>
- Fouletier-Dilling, C. M., P. Bosch, A. R. Davis, J. A. Shafer, S. L. Stice, Z. Gugala, F. H. Gannon and E. A. Olmsted-Davis (2005). "Novel compound enables high-level adenovirus transduction in the absence of an adenovirus-specific receptor." *Hum Gene Ther* 16(11): 1287-1297.
- Francis, R. S. (1985). "Small animal traumatizer." *J Appl Physiol* 59: 658-659.
- Frink, M., H. Andruszkow, C. Zeckey, C. Krettek and Hildebrand F. (2011). "Experimental trauma models: An update." *J Biomed Biotech Article ID 797383*: 1-15.
- Funama, Y., S. Oda, D. Utsunomiya, K. Taguchi, T. Shimonobo, Y. Yamashita and K. Awai (2012). "Coronary artery stent evaluation by combining iterative reconstruction and high-resolution kernel at coronary CT angiography " *Acad Radiol* 19(11): 1324-1331.
- Gakhal, M. S. and K. A. Sartip (2009). "CT angiography signs of lower extremity vascular trauma." *Am J Roentgenol* 193(1): W49-W57.
- Gierer, P., T. Mittlmeier, R. Bordel, K. D. Schaser, G. GRADL and B. Vollmar (2005). "Selective cyclooxygenase-2 inhibition reverses microcirculatory and inflammatory sequelae of closed soft-tissue trauma in an animal model." *J Bone Joint Surg* 87: 153-159.
- Gierer, P., J. Röther, T. Mittlmeier, G. Gradl and B. Vollmar (2010). "Ebselen reduces inflammation and microvascular perfusion failure after blunt skeletal muscle injury of the rat." *J Trauma Acute Care Surg* 68(4): 853-858.
- Gilbert, S. F. (2006). *Developmental biology*. Sinauer Associates, Inc. Sunderland, MA, USA: 817.
- Gill, A. L. and C. N. A. Bell (2004). "Hyperbaric oxygen: its uses, mechanisms of action and outcomes." *QJM* 97(7): 385-395.
- Gillies, A. R. and R. L. Lieber (2011). "Structure and function of the skeletal muscle extracellular matrix." *Muscle & Nerve* 44(3): 318-331.
- Goodman, C. C. and K. S. Fuller (2014). "Pathology: Implications for the physical therapist." 1800.
- Gourgiotis, S., C. Villias, S. Germanos, A. Foukas and M. P. Ridolfini (2007). "Acute limb compartment syndrome: a review." *J Surg Educ* 64(3): 178-186.
- Greenhalgh, D. G. (1998). "The role of apoptosis in wound healing." *Int J Biochem Cell Biol* 30(9): 1019-1030.

- Grounds, M. D. and J. Torrisi (2004). "Anti-TNFalpha (Remicade) therapy protects dystrophic skeletal muscle from necrosis." *Am Soc Exp Biol* 18(6): 676-682.
- Guldberg, R. E., A. S. Lin, R. Coleman, G. Robertson and C. Duvall (2004). "Microcomputed tomography imaging of skeletal development and growth." *J Birth Defects Res* 72(Part C): 250-259.
- Hallouard, F., N. Anton, P. Choquet, A. Constantinesco and T. Vandamme (2010). "Iodinated blood pool contrast media for preclinical X-ray imaging applications – a review." *Biomaterials* 31(24): 6249-6268.
- Hausman, M. R., M. B. Schaffler and R. J. Majeska (2001). "Prevention of fracture healing in rats by an inhibitor of angiogenesis." *Bone* 29(6): 560-564.
- Heil, M., I. Eitenmüller, T. Schmitz-Rixen and W. Schaper (2006). "Arteriogenesis versus angiogenesis: similarities and differences." *Journal of Cellular and Molecular Medicine* 10(1): 45-55.
- Heil, M. and W. Schaper (2004). "Influence of mechanical, cellular, and molecular factors on collateral artery growth (arteriogenesis)." *Circ Res* 95: 449-458.
- Heil, M., S. Wagner and W. Schaper (2004). "Arterial regeneration by collateral artery growth (arteriogenesis)." *Drug Discovery Today: Disease Models* 1(3): 265-271.
- Herrera, E., M. C. Sandoval, D. M. Camargo and T. F. Salvini (2011). "Effect of walking and resting after three cryotherapy modalities on the recovery of sensory and motor nerve conduction velocity in healthy subjects." *Brazilian Journal of Physical Therapy* 15: 233-240.
- Hershey, J. C., E. P. Baskin, J. D. Glass, H. A. Hartman, D. B. Gilberto, I. T. Rogers and J. J. Cook (2001). "Revascularization in the rabbit hindlimb: dissociation between capillary sprouting and arteriogenesis." *Cardiovasc Res* 49(3): 618-625.
- Hershey, J. C., E. P. Baskin, J. D. Glass, H. A. Hartman, D. B. Gilberto, I. T. Rogers and J. J. Cook (2001). "Revascularization in the rabbit hindlimb: dissociation between capillary sprouting and arteriogenesis." *Cardiovasc Res.* 49(3): 618-625.
- Herzog, S., H. Sager, E. Khmelevski, A. Deylig and W. D. Ito (2002). "Collateral arteries grow from pre-existing anastomoses in the rat hindlimb." *Am J Physiol Heart Circ Physiol* 283(5): 2012-2020.
- Hildebrand, T. and P. Rügsegger (1997). "A new method for the model-independent assessment of thickness in three-dimensional images." *J Microsc* 185(1): 67-75.
- Hodde, J. and M. Hiles (2007). "Constructive soft tissue remodelling with a biologic extracellular matrix graft: overview and review of the clinical literature." *J Acta Chir Belg* 107(6): 641-647.
- Honda, H., H. Kimura and A. Rostami (1990). "Demonstration and phenotypic characterization of resident macrophages in rat skeletal muscle." *Immunology* 70(2): 272-277.
- Hopf, H. W., J. J. Gibson, A. P. Angeles, J. S. Constant, J. J. Feng, M. D. Rollins, M. Zamirul Hussain and T. K. Hunt (2005). "Hyperoxia and angiogenesis." *Wound Repair Regen* 13(6): 558-564.

- Howatson, G., D. Gaze and K. A. Van Someren (2005). "The efficacy of ice massage in the treatment of exercise-induced muscle damage." *Scand J Med Sci Sports* 15(6): 416-422.
- Hoy, A. J., G. E. Peoples and P. L. McLennan (2009). "The effect of vasoconstrictors on oxygen consumption in resting and contracting skeletal muscle of the autologous pump-perfused rat hindlimb." *J Physiol Pharmacol* 60(3): 155-160.
- Huard, J., Y. Li and F. H. Fu (2002). *Muscle Injuries and Repair: Current Trends in Research*. 84: 822-832.
- Huard, J., Y. Li and F. H. Fu (2002). "Muscle injuries and repair: Current trends in research." *J Bone Joint Surg* 84(5): 822-832.
- Hubbard, T. J. and C. R. Denegar (2004). "Does cryotherapy improve outcomes with soft tissue injury?" *J Athl Train* 39(3): 278-279.
- Hunt, T. K. (1988). "The physiology of wound healing." *Ann Emerg Med* 17(12): 1265-1273.
- Hussain, T. Z. and M. Agdi (2012). Intravasation of water-soluble contrast agent into the internal iliac vein during hysterosaplingography. *Pakistan J Med Sci*. 28.
- International Organization for Standardization (ISO) (1994). "Accuracy (trueness and precision) of measurement method and results. Part 1. General principles and definitions." ISO, Geneva, Switzerland, ISO 5725-1.
- Ishii, Y., T. Ushida, T. Tateishi, H. Shimojo and Y. Miyanaga (2002). "Effects of different exposures of hyperbaric oxygen on ligament healing in rats." *J Orthop Res* 20(2): 353-356.
- Jackowski, M., X. Papademetris, L. Dobrucki, A. Sinusas and L. Staib (2005). Characterizing vascular connectivity from microCT images. *Medical image computing and computer-assisted intervention – MICCAI 2005*. J. Duncan and G. Gerig, Springer Berlin Heidelberg. 3750: 701-708.
- Järvinen, M. (1976). "Healing of a crush injury in rat striated muscle. 3. A micro-angiographical study of the effect of early mobilization and immobilization on capillary ingrowth." *Acta Pathol Microbiol Scand A*. 84(1): 85-94.
- Järvinen, M. (1977). "Immobilization effect on the tensile properties of striated muscle: an experimental study in the rat." *J Arch Phys Med* 58: 123-127.
- Järvinen, M. and M. U. Lehto (1993). "The effect of early mobilization and immobilization on the healing process following muscle injuries." *J Sports Med* 15: 78-89.
- Järvinen, T. A., T. L. Järvinen, M. Kääriäinen, H. Kalimo and M. Järvinen (2005). "Muscle injuries: Biology and treatment." *Am J Sports Med* 33: 745
- Järvinen, T. A. H., T. L. N. Järvinen, M. Kääriäinen, V. Äärimaa, S. Vaittinen, H. Kalimo and M. Järvinen (2007). "Muscle injuries: optimising recovery." *Best Practice Res Clin Rheumatol* 21(2): 317-331.
- Jensen, P. J., P. K. Andersen and C. Thøgersen (1994). "The reproducibility of measurement of right ventricular ejection fraction and cardiac output by the thermodilution technique in patients on mechanical ventilation." *Acta Anaesthesiol Scand* 38(5): 486-489.

- Jia, F., P. Françoise, L. Malaval, V. Laurence and L. P. Marie-Hélène (2010). "Imaging and quantitative assessment of long bone vascularization in the adult rat using microcomputed tomography." *Anat Rec: Adv Integr Anat Evol Biol* 293(2): 215-224.
- Jing, X. L., A. S. Farberg, L. A. Monson, A. Donneys, C. N. Tchanque-Fossuo and S. R. Buchman (2012). "Radiomorphometric quantitative analysis of vasculature utilizing micro-computed tomography and vessel perfusion in the murine mandible." *Craniofacial Trauma Reconstr* 5(4): 223-230.
- Jutte, L. S., M. A. Merrick, C. D. Ingersoll and J. E. Edwards (2001). "The relationship between intramuscular temperature, skin temperature, and adipose thickness during cryotherapy and rewarming." *Arch Phys Med Rehab* 82(6): 845-850.
- Kadam, P. and S. Bhalerao (2010). "Sample size calculation." *Int J Ayurveda Res* 1(1): 55-57.
- Källicke, T., U. Schlegel, G. Printzen, E. Schneider, G. Muhr and S. Arens (2003). "Influence of a standardized closed soft tissue trauma on resistance to local infection. An experimental study in rats." *J Orthop Res* 21(2): 373-378.
- Kanlayanaphotporn, R. and P. Janwantanakul (2005). "Comparison of skin surface temperature during the application of various cryotherapy modalities." *Arch Phys Med Rehab* 86(7): 1411-1415.
- Kannus, P. (2000). "Immobilization or early mobilization after an acute soft-tissue injury?" *Phys Sportsmed* 28(3): 55-63.
- Kano, Y., Shimegi, Takahashi, Masuda and Katsuta (2000). "Changes in capillary luminal diameter in rat soleus muscle after hind-limb suspension." *Acta Physiologica Scandinavica* 169(4): 271-276.
- Kano, Y., S. Shimegi, H. Takahashi, K. Masuda and S. Katsuta (2000). "Changes in capillary luminal diameter in rat soleus muscle after hind-limb suspension." *Acta Physiol Scand* 169: 271-276.
- Khattak, M. J., T. Ahmad, R. Rehman, M. Umer, Hasan S.H. and Ahmed M. (2010). "Muscle healing and nerve regeneration in a muscle contusion model in the rat." *J Bone Joint Surg* 92(6): 894-899.
- Kindig, C. A., T. I. Musch, R. J. Basaraba and D. C. Poole (1999). "Impaired capillary hemodynamics in skeletal muscle of rats in chronic heart failure." *J Appl Physiol* 87(2): 652-660.
- Knobloch, K., R. Grasmann, M. Spies and P. M. Vogt (2007). "Intermittent KoldBlue cryotherapy of 3×10 min changes mid-portion Achilles tendon microcirculation." *Br J Sports Med* 41(6): e4.
- Korthius, R. J., D. N. Granger, M. I. Townsley and A. E. Taylor (1985). "The role of oxygen-derived free radicals in ischaemia-induced increases in canine skeletal muscle vascular permeability." *J Circ Res* 57: 599-609.
- Krucker, T., A. Lang and E. P. Meyer (2006). "New polyurethane-based material for vascular corrosion casting with improved physical and imaging characteristics." *Microsc Res Tech* 69(2): 138-147.
- Landry, P. S., A. A. Marino, K. K. Sadasivan and J. A. Albright (2000). "Effect of soft-tissue trauma on the early periosteal response of bone to injury." *J Trauma* 48: 479-483.

- Lee, C., J. Pardun, R. Buntic, M. Kiehn, D. Brooks and H. Buncke (2007). "Severe frostbite of the knees after cryotherapy." *Orthop* 30(1): 63-64.
- Lee, H., H. Natsui, T. Akimoto, K. Yanagi, N. Ohshima and I. Kono (2005). "Effects of cryotherapy after contusion using real-time intravital microscopy." *Med Sci Sports Exerc* 37(7): 1093-1098.
- Lee, J., D. Koh and C. N. Ong (1989). "Statistical evaluation of agreement between two methods for measuring a quantitative variable." *Comput Biol Med* 19(1): 61-70.
- Legan, M. (2005). "New marker of angiogenesis CD105 (endoglin): diagnostic, prognostic and therapeutic role: review." *Radiol Oncol* 39(4): 253-259.
- Levin, S. L. and D. P. Condit (1996). "Combined injuries—soft tissue management." *J Clin Orthop* 327: 172–181.
- Li, J., J. Chen and R. Kirsner (2007). "Pathophysiology of acute wound healing." *Clin Dermatol* 25: 9–18.
- Li, J., Z. Zhong, R. Lidtke, K. E. Kuettner, C. Peterfy, E. Aliyeva and C. Muehleman (2004). "Radiography of soft tissue of the foot and ankle with diffraction enhanced imaging." *J Am Podiatr Med Assoc* 94(3): 315-322.
- Linares, H. A. (1996). "From wound to scar." *Burns* 22(5): 339-352.
- Lomas-Niera, J. L., M. Perl, C. S. Chung and A. Ayala (2005). "Shock and hemorrhage: an overview of animal models." *J Shock* 24(1): 33–39.
- Longo, U. G., M. Loppini, A. Berton, F. Spiezia, N. Maffulli and V. Denaro (2012). "Tissue engineered strategies for skeletal muscle injury." *Stem Cells Int* 2012: 13.
- Lovering, R. M. (2008). "Skeletal muscle damage and repair." *J Phys Ther Interven*: 219–230.
- Lu, W., Z. Dong, Z. Liu, W. Fu, Y. Peng, S. Chen, T. Xiao, H. Xie, G. Du, B. Deng and X. Zhang (2010). "Detection of microvasculature in rat hind limb using synchrotron radiation." *J Surg Res* 164(1): e193-e199.
- Mac Auley, D. C. (2001). "Ice therapy: How good is the evidence?" *Int J Sports Med* 22(05): 379-384.
- Marc, E. S., M. P. Shayn and K. Kimberly (2011). "Rapid analysis of vessel elements (RAVE): A tool for studying physiologic, pathologic and tumor angiogenesis." *PLoS ONE*.
- Marks, P. C., M. Preda, T. Henderson, L. Liaw, V. Lindner, R. E. Friesel and I. M. Pinz (2013). "Interactive 3D analysis of blood vessel trees and collateral vessel volumes in magnetic resonance angiograms in the mouse ischemic hindlimb model." *Open Med Imaging J* 7: 19-27.
- Mars, M., B. Hadebe and M. Tufts (2006). "The effect of icepack cooling on skin and muscle temperature at rest and after exercise." *SAJSM* 18(3).
- Marxen, M., M. M. Thornton, C. B. Chiarot, G. Klement, J. Koprivnikar, J. G. Sled and R. M. Henkelman (2004). "MicroCT scanner performance and considerations for vascular specimen imaging." *J Med Phys* 31: 305-313.
- Matharu, G. S., P. S. Najran and K. M. Porter (2010). "Soft-tissue ankle injuries." *J Trauma* 12: 105–115.

- Mayer, J. M., V. Mooney, L. N. Matheson, G. N. Erasala, J. L. Verna, B. E. Udermann and S. Leggett (2006). "Continuous low-level heat wrap therapy for the prevention and early phase treatment of delayed-onset muscle soreness of the low back: A randomized controlled trial." *Arch Phys Med Rehab* 87(10): 1310-1317.
- McMaster, W. C. (1977). "A literary review on ice thera in injuries." *Am J Sports Med* 5(3): 124-126.
- McMaster, W. C., S. Liddle and T. R. Waugh (1978). "Laboratory evaluation of various cold therapy modalities." *Am J Sports Med* 6(5): 291-294.
- Melnyk, M., T. Henke, L. Claes and P. Augat (2008). "Revascularisation during fracture healing with soft tissue injury." *J Arch Orthop Trauma Surg* 128: 1159-1165.
- Merrick, M. A. (2002). "Secondary injury after musculoskeletal trauma: A review and update." *Journal of Athletic Training* 37(2): 209-217.
- Merrick, M. A. (2002). "Secondary injury after musculoskeletal trauma: A review and update." *J Athl Train* 37(2): 209-217.
- Merrick, M. A., K. L. Knight, C. D. Ingersoll and J. A. Potteiger (1993). "The effects of ice and compression wraps on intramuscular temperatures at various depths." *J Athl Train* 28(3): 236-245.
- Metcalfe, D. D., D. Baram and Y. A. Mekori (1997). "Mast cells." *J Physiol Rev* 77(4): 1033-1079.
- Michlovitz, S. L., J. W. Bellew and T. P. Nolan Jr (2011). *Modalities for therapeutic intervention*. Fifth edition. PA, USA, F.A. Davis: 460.
- Mitzner, W., R. Brown and W. Lee (2001). "In vivo measurement of lung volumes in mice." *Physiol Genomics* 4: 215-221.
- Moding, E. J., D. P. Clark, Y. Qi, Y. Li, Y. Ma, K. Ghaghada, G. A. Johnson, D. G. Kirsch and C. T. Badea "Dual-energy micro-computed tomography imaging of radiation-induced vascular changes in primary mouse sarcomas." *Int J Radiation Oncolo Biol Phys* 85(5): 1353-1359.
- Moore, D. (2011). "Tscherne classification." *Orthobullets*. MA, USA. from <http://www.orthobullets.com/trauma/1002/tscherne-classification>
- Morcos, S. K., P. Dawson, J. D. Pearson, J. Y. Jeremy, A. P. Davenport, M. S. Yates, P. Tirone, P. Cipolla, C. de Haën, P. Muschick, W. Krause, H. Refsum, C. J. Emery, P. Liss, A. Nygren, J. Haylor, N. D. Pugh and J. O. G. Karlsson (1998). "The haemodynamic effects of iodinated water soluble radiographic contrast media: a review." *Eur J Radiol* 29(1): 31-46.
- Müller, R. (2009). "Hierarchical microimaging of bone structure and function." *Nat Rev Rheumatol* 5(7): 373-381.
- Müller, R. and P. Büttner (1994). "A critical discussion of intraclass correlation coefficients." *Stat in Med* 13(23-24): 2465-2476.
- Murohara, T., T. Asahara, M. Silver, C. Bauters, H. Masuda, C. Kalka and J. M. Isner (1998). "Nitric oxide synthase modulates angiogenesis in response to tissue ischemia." *J Clin Invest* 101(11): 2567-2578.
- Myburgh, K. H., M. J. Kruger and C. Smith (2012). "Accelerated skeletal muscle recovery after in vivo polyphenol administration." *J Nutr Biochem* 23(9): 1072-1079.

- National Health and Medical Research Council. (2013). "Australian code for the care and use of animals for scientific purposes." 8th edition, Natl Health and Med Res Council. Canberra. from http://www.nhmrc.gov.au/files/nhmrc/publications/attachments/ea28_code_care_use_animals_130728.pdf
- Nauta, A., G. C. Gurtner and M. T. Longaker (2011). "Wound healing and regenerative strategies:invited medical review." *J Oral Dis* 17: 541–549.
- Nebuloni, L., G. A. Kuhn and R. Müller (2013). "A comparative analysis of water-soluble and blood-pool contrast agents for in vivo vascular imaging with micro-CT." *Acad Radiol* 20(10): 1247-1255.
- Nebuloni, L., G. A. Kuhn, J. Vogel and R. Müller (2014). "A novel in vivo vascular imaging approach for hierarchical quantification of vasculature using contrast enhanced micro-computed tomography." *PLoS ONE* 9(1): e86562.
- Niemistö, A., V. Dunmire, O. Yli-Harja, W. Zhang and I. Shmulevich (2005). "Robust quantification of in vitro angiogenesis through image analysis." *IEEE Trans Med Imaging* 24(4): 549-553.
- Norris, L. A. (2003). "Blood coagulation." *Best Practice Res Clin Obstet Gynaecol* 17(3): 369-383.
- Novak, M. L., E. M. Weinheimer-Haus and T. Koh, J., (2014). "Macrophage activation and skeletal muscle healing following traumatic injury." *J pathol* 232(3): 344-355.
- Nyangoga, H., P. Mercier, H. Libouban, M. F. Baslé, D. Chappard and S. Basu (2011). "Three-dimensional characterization of the vascular bed in bone metastasis of the rat by microcomputed tomography (micro-CT)." *PLOS One*.
- Ochman, S., S. Frey, M. J. Raschke, J. N. Deventer and R. H. Meffert (2011). "Local application of VEGF compensates callus deficiency after acute soft tissue trauma-results using a limb-shortening distraction procedure in rabbit tibia." *J Orthop Res*: 1-5.
- Oliveira, N. M. L. I., A. D. I. I. Gava and T. F. I. I. Salvini (2007). "The effect of intermittent cryotherapy and compression on muscle injuries in rats: a morphometric analysis." *Braz J Phys Ther* 11(5): 403-410.
- Orbay, H., H. Hong, J. M. Koch, H. F. Valdovinos, T. A. Hacker, C. P. Theuer, T. E. Barnhart and W. Cai (2013). "Pravastatin stimulates angiogenesis in a murine hindlimb ischemia model: a positron emission tomography imaging study with (64)Cu-NOTA-TRC105." *Am J Transl Res* 6(1): 54-63.
- Oses, P., M. A. Renault, I. R. Chauve, L. Leroux, C. Allières, B. Séguy, J. M. Lamazière, P. Dufourcq, T. Couffinal and C. Duplâa (2009). "Mapping 3-dimensional neovessel organization steps using micro-computed tomography in a murine model of hindlimb ischemia-brief report." *Arterioscler Thromb Vasc Biol* 29(12): 2090-2092.
- Perilli, E., V. Le, B. Ma, P. Salmon, K. Reynolds and N. L. Fazzalari (2010). "Detecting early bone changes using in vivo micro-CT in ovariectomized, zoledronic acid-treated, and sham-operated rats." *Osteoporosis International* 21(8): 1371-1382.
- Qian, D. and P. Bottomley (2012). "High-resolution intravascular magnetic resonance quantification of atherosclerotic plaque at 3T." *J Cardiovasc Magnetic Resonance* 14(1): 20.

- Qin, L., H. K. Genant, J. F. Griffith and K. S. Leung (2007). "Advanced bioimaging technologies in assessment of the quality of bone and scaffold materials: Techniques and applications." 700.
- Radley, H. G., M. J. Davies and M. D. Grounds (2008). "Reduced muscle necrosis and long-term benefits in dystrophic mdx mice after cV1q (blockade of TNF) treatment." *Neuromusc Disord* 18: 227-238.
- Raines, A. L., M. Sunwoo, A. A. Gertzman, K. Thacker, R. E. Guldberg, Z. Schwartz and B. D. Boyan (2011). "Hyaluronic acid stimulates neovascularization during the regeneration of bone marrow after ablation." *J Biomed Mater Res* 96(3): 575-583.
- Rakobowchuk, M., C. L. McGowan, P. C. de Groot, J. W. Hartman, S. M. Phillips and M. J. MacDonald (2005). "Endothelial function of young healthy males following whole body resistance training." 98(6): 2185-2190.
- Ramos-Vara, J. A. (2005). "Technical aspects of immunohistochemistry." *J Vet Pathol* 42(4): 405-426.
- Relaix, F. and P. S. Zammit (2012). "Satellite cells are essential for skeletal muscle regeneration: the cell on the edge returns centre stage." *Development* 139(16): 2845-2856.
- Rivenburgh, D. W. (1992). "Physical modalities in the treatment of tendon injuries." *Clin Sports Med* 11(3): 645-659
- Rodriguez, P. G., F. N. Felix, D. T. Woodley and E. K. Shim (2008). "The Role of oxygen in wound healing: A review of the literature." *Dermatol Surg* 34(9): 1159-1169.
- Rosner, B. (2010). *Fundamentals of biostatistics*. Cengage Learning, Inc. Boston, USA.
- Rüedi, T. P. and W. M. Murphy. (2007). "Classification of fractures with soft tissue injury: AO publishing." Switzerland. from https://www2.aofoundation.org/wps/portal/!ut/p/c0/04_SB8K8xLLM9MSSzPy8xBz9CP0os3hng7BARYdDRwN39yBTAYMvLwOLUA93I4MQE_2CbEdFAF3RnT4!/?contentUrl=%2Fsrq%2Fpopup2Ffurther_reading%2FPrinciples%2FClassification%2FSftTissue-Classfctn-neu.jsp&popupStyle=diagnosis&soloState=true&bone=Radius&segment=Shaft&BackMode=true
- Rüegg, M. A. and S. Meinen (2011). *Histopathology in hematoxylin & eosin stained muscle sections*. Treat-NMD. S. (MDC1A_M.1.2.004). Switzerland, Biozentrum, University of Basel, Basel, Switzerland. 1.
- Sanders, J. E., B. S. Goldstein and D. F. Leotta (1995). "Skin response to mechanical stress: adaptation rather than breakdown--a review of the literature." *J Rehabil Res Dev* 32(3): 214-226.
- Savai, R., A. C. Langheinrich, R. T. Schermuly, S. S. Pullamsetti, R. Dumitrescu, H. Traupe, W. S. Rau, W. Seeger, F. Grimminger and G. A. Banat (2009). "Evaluation of angiogenesis using micro-computed tomography in a xenograft mouse model of lung cancer." *Neoplasia* 11(1): 48-56.
- Scanco Medical. (SCANCO Medical microCT systems: 3D analysis). "Brüttisellen, Switzerland ". from http://www.scanco.ch/index.php?id=3d_analysis
- Schambach, S. J., S. Bag, C. Groden, L. Schilling and M. A. Brockmann (2010). "Vascular imaging in small rodents using micro-CT." *J Methods* 50(1): 26-35.

- Schaser, K. D., H. J. Bail, L. Schewior, J. F. Stover, I. Melcher, N. P. Haas and T. Mittlmeier (2005). "Acute effects of N-acetylcysteine on skeletal muscle microcirculation following closed soft tissue trauma in rats." *J Orthop Res* 23: 231-241.
- Schaser, K. D., A. C. Disch, J. F. Stover, A. Lauffer, H. J. Bail and T. Mittlmeier (2007). "Prolonged superficial local cryotherapy attenuates microcirculatory impairment, regional inflammation, and muscle necrosis after closed Soft tissue injury in rats " *Am J Sports Med* 35(1): 93-102
- Schaser, K. D., J. F. Stover, I. Melcher, A. Lauffer, N. P. Haas, H. J. Bail, U. Stöckle and T. W. Mittlmeier (2006). "Local cooling restores microcirculatory hemodynamics after closed soft-tissue trauma in rats." *J Trauma: Injury, Infect, Critl Care* 61(3): 642-649.
- Schaser, K. D., B. Vollmar, M. D. Menger, L. Schewior, S. N. Kroppenstedt, M. Raschke, Lübbe, A.S., , N. P. Haas and T. Mittlmeier (1999). "In vivo analysis of microcirculation following closed soft-tissue injury." *J Orthop Res* 17: 678-685.
- Schaser, K. D., L. Zhang, N. P. Haas, T. Mittlmeier, G. Duda and H. J. Bail (2003). "Temporal profile of microvascular disturbances in rat tibial periosteum following closed soft tissue trauma." *J Langenbecks Arch Surg* 388: 323-330.
- Schmalbruch H. (2006). "The satellite cell of skeletal muscle fiber: review." *Braz J morphol Sci* 23(2): 159-172.
- Schmidt, A., K. Brixius and W. Bloch (2007). "Endothelial precursor Cell migration during vasculogenesis." *Circ Res* 101(2): 125-136.
- Scholz, D., T. Ziegelhoeffer, A. Helisch, S. Wagner, C. Friedrich, T. Podzuweit and W. Schaper (2002). "Contribution of arteriogenesis and angiogenesis to postocclusive hindlimb perfusion in mice." *J Mol Cell Cardiol* 34(7): 775-787.
- Scholz, D., Ziegelhoeffer, T, Helisch, A, Wagner, S, Friedrich, C, Podzuweit, T, and Schaper, W, (2002). "Contribution of arteriogenesis and angiogenesis to postocclusive hindlimb perfusion in mice." *J Mol Cell Cardiol* 34: 775-787.
- Shireman, P. K., V. Contreras-Shannon, S. M. Reyes-Reyna, S. C. Robinson and L. M. McManus (2006). "MCP-1 parallels inflammatory and regenerative responses in ischemic muscle." *J Surg Res* 134(1): 145-157.
- Sider, K. L., J. Song and J. E. Davies (2010). "A new bone vascular perfusion compound for the simultaneous analysis of bone and vasculature." *Microsc Res Tech* 73(7): 665-672.
- Sillman, D. (2007). *Biology: review of rat muscles*. PA, USA, Penn State University.
- Smith, C., M. J. Kruger, R. M. Smith and K. H. Myburgh (2008). "The inflammatory response to skeletal muscle injury." *J Sports Med* 38(11): 947-969.
- Smith, T. L., W. W. Curl, C. George and E. Rosencrance (1994). "Effects of contusion and cryotherapy on microvascular perfusion in rat dorsal skeletal muscle." *Pathophysiol* 1(4): 229-233.
- Smith, T. L., W. W. Curl, B. P. Smith, M. B. Holden, T. Wise, A. Marr and K. Andrew, L., (1993). "New skeletal muscle model for the longitudinal study of alterations in microcirculation following contusion and cryotherapy." *Microsurg* 14(8): 487-493.
- Sprawls, P. (1995). "The physical principles of medical imaging."

- Stadelmann, W. K., A. G. Digenis and G. R. Tobin (1998). "Physiology and healing dynamics of chronic cutaneous wounds." *Am J Surg* 176(2, Supplement 1): 26S-38S.
- Starke, R. D., F. Ferraro, K. E. Paschalaki, N. H. Dryden, T. A. J. McKinnon, R. E. Sutton, E. M. Payne, D. O. Haskard, A. D. Hughes, D. F. Cutler, M. A. Laffan and A. M. Randi (2011). "Endothelial von Willebrand factor regulates angiogenesis." *Blood* 117(3): 1071-1080.
- Stratos, I., J. Graff, R. Rotter, T. Mittlmeier and B. Vollmar (2010). "Open blunt crush injury of different severity determines nature and extent of local tissue regeneration and repair." *J Orthop Res* 28(7): 950-957.
- Stroncek, J. D. and M. W. R. Reichert (2007). *Overview of wound healing in different tissue types. Indwelling neural implants*, CRC Press: 3-38.
- Sudhakar, S. and N. Arun (2012). "Biochemical markers an indirect method for evaluating delayed onset muscle soreness among recreational athletes." *Int J Biol Med Res* 3(2): 1624- 1626.
- Südkamp, N. P. (2004) "Soft tissue injuries of the tibia." *J AO Foundation* DOI: http://www2.aofoundation.org/wps/portal!/ut/p/c0/04_SB8K8xLLM9MSSzPy8xBz9CP0os3hng7BARydDRwN39yBTAYMvLwOLUA93I4MQE_2CbEdFAF3RnT4!/?segment=Shaft&bone=Tibia&soloState=true&popupStyle=diagnosis&contentUrl=srg/popup/further_reading/PFxM2/42/16_465_Sft-tiss_injry_tibia.jsp#JumpLabelNr2.
- Swenson, C., L. Swärd and J. Karlsson (2007). "Cryotherapy in sports medicine." *Scand J Med Sci Sports* 6(4): 193-200.
- Takagi, R., N. Fujita, T. Arakawa, S. Kawada, N. Ishii and A. Miki (2011). "influence of icing on muscle regeneration after crush injury to skeletal muscle in rats." *J Appl Physiol* 110: 382-388.
- Takagi, R., N. Fujita, T. Arakawa, S. Kawada, N. Ishii and A. Miki (2011). "Influence of icing on muscle regeneration after crush injury to skeletal muscles in rats." *Journal of Applied Physiology* 110(2): 382-388.
- Tata, D. A. and B. J. Anderson (2002). "A new method for the investigation of capillary structure." *J Neurosci Methods* 113(2): 199-206.
- Thompson, H. J., J. N. McGinley, K. K. Knott, N. S. Spoelstra and P. Wolfe (2002). "Vascular density profile of rat mammary carcinomas induced by 1-methyl-1-nitrosourea: implications for the investigation of angiogenesis." *Carcinogenesis* 23(5): 847-854.
- Thompson, M. K. (2013). *Statistical outlier detection for jury based grading systems*. 120th Am Soc Eng Edu (ASEE) Ann Conf and Expo. Atlanta, Georgia, USA, ASEE.
- Tomlinson, R. E., J. A. McKenzie, A. H. Schmieder, G. R. Wohl, G. M. Lanza and M. J. Silva (2013). "Angiogenesis is required for stress fracture healing in rats." *Bone* 52(1): 212-219.
- Tonnesen, M. G., X. Feng and R. A. F. Clark (2000). "Angiogenesis in wound healing." *J Invest Dermatol Symp Proceed* 5: 40-46.
- Tscherne, H., L. Gotzen and T. C. Telger (1984). *Fractures with Soft tissue injuries*. New York, Springer-Verlag.

- Tseng, C. Y., J. P. Lee, Y. S. Tsai, S. D. Lee, C. L. Kao, T. C. Liu, C. H. Lai, M. B. Harris and C. H. Kuo (2013). "Topical cooling (icing) delays recovery from eccentric exercise-induced muscle damage." *J Strength Condition Res* 27(5): 1354-1361.
- Tsivitse, S. K., T. J. McLoughlin, J. M. Peterson, E. Mylona, S. J. McGregor and F. X. Pizza (2003). "Downhill running in rats: influence on neutrophils, macrophages, and MyoD+ cells in skeletal muscle." *Eur J Appl Physiol* 90(5-6): 633-638.
- Tu, Y. K., G. On Tong, C. H. Wu, K. Sananpanich and R. Kakinoki (2008). "Soft tissue injury in orthopaedic trauma." *J Injury* 3954: 53-57.
- Turner, N. J. and S. F. Badylak (2012). "Regeneration of skeletal muscle." *Cell Tissue Res* 347(3): 759-774.
- Uhrig, B. A., J. D. Boerckel, N. J. Willett, M. T. Li, N. Huebsch and R. E. Guldberg (2013). "Recovery from hind limb ischemia enhances rhBMP-2-mediated segmental bone defect repair in a rat composite injury model." *Bone* 55(2): 410-417.
- Ungersma, S. E., G. Pacheco, C. Ho, S. F. Yee, J. Ross, N. van Bruggen, F. V. J. Peale, S. Ross and R. A. Carano (2010). "Vessel imaging with viable tumor analysis for quantification of tumor angiogenesis." *Magn Reson Med* 63(6): 1637-1647.
- Valeria, B., G. Maddalena, V. Enrica, T. Onofrio and B. Gaetano (2008). "Endoglin (CD105) expression in the human heart throughout gestation: An immunohistochemical study." *Reprod Sci* 15(10): 1018-1026.
- van Oostrom, M. C., O. van Oostrom, P. Quax, M. Verhaar and I. E. Hoefer (2008). "Insights into mechanisms behind arteriogenesis: what does the future hold?" *J Leukoc Biol* 86(6): 1379-1391.
- van Wessel, T., A. de Haan, W. J. van der Laarse and R. T. Jaspers (2010). "The muscle fiber type-fiber size paradox: hypertrophy or oxidative metabolism?" *Eur J Appl Physiol* 110(4): 665-694.
- Veikkola, T. and K. Alitalo (1999). "VEGFs, receptors and angiogenesis." *Semin in Cancer Biol* 9(3): 211-220.
- Voeltz, M. D., M. A. Nelson, M. C. McDaniel and S. V. Manoukian (2007). "The important properties of contrast media: Focus on viscosity." *J Invasive Cardiol* 19: 1-9.
- Webber, W. (2013). "Approximate recall confidence intervals." *ACM Trans Inf Syst* 31(1): 1-33.
- White, G. E. and G. D. Wells (2013). "Cold-water immersion and other forms of cryotherapy: physiological changes potentially affecting recovery from high-intensity exercise." *Extreme Physiol Med* 2: 26-26.
- Wilke, B. and R. D. Weiner (2003). "Postoperative cryotherapy: risks versus benefits of continuous-flow cryotherapy units." *Clin Podiatric Med Surg* 20(2): 307-322.
- Williamson, D. and K. Hardingb (2004). "Wound healing." *J Med* 32(12): 4-7.
- Winkler, T., P. von Roth, G. Matziolis, M. R. Schumann, S. Hahn, P. Strube, G. Stoltenburg-Didinger, C. Perka, G. N. Duda and S. V. Tohtz (2011). "Time course of skeletal muscle regeneration after severe trauma: Muscle function against the background of MRI and histological findings." *Acta Orthop* 82(1): 102-111.
- Wolfard, A., J. Császár, L. Gera, A. Petri, J. A. Simonka, A. Balogh and M. Boros (2002). "Endothelin-a receptor antagonist treatment improves the periosteal

- microcirculation after hindlimb ischemia and reperfusion in the rat." *J Microcirc* 9: 471-476.
- Woodard, C. (1954). "What is active treatment?" *J Sports Med*: 1-14.
- Wullschleger, M. E. (2010). Effect of surgical approach on bone vascularization, fracture and soft tissue healing: comparison of less invasive to open approach. PhD, Queensland University of Technology.
- Yeung, A. K., M. Atri, L. Sugar and L. Klotz (2011). "Feasibility and safety of silicone rubber contrast-enhanced microcomputed tomography in evaluating the angioarchitecture of prostatectomy specimens." *Transl Oncol* 4(3): 173-177.
- Yeung, A. K. e. a. (2011). "Feasibility and Safety of Silicone Rubber Contrast-Enhanced Microcomputed Tomography in Evaluating the Angioarchitecture of Prostatectomy Specimens." *Transl Oncol*. 4(3): 173-177.
- Zagorchev, L., P. Oses, Z. W. Zhuang, K. Moodie, M. J. Mulligan-Kehoe, M. Simons and T. Couffinhal (2010). "Micro computed tomography for vascular exploration." *J Angiogenesis Res* 2(7): 1:11.
- Zemke, J. E., J. C. Anderson, W. K. Guion, J. McMillan and A. B. Joyner (1998). "Intramuscular temperature responses in the human leg to two forms of cryotherapy: Ice massage and ice bag." *J Orthop Sports Phys Ther* 27(4): 301-307.
- Zhang, L., H. Bail, T. Mittlmeier, N. P. Haas and K. D. Schaser (2003). "Immediate microcirculatory derangements in skeletal muscle and periosteum after closed tibial fracture." *J Trauma* 54: 979-985
- Zhang, L. and L. Shuqian (2011). "Micro soft tissues visualization based on X-Ray phase-contrast imaging." *Open Med Inform J* 5: 19-25.
- Zhu, J., Y. Li, A. Lu, B. Gharaibeh, J. Ma, T. Kobayashi, A. J. Quintero and J. Huard (2011). "Follistatin improves skeletal muscle healing after injury and disease through an interaction with muscle regeneration, angiogenesis, and fibrosis." *Am J Pathol* 179(2): 915-930.
- Zhuang, Z. W., L. Gao, M. Murakami, J. D. Pearlman, T. J. Sackett, M. Simons and E. D. de Muinck (2006). "Arteriogenesis: noninvasive quantification with multi-detector row CT angiography and three-dimensional volume rendering in rodents." *Radiology* 240(3): 698-707.
- Zhuang, Z. W., L. Gao, M. Murakami, J. D. Pearlman, T. J. Sackett, M. Simons and E. D. de Muinck (2006). "Arteriogenesis: Noninvasive quantification with multi-detector row CT angiography and threedimensional volume rendering in rodents." *J Radiol* 240(3): 698-707.
- Zudaire, E., L. Gambardella, C. Kurcz, S. Vermeren, E. Zudaire, L. Gambardella, C. Kurcz and S. Vermeren (2011). "A computational tool for quantitative analysis of vascular networks." *PLoS One* 6(11): e27385.

Appendix A

NUMERICAL TABLES

A-1 Impact device characterisation

Table A-1: The numerical data determined from analytical calculations are given for the impactor velocity, kinetic energy and impulse at 18 height points between the starting point and the impact surface.

Number of calculations	Impactor Mass (Kg)	Dropped Height (m)	Velocity (m/s)	Kinetic Energy (J)	Impulse (Kgm/s)
1	0.13	1.66	5.70	2.14	0.75
2	0.13	1.57	5.54	2.02	0.73
3	0.13	1.47	5.36	1.89	0.70
4	0.13	1.37	5.17	1.76	0.68
5	0.13	1.27	4.98	1.63	0.65
6	0.13	1.17	4.78	1.50	0.63
7	0.13	1.07	4.57	1.37	0.60
8	0.13	0.97	4.35	1.24	0.57
9	0.13	0.87	4.12	1.11	0.54
10	0.13	0.77	3.87	0.99	0.51
11	0.13	0.67	3.61	0.86	0.47
12	0.13	0.57	3.33	0.73	0.44
13	0.13	0.47	3.02	0.60	0.40
14	0.13	0.37	2.67	0.47	0.35
15	0.13	0.27	2.28	0.34	0.30
16	0.13	0.17	1.80	0.21	0.24
17	0.13	0.10	1.40	0.13	0.18
18	0.13	0.07	1.13	0.08	0.15

A-2 Total segmented volume obtained from vascular injury model

(ROI)

Table A- 2: The quantitative comparisons of the total vessel volume (TSV) obtained from the ROIs (n=6) are illustrated as mean values for non-injured and injured hindlimbs one day after trauma (Mean \pm SD).

Total segmented volume (TSV) (mm ³)	Bone volume	Non-injured	Injured
Mean \pm SD	297.6 \pm 10.1	401.9 \pm 56.0	496 \pm 102.8

A-3 Vascular morphometric parameters (biopsies)

Table A- 3: The original data of the quantified vascular parameters (Mean \pm SD) obtained from the vascular injury model presented for non-injured and injured biopsy samples (n=6) one day after trauma.

Vascular morphometric Parameters	Non-injured	Injured
VV (mm ³)	0.372 \pm 0.17	0.729 \pm 0.30
VD (mm)	0.069 \pm 0.02	0.069 \pm 0.01
VN (1/mm)	1.348 \pm 0.24	1.25 \pm 0.16
VSp (mm)	0.765 \pm 0.15	0.817 \pm 0.10
VConn (1/mm ³)	1.090 \pm 1.20	5.296 \pm 5.66
DA [1]	1.393 \pm 0.18	1.452 \pm 0.20

A-4 Vasodilation verification for the vascular injury model

Table A-4: The vessel diameter values (Mean \pm SD) of the large vessels (n=10) obtained from histology sections are presented as absolute values obtained from the non-injured and injured hindlimbs at day 1 for verification of vasodilation.

Vessel diameter (μ m)		
Day1	Non-injured	Injured
	17.3 \pm 5.8	45.7 \pm 12.7

Icing study

A-5 Quantitative analysis of CSTT inflamed areas

Table A-5: The CSTT and muscle injury quantitative results are presented in this table indicating the changes in the haematoma size (inflamed areas) at time points of 1, 3 and 7 days post injury after excluding the outlier values.

CSTT area (cm ²)	Time points	Inflamed
Sham	Day 1	5.18 ± 0.63
	Day 3	0.76 ± 0.18
	Day 7	0.36 ± 0.31
Icing	Day 1	2.53 ± 0.92
	Day 3	1.06 ± 0.18
	Day 7	1.05 ± 0.90

A-6 The normalised total vessel volume (ROI)

Table A-6: The normalised mean values are presented for perfused total vessel volume (TSV) obtained from sham and icing groups at different time points (Mean ± SD).

Time point	Total segmented volume (TSV) %				
	Day 0	Day 1	Day 3	Day 7	Day 28
Control	96.5 ± 3.1				
Sham		124.1 ± 10.6	112.0 ± 9.0	110.1 ± 5.5	110.2 ± 7.7
Icing		113.9 ± 8.7	103.1 ± 1.8	105.2 ± 13.9	112.3 ± 4.3

A-7 Vasodilation verification (icing study)

Table A-7: The vessel diameter values (Mean ± SD) of the large vessels (n=10) obtained from histology sections are presented as normalised values for the sham and icing groups at day 1 indicating higher vasodilation in the sham group.

Vessel diameter%	
Day 1	
Sham	267.8 ± 18.4
Icing	154.8 ± 26.0

A-8 The normalised vascular morphometric parameters (biopsies)

Table A-8: The normalised (non-injured/injured×100) vascular parameters (Mean ± SD) obtained from biopsy samples presented for all groups.

Normalised original values of the vascular morphometric Parameter (%)							
Groups	Time points	VV	VD	VN	VSp	VConn	DA
Control	Day 0	232.3 ± 200.4	172.8 ± 114.7	106.1 ± 23.4	100.2 ± 26.1	246.6 ± 254.9	98.9 ± 11.4
	Day 1	350.4 ± 233.3	121.5 ± 70.9	105.2 ± 16.8	98.6 ± 16.2	8035.1 ± 8554.5	115.2 ± 21.6
Sham	Day 3	364.0 ± 72.5	168.4 ± 88.6	105.8 ± 19.8	98.4 ± 22.4	4621.5 ± 5142.8	102.8 ± 9.9
	Day 7	733.6 ± 892.9	413.9 ± 594.4	97.5 ± 17.6	108.0 ± 36.9	17398 ± 29581	107.3 ± 5.0
	Day 28	150.3 ± 63.6	116.5 ± 52.6	114.3 ± 8.0	88.1 ± 5.8	598.9 ± 677.3	81.1 ± 5.2
	Day 1	1203.9 ± 1941.9	189.2 ± 119.9	90.9 ± 9.8	98.6 ± 16.2	387.6 ± 401.7	98.9 ± 13.9
Icing	Day 3	115.6 ± 37.0	109.5 ± 38.6	84.9 ± 11.4	98.4 ± 22.4	244.6 ± 228.9	84.6 ± 5.4
	Day 7	183.1 ± 90.7	170.4 ± 67.2	102.2 ± 11.6	108.0 ± 36.9	240.1 ± 160.8	105.4 ± 14.4
	Day 28	241.6 ± 106.6	119.7 ± 23.6	124.5 ± 36.3	88.1 ± 5.8	557.9 ± 531.6	91.9 ± 10.9
	Day 1	1203.9 ± 1941.9	189.2 ± 119.9	90.9 ± 9.8	98.6 ± 16.2	387.6 ± 401.7	98.9 ± 13.9

A-9 The perfused vessel number

Table A-9: The perfused vessel number (PVN) per area of tissue (Mean \pm SD) obtained from histological analysis is presented for the sham and icing groups at different time points.

Perfused vessel number (PVN)/mm ²					
	Day 0	Day 1	Day 3	Day 7	Day 28
Control	0.16 \pm 0.01				
Sham		0.20 \pm 0.06	0.21 \pm 0.08	0.28 \pm 0.05	0.27 \pm 0.14
Icing		0.13 \pm 0.03	0.13 \pm 0.03	0.21 \pm 0.06	0.26 \pm 0.09

Appendix B

IMMUNOHISTOCHEMISTRY TECHNIQUES

Immunohistochemistry (IHC) uses antibodies as histological tools to identify different patterns of antigen distribution within tissues. Antibodies are usually pre-made and can bind to a specific protein (antigen) (Ramos-Vara 2005). These antibodies are then tagged with a fluorescent chemical or an enzyme such as fluorescing or rhodamine which converts them to a visible dye. The tagged antibodies within the tissue are incubated and after washing the unbound antibodies away, the bound antibodies distribution is revealed by fluorescence or light microscopy. The assumption is that the antibody distribution can show the antigen distribution. In this research, IHC was utilised to evaluate the expression level of different antigens associated with revascularisation (angiogenesis). The von Willebrand Factor (vWF) is commonly used as vascular endothelial cell marker for studying angiogenesis and neovascularisation (Starke *et al.* 2011).

Histological section preparation

The general section preparation for the immunohistochemistry analysis was the same as H&E staining explain in 3.2.5.

Staining methods

For immunohistochemistry staining, the deparaffinised sections were treated by agents to suppress the non-specific background staining. For this purpose usually two agents are used including: the hydrogen peroxidase (H₂O₂ 3%, for 20 min) to suppress the tissue and cells endogenous peroxidase activity, and bovine serum albumin (BSA 2% for 60 min) which carries antibodies to block reactive sites and sticky proteins.

Heat-induced antigen retrieval (unmasking the antigens) was also carried out with a tri-sodium citrate buffer (Sigma-Aldrich, NSW, Australia) for 30 minutes at 70°C in an oven (Cole-Parmer StableTemp oven, NSW, Australia). Incubation of the sections was performed overnight at 4°C followed by adding the primary antibodies, rabbit polyclonal anti-human vWF (Ready-to-use; DAKO, California, USA), to detect the vascular endothelial cells and entire blood vessels including pre-existing and newly formed. The sections were then incubated for 30 minutes with a goat anti-mouse and anti-rabbit secondary antibody conjugated with horseradish peroxidase (DAKO, California, USA). Colour (brown) was produced using a 3,3-diaminobenzidine (DAB substrate kit; DAKO, California, USA) which is insoluble in alcohol, xylene and also resistance to heat along with counter staining with Mayer's haematoxylin. Negative and positive controls were conducted simultaneously to the test the tissue samples. Positive control is applied for testing the protocol to ensure it works properly, whereas negative control is to test that the involved antibody is specific. The exclusion of the primary antibody as well as an isotype control (Mouse IgM isotype control; BD Pharmingen, San Diego, USA) served as negative controls, whereas samples known to have specific cells and tissues were used as positive controls. Rat femur scaffold samples were obtained from previous work within the bone tissue morphology group, and used as positive controls.

Other methods including imaging of histological sections were similar to H&E imaging (3.2.5). Finally, positively stained blood vessels and capillaries by vWF were identified and then all groups were compared.

Appendix C



Standard Operating Procedures (SOPs) for the “Impact Device”

Developed by:

Zohreh Barani Lonbani

Institute of Health and Biomedical Innovation (IHBI),
Faculty of Science and Engineering,
Queensland University of Technology,
Brisbane, QLD, Australia

SOP Number:	Preparation Date:
KGQ-SOP-IM-D-23	23/11/2011
Author:	Review Date:
Zohreh Barani Lonbani	23/11/2011
Approved By:	Approval Date:
Dr. Roland Steck	15/12/2011
First update by:	First Update Date:
Zohreh Barani Lonbani	21/06/2012

Abbreviations

- ✚ CSTT: Closed soft tissue trauma
- ✚ PPE: Personal protection equipment e.g. gloves, gown, safety glasses, suitable shoes
- ✚ PC2: Physical containment level 2

Purpose and scope

This document has been developed to present safe operating procedures and standard protocols for utilizing the “impact device” located at MERF, Prince Charles Hospital, QUT, Brisbane, Australia. The repair or maintenance of this device is not the purpose of this guideline.

Guidelines for the impact device

The impact device has been developed to create a controlled reproducible closed soft tissue trauma (CSTT) on the hindlimb muscle (biceps femoris) of rats using anaesthetised rats or cadavers. This device has been designed to apply an impact with variable drop weights at different impact speeds to produce different degrees of CSTT.

Responsibilities

This document covers only basic information regarding the safe operating of the impact device. Therefore, as this guideline does not provide specific details regarding different experiments, operators will be required to be specifically trained for their particular tests. Users are responsible to operate the device according to the protocols presented in this guideline. Users are expected to be familiar with the terms and conditions described in this document and if necessary training must be taken before operating this device.

Precautions

The device is operated in a PC2 environment, and using PPE equipment is essential while operating this instrument especially if the user is working with animal specimens and there is a chance of contamination by blood.

The Safety cabinet door and front lid must be closed while the test is running to prevent injuries from the drop weight.

Impact device structure

The following figures illustrate the components of the impact device.

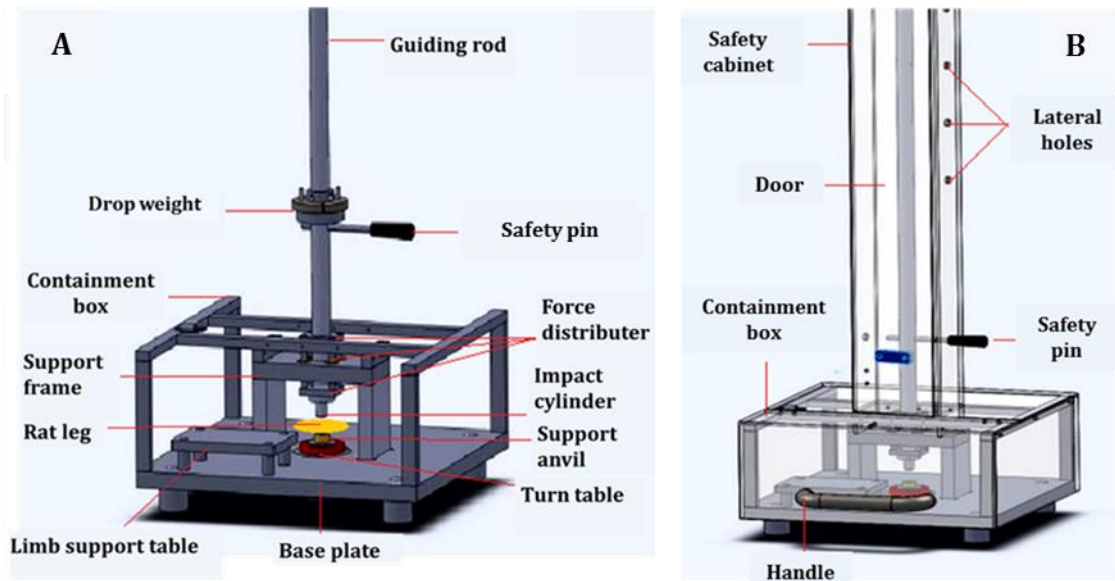


Figure C-6-2: The schematic of the impact device's structure.

This schematic shows two views of the impact device's structure including the internal (A) and external (B) components. A: The top part of the impact device consists of a guiding rod, along which the drop weight slides down. The lower part of the device is comprised of a base plate, a support frame, an impact cylinder, and force distributors to transfer the force from the drop weight to the impact cylinder and a height-adjustable support anvil. Two safety pins were also used in the upper and lower parts of the device to secure the drop weight in its location. Since the height of the guiding rod was 1.66 m, here only the lower part of the device is shown. The positioning of the specimen (rat leg) between the impact cylinder and the support anvil is schematically exhibited. To reduce the risk of any injury to the researchers using this device, the entire impact device was encased by a frame made from Perspex panels, with lateral holes for locating the safety pins (B).

Procedure

Before commencing a test, ensure there is appropriate PPE. While not in use, the impact device must be kept with the cabinet safety door and front lid closed while the calibrated drop weight is held at its lowest position by the lower safety pin.

- ✚ Open the safety cabinet door gently.
- ✚ Hold the drop weight while removing the lower safety pin.

- ✚ Slide the drop weight up to the desired height.
- ✚ Hold the drop weight at the desired height and secure it using the upper safety pin. The drop height determines the impact velocity as per Table 1.
- ✚ Make sure the lower safety pin is in place.
- ✚ Add more drop weights if necessary using additional plasticine.
- ✚ Close the safety cabinet door gently.
- ✚ Open the front lid gently.
- ✚ Pull the force distributors upwards and place the sample between the anvil and impact cylinder.
- ✚ The vertical position of the bottom anvil and sample can be adjusted with the two screws located on the base plate. Use the top screw to change the vertical position and the bottom screw to lock into position.
- ✚ Close the front lid gently.
- ✚ Remove the lower safety pin.
- ✚ Release the upper pin and the drop weight will slide down the rod and impact the sample.
- ✚ Open the safety cabinet door.
- ✚ Pull the force distributors up with one hand and remove the sample using the other hand.
- ✚ Hold the drop weight at its lowest position and secure it with the lower safety pin.
- ✚ Make sure the safety pins are placed in the right holes to prevent the drop weight from falling.
- ✚ When your experiment is finished, clean the device with ethanol.
- ✚ Close the cabinet door.

What are the risks?

- ✚ Impact injuries caused by the drop weight.
- ✚ Animal bites.
- ✚ Animal tissue/fluid (i.e. splashing fluids or blood into eyes).
- ✚ Contamination with animal fluid and tissue.
- ✚ Unexpected debris from the sample.
- ✚ Injuries to back and neck muscles due to inappropriate body posture during lengthy experimental tests.

What are the controls?

- ✚ The Impact device is designed with shields and guards in place to protect the operator.
- ✚ Operators should start with a light weight during calibration of the device, and increase the weight as necessary.
- ✚ Only trained operators should use the device.
- ✚ The device should be placed in a secure location away from foot traffic.
- ✚ Appropriate PPE (safety glasses, gloves and lab coat) must be used.
- ✚ Anyone wishing to work with this device must be trained in animal handling.
- ✚ Animals should only be handled briefly to transfer them from a cage into the pre-anaesthesia chamber.
- ✚ Follow SOP's for gas anaesthesia of rats.
- ✚ Users should take a Vaccination against Hepatitis B.
- ✚ Place the device on a stable bench or table at the correct height so users can work with the device safely and comfortably. Provide a suitable stand for safe access to the top of the drop tower. Sit in an ergonomic position while working.

Authority

Only people who have completed a full laboratory induction including animal handling and impact device training are authorised to work with this instrument.

Notes

This SOP has been reviewed and approved by Dr Roland Steck and Dr. Lauren Bautler.

Appendix D



Standard Operating Procedures (SOPs) for the “Rat Perfusion”




Developed by:

Zohreh Barani Lonbani

Institute of Health and Biomedical Innovation (IHBI),
School of Chemistry, Physics and Mechanical Engineering,
Queensland University of Technology,
Brisbane, QLD, Australia

SOP Number:	Preparation Date:
IHBI_TGR_RP_23	23/06/2012
Author:	Review Date:
Zohreh Barani Lonbani	24/06/2012
Approved By:	Approval Date:
Dr. Roland Steck	06/07/2012

Abbreviations

-  CSTT: closed soft tissue trauma
-  PPE: personal protection equipment e.g. gloves, gown, safety glasses, suitable shoes
-  PC2: Physical containment level 2

Purpose and scope

This document has been developed to present safe operating procedures and standard protocols for perfusing a solution through rat's vessels for various applications at MERF, Prince Charles Hospital, Brisbane, Australia.

Guidelines for rat perfusion

The rat perfusion protocol has been developed to help investigate microvasculature whether it has been injured by closed soft tissue trauma (CSTT) or is non-injured, using micro CT on anaesthetised rats or cadavers. Depending on the experiment, a variety of solutions can be used to perfuse through the microvasculature. This particular SOP is designed for perfusing a saline-heparin mixture to flush the blood from the microvasculature and also to perfuse a contrast agent (microfil) through the vasculature.

Animal preparation

The animal housing and welfare are based on the Australian code for the care and use of animals for scientific purposes (National Health and Medical Research Council 2013). Animals are accommodated in enclosed, safe and clean cages where they can freely have access to water and nutritious pellets as well as social and physical activity. Prior to the initiation of the impact, the anaesthetised animals are injected with analgesic subcutaneously (Buprenorphine: 0.2 mg/ml, 0.05 mg/kg) and then transferred to the impact device. After impact, animals should be kept warm during recovery while their vital signs are monitored. The post-operative pain can be managed by injecting one dose of Buprenorphine 12 hours after impact. The rats are euthanized 24 hours after impact according to the standard operating protocol (SOP) #261 of the Medical Engineering Research Facility (MERF) at QUT.

Responsibilities

This document covers only basic information regarding the safe operating procedure for rat microvasculature perfusion. Therefore, as this guideline does not provide specific details regarding different experiments, operators will be required to be specifically trained for their particular tests. Users are responsible to perform the perfusion according to the protocols presented in this guideline. Users are expected to be familiar with the terms and conditions described in this document and if necessary training must be taken before initiating the perfusion procedure.

Precautions

The surgery and perfusion are performed in a PC2 environment as there is a chance of contamination by blood or tissue fluid. Using PPE is essential during this procedure.

Procedures

- ✚ Before commencing the test, appropriate PPE must be used.
- ✚ Turn the hood and blower on.
- ✚ Be familiar with the rat's anaesthesia and euthanasia procedures described below.

Rat anaesthesia protocols

- ✚ Connect the oxygen to the tank, then open the oxygen tank valve. If the oxygen tank is empty, check with the relevant MERF staff to arrange tank replacement.
- ✚ Fill the anaesthetics machine with isoflurane.
- ✚ Obtain the isoflurane key to connect the isoflurane to the anaesthetic machine from the relevant MERF staff.

- ✚ Insert the key into the bottle.
- ✚ Insert the other end of the key into the anaesthetics machine (2 holes pointing to the right), then secure with a screw.
- ✚ Turn the bottle upside down and open the valve, then fill the anaesthetics machine until the maximum line is reached.
- ✚ Close the valve and turn the bottle back on its base, shaking the remaining isoflurane back into the bottle.
- ✚ Remove the key from the anaesthetic machine and bottle.
- ✚ Induce anaesthesia.
- ✚ Hold the animal by its tail and carry it from its cage to the anaesthesia chamber.
- ✚ Place the animal inside the induction chamber and tighten up the chamber lid.
- ✚ Connect the scavenger tube to the carbon tank (or exhaust via fume hood).
- ✚ Turn the switch so the anaesthetics flows into the induction chamber.
- ✚ Adjust oxygen flow (right valve) to 2-3L Oxygen/minutes and 5% isoflurane.
- ✚ Once the animal is unconscious/anaesthetised, stop gas/oxygen flow.
- ✚ Maintain anaesthesia.
- ✚ Place the animal on a surgical table with its nose inside the nose piece.
- ✚ Reconnect the nose piece to the anaesthetics machine.
- ✚ Reconnect the scavenger hose to the carbon tank (or exhaust via fume hood).
- ✚ Switch the gas flow to go through to the nose piece.

- ✚ Adjust oxygen flow (left valve) to 1-1.5l O₂/min at 2-2.5% isoflurane.
- ✚ Ensure that the animal is put to sleep properly.

Rat Euthanasia

- ✚ Placed the rat in a plastic container under a laboratory hood.
- ✚ Connected the container to CO₂ and seal the lid to prevent the gas leaking outside.
- ✚ Verify death of the rat (refer to the NHMRC Guidelines to promote the wellbeing of animals used for scientific purposes: the assessment and alleviation of pain and distress in research animals. 2008).

The PC2 preparation room

- ✚ Before commencing the test, ensure the appropriate PPE is used.
- ✚ Prepare the perfusion setup (perfusion pumps, the connectors, heparinised saline and microfil contrast agent).
- ✚ Prepare a plastic net over an open plastic container for collecting blood and solution.
- ✚ Prepare the surgery setup (bladed scalpel, a pair of scissors, tweezers and clamps).
- ✚ Make sure the perfusion pump is working properly then connect one tip of the tube to the heparinised saline prepared in a glass (250 ml) and the other tip to the three-way connector.
- ✚ Open the rat's chest using a bladed scalpel and a pair of scissors section to expose the heart.
- ✚ Dry the heart with a paper towel.

- ✚ Insert the 22 G angiocath into the left ventricle and secure it with super glue.
- ✚ Transfer the rat onto the plastic net in the supine position and attach the angiocath to the three-way connector.
- ✚ Open the right atrium delicately to facilitate the drainage of solutions using a needle.
- ✚ Turn on the perfusion pump so the heparinised saline flows through the vasculature.
- ✚ When the output has become clear of blood, prepare the microfil contrast agent in a disposable glass and connect that to the second pump for perfusion.
- ✚ After completing the contrast agent perfusion, transfer the rat into the fridge and keep it there at 4°C overnight.
- ✚ The day after dissection put the legs in NBF at 10% concentration for future micro-CT imaging.

What are the risks?

- ✚ Contamination with anaesthesia gas (isoflourane).
- ✚ Injuries caused by the blade.
- ✚ Injuries caused by the needle.
- ✚ Animal bites.
- ✚ Animal Tissue/Fluid: Splashing fluids or blood into eyes.
- ✚ Contamination with animal fluid and tissue during surgery.
- ✚ Unexpected debris from the sample.
- ✚ Injuries to back and neck muscles due to inappropriate body posture during the procedure.
- ✚ Contamination with chemical materials (i.e. microfil).

What are the controls?

- ✚ Be familiar with anaesthesia SOPs.
- ✚ The hood and blower must be on in all times during anaesthesia.
- ✚ The animal chamber must be closed tightly during anaesthesia.
- ✚ The isofloarane lid must be tightened properly after use.
- ✚ Appropriate PPE (mask, safety glasses, gloves, covered shoes, gown with long sleeves, and hair net) must be used.
- ✚ If there are any concerns regarding the gloves being torn during the surgery, two or even three gloves should be worn.
- ✚ To prevent risks associated with the blade, inserting the blade into the scalpel and cutting of the tissue must be carried out by a trained person or under expert supervision. Holding the scalpel like a pen is the safest position when cutting the tissue.
- ✚ After using scalpel, the blade must be immediately disposed of safely.
- ✚ Only trained personnel should perform the surgery.
- ✚ Surgical instruments such as the scalpel should be stored in a secure location away from foot traffic.
- ✚ All consumables used for the perfusion should be disposed of properly after surgery.
- ✚ All personnel who wish to perform the surgery must be trained in animal handling.
- ✚ Users should take a Vaccination against Hepatitis B.
- ✚ Sit in an ergonomic position while working.
- ✚ The safest way to carry the animal from its cage to the anaesthesia chamber is by its tail.
- ✚ The scavenger system should be used to prevent chemical exposure.

Authority

Only people who have completed a full laboratory induction including animal handling and have trained to work with hazardous materials are authorised to work using these protocols.

Appendix E

RADIOLOGICAL SOCIETY OF NORTH AMERICA
820 JORIE BLVD. OAK BROOK, IL 60523
TEL 1-630-571-2670 FAX 1-630-571-7837
RSNA.ORG



December 22, 2014

Zohreh Barani Lonbani
QUT Institute of Health and Biomedical Innovation
Brisbane QLD 4059
Australia

Dear Zohreh Barani Lonbani:

The Radiological Society of North America (RSNA[®]) is pleased to grant you permission to reproduce the following figures in print and electronic formats for educational, non-profit use in your PhD thesis, provided you give full credit to the authors of the original publication.

Figures 1a, 1b
Zhuang Z W, Gao L, Murakami M, et al. Arteriogenesis: Noninvasive quantification with multi-detector row CT angiography and three-dimensional volume rendering in rodents. *Radiology* 2006;240:698-707.

This permission is a one-time, non-exclusive grant for English-language use and is exclusively limited to the usage stated and underlined above. The requestor guarantees to reproduce the material as originally published. Permission is granted under the condition that a full credit line is prominently placed (i.e. author name(s), journal name, copyright year, volume #, inclusive pages and copyright holder).

This permission becomes effective upon receipt of this signed contract. Please sign a copy of this agreement, return a signed copy to me and retain a copy for your files. Thank you for your interest in our publication.

[Print Name]: Zohreh Barani Lonbani

SIGNATURE: Zohreh Barani Date: 21,01,2015

Sincerely,

A handwritten signature in black ink that reads 'Ashley E. Daly'.

Ashley E. Daly
Senior Manager, Journal Rights & Communications
Publications

Phone: 630-590-7771
Fax: 630-590-7724
E-mail: permissions@rsna.org